Defense Nuclear Agency
Alexandria, VA 22310-3398

DNA-TR-94-124

Weighmat Sensor Investigation

Richard B. Underwood III
Steven C. Lofton
Applied Research Associates, Inc.
4300 San Mateo Blvd. NE
Suite A220
Albuquerque, NM 87110-1260

June 1995

CONTRACT No. DNA-MIPR-93-625

DISCLAIMER

Review of this material does not imply Department of Defense Indorsement of factual accuracy or opinion.

Destroy this report when it is no longer needed. Do not return to sender.

PLEASE NOTIFY THE DEFENSE NUCLEAR AGENCY, ATTN: CSTI, 6801 TELEGRAPH ROAD, ALEXANDRIA, VA 22310-3398, IF YOUR ADDRESS IS INCORRECT, IF YOU WISH IT DELETED FROM THE DISTRIBUTION LIST, OR IF THE ADDRESSEE IS NO LONGER EMPLOYED BY YOUR ORGANIZATION.

REPORT DOCUMENTATION PAGE

Form Approved OMB No. 0704-0188

1. AGENCY USE ONLY (Leave blank)	2. REPORT DATE	3. REPORT TYPE AND DATES COVERED
	950601	Technical 931001 – 940630

4. TITLE AND SUBTITLE

Weighmat Sensor Investigation

5. FUNDING NUMBERS

C - DNA-MIPR-93-625

6. AUTHOR(S)

Robert B. Underwood III and Steven C. Lofton (Applied Research) and
Andres Peekna (Innovative Mechanics)

7. PERFORMING ORGANIZATION NAME(S) AND ADDRESS(ES)

Applied Research Associates, Inc.
4300 San Mateo Blvd. NE
Suite A220
Albuquerque, NM 87110-1260

8. PERFORMING ORGANIZATION REPORT NUMBER

9. SPONSORING/MONITORING AGENCY NAME(S) AND ADDRESS(ES)

Defense Nuclear Agency
6801 Telegraph Road
Alexandria, VA 22310-3398
VTSA/Simelton

10. SPONSORING/MONITORING AGENCY REPORT NUMBER

DNA-TR-94-124

11. SUPPLEMENTARY NOTES

12a. DISTRIBUTION/AVAILABILITY STATEMENT

Approved for public release; distribution is unlimited.

12b. DISTRIBUTION CODE

13. ABSTRACT *(Maximum 200 words)*

This research investigated questions which arose from earlier work examining the potential application of thin-film piezoresistive mats in weighing military trucks as part of treaty verification operations. The object of this research was to investigate the properties of the sensor elements to recommend suitable methods to control their impacts on accuracy. Applied Research Associates tested the sensor element at the Waterways Experiment Station to evaluate pressure sensitivity variations, temperature effects, and alternative calibration methods. The sensor element was found sensitive to temperature changes, becoming non-repeatable above the 100 degrees F. The element produced repeatable measurements within its operable temperature range. The sensor's response was confirmed to be nonlinear and hysteretic. Static creep was found to be predictable; hysteresis and sensor fatigue were found to be relatively minor factors in weighing vehicles. Short term memory of the element could affect accuracy if vehicles are weighed in close succession. The element's sensitivity to temperatures above 100 degrees F makes it currently impractical as a part of a field measurement device. However, it could be used under controlled temperatures in a screening/gating device. The principal recommendation of this study is to develop a piezoresistive material with a higher working temperature range.

14. SUBJECT TERMS

Shock
Weigh-In-Motion
Piezo-Resistive Sensors
Military Vehicles
Sensor Technology

15. NUMBER OF PAGES

184

16. PRICE CODE

17. SECURITY CLASSIFICATION OF REPORT	18. SECURITY CLASSIFICATION OF THIS PAGE	19. SECURITY CLASSIFICATION OF ABSTRACT	20. LIMITATION OF ABSTRACT
UNCLASSIFIED	UNCLASSIFIED	UNCLASSIFIED	SAR

CLASSIFIED BY:

N/A since Unclassified.

DECLASSIFY ON:

N/A since Unclassified.

7. PERFORMING ORGANIZATION NAMES(S) AND ADDRESS(ES) (Continued).

Innovative Mechanics Inc.
265 Coe Road
Clarendon Hills, IL 60514-1029

9. SPONSORING/MONITORING AGENCY NAME(S) AND ADDRESS(ES) (Continued).

U.S. Army Engineer Waterways Experiment Station
3909 Halls Ferry Road
Vicksburg, MS 39180-6199

PREFACE

This project's objective was to characterize the performance of piezoresistive thin-film pressure sensors. The investigation involved experimentation in the laboratory. This project was conducted from October 1993 through June 1994, and was conducted under Contract Number DACA39-93-C-0134, US Army Engineer Waterways Experiment Station (WES). The Contracting Officer's Technical Representative for this project was Mr. Richard Bradley, Geotechnical Laboratory, WES.

The Principal Investigator for this work was Mr. Robert B. Underwood III, Applied Research Associates, Inc. (ARA). Dr. Andres Peekna, Innovative Mechanics, Inc. and Mr. Steve Lofton, ARA executed the experiments and analyzed the data. Ms. Virginia Hoeppel, ARA, prepared and edited the report. Mr. Tommy Carr and Ms. August Williamson, Instrumentation Services Division, WES, set up and operated the WES laboratory environmental chamber and numerically-controlled loading device used for the experiments. Ms Jody Rhodes assisted in preparing tables, graphs and figures for the report.

This report describes the work accomplished, the observations from the investigations, and recommendations for further investigations.

CONVERSION TABLE

Conversion factors for U.S. Customary to metric (SI) units of measurement.

MULTIPLY → / ← TO GET	BY → / ← BY	TO GET → / ← DIVIDE
atmosphere (normal)	1.013 25 X E +2	kilo pascal (kPa)
bar	1.000 000 X E +2	kilo pascal (kPa)
calorie (thermochemical)	4.184 000	joule (J)
cal (thermochemical/cm^2)	4.184 000 X E -2	mega joule/m^2 (MJ/m^2)
degree (angle)	1.745 329 X E -2	radian (rad)
degree Centrigrade	add: 273.16	degree kelvin (K)
degree Fahrenheit	$t_k = (t°f + 459.67)/1.8$	degree kelvin (K)
erg	1.000 000 X E -7	joule (J)
erg/second	1.000 000 X E -7	watt (W)
foot	3.048 000 X E -1	meter (m)
foot-pound-force	1.355 818	joule (J)
inch	2.540 000 X E -2	meter (m)
kilofoot (kft)	0.3048	kilometer (km)
kilotons	4.183	terajoules
kip (1000 lbf)	4.448 222 X E +3	newton (N)
kip/$inch^2$ (ksi)	6.894 757 X E +3	kilo pascal (kPa)
megaton (MT)	4183	terajoules (TJ)
micron	1.000 000 X E -6	meter (m)
mil	2.540 000 X E -5	meter (m)
mile (international)	1.609 344 X E +3	meter (m)
nautical mile (nmi)	1852	meter (m)
ounce	2.834 952 X E -2	kilogram (kg)
pound-force (lbs avoirdupois)	4.448 222	newton (N)
pound-force/$inch^2$ (psi)	6.894 757	kilo pascal (kPa)
pound-$inch^2$ (psi)	1/0.145	kilopascal (kPa)
pound-mass (lbm avoirdupois)	4.535 924 X E -1	kilogram (kg)

TABLE OF CONTENTS

TABLE OF CONTENTS (Continued)

FIGURES

FIGURES (Continued)

FIGURES (Continued)

FIGURES (Continued)

TABLES

TABLES (Continued)

SECTION 1

INTRODUCTION

1.1 BACKGROUND.

There is a need for lightweight, portable, and accurate weigh scales capable of measuring heavy vehicles. Traditional weighing methods have not allowed both portability and accuracy. Electro-optical and piezoelectric tactile sensing devices which have been developed for robotics applications have demonstrated their own limitations in accurately measuring weights. Technological breakthroughs in piezoresistive thin film circuits offered the potential of allowing the development of a vehicle weighing system that is both portable and accurate. The basic technology is manufactured by Tekscan, Inc. (Boston, MA) for use in the medical field for dental and orthopedic pressure sensors.

ARA packaged a pressure sensing system for use in weighing vehicles - *Weighmat*. The basic sensor inside the Weighmat consists of a printed circuit grid applied to polyester films, with a pressure sensitive semi-conductive material sandwiched between. The resistance of the sandwiched material is inversely related to an applied force. The grid senses a pressure distribution over time and this pressure distribution is integrated over the area to obtain a force (weight). Grids are connected through a signal conditioning circuit and a receiver circuit to a personal computer. Computer software allows the display of force and pressure distributions and time histories. The sensor chosen for the Weighmat system has a sensing area of 16.67 in. by 19.09 in. with a nominal pressure range of 75 psi.

There are several advantages to using this piezoresistive type grid sensor. In addition to giving a load reading, the sensor gives a pressure distribution under a load. This distribution can gives useful information not obtainable by static scales which give a total load reading only. The system is also capable of weighing vehicles in motion. An advantage of the piezoresistive sensor over piezoelectric type sensors is that the piezoresistive sensor can measure static loads. This is because a piezoelectric sensor relies on a change in current due to a change in force allowing readings of dynamic forces only. The high output impedance of piezoelectric sensors also makes them more vulnerable to environmental factors such as moisture. Because the piezoresistive sensor relies simply on the resistance of the pressure sensitive material, static readings are possible with this type of sensor.

This project addresses some technical issues raised by our Proof of Concept project[1]. In the Proof of Concept project we found that this technology offered the possibility of overcoming the technical hurdles of weight and dynamic response if certain sensor properties were more fully understood. We found that temperature changes affected accuracy. We also found the sensor to be subject to creep and hysteresis and sensel-to-sensel variations in sensitivity. In this project our objective was to quantify and bound the most important factors affecting accuracy for the application of weighing either stationary or slow moving vehicles.

1.2 SCOPE.

This work focused on the performance characteristics of the sensor elements. We designed our experiments with respect to the critical variables identified in our previous effort. We

---

[1] Underwood, R.B. III and Dr. Andres Peekna, Weighmat Proof of Concept Final Report, prepared for USAE Waterways Experiment Station, Vicksburg, Mississippi, January 1993.

performed experiments using two different loading devices, an inflatable bladder to provide gradual, even loads, and a tire-treaded platen which provided rapid and repeated uneven loads. We conducted the preponderance of our experiments in the laboratory under controlled environmental conditions by using an environmental chamber. We briefly examined the sensors under vehicle loads to test several hypotheses. These activities enabled us to examine the sensor's response to varying temperatures, loading pressures, patterns, durations, frequencies, and repetitions.

1.3 CONCLUSIONS.

The concept of using a gridded array of sensels to weigh a vehicle wheel has advantages over single reading static type scales. The gridded sensor provides valuable information on pressure distribution under the tire and loading area. An advantage of the particular sensor system which was evaluated is that it can be used to weigh vehicles in motion. The sensors used in the Weighmat study possess many characteristics which affect their accuracy. Accuracy is affected by nonlinearity, temperature sensitivity, eratic creep, hysteresis, and sensel-to-sensel variations in sensitivity. Influences on accuracy of the sensor due to these inherent characteristics were evaluated in this project. Sensor behavior begins to become eratic above 100 degrees F. Results indicated the current sensor should obtain an accuracy of 10 percent making it suitable for screening type weight measurements. At present, the sensor element is not ready for use as a precision vehicle weighing device under field conditions. Improved resistive inks could improve the accuracy of these piezoresistive type sensors. Also, another type of element which could be used in the grid configuration could be explored for future development of a portable weighing system.

SECTION 2

TECHNICAL APPROACH

2.1 INTRODUCTION.

Applied Research Associates, Inc. (ARA) determined the performance characteristics of the Weighmat sensor element by conducting a set of laboratory experiments, applying uniform statically and non-uniform loads statically and dynamically, followed by brief experiments using two different vehicles.

Our laboratory experiments were conducted to investigate the sensor element's performance in the following areas: sensel-to-sensel variations, repeatability, temperature sensitivity, non-linearity, static creep, hysteretic behavior, fatigue, memory and recovery. We applied two different kinds of loads, a uniform bladder load using the manufacturer's equilibration device and a non-uniform platen load using a military tire tread section. The platen loads were applied by an MTS machine both statically and dynamically to approximate a slow moving vehicle.

2.2 SYSTEM.

ARA obtained the necessary system components for this effort. Our system consisted of a mat sensor, two handle/cable assemblies, an IBM-compatible computer interface board, a personal computer, data analysis software, and a color inkjet printer (Figure 2-1). The mat sensor, handle/cable assemblies, computer interface board and software were obtained from Tekscan.

We used a "seat" sensor for evaluation (Figure 2-2). This sensor type consisted of two printed sheets of polyester (Mylar) film glued together around the edge. The column circuits were printed on one sheet and the row circuits were printed on the other. On top of the circuitry of each sheet was printed a layer of resistive ink; these ink layers (each about 0.001-inch thick) provide the piezoresistive properties for each individual sensel. The seat sensors were obtained from the manufacturer in a nominal range of 75 psi with a sensing area of 16.67"x19.09". The seat sensors had 48 columns and 42 rows for a total of 2016 sensels; each sensel was a square of 0.397 inch on a side, nominally having an area of 0.16 square inch. We found that quality control of sensor elements shipped to us was poor; four of ten sensors in one shipment required exchange due to row ghosting. These sensors should be carefully checked before use. We checked each row of each sensor for proper response with a hand-held loading element.

For the laboratory experiments we used a variety of measures to package the sensors which will be described later in this report. For the vehicle tests we mounted the sensors on aluminum base plates measuring 24"x30"x0.125" and weighing approximately 8 pounds. The base plates were selected to ensure a stable platform for our preliminary tests, and were half as thick as the plate used in the proof of concept project. Above and below the sensor we placed fabric-reinforced rubber blankets, with about 0.1 inch on top of the sensor and 0.035 inch between the sensor and the base plate. These blankets served to protect the sensor and distribute the tire load. Between the sensor and the blankets we placed 0.005-inch thick pieces of Teflon sheet to reduce shear between the blankets and the sensor. The total weight of the blankets was about 2 pounds.

The sensors connected to data handles supplied by Tekscan (Figure 2-3). The handle's purpose was to multiplex the signals from the sensel array and transmit the analog data to an

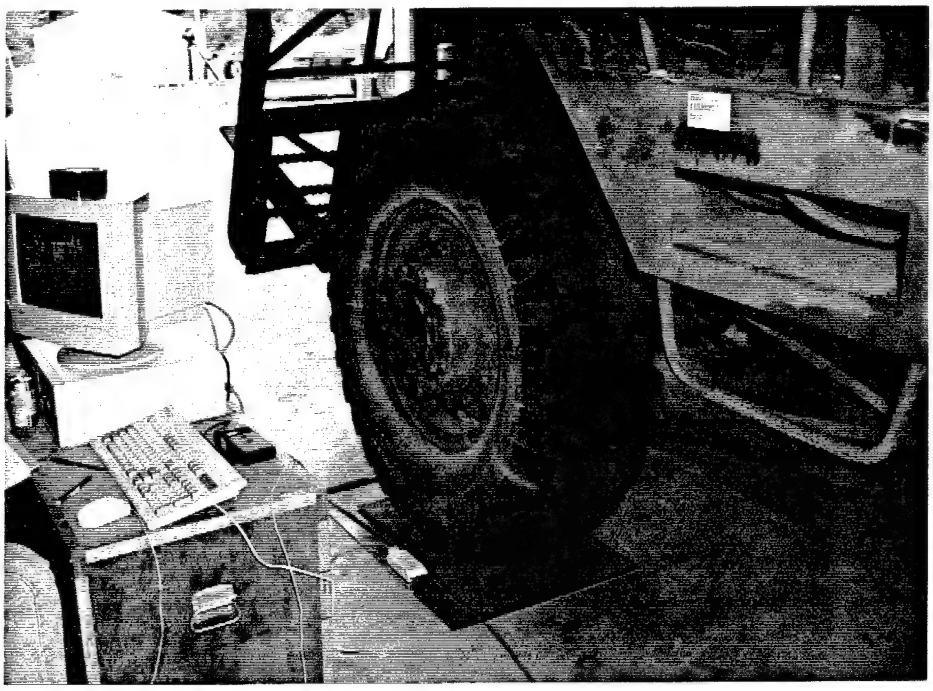

Figure 2-1. Sensor system and computer during a vehicle weighing. Note data handle on floor immediately to the left of the tire.

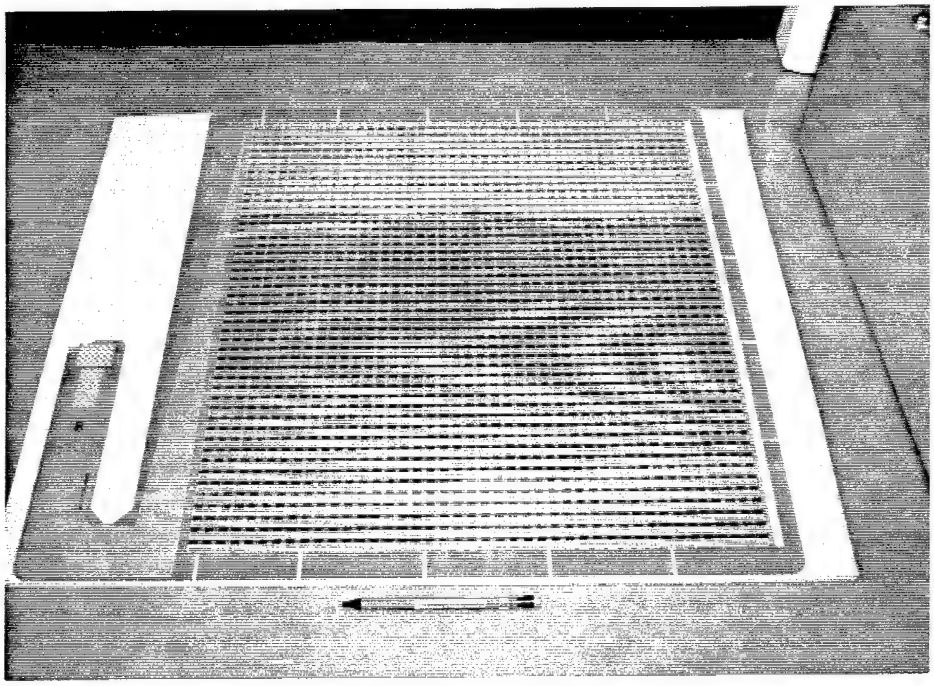

Figure 2-2. We used a "seat" sensor with nominal 75 psi rating consisting of 2016 individual sensels.

A/D board mounted in the expansion slot of the laptop computer. The plastic data handle used spring loaded pins to contact with the contact points on the sensors; its design allowsthe use of different sensor designs and grid configurations. The handles connected with the A/D board by standard 6 pin computer cables.

We used an ordinary Intel 486-based personal computer. We used Tekscan's proprietary software for data display and analysis (Figure 2-4). We found the complete system to be satisfactory for our immediate purposes, with the Tekscan software getting high marks for ease of use, functionality and stability.

2.3 LABORATORY TESTING.

Our laboratory tests were conducted at the Material Research and Construction Technology Laboratory, Geotechnical Laboratory, Waterways Experiment Station (WES) (Figure 2-5). We used two devices for loading the sensors. The bladder device obtained from Tekscan provided uniform loads up to 90 psi and an MTS provided loads up to 10,000 pounds, which was the capacity of the load cell. The MTS was numerically controlled and could generate a pulsed loading waveform. An environmental chamber provided low temperatures via the venting of liquid nitrogen, and it provided warmer temperatures from an internal heater (Figure 2-6).

2.3.1 Uniform (Bladder) Loadings.

These loadings were accomplished by using the Tekscan bladder loading device which we used for equilibration (Figure 2-7). The bladder loading device consisted of an aluminum frame within which is a rubber bladder. Gas pressure is supplied from a standard nitrogen bottle through a control mechanism supplied by the manufacturer. We used the bladder device on a bench for equilibrations and for room temperature tests. For higher and lower temperatures, we were able to fit the bladder within the environmental chamber, running the lead to the sensor, the nitrogen gas line, and a temperature probe up through the hole in the bottom of the chamber.

2.3.2 Compressibility Effects on Temperature.

It is well known that pressurizing a volume of gas increases its temperature. Transfer of heat to or from the solid walls of the apparatus decreases these temperature changes. Loading the air bladder with liquid was considered, but abandoned on advice from Tekscan personnel, who pointed out that liquids such as hydraulic fluid may tend to dissolve the pressure-sensitive adhesive that holds the air bladder together. Thus, nitrogen gas was used to load the bladder.

On the advice of Tekscan personnel, a thermocouple was inserted between the air bladder and a sensor to check out possible compressibility effects. A no longer usable sensor, left over from the previous Proof of Concept tests, was used, as we were warned that the thermocouple would tend to put a crease into the sensor. The thermocouple output was monitored as the pressure was changed from zero gage pressure to 90 psi, and from 90 psi to zero gage pressure. Each change was as fast as the apparatus would allow (on the order of 10 seconds). Resulting fluctuations in the output of the thermocouple averaged 0.5 degree F, and 0.6 degree F was the greatest fluctuation observed. These temperature changes were probably this small due to the low volume of the air bladder (the gas volume was less than 0.1-inch or 2.5-mm thick) and the relatively large thermal mass of the equilibration device.

When performing tests with uniform loading at much lower temperatures, an additional concern arose because the tank of compressed nitrogen was located outside the environmental

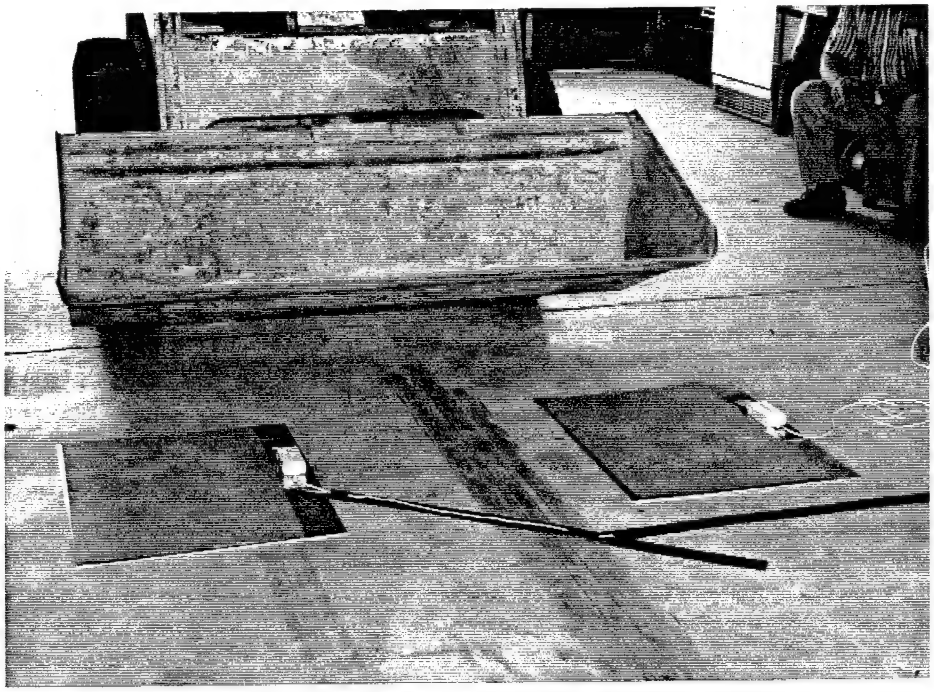

Figure 2-3. Two-handle system allows simultaneous capture of both vehicle wheel traces.

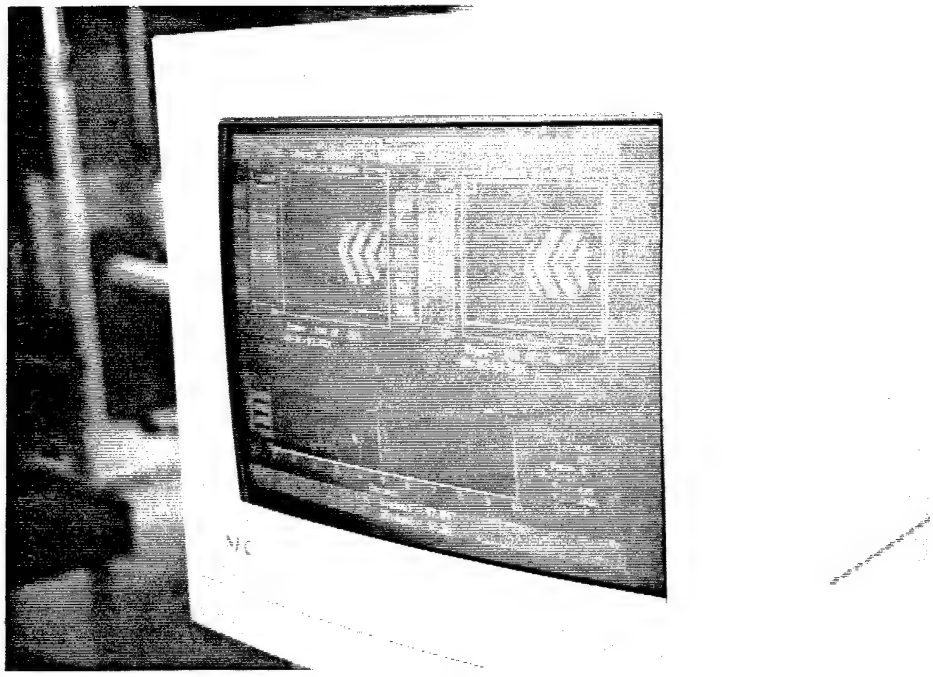

Figure 2-4. System software allows data from each handle to be viewed real-time and in a playback mode.

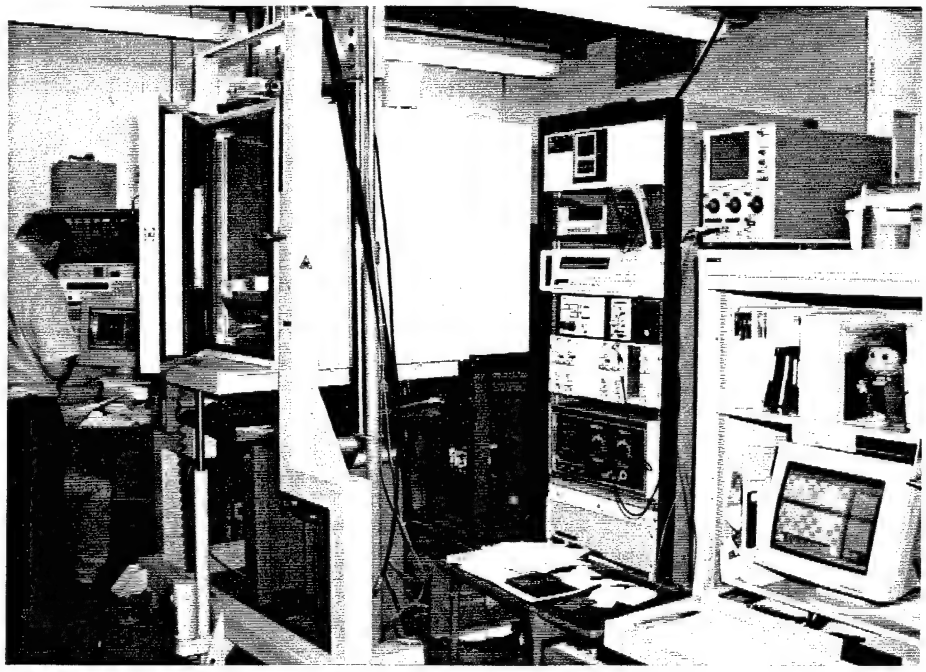

Figure 2-5. Experiments were conducted at the Geotechnical Laboratory, Waterways Experiment Station. Pictured is the numerically-controlled MTS loading system with environmental chamber.

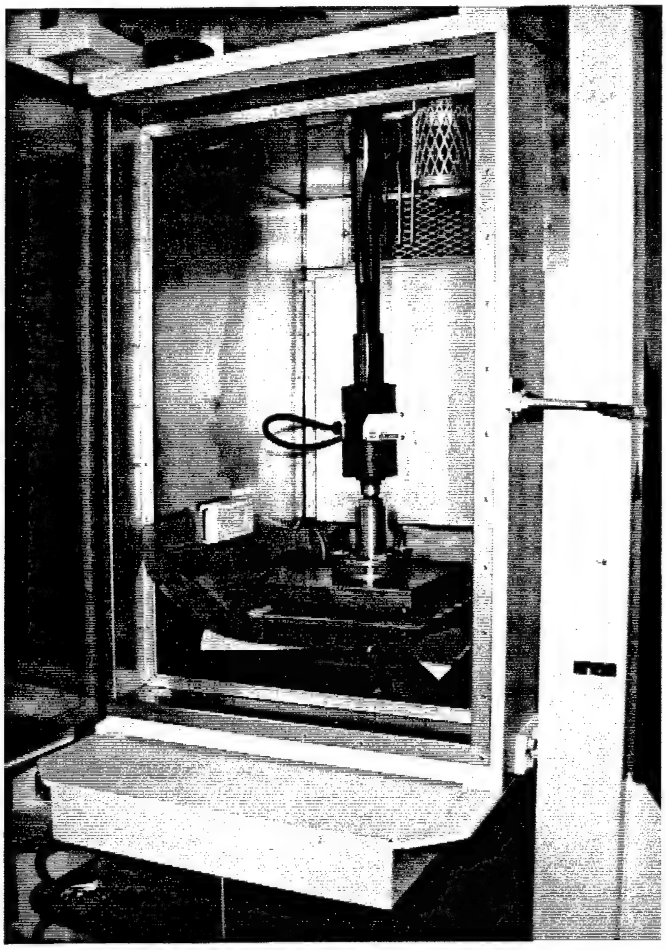

Figure 2-6. The environmental chamber provided test temperatures from -20 degrees F to 110 degrees F for our experiments. Shown inside is the platen loading device with 10,000-pound load cell.

chamber. This brought in the additional effect of piping room-temperature nitrogen into the cold air bladder loader. To check this out, the same sort of tests were also repeated at -16 degrees F. Resulting temperature fluctuations were 0.8 degree F or less. It was concluded that effects of compressibility on temperature in the air bladder equilibrations and uniform loading tests were not significant enough to require correction.

2.3.3 Non-uniform (Platen) Loadings.

One of our objectives was to evaluate the effects of dynamic, non-uniform loads imposed by aggressively-treaded military type tires under various temperatures and pressures. In order to do this we were constrained to using the MTS system with environmental chamber. We obtained a Goodyear tire for a Light Amphibious Vehicle (LAV) and mounted a patch of it on a steel plate (Figure 2-8). We selected the tire for its aggressive chevron-shaped tread pattern. Our patch was cut large enough to include three pitches of the tread pattern. We then mounted the treaded platen to the loading device (Figure 2-9).

The MTS applied the platen loads statically or as programmed pulses and increments (Figure 2-10). Data cable fed back to the computer for storage and later analysis (Figure 2-11).

2.3.4 Sensor Packaging for Platen Loading Tests with Tire Tread and for Vehicle Loadings.

In the previous Proof of Concept tests, the sensor was protected by three fabric reinforced rubber printing blankets above and one beneath. The fabric reinforcing minimizes lateral strain under load. Minimizing lateral strain was considered beneficial in that it would tend to minimize in-plane tensile strain in the sensor itself. The printing blankets also have a foam-rubber "compressible" layer, which is intended to provide local compressibility even under conditions of little or no lateral strain. Such compressibility is desirable in evening out the effects of local high compression, as due to sand grains. The smoothness and even thickness of the printing blankets were also in their favor when considering the needs of this measurement application.

In the Proof of Concept tests, the printing blankets were held together at their outer edges by double-stick tape; rubber adhesive could also be used. The sensor itself was held on one edge only. Otherwise, it was left free to move in the Weighmat pocket. This proved quite successful, except for some symptoms of the sensor tending to form a crease within the pocket; this would iron itself out in time. To hasten the ironing out of such a possible crease, and to help prevent its formation to begin with, it was decided that including a layer of slippery Teflon immediately above and below the sensor would be a good idea. A thickness of 0.005 inch for the Teflon was considered adequate, while a 0.002-inch thick sample appeared too thin in that it itself may tend to wrinkle. For this round of testing, 0.005-inch thick Teflon was procured.

The reason for only one printing blanket layer under the sensor (versus three above) was that while some protection (including against small sand grains) under the sensor element is desired, excessive compressibility between the sensor and its base plate would result in excessive flexure of the sensor under the tire lugs. Indeed, if the Weighmat were to be adhered directly to its base plate, it may be better to omit the printing blanket on the bottom.

Prior to final selection of sensor packaging, tests were done with platen loading with the tire tread, involving various combinations of layers of printing blankets above and below the sensor, also with and without the Teflon layers. The number of printing blankets below the sensor (next to the smooth base plate) varied between zero and one, and the number of printing blankets above the sensor (facing the tire tread) was varied between zero and three. The resulting distributions of indicated stress were examined for excessive smoothing (as

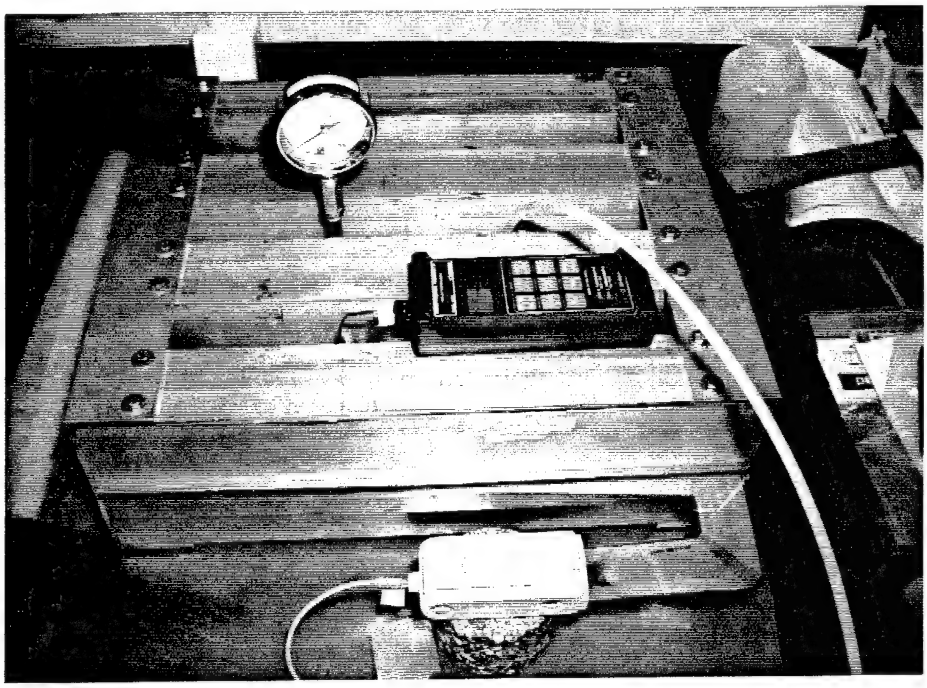

Figure 2-7. A bladder loading device provided uniform loads up to 90 psi. Note the sensor insertion and its data handle at bottom of photo. On the device is a temperature gage and pressure gage.

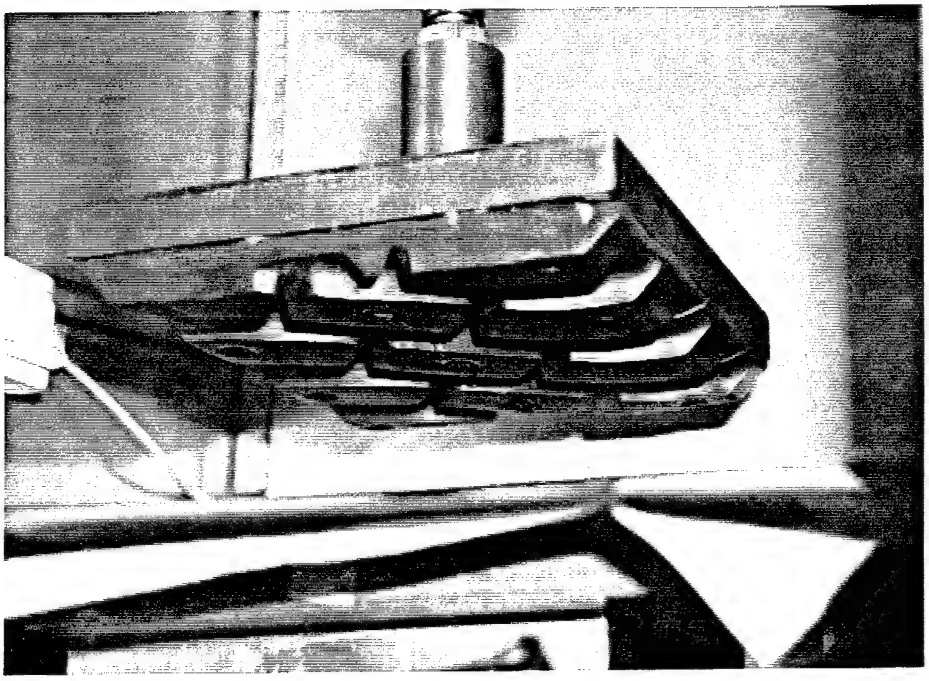

Figure 2-8. For non-uniform load conditions we mounted a patch of tire tread on a steel plate.

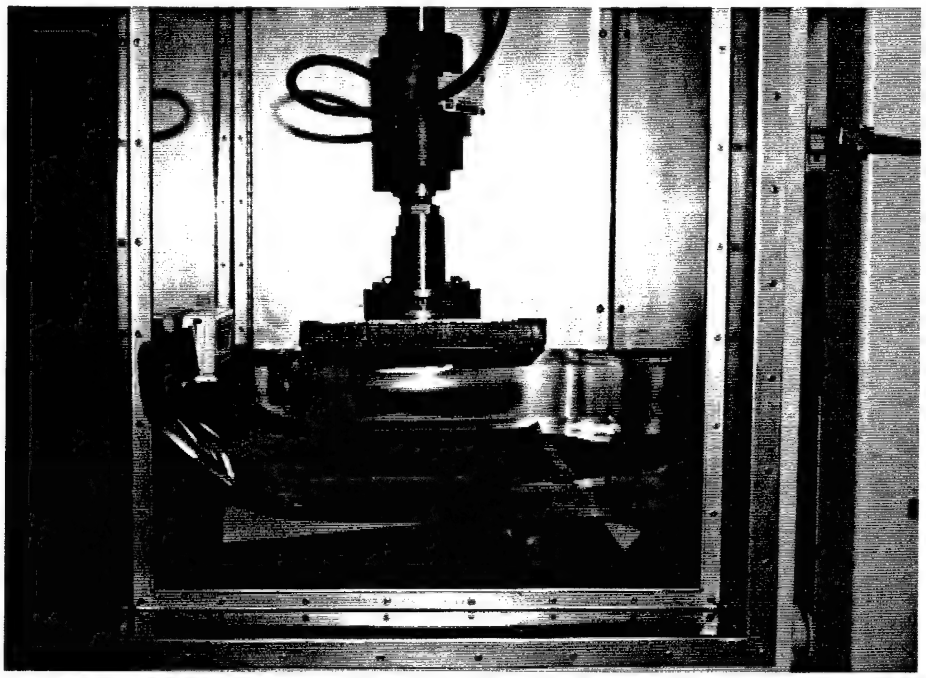

Figure 2-9. We then attached the treaded platen to the loading device. Note the 10,000-pound load cell used for reference.

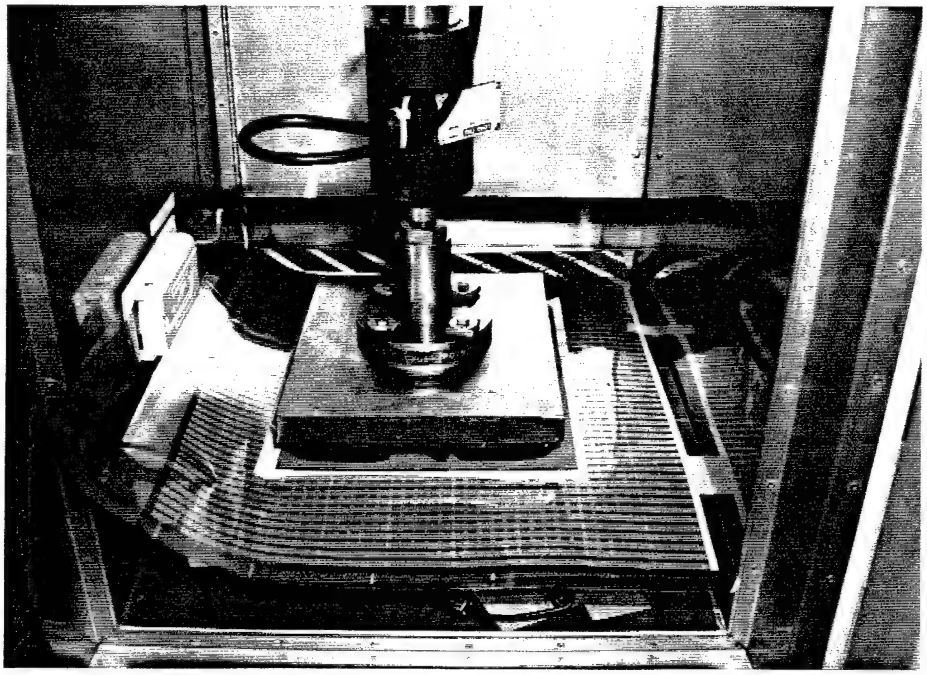

Figure 2-10. Platen load applied to the sensor element.

from too many blankets) and other adverse symptoms.

In the end, the final choice settled on two printing blankets on top, one on the bottom, and a layer of Teflon immediately above and below the sensor, as providing a reasonable optimum (Figure 2-12). Two of the particular printing blankets used on top of the sensor in this round of tests had about the same total compressibility as the top layer of three printing blankets used in the Proof of Concept tests. The total compressibility is such that it would take an 0.010-inch compressive deformation to "bottom out" the compressible layers. This "bottoming out" would occur at close to 200 psi. This deformation could be exceeded locally, as under a sand grain, by producing localized lateral strain within the printing blankets. This combination of printing blanket and Teflon layers, deemed reasonably optimum for field use, was used in taking all the platen loading test data presented in this report.

2.4 VEHICLE TESTING.

We used two different vehicles. One was a small front end loader called a Bobcat (Figure 2-13). The other was a military rough terrain forklift having large off road tires with an aggressive tread pattern (Figure 2-14). We tested the vehicles inside a shed at WES. The test area was shaded and the pavement temperature remained constant and well within the operating range of the sensor element.

2.5 EXPERIMENTAL PARAMETERS.

Our experiments covered a wide range of environmental and loading parameters. We varied temperature, load magnitudes and frequencies, and placements. Due to time and laboratory availability constraints we were challenged to gather enough samples to make valid conclusions. By carefully controlling our variables while conducting the experiments, we have been able to do so.

We used the bladder device to apply static loads and the platen device to apply static and dynamic loads. Generally bladder loads ranged from 10 to 90 psi according to the temperature regime. The higher sensitivity exhibited at higher temperatures made higher pressure loadings saturate sensor response. Therefore we used lower pressures at higher temperatures and higher pressures at low temperatures.

Platen loads were applied with a similar philosophy, with loads applied to exercise the sensor at their low, mid and upper ranges. Bladder loading was used to examine long duration (20-second) static creep, nonlinearity, temperature sensitivity, and hysteresis. Platen loadings were used to investigate nonlinearity, temperature sensitivity, static creep, hysteresis, fatigue, memory, and pulse train behavior.

Temperatures ranged from -20 to 110 degrees Fahrenheit. We performed as many experiments as possible at room temperature. Temperature variations were important in investigating nonlinearity, static creep, hysteretic behavior, and fatigue. Load duration frequencies ranged from static to repeated dynamic loads approximating a column of slow moving four-axled vehicles. Load plateaus ranged from tenths of seconds to hours.

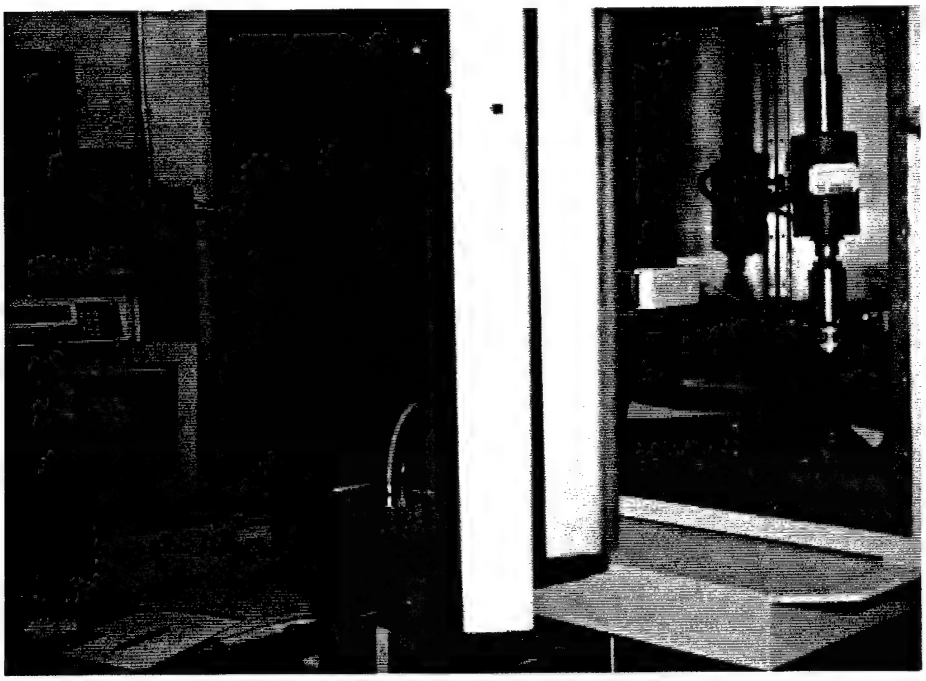

Figure 2-11. Test setup with platen load applied to sensor real time data displayed on monitor.

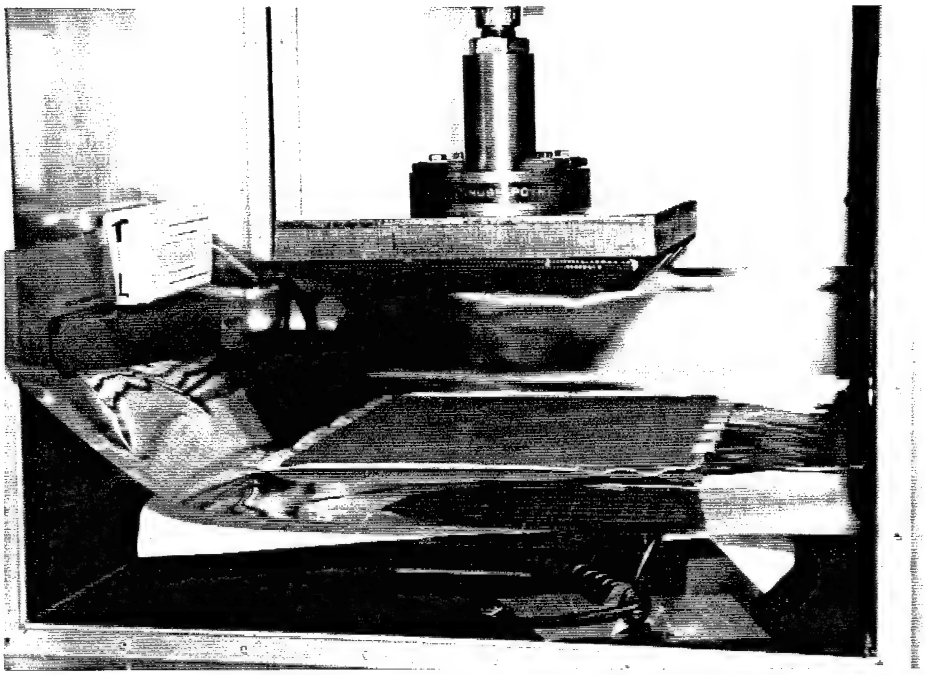

Figure 2-12. For platen and vehicle loads the sensor was packaged with printing blankets and Teflon sheets. Note data handle at left and temperature probe underneath.

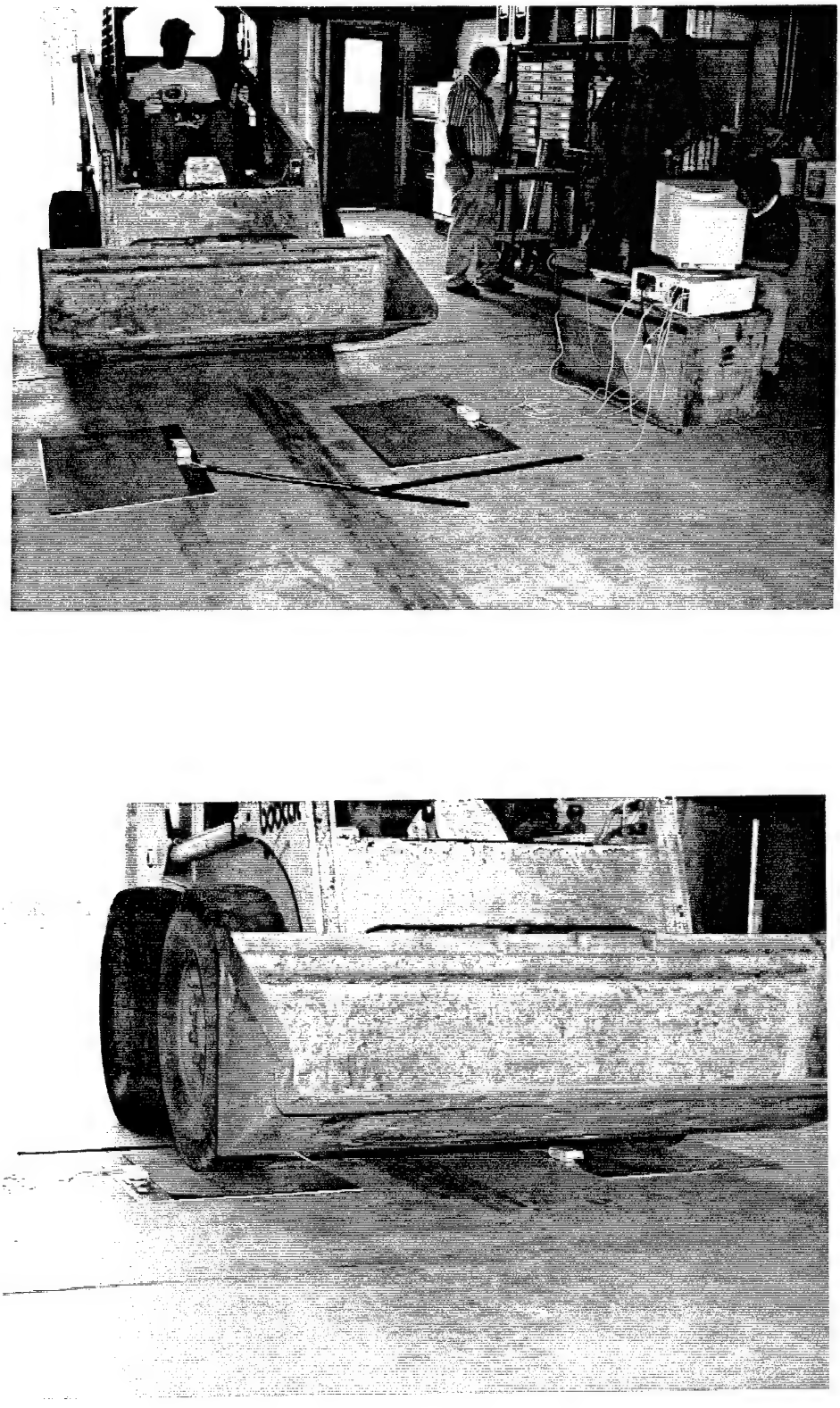

Figure 2-13. A Bobcat loader was used for vehicle tests.

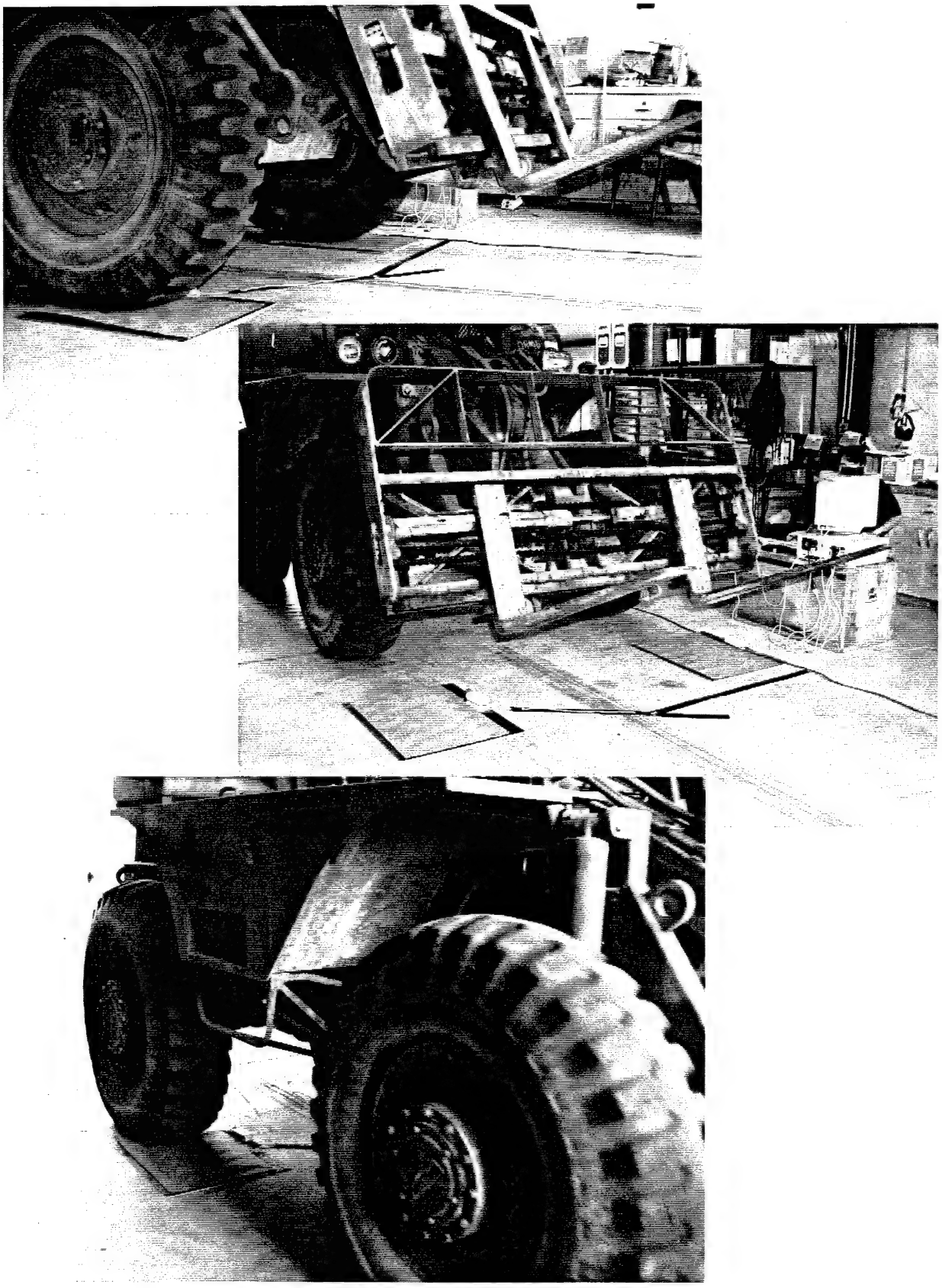

Figure 2-14. One vehicle used was a military rough terrain forklift with large aggressively-treaded tires.

SECTION 3

OBSERVATIONS

3.1 SENSEL-TO-SENSEL VARIATIONS AND EQUILIBRATION.

Significant variations in sensitivity depending on position of a tire's contact on the sensor were found in the previous Proof of Concept tests. At that time, Tekscan was aware of the problem of variations in sensitivity between the various individual row-column junctions, or sensels, and was working on a software fix to compensate for the problem. This feature, denoted *equilibration* by the manufacturer, works as follows. Upon choosing the equilibration feature and activating with the computer mouse, a calibration is generated in which the output of each sensel is corrected to the output averaged over the entire sensor. If, at this time, the sensor is loaded with uniform pressure (an air bladder device is convenient for this purpose), the result is an even sensitivity map for the sensor, at least at this particular pressure. Sensel-to-sensel variations in nonlinearity, static creep, and sensitivity to temperature can cause deviations from a precisely even sensitivity map when parameters such as loading pressure, duration, and temperature are varied.

The equilibration feature became available in time for this phase of the investigation. The results of an equilibration can be saved in a calibration file. Using such a file to make a data recording will record raw digital output (0 to 255); the output will not be calibrated in magnitude.

A subsequent force calibration can provide equilibrated output also calibrated in magnitude. First, the desired equilibration file is loaded. Then a force calibration is performed by selecting this option, entering the total applied load, and clicking the computer mouse at the desired instant. (In case of loading by uniform pressure, as with an air bladder, the entered applied load is the pressure times the loaded nominal area. For these particular sensors, the nominal area of each sensel is 0.16 square inches.) The result is an equilibrated calibration with the output also calibrated in magnitude. This can also be saved, in an additional calibration file. (A force calibration can also be performed without preceding equilibration, if desired.)

The distribution of indicated stress from a sensor without equilibration, loaded with uniform pressure, is shown in Figure 3-1. Figure 3-1 is a Tekscan "3-D" plot, an isometric view of the stress distribution in which the vertical distance is proportional to the indicated stress. The color scale at the bottom of the figure provides another clue to the relative stress magnitude. In Figure 3-1 and in the other stress distributions illustrating observations concerning equilibration in this report, the color scale has been adjusted so that the deep red represents a digital output per sensel of 255, which is the maximum, or saturation output.

If the sensor had constant sensitivity all across its area, the stress distribution in Figure 3-1 would look like a flat rectangle. More problematic than the short-distance variations between adjacent sensels (appearing as roughness in Figure 3-1) are the variations between whole regions over longer distances (appearing as waviness in Figure 3-1). In particular, note a significant wavelike rise in sensitivity near the sensor edge at the top left in Figure 3-1. A tire contact patch in this region would register a significantly higher load than would be the case if it were located close to the central part of the sensor edge at the bottom left (bluish area).

The dramatic improvement brought about by equilibration is shown in Figure 3-2. In the recording that produced 3-2, the Tekscan sensor-connector "handle" was *not* the same one as

used in the preceding equilibration. A distribution of indicated stress obtained with the same sensor-connector as used in the preceding equilibration is shown in Figure 3-3. This shows a further slight improvement, although it is clear that the big advance was in performing an equilibration at all. The saturated sensel in the back row (sharp red peak, Figure 3-3) may be the result of a load concentration imparted by the edge of the plastic air bladder; it is possible that the sensor was positioned not far enough inward in the air bladder loading device.

However, *comparing the sensitivities averaged over the entire sensor area* (in terms of total indicated load) *with the same sensor under the same conditions under uniform loading except for an exchange in the sensor-connectors showed a repeatable difference of 2.4 percent.* It appears that the sensitivity, and to some extent the equilibration, can depend on the specific sensor-connector, or "handle" used. Switching the sensor-connector output connector to the other port in the Tekscan electronic card in the computer had no effect. This suggests that *for best accuracy, calibrations for a given sensor should be performed with the same sensor-connector, or "handle", as is to be used in the measurements.* This applies especially to force calibrations; there may be somewhat greater flexibility with the equilibrations.

For all the subsequent laboratory data taken for this report, all calibrations, both equilibrations and force calibrations, were performed with the same sensor-connector as was later used to take the data.

One of the two sensor-connectors, or "handles", also showed symptoms of a marginal connection to one of the sensor rows (with more than one sensor). This would sometimes require release and slight repositioning of the sensor neck inside the "handle". The better of the two sensor-connectors was chosen for our laboratory calibrations and data-taking.

It was noticed that when an equilibration was performed after a given time interval after the application of pressure, in a subsequent application of uniform pressure the evenness of the distribution of indicated stress would increase as that time interval is approached, and decrease thereafter. This is evidently due to sensel-to-sensel variations in static creep rates. *We standardized our calibration procedures to perform all equilibrations at 20 seconds after the desired applied pressure is attained, and similarly, all force calibrations for taking laboratory data were performed 20 seconds after application of a static load.*

For several sensors, equilibrations were performed at three applied pressures, around 20 psi, 45 psi, and 70 psi. All equilibrations were performed at room temperature. Upon loading with uniform pressures other than the equilibration pressure at temperatures in the same (room temperature) range, the resulting indicated stress distributions look best (most even) when the preceding equilibration pressure was the same as the applied pressure. When the applied pressure was *not* the same, the indicated stress distribution was more uneven at applied pressures higher than the equilibration pressure, than when the respective pressure magnitudes were the other way around. Figures 3-4 and 3-5 illustrate the effects of switching equilibration and loading pressures of 20 psi and 70 psi.

The observations at temperatures significantly lower or higher were somewhat different in that it became clear that it's not the absolute magnitude of the pressure, but its effect on producing indicated output as a percentage of sensor saturation is what's important here. In tests involving temperatures around -23 degrees F, there were no great differences between the indicated stress distributions obtained by using the different equilibration files, which were all generated at room temperature. But nevertheless, the indicated stress

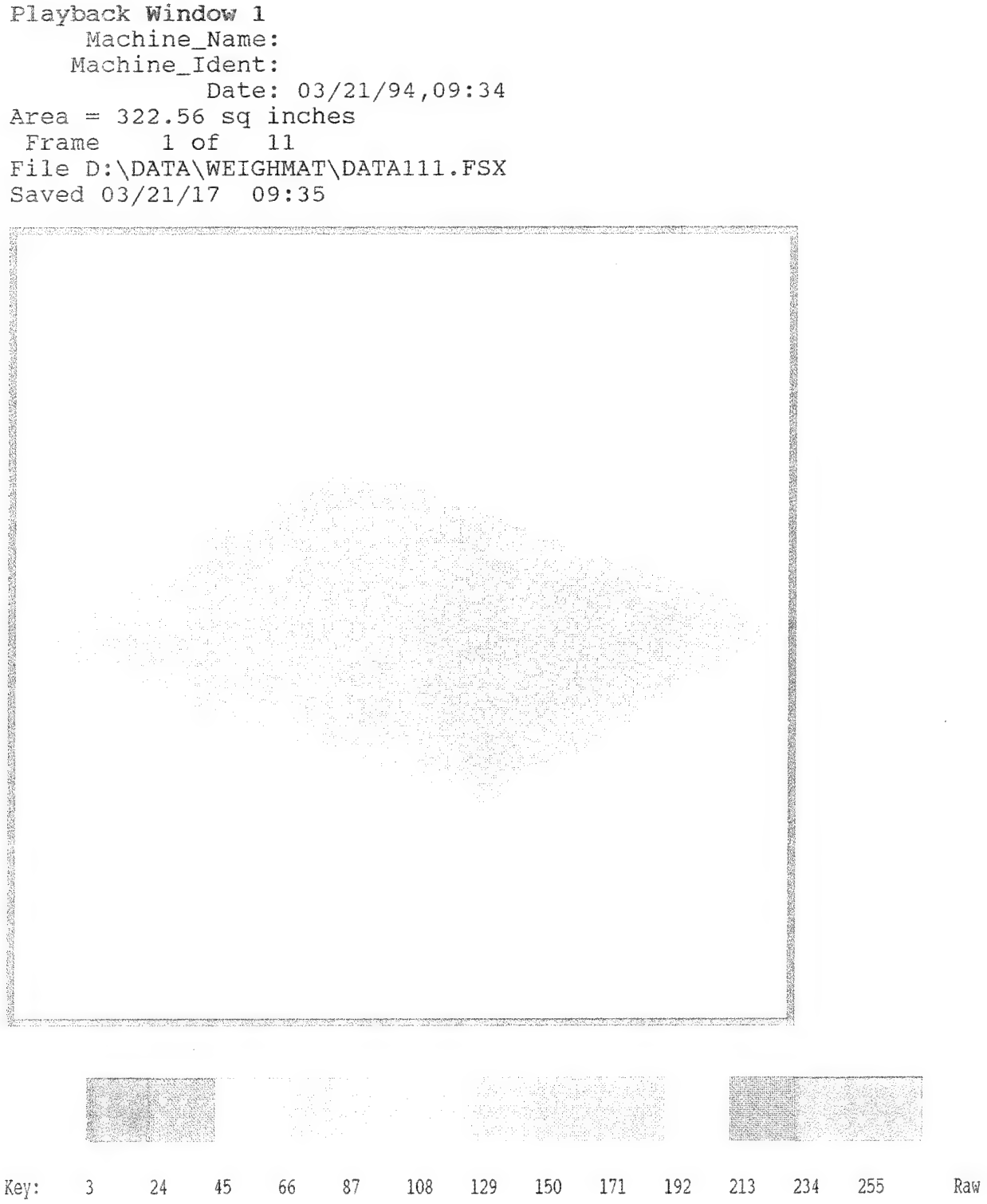

Figure 3-1. Sensor without equilibration, loaded with 60 psi uniform pressure. Temperature 71 degrees F.

```
Playback Window 2
     Machine_Name:
    Machine_Ident:
             Date: 03/21/94,10:42
Area = 322.56 sq inches
 Frame    1 of   11
File D:\DATA\WEIGHMAT\DATA141.FSX
Saved 03/21/17  10:49
```

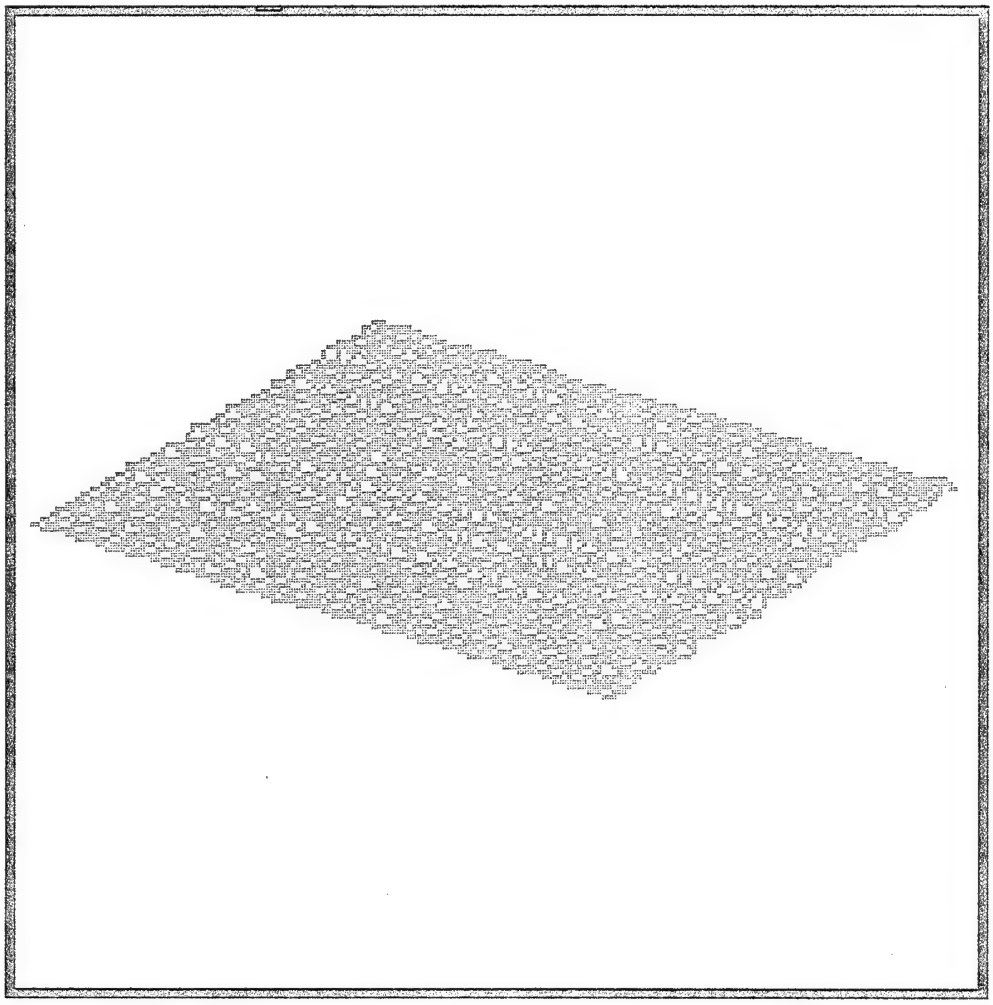

Key: 3 24 45 66 87 108 129 150 171 192 213 234 255 PSI

Figure 3-2. Same sensor as in Figure 3-1, after equilibration. 60 psi, at 71 degrees F. Sensor-connector used in taking this recording was not the same one as used in the equilibration.

```
Playback Window 1
     Machine_Name:
    Machine_Ident:
             Date: 03/24/94,19:38
Area = 322.56 sq inches
 Frame   28 of   41
File D:\DATA\WEIGHMAT\E3241945.FSX
Saved 03/24/17  19:46
```

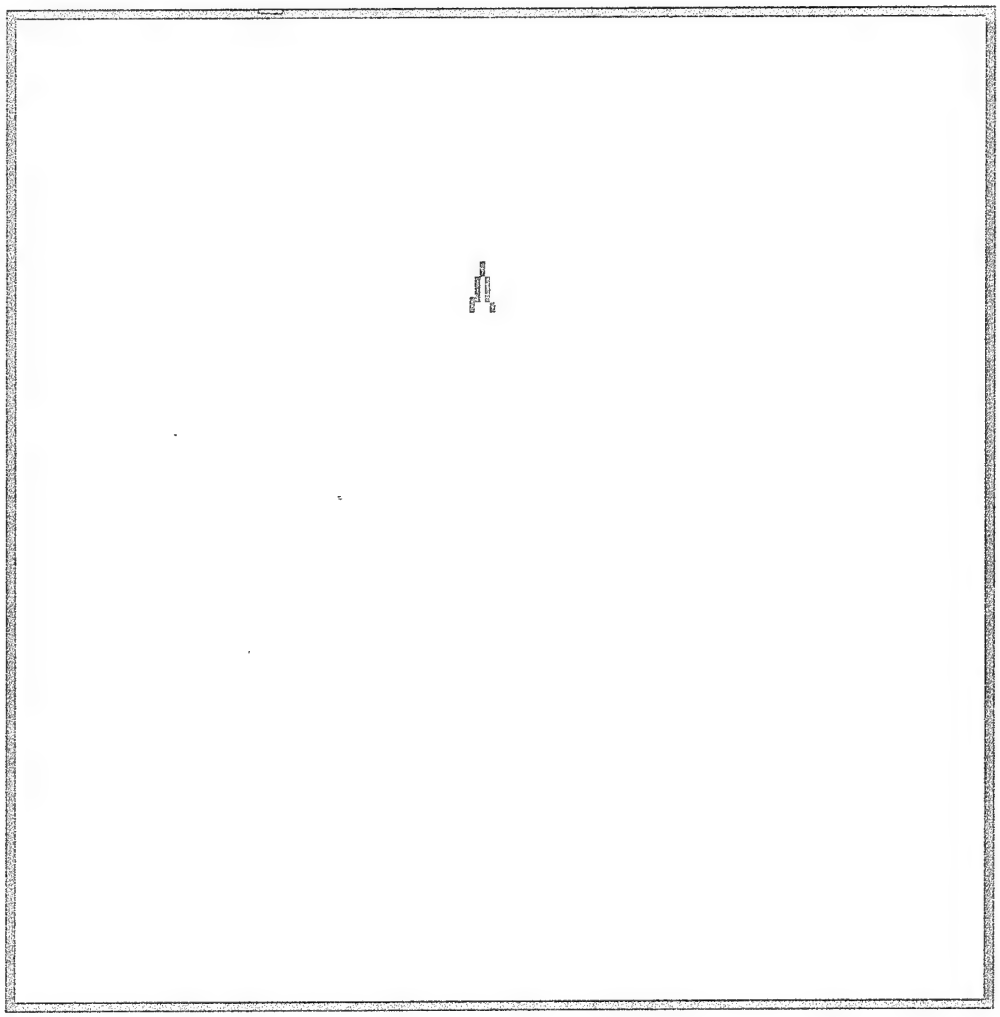

Key: 3 24 45 66 87 108 129 150 171 192 213 234 255 PSI

Figure 3-3. Sensor equilibrated at 70 psi, 70.6 degrees F, loaded by 70.5 psi at 74.1 degrees F. Sensor-connector was the same as used in the equilibration.

```
Playback Window 2
     Machine_Name:
    Machine_Ident:
             Date: 03/25/94,13:35
Area = 322.56 sq inches
 Frame   29 of   41
File D:\DATA\WEIGHMAT\E3251335.FSX
Saved 03/25/17  13:37
```

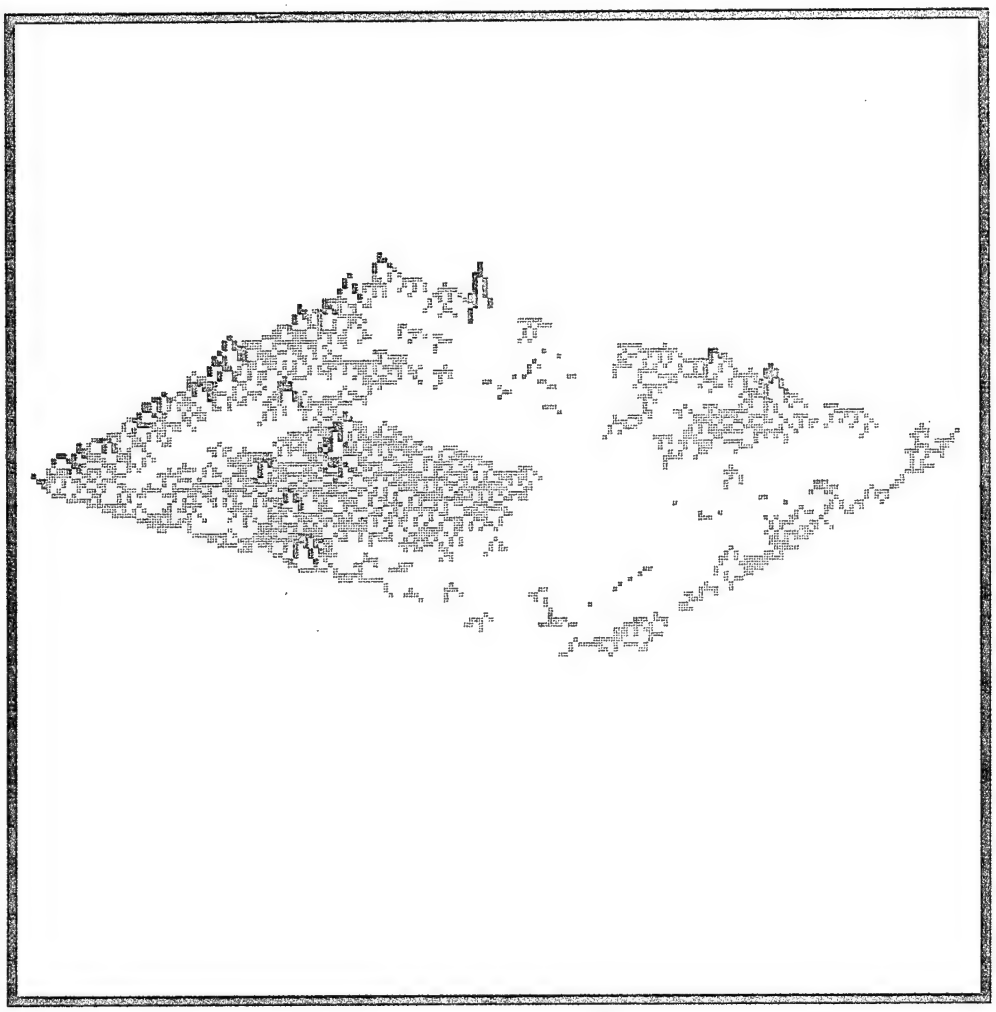

Key: 3 24 45 66 87 108 129 150 171 192 213 234 255 PSI

Figure 3-4. Sensor equilibrated at 19.5 psi, 70.6 degrees F, loaded by 70 psi at 72.4 degrees F.

```
Playback Window 2
     Machine_Name:
    Machine_Ident:
             Date: 03/25/94,14:10
Area = 322.56 sq inches
 Frame   28 of   41
File D:\DATA\WEIGHMAT\E3251411.FSX
Saved 03/25/17  14:13
```

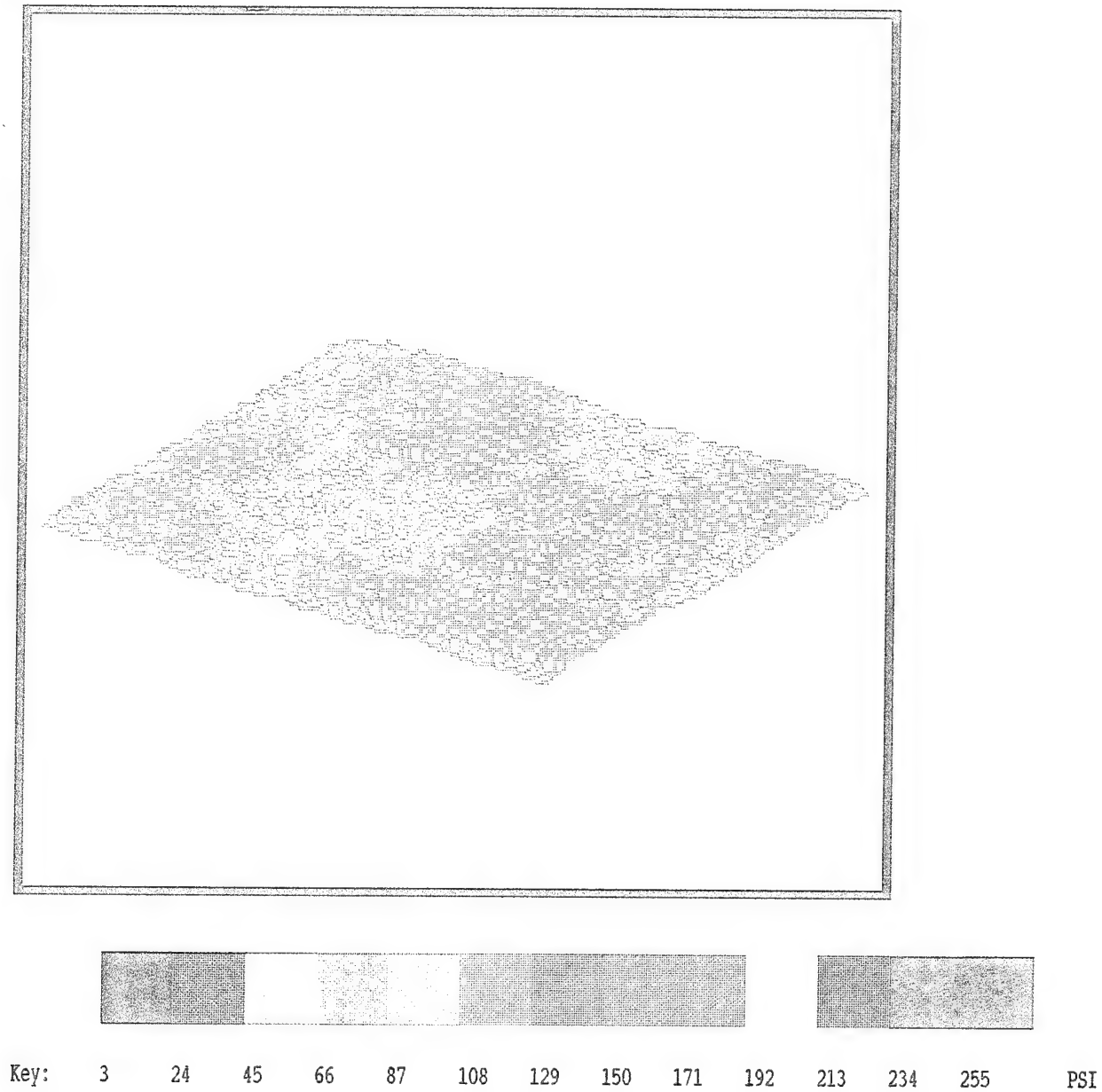

Figure 3-5. Sensor equilibrated at 70 psi, 70.6 degrees F, loaded by 20 psi at 72.6 F.

distributions obtained at 70 psi loading pressure at this low temperature look more even when based on room temperature equilibration pressures around 20 psi than at the higher pressures of 70 psi or 45 psi. The differences are small but detectable. To enhance the differences the color scales on the computer screen, which also control the height on a 3-D plot, can be adjusted at both the low and high ends. (The stress distributions with differences enhanced are not shown here.) Comparing Figure 3-6, produced by loading by 70 psi at -23.2 degrees F, with Figure 3-5, which was produced by loading with 20 psi in the room temperature range, shows that under these two sets of conditions the sensor is producing similar levels of output when expressed as a percentage of saturation.

The importance of the equilibration pressure producing similar levels of indicated output as a percentage of sensor saturation as in the data-taking was clearer in the tests in the higher-temperature, 102-degree F range. In Figure 3-7, which was produced by loading a sensor previously equilibrated at 70 psi at room temperature and loaded by 30 psi at 102.5 degrees F, the closeness to saturation is close to the level in Figure 3-3, for which the sensor was both equilibrated and loaded by approximately 70 psi at room temperature. The distribution of indicated stress in Figure 3-7 is also reasonably even.

On the other hand, the indicated stress distribution in Figure 3-8, which was produced by equilibrating at 19.5 psi at room temperature and loading with essentially the same pressure, 20 psi, at 102.5 degrees F is much more uneven. The evenness of the indicated stress distribution produced by loading the sensor at 20 psi using the 70 psi equilibration file is very similar to what's seen in Figure 3-7 (this is not shown separately).

Comparisons of Figures 3-6 and 3-7 with Figure 3-3 also demonstrate that the effect of equilibration is not seriously compromised when taking data at temperatures other than the equilibration temperature, provided that the output levels relative to saturation are pretty much the same.

Although the generation of equilibration files close to the temperature of intended use would provide the highest accuracy, generation of equilibration files at room temperature could be considered adequate for many purposes. It is a good idea to generate equilibration files at several different pressures. Later, selection among these files can be made such that the output level in terms of closeness to saturation is at or near the corresponding levels with the highest pressures or loads in intended use.

3.2 REPEATABILITY.

Repeatability of the sensor was investigated for static uniform and non-uniform loadings as well as non-uniform pulse loadings. The effect of varying the loading locations on the mat was also studied.

3.2.1 General Repeatability.

The repeatability of a given sensor to duplicate output for a constant input was studied for the static uniform and non-uniform loadings. For static loadings a load was applied and a reading was taken after 20 seconds. Limited non-uniform pulse data were also obtained to investigate loading rate effects on repeatability of readings. In order to quantify the effect of repeatability, a coefficient of variation was obtained for various readings of a given sensor at a constant input load and constant temperature. The coefficient of variation is simply a way to look at variance in a normalized fashion. The coefficient of variation is the sample standard deviation over the nominal value times 100 percent.

```
Playback Window 2
     Machine_Name:
    Machine_Ident:
             Date: 03/30/94,15:19
Area = 322.56 sq inches
 Frame    29 of    41
File D:\DATA\WEIGHMAT\E3301520.FSX
Saved 03/30/17  15:22
```

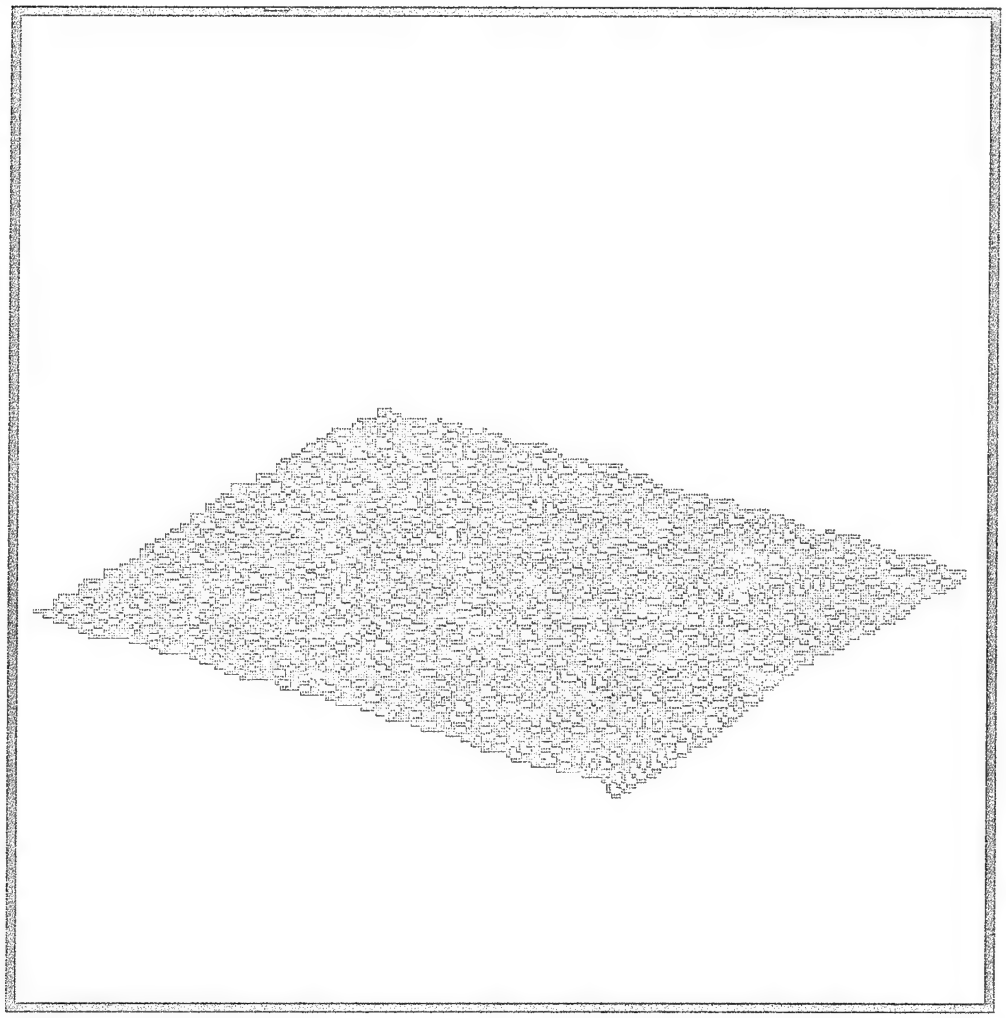

Key: 3 24 45 66 87 108 129 150 171 192 213 234 255 PSI

Figure 3-6. Sensor equilibrated at 19.5 psi, 70.6 degrees F, loaded by 70 psi at -23.2 degrees F.

```
Playback Window 1
     Machine_Name:
    Machine_Ident:
             Date: 04/01/94,16:43
Area = 322.56 sq inches
 Frame   41 of   41
File D:\DATA\WEIGHMAT\H4011714.FSX
Saved 04/01/17  17:16
```

Key: 3 24 45 66 87 108 129 150 171 192 213 234 255 PSI

Figure 3-7. Sensor equilibrated at 70 psi, 70.4 degrees F, loaded by 30 psi at 102.5 degrees F.

```
Playback Window 2
     Machine_Name:
    Machine_Ident:
             Date: 04/01/94,17:40
Area = 322.56 sq inches
 Frame    29 of    41
File D:\DATA\WEIGHMAT\H4011740.FSX
Saved 04/01/17  17:42
```

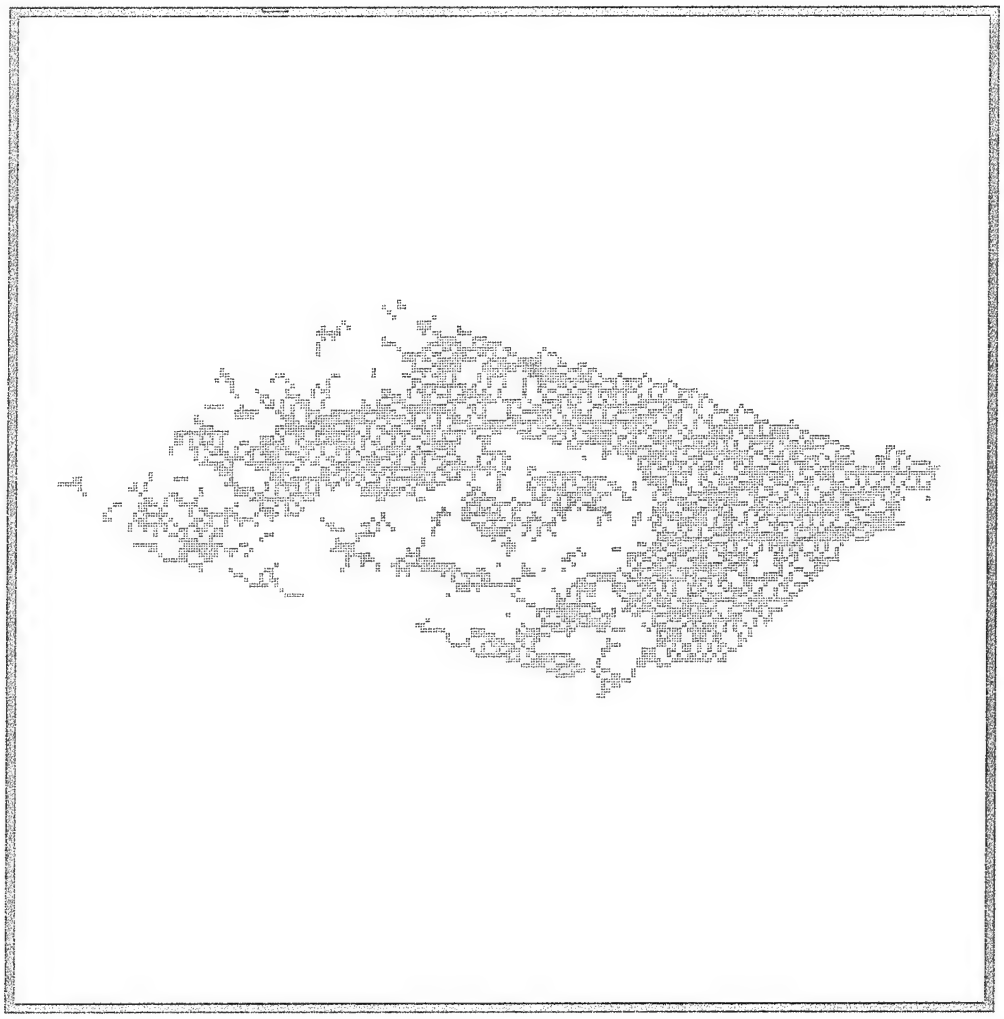

Key: 3 24 45 66 87 108 129 150 171 192 213 234 255 PSI

Figure 3-8. Sensor equilibrated at 19.5 psi, 70.9 degrees F, loaded by 20 psi at 102.5 degrees F.

Plots of coefficients of variation versus temperature and pressure for the uniform static loading are shown in Figures 3-9 and 3-10. Non-uniform static loading yielded the results in Figures 3-11 and 3-12, and the pulse data are presented in Figures 3-13 and 3-14. Based on all the data, no load magnitude-dependent trends could be inferred. The two worst-case data points for the uniform static loading occurred at 103 degrees F. A breakdown in repeatability is indicated at the high end of the temperature scale. Below 103 degrees F, no temperature dependent trends were obvious from the data. In general, all readings were quite repeatable. Uniform static loadings were most repeatable with an average coefficient of variation of 0.836 percent. The non-uniform static loadings yielded an average coefficient of variation of 2.62 percent, and the non-uniform pulse loadings gave an average coefficient of variation of 2.86 percent. Based on these findings, non-uniformity of the load *appears* to be a bigger factor on repeatability than is the loading rate. In any case, non-uniform loadings were less repeatable than uniform loadings.

3.2.2 Load Location Variability.

Variability of a reading due to the a change in location on the mat was studied at room temperature. The plate mounted-tire tread was used to statically load five sensors at three locations each. A reading was taken 20 seconds after the load was applied. The locations 180 and 270 degrees out of phase with the lugs of the tire tread were chosen (see Figure 3-15).

Results are shown in Figure 3-16. The output was divided by the input in order to eliminate any influence of the slight variations in the input. Corrections were made for temperature fluctuation encountered during testing. The curves do not cross; therefore, a consistent trend of magnitude change for a change in load location is indicated. The variability in reading is increased at lower loads due to the nonlinearity of the sensor. The worst-case variability is at the 340-pound load comparing positions 1 and 2 where the change in location represents a difference in reading of 6.4 percent.

3.2.3 Summary.

Repeatability of the sensor is quite good for all data obtained. Uniform static loading was exceptionally repeatable (0.8-percent variation) whereas repeatability of non-uniform static loading was less so (2.62-percent variation). Limited non-uniform pulse loading data revealed slightly less repeatability (2.86-percent variation) than the static non-uniform loadings.

Variable load location on the mat caused a noticeable difference in readings obtained, particularly at low loads. Variability of as much as 6.4 percent was obtained. This variability will be avoided in field use of the Weighmat system as long as the average of several readings are taken while the vehicle is travelling across the mat.

3.3 TEMPERATURE EFFECTS.

The polymer material from which the resistive ink in the Weighmat sensor is made is very sensitive to changes in temperature. An increase in temperature causes more plastic flow of the material, thus, the reading for a given load will tend to be higher at a higher temperature. The uniform and nonuniform static 20 second loadings were used to quantify the effect temperature plays on sensor behavior.

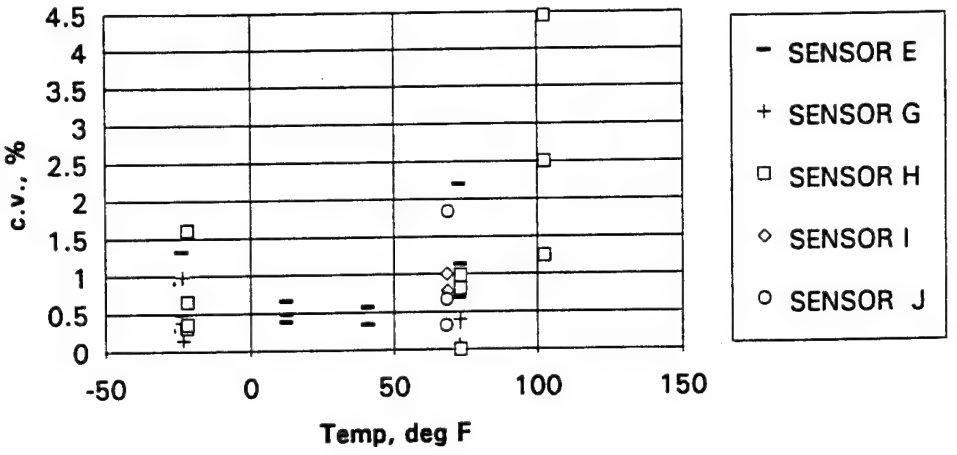

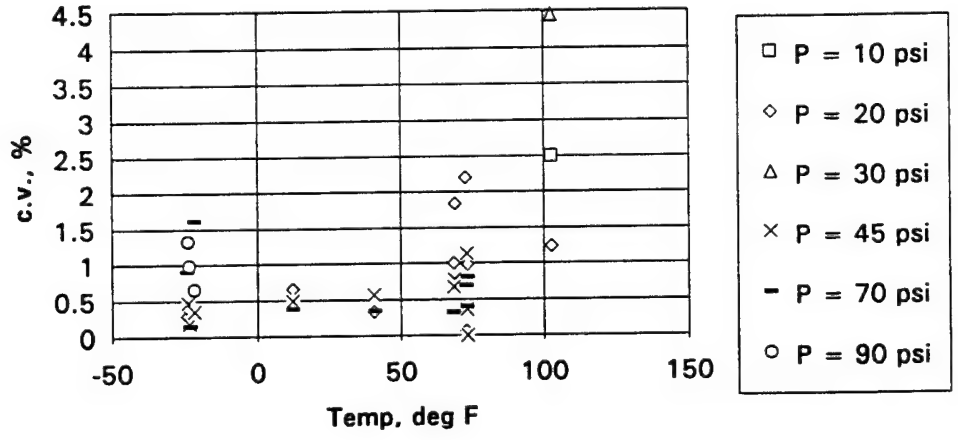

Figure 3-9. Uniform loading - effect of temperature on repeatability.

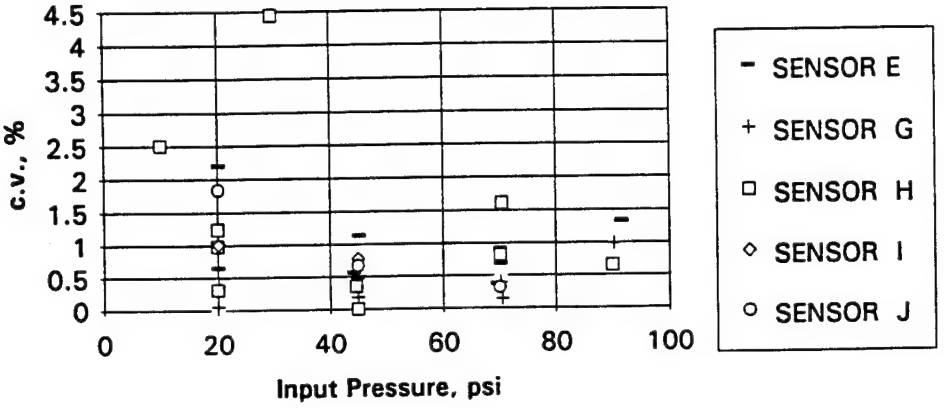

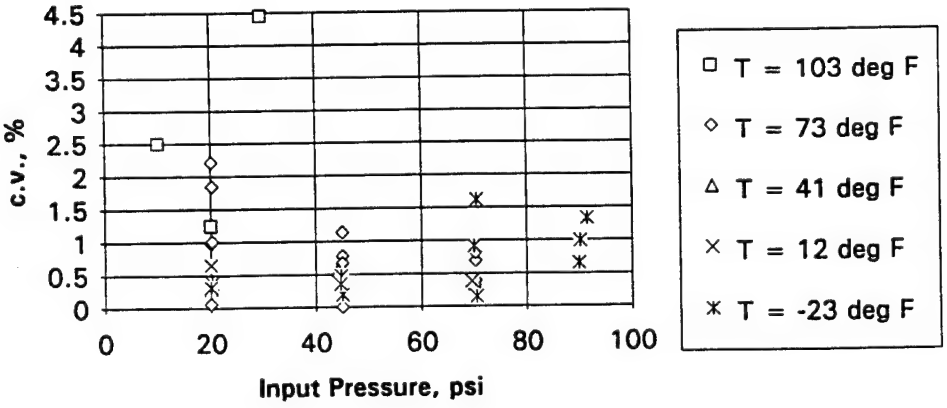

Figure 3-10. Uniform loading - effect of pressure on repeatability.

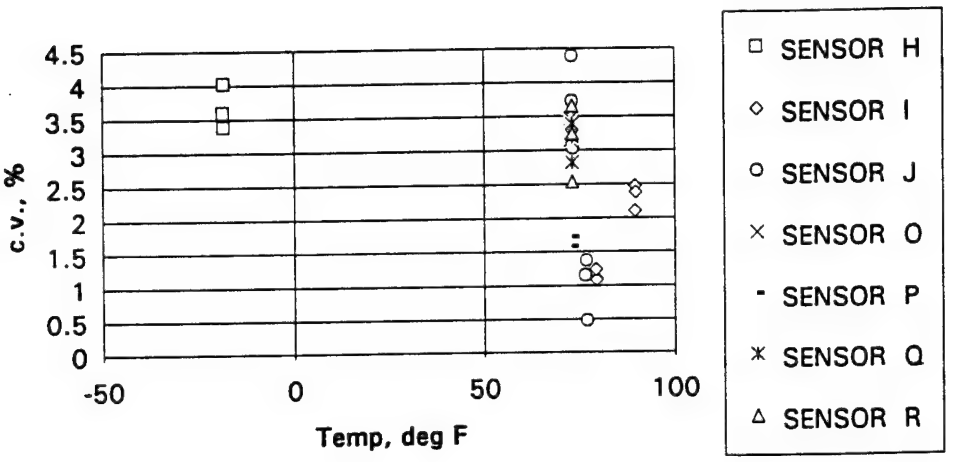

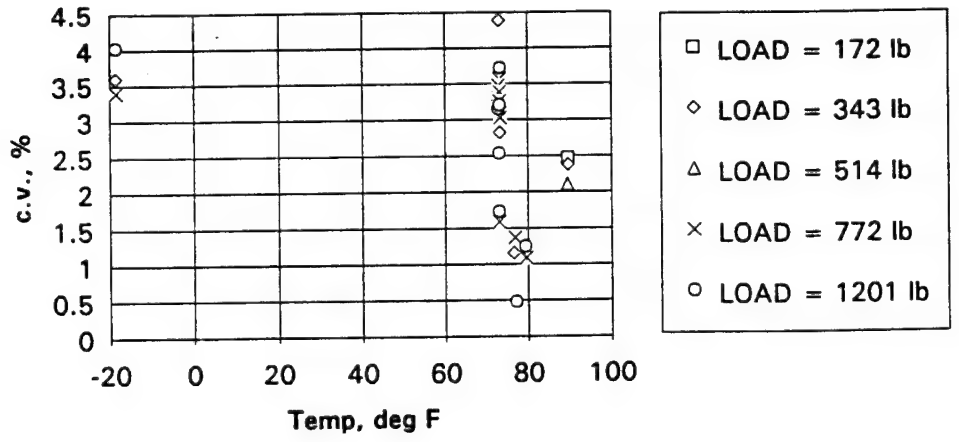

Figure 3-11. Non-uniform loading - effect of temperature on repeatability.

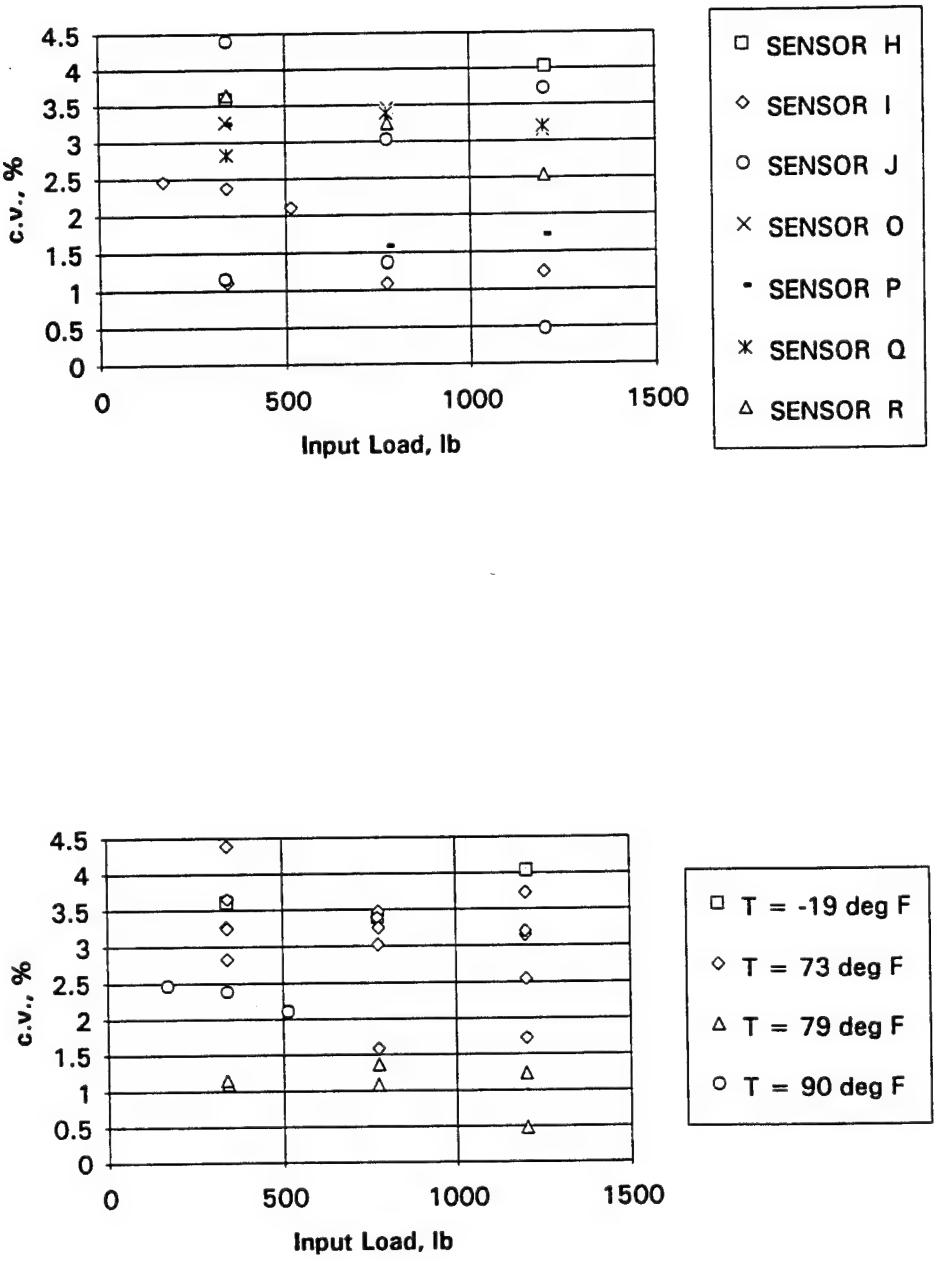

Figure 3-12. Non-uniform loading - effect of input load on repeatability.

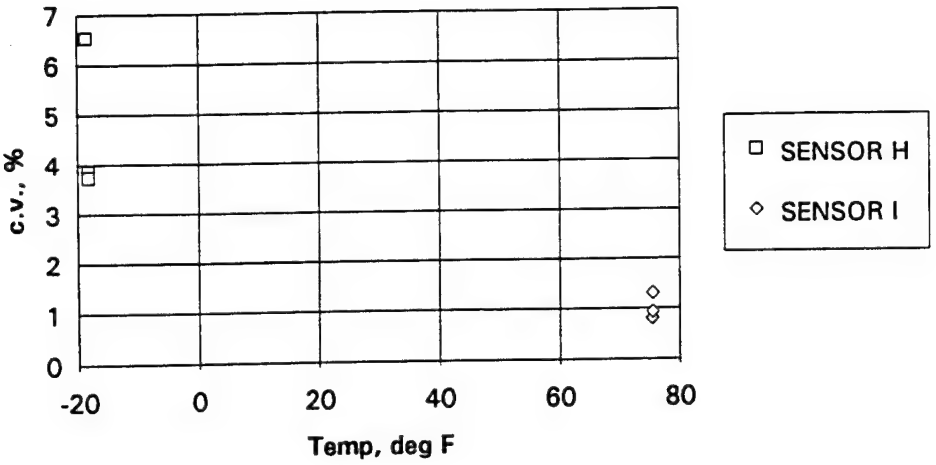

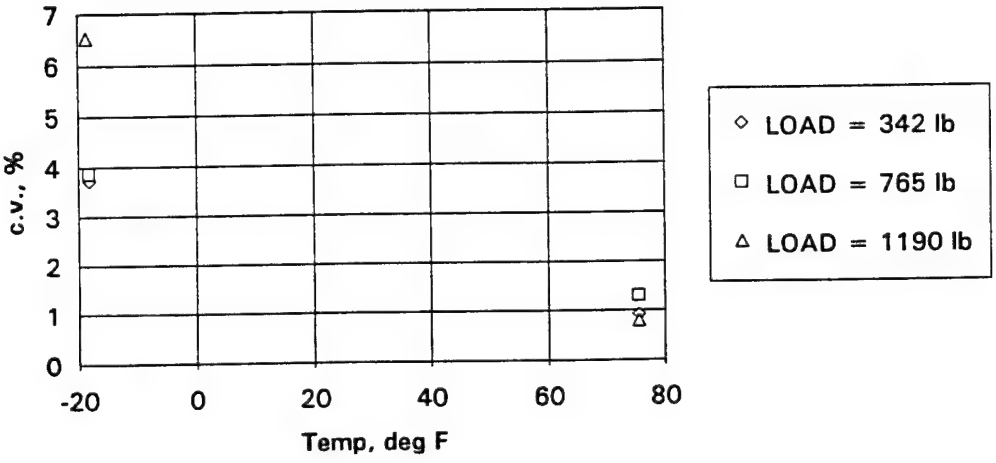

Figure 3-13. Pulse loading - effect of temperature on repeatability.

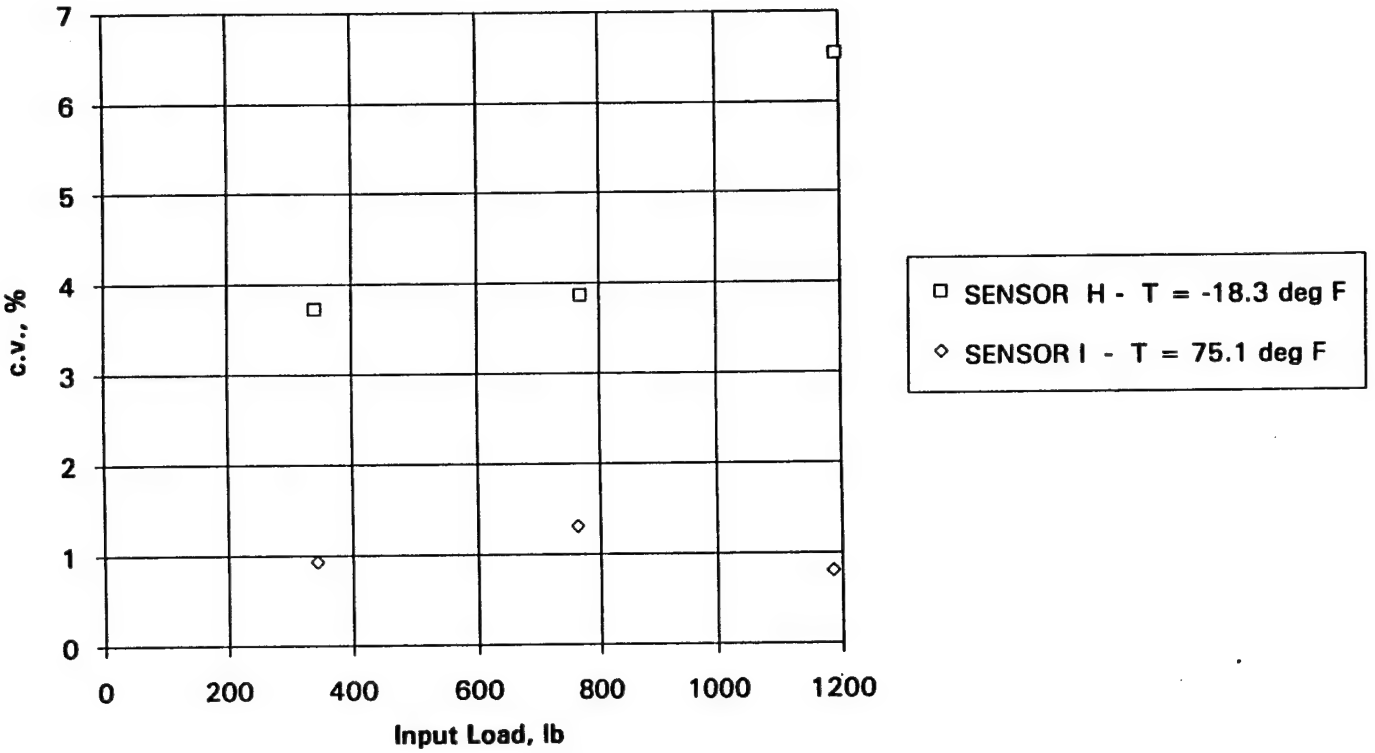

Figure 3-14. Pulse loading - effect of input loan on repeatability.

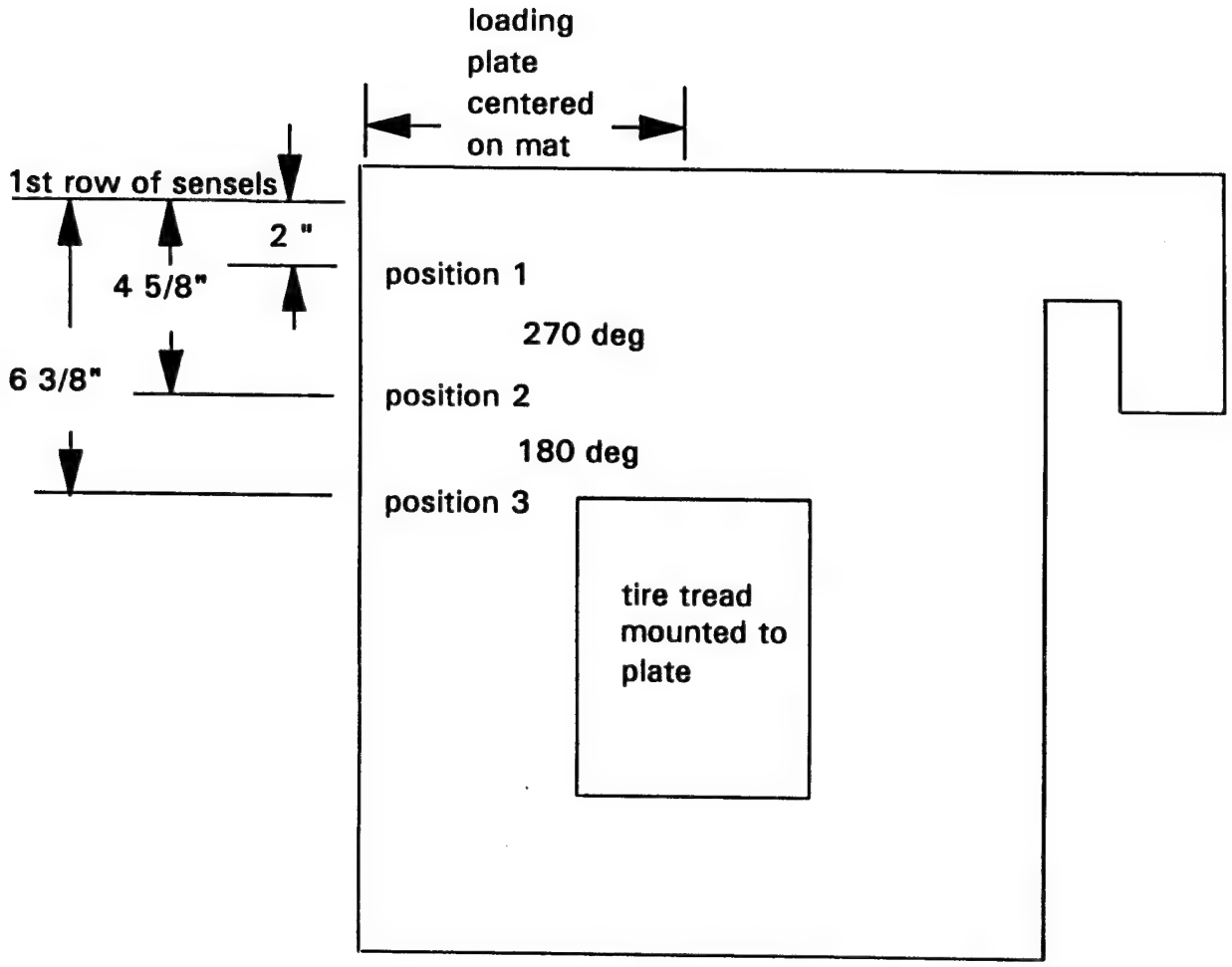

Figure 3-15. Position variations on weighmat.

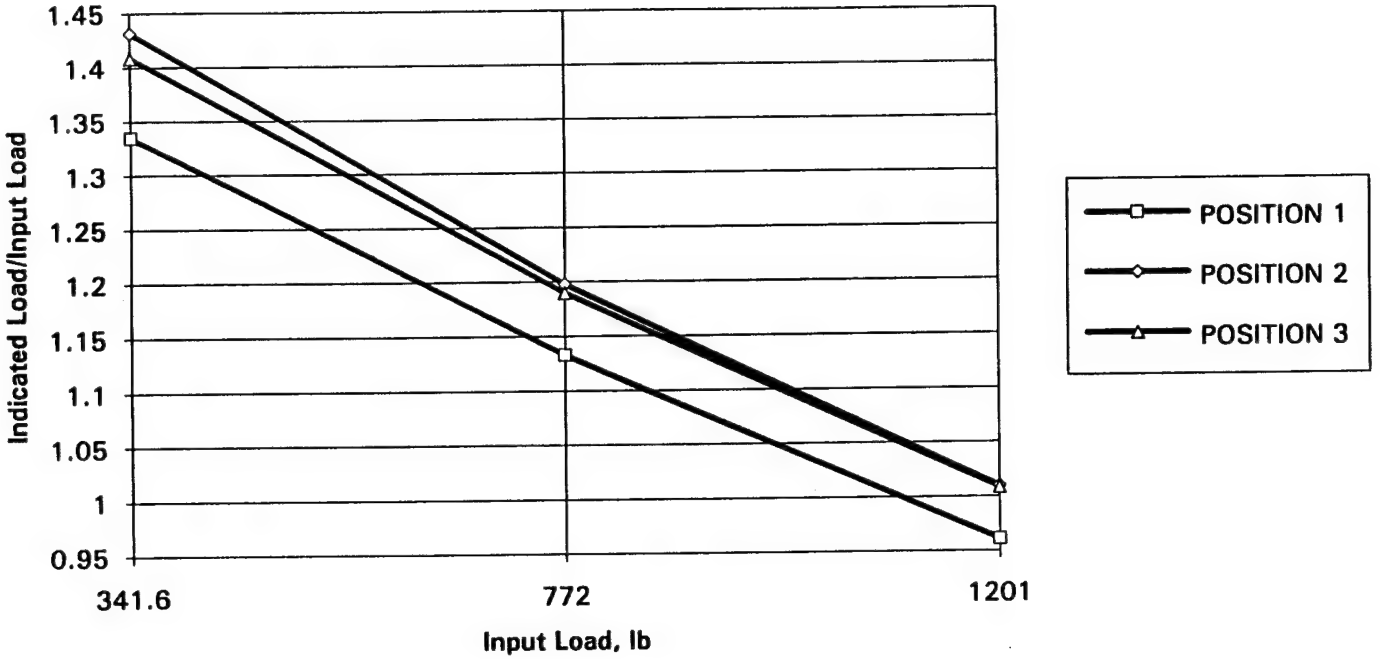

Figure 3-16. Effect of varied positions.

3.3.1 Uniform Loading.

Bladder loadings at 20, 45, and 70 psi were performed at temperatures varying from -23 degrees F to 103 degrees F. The data are shown in Figures 3-17 - 3-19 and a summary plot is shown in Figure 3-20. The summary plot shows the curves to be a family of nearly parallel curves in linear-log space. The one point which does not follow the trend of all other points is the one at 20 psi and 103 degrees F; a much higher reading was obtained for these conditions. The manufacturer predicts a breakdown of the resistive inks at between 115 and 120 degrees F. According to the data obtained here, the sensor becomes much more sensitive to changes in temperature above 100 degrees F.

Table 3-1 gives the data from Figure 3-20 in tabulated form. An increase in digital output per degree F is included which was calculated for each step in temperature for a given pressure. The increases obtained at a given pressure are of the same order across the temperature ranges tested. The one exception to this trend is the increase of output obtained at 20 psi when comparing output at 71 degrees F and 103 degrees F. The increase is much higher here due to the exaggerated sensitivity of the sensor at the high temperature.

3.3.2 Non-uniform Loading.

The sensor was loaded in the environmental chamber with the plate mounted tire tread ("platen load") at temperatures ranging from -19 degrees F to 90 degrees F. Digital output versus input load are plotted in Figures 3-21 - 3-23 and a summary plot is included in Figure 3-24. The summary curves are parallel in linear-log space, as they are for the uniform loading. The trend of the curves is consistent for the full range of temperatures. That is, the sensitivity increase for a given load for varying temperature is fairly constant up to 90 degrees F. Based on the results of both uniform and non-uniform loadings, somewhere between 90 degrees F and 103 degrees F the sensor becomes hyper-sensitive to temperature. Table 3-1 gives increases in digital output per degree F for the changes in temperature for a given load. It should be noted that the increase found between 73 and 78 degrees F should be interpreted with some scrutiny. The small change in temperature may cause an increase or slope between these points to be exaggerated.

3.3.3 Summary.

Temperature sensitivity was investigated for a large range of temperatures and loading conditions. The curves obtained indicated near-constant sensitivity changes in temperature from -20 degrees to 90 degrees for a given load. Because the curves were consistently parallel, interpolating values from these curves should give reasonable results below 90 degrees F. Somewhere between 90 degrees F and 103 degrees F the sensors sensitivity rate becomes higher with an increase in temperature.

3.4 NONLINEARITY.

Previous testing under the Proof of Concept project indicated nonlinearity in load versus reading for the Weighmat sensor. Under this project we tested to characterize the nonlinearity of the sensor for varied temperature (-23 degrees F to 103 degrees F) and loading conditions (uniform and non-uniform loading).

Nonlinearity was tested primarily by statically loading the sensor. The sensor was loaded by both the equilibration device (uniform loading) and the MTS loader with the plate-mounted tire tread (non-uniform loading). Static load readings were taken 20 seconds after application of the load, at which time most static creep had leveled out sufficiently. An additional set of

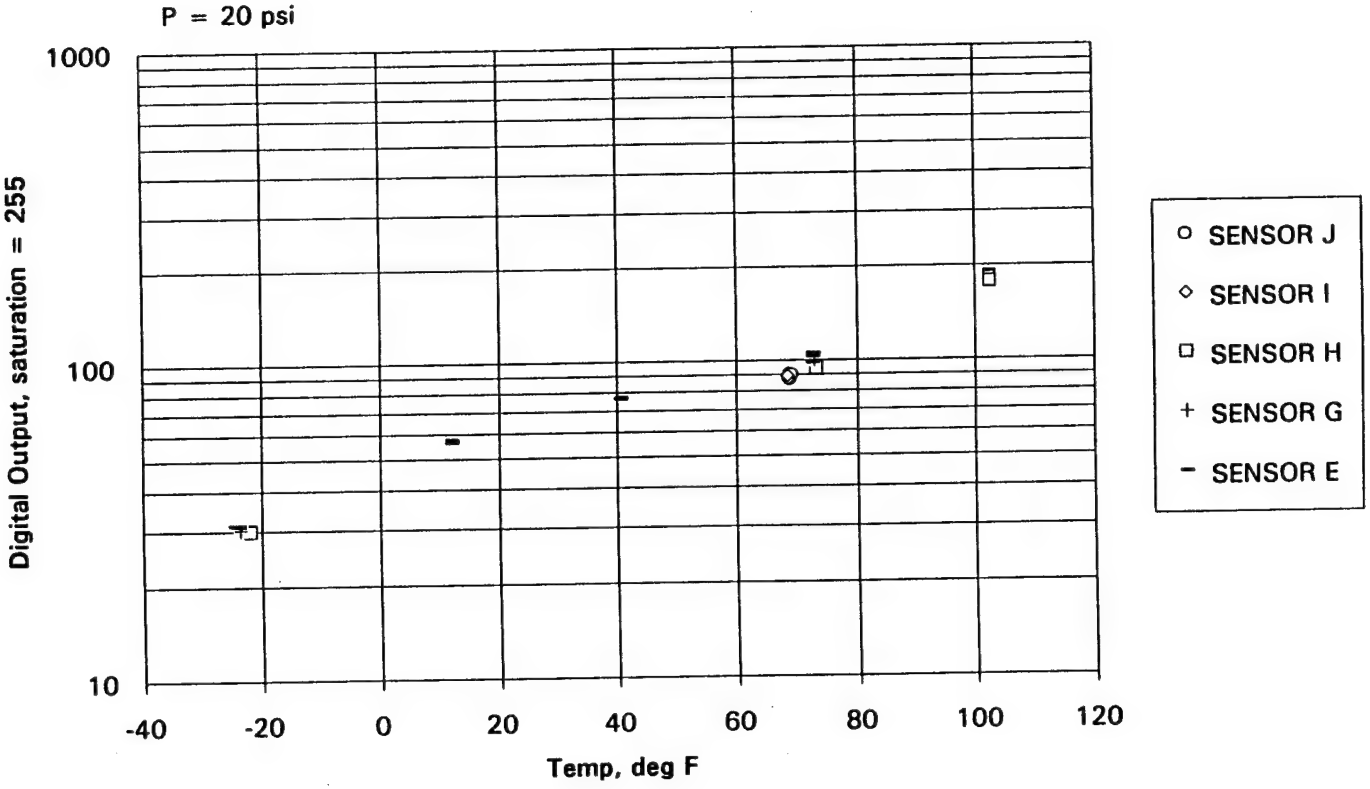

Figure 3-17. Uniform loading at 20 psi.

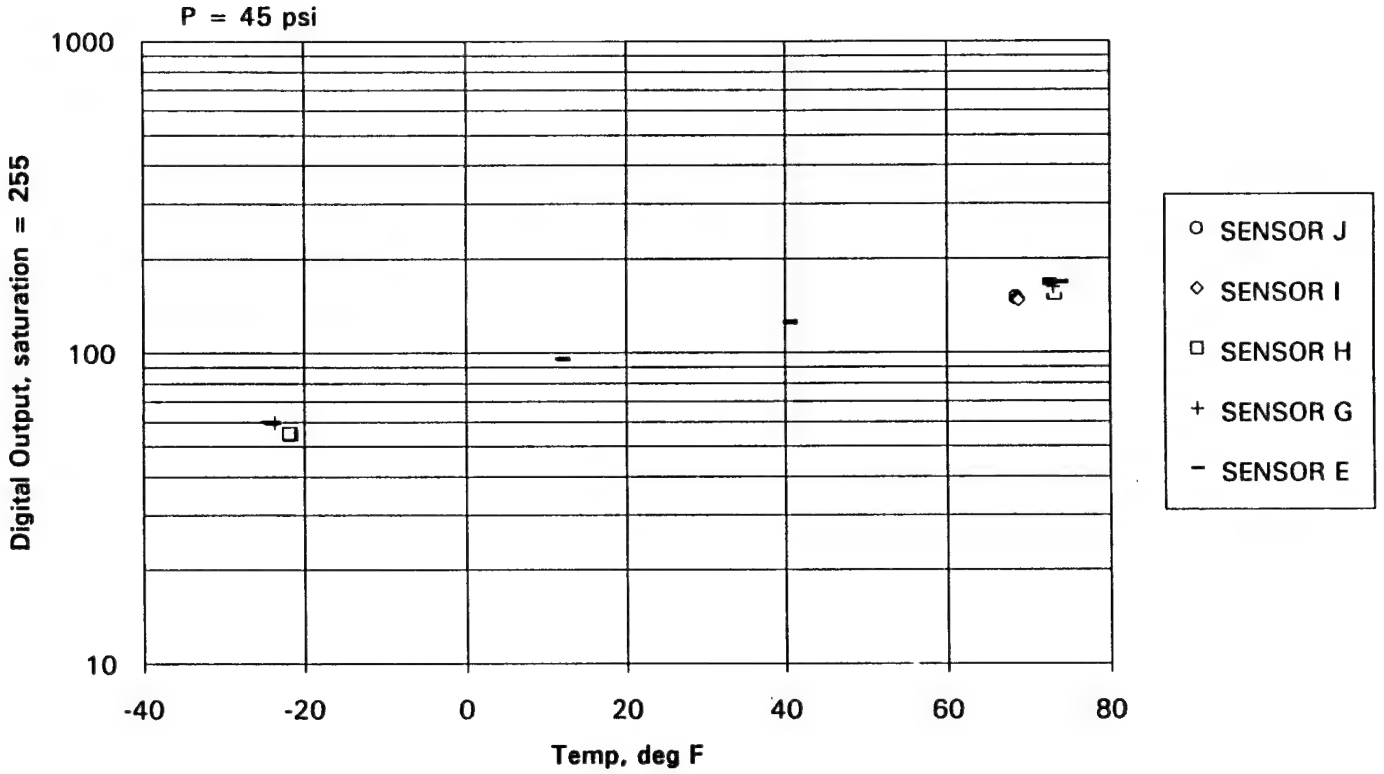

Figure 3-18. Uniform loading at 45 psi.

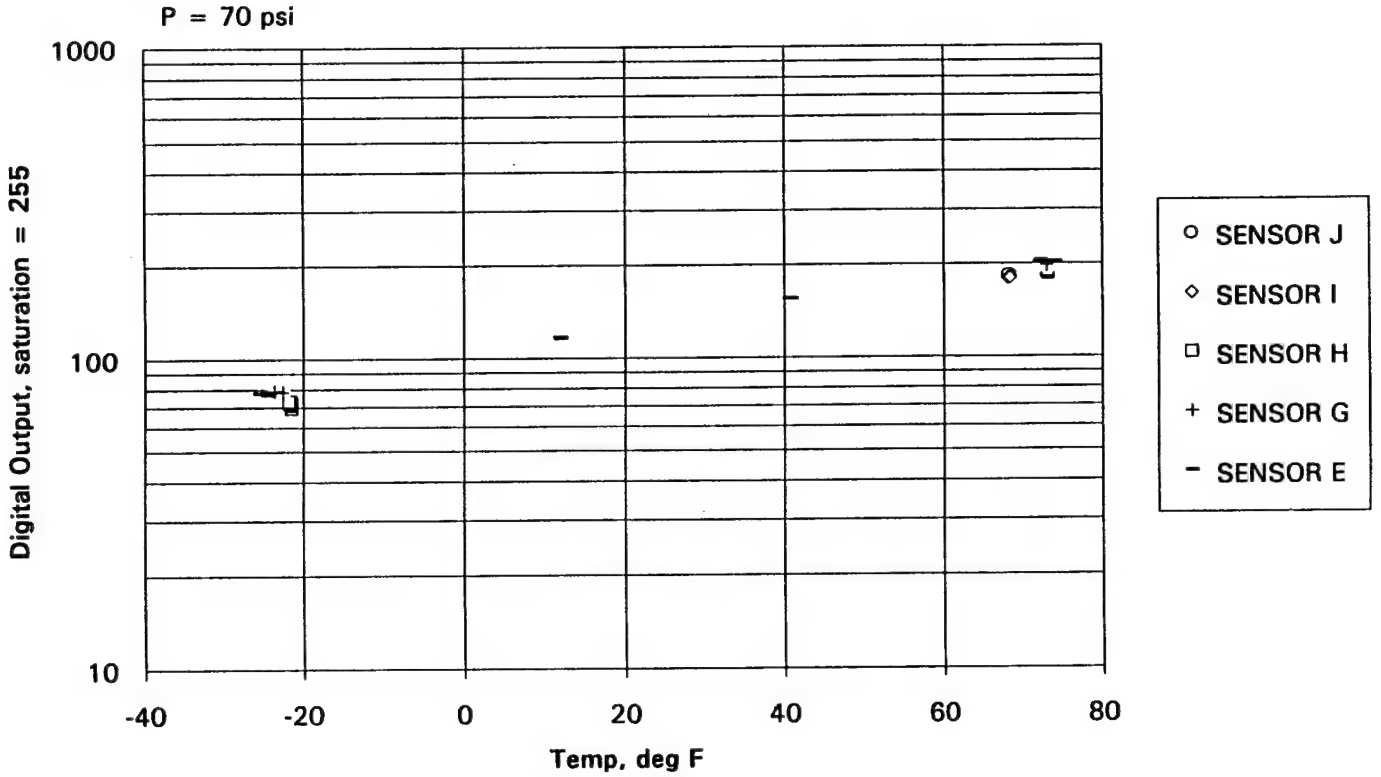

Figure 3-19. Uniform loading at 70 psi.

Table 3-1. Tabulated results of uniform and non-uniform loading.

Temperature Effects
Average of Several Sensors

Uniform loading

Pressure, psi	Temp, deg F	DO@20sec	Increase do/deg F	increase, % %/deg F
20 (20.04) psi	-23.09	30.49		
	12.20	56.90	0.75	1.71
	40.67	76.64	0.69	1.04
	71.61	97.85	0.69	0.79
	102.57	171.60	2.38	1.77
45 (44.758)psi	-22.99	57.66		
	12.13	95.36	1.07	1.40
	40.64	125.00	1.04	0.94
	71.71	159.50	1.11	0.78
70 (70.065)psi	-23.03	75.14		
	12.06	116.78	1.19	1.24
	40.74	155.56	1.35	0.99
	71.66	193.57	1.23	0.70

Nonuniform Loading

Load, lb	Temp, deg F	DO@20sec	Increase do/deg F	increase, % %/deg F
342.25	-18.63	29.37		
	73.19	59.35	0.33	0.74
	78.85	64.63	0.93	1.51
	89.67	71.62	0.65	0.95
772.60	-18.55	40.66		
	73.22	88.72	0.52	0.81
	78.88	93.44	0.83	0.92
1201.14	-18.53	44.39		
	73.19	103.08	0.64	0.87
	78.87	107.12	0.71	0.68

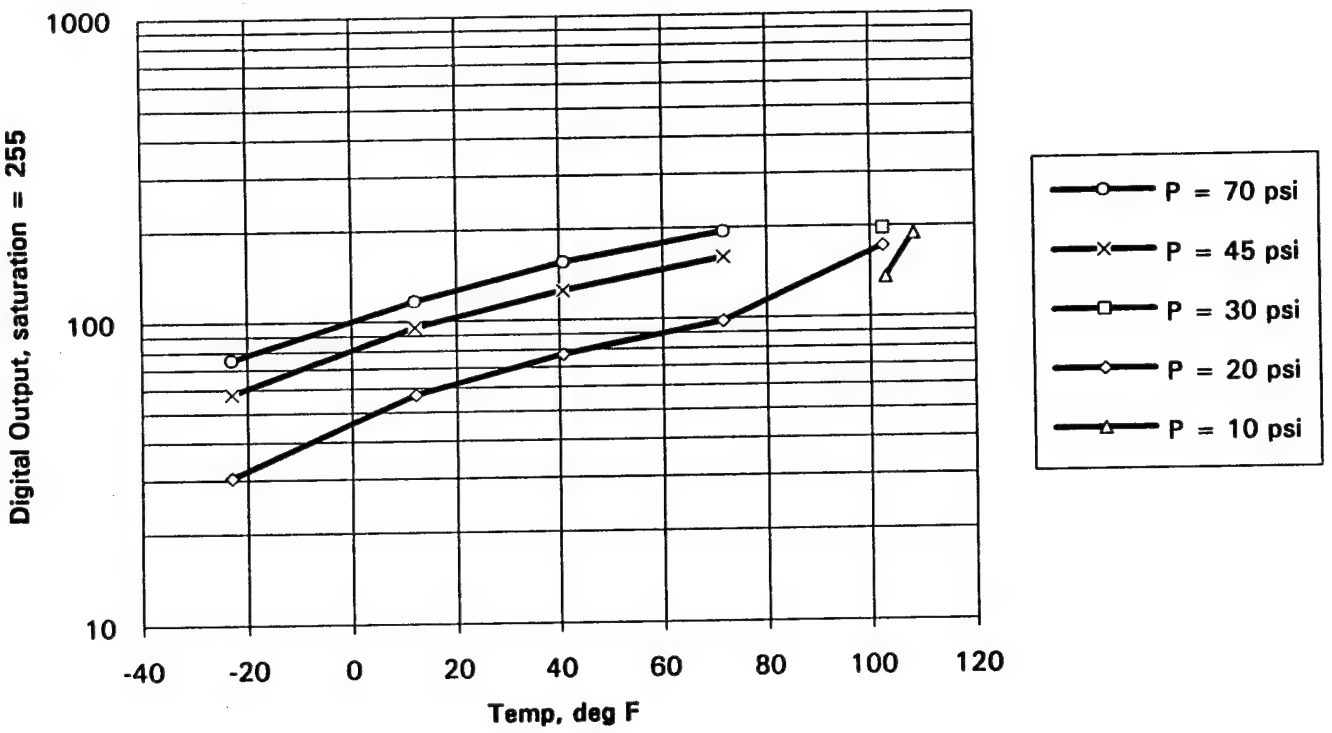

Figure 3-20. Summary of uniform loading.

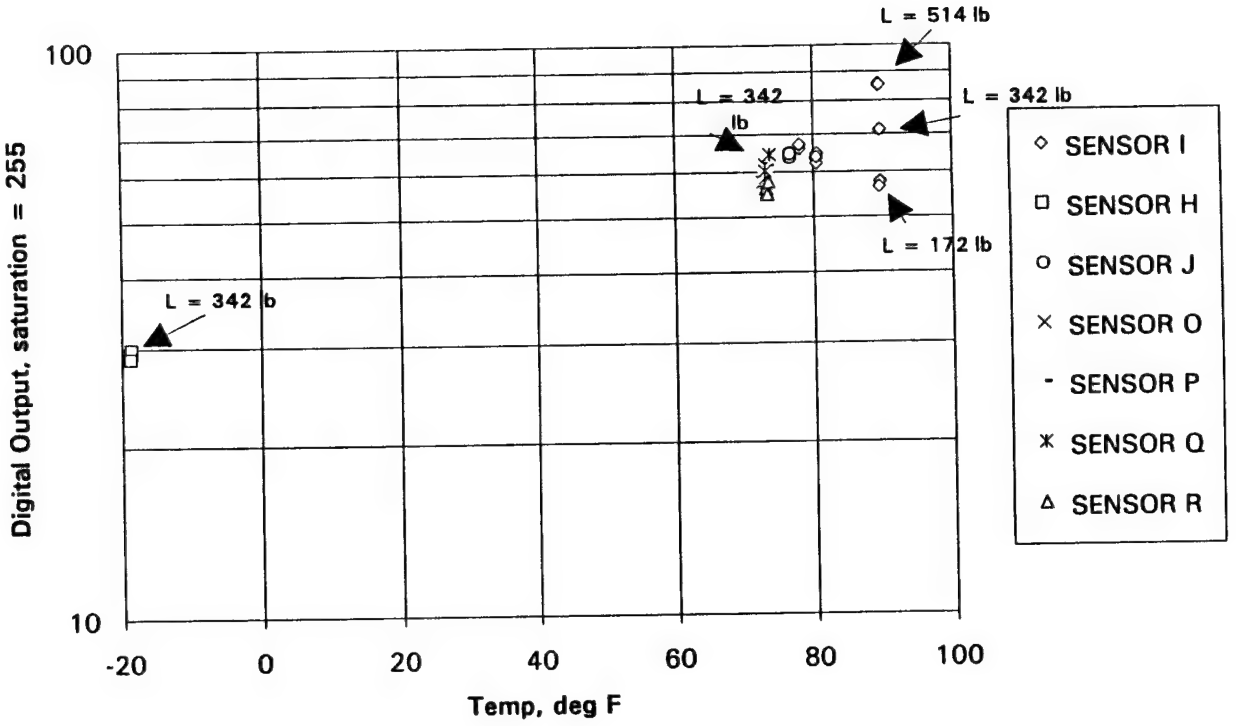

Figure 3-21. Non-uniform loading at 172, 342, and 514 pounds.

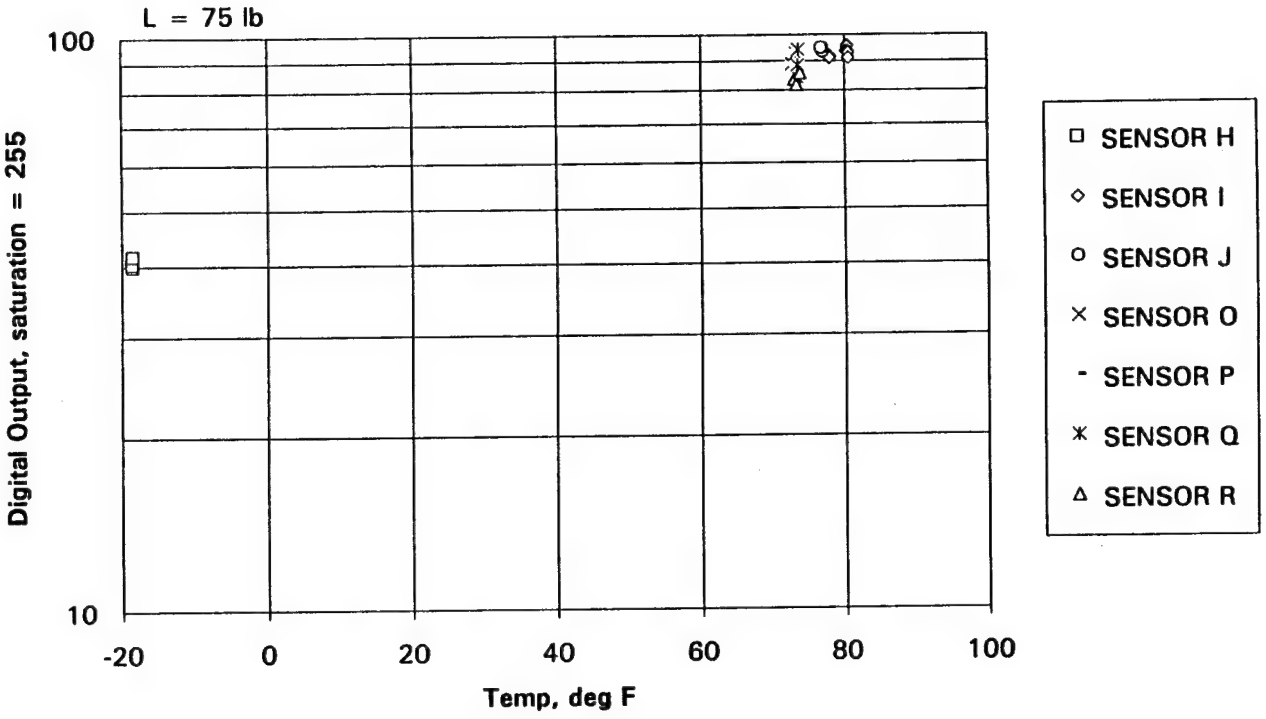

Figure 3-22. Non-uniform loading at 775 pounds.

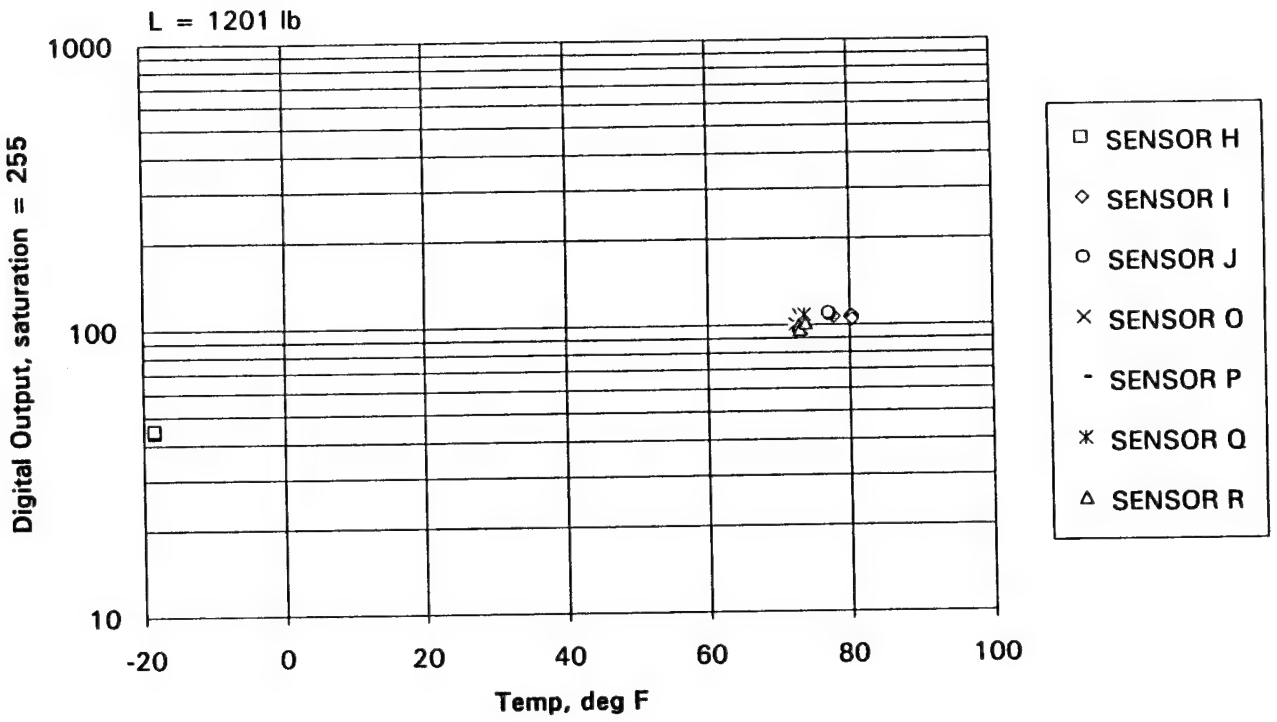

Figure 3-23. Non-uniform loading at 1201 pounds.

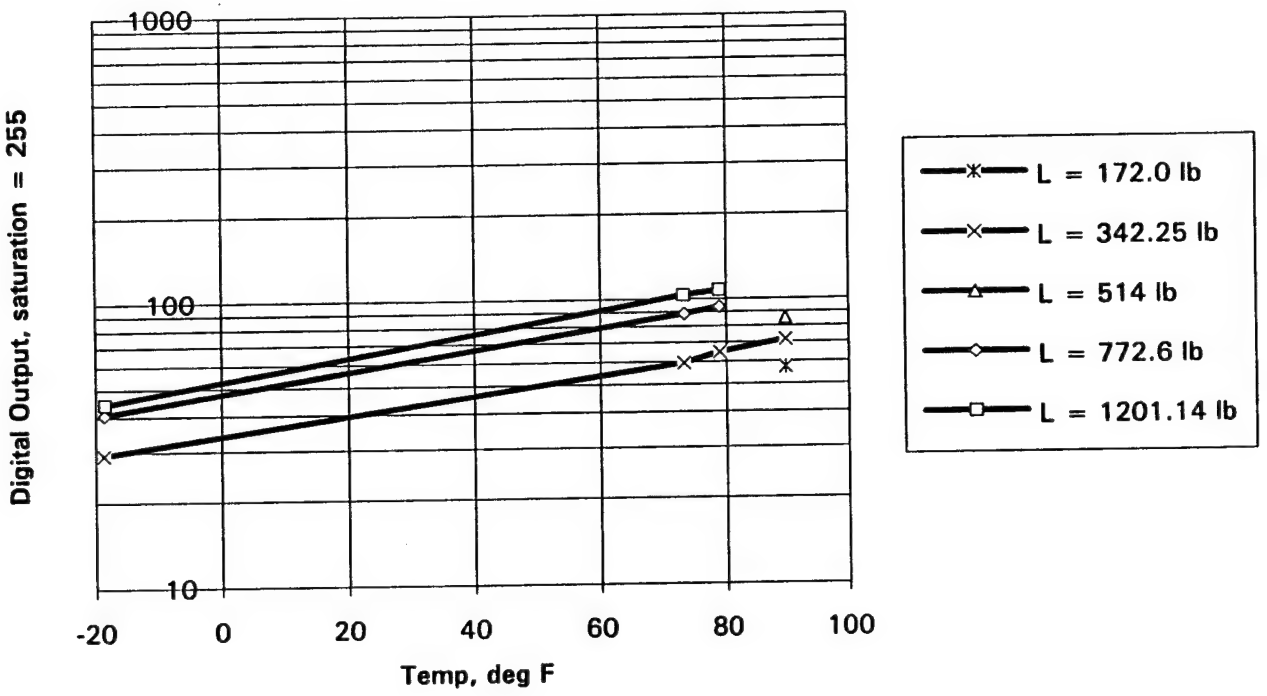

Figure 3-24. Summary of non-uniform loading.

nonlinearity data was taken for 1-second pulse loadings of the MTS loader. Prior to all testing and calibration, sensors were exercised as advised by the manufacturer.

3.4.1 Uniform Static Loading.

Uniform static loading was accomplished with the equilibration device which was loaded into the environmental chamber for all tests except those at room temperature. Equilibration calibrations obtained at 70 degrees F for three pressures (20, 45 and 70 psi) were used for uniform static loadings at all temperatures.

Test data showing input pressure versus digital output of the sensor are shown for static uniform loadings in Figures 3-25 and 3-26 and a summary plot is given in Figure 3-27. Data points in Figure 3-27 represent averages of pressure and digital output at a given temperature. At the lowest temperature (-23 degrees) the sensor exhibits less nonlinear behavior. A monotonic trend exists, whereby, with increased temperature, nonlinearity of the sensor is increased.

3.4.2 Non-Uniform Static Loading.

Non-uniform static loading of the sensor was performed in the environmental chamber with the plate-mounted tire tread. Equilibration calibrations from 70 degrees F for three pressures (20, 45, and 75 psi) were loaded for each sensor and force calibrations were performed at each temperature prior to testing. Force calibrations were made by loading the sensor with the highest loading at a given temperature.

For comparison to the uniform loadings, an average pressure along with a digital output were obtained from the non-uniform test data. The average pressure was calculated by dividing the input load by the Weighmat loaded area. The digital output was obtained by dividing the Weighmat load by the Weighmat sensed area and dividing this average pressure by the scale factor. These data are provided in Figures 3-28 and 3-29 and a summary plot of the averages of these data is shown in Figure 3-30. The comparison of the uniform and non-uniform loading in Figure 3-31 show that less digital output was obtained from the non-uniform loading for the same average input pressure. The cause for this lower reading from non-uniform loadings is due to partial loading of sensels at the edge of the loaded area. A sensel reading is the average of sixteen node points across the sensel area. If a sensel is partially loaded the reading from the portion of the sensel loaded is averaged over the entire area of the sensel (0.16 in^2) and thus the reading is lowered.

Loads read by the Weighmat versus the input loads are shown in Figures 3-32 and 3-33 for the non-uniform loadings. A summary plot of the averages of these data for a given temperature and input load is shown in Figure 3-34. In general, the load indicated by the Weighmat was high versus the input load. This could indicate a lack of sufficient exercise prior to taking a force calibration, but more probably is the result of nonlinearity. No temperature dependent trends can be inferred from the output versus input load curves.

3.4.3 Pulse Loadings.

Pulse loadings of 1 second in duration at -18 and 75 degrees F were taken with only one sensor at each temperature. The same force calibration files used for the static loadings were used for the pulse loadings.

Pulse loadings data and averages are shown in Figure 3-35. A summary plot of the pulse loadings versus the uniform and non-uniform static loads is shown in Figure 3-36. Because the force calibrations were made after the sensor was loaded for 20 seconds and allowed to

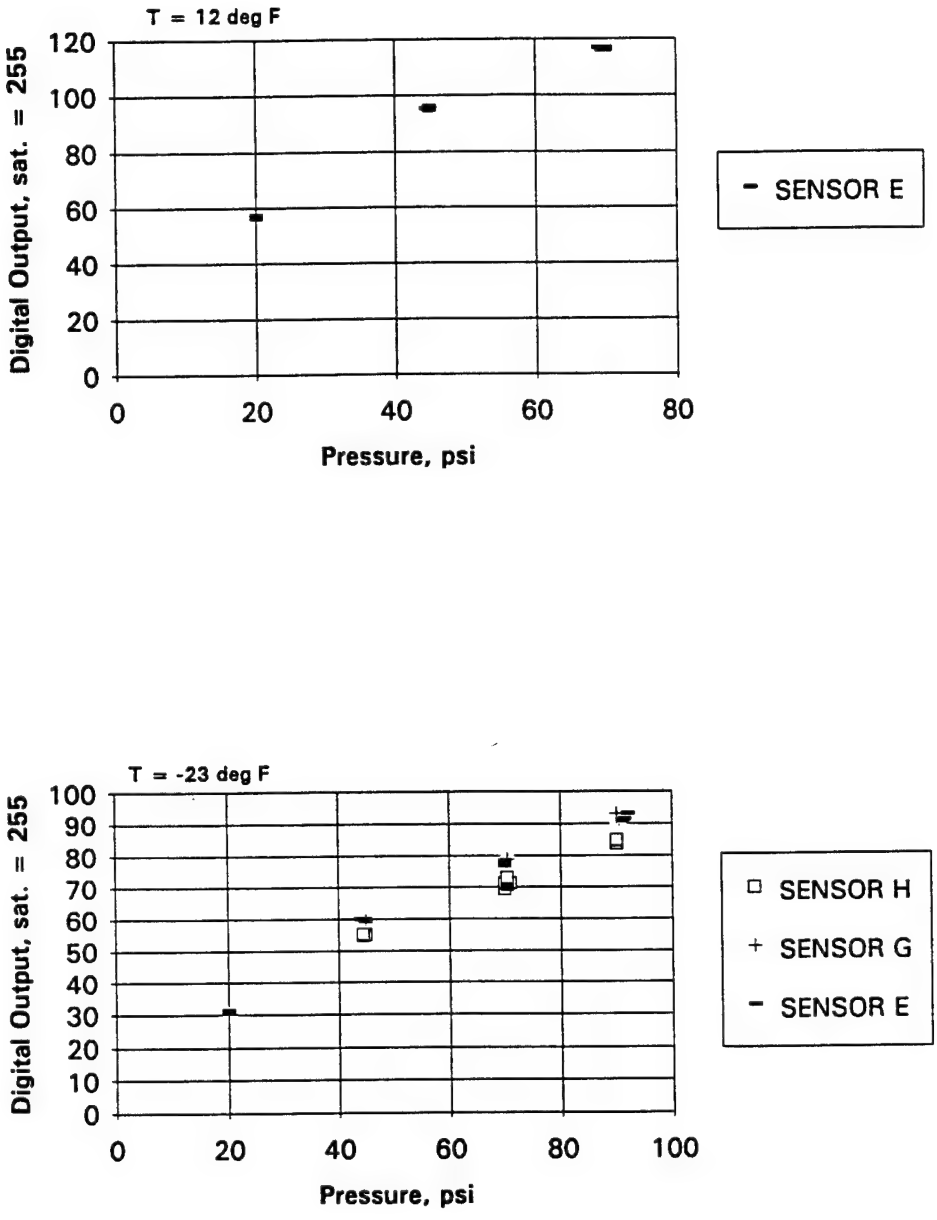

Figure 3-25. Uniform loading at -23 degrees and 12 degrees F.

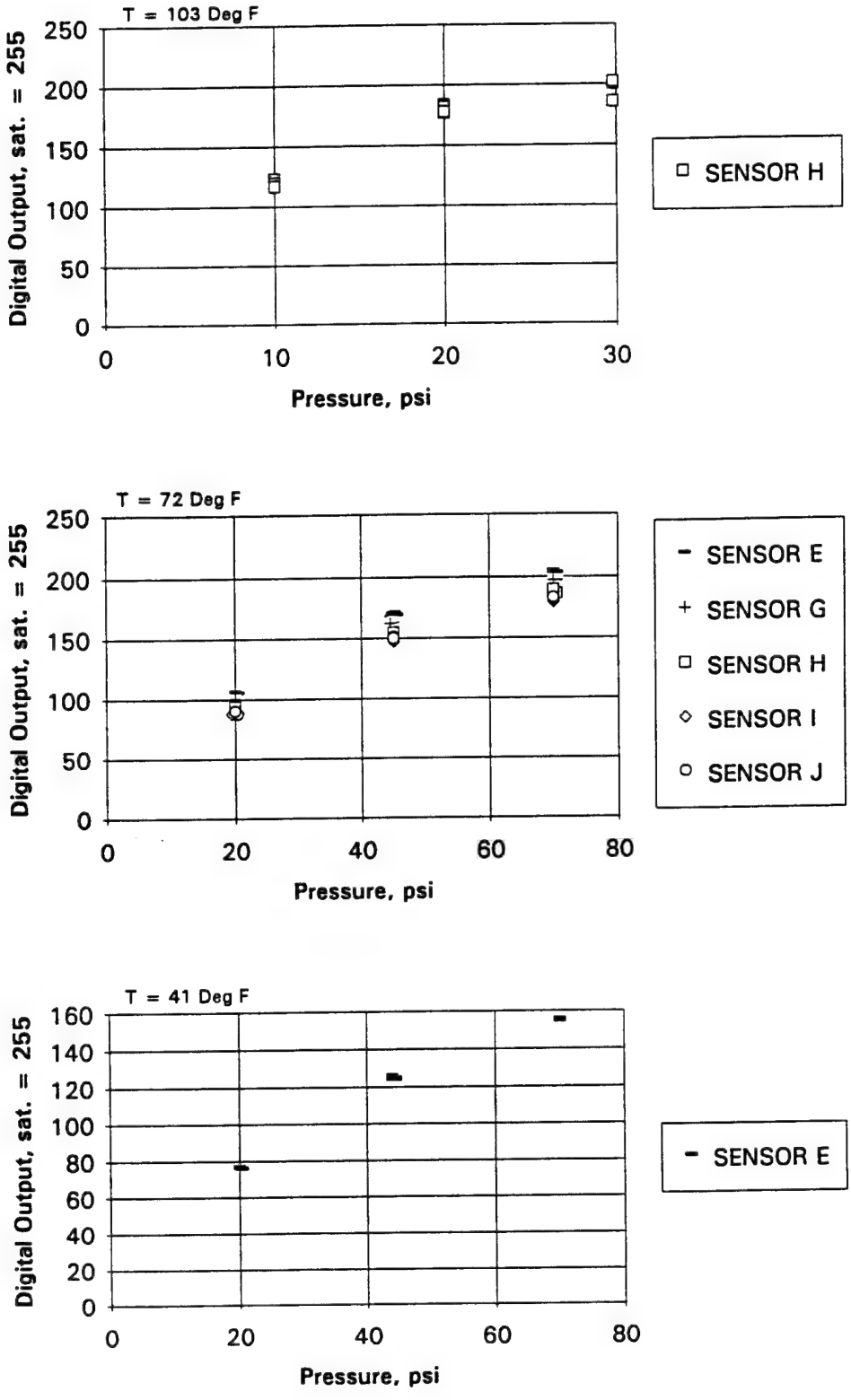

Figure 3-26. Uniform loading at 41 degrees, 72 degrees, and 103 degrees F.

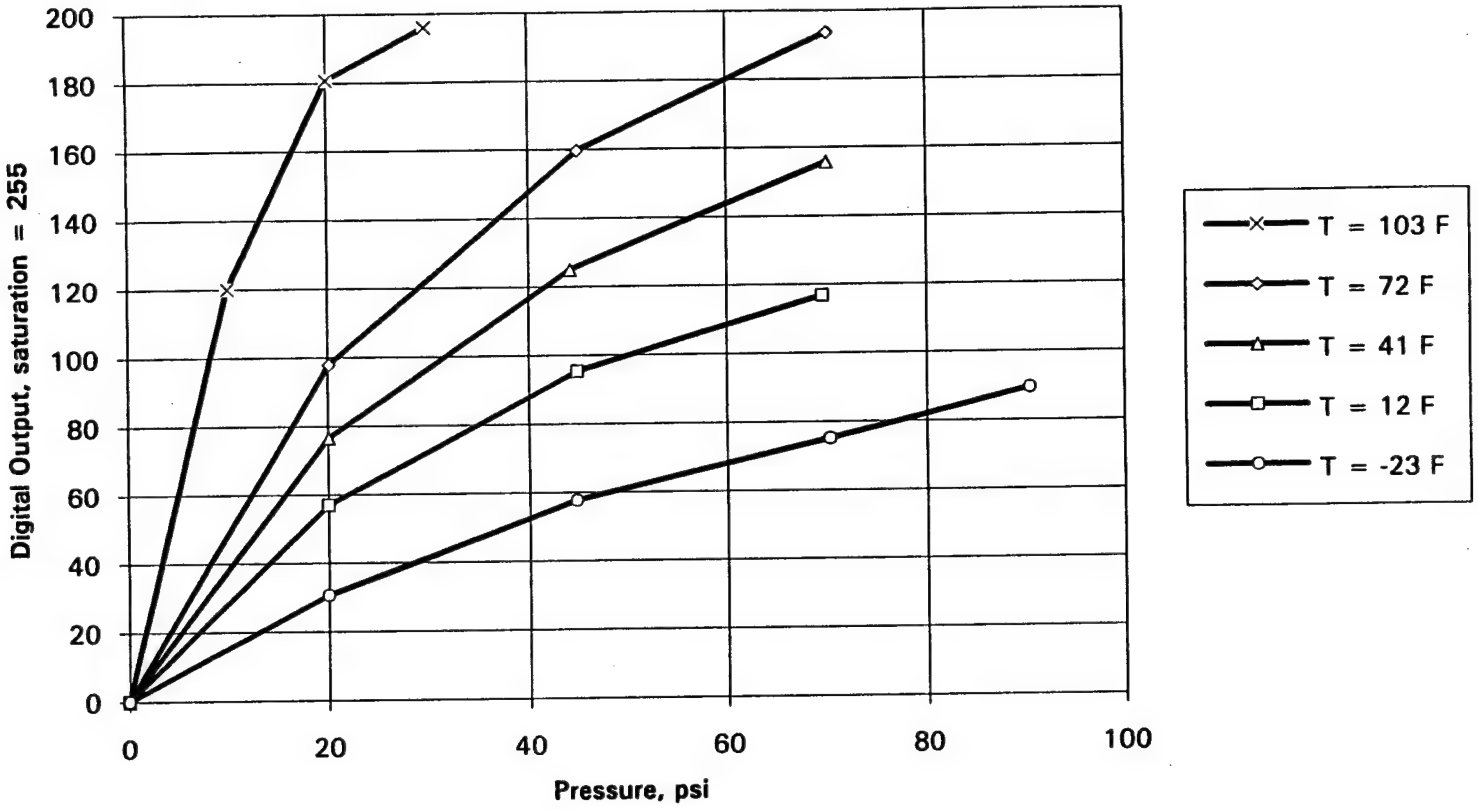

Figure 3-27. Summary of uniform loading.

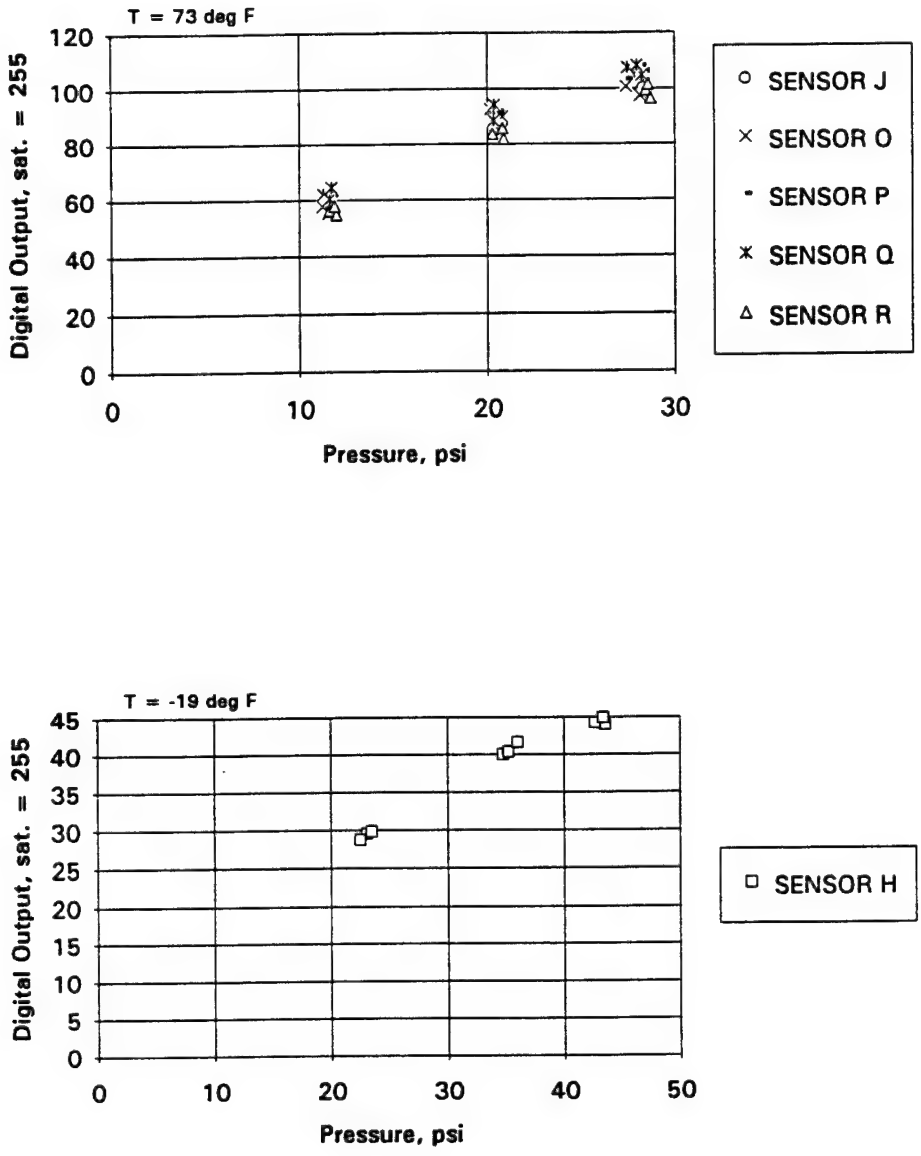

Figure 3-28. Non-uniform loading at -19 degrees and 73 degrees F - digital output versus input pressure.

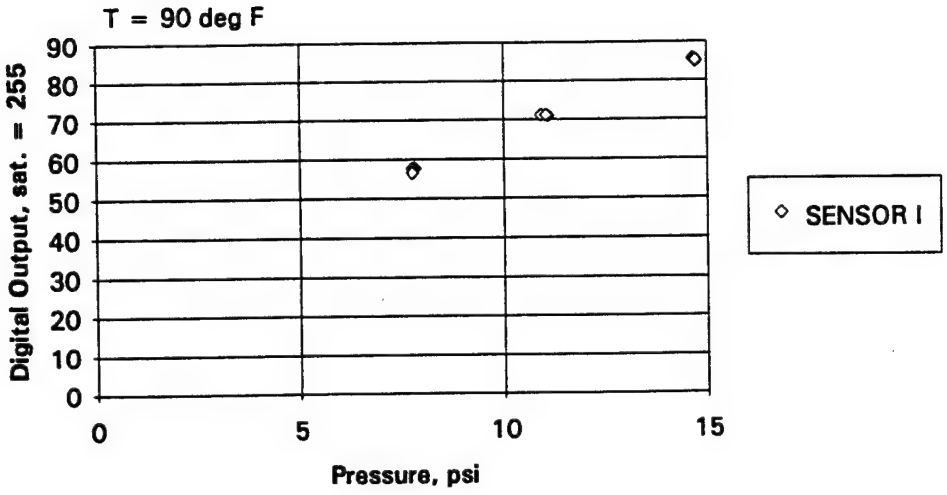

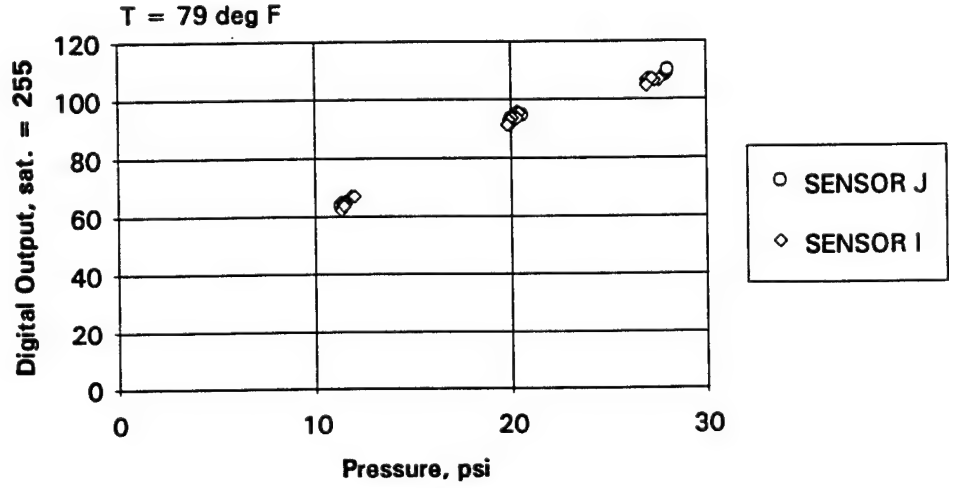

Figure 3-29. Non-uniform loading at 79 degrees and 90 degrees F - digital output versus input pressure.

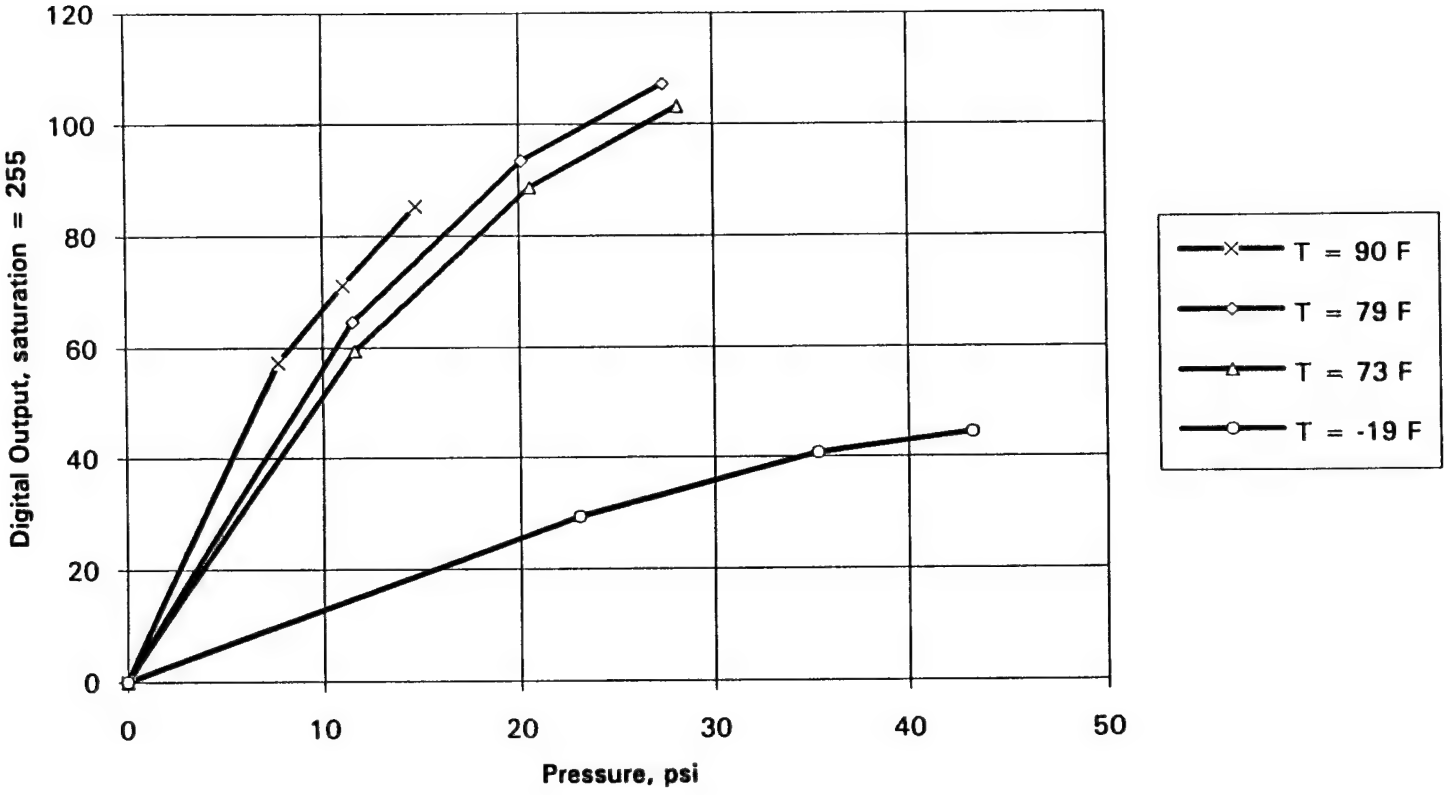

Figure 3-30. Summary of non-uniform loading. Digital output versus input pressure.

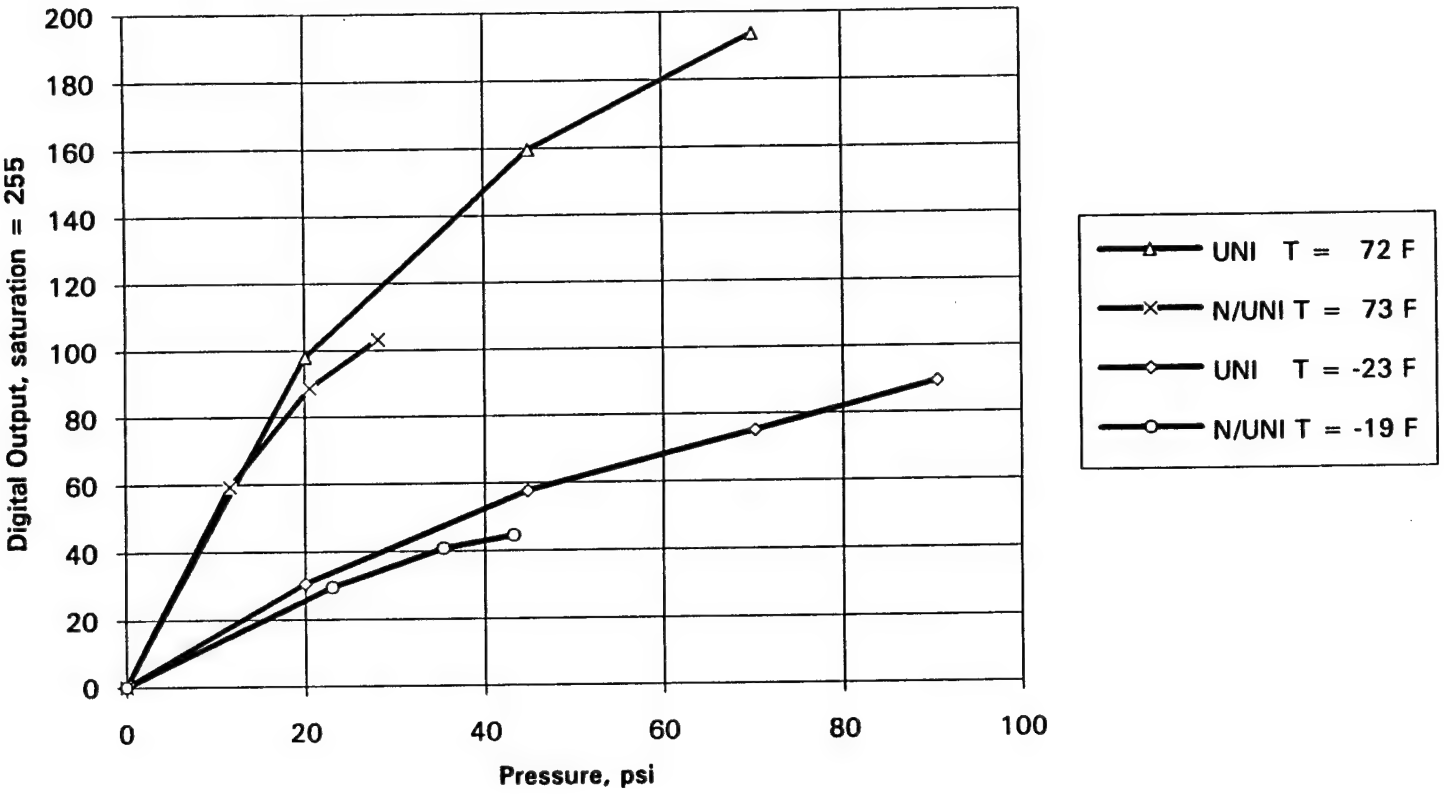

Figure 3-31. Uniform loading versus non-uniform loading.

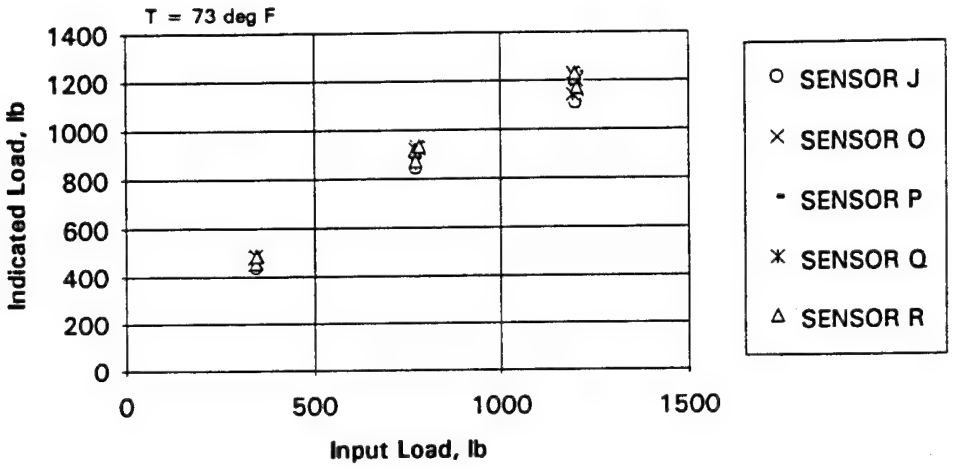

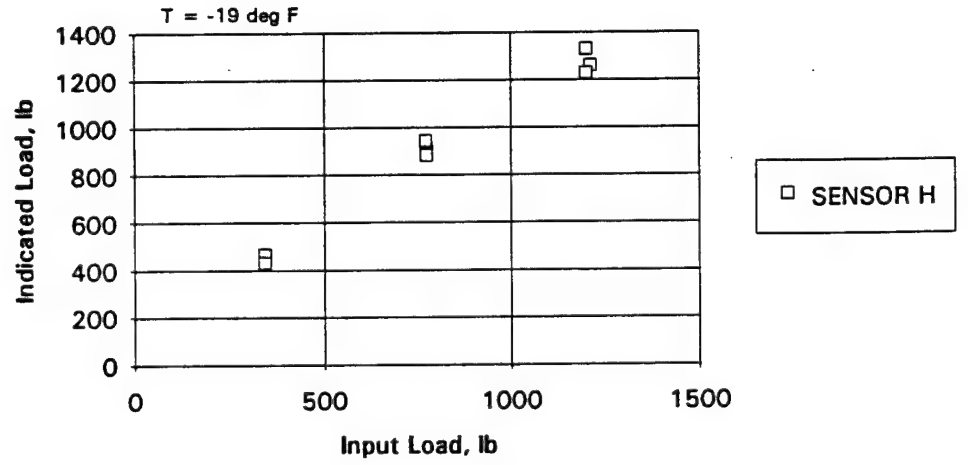

Figure 3-32. Non-uniform loading at -19 degrees and 73 degrees F - indicated load versus input load.

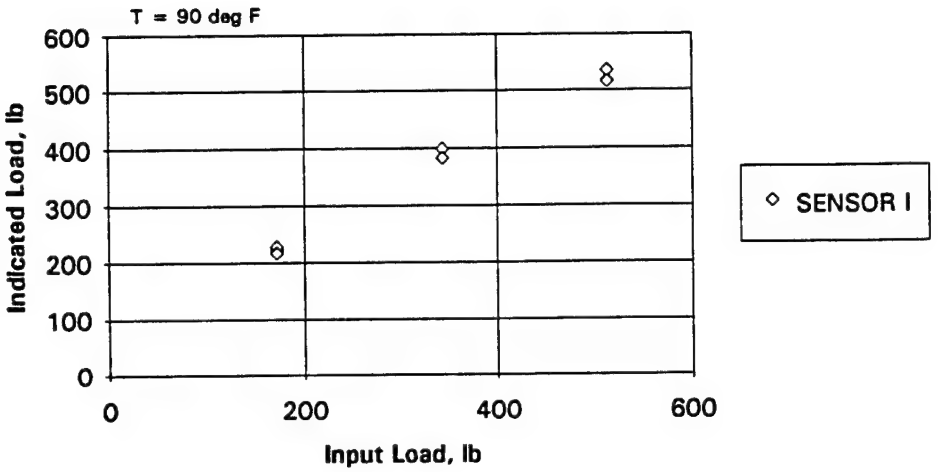

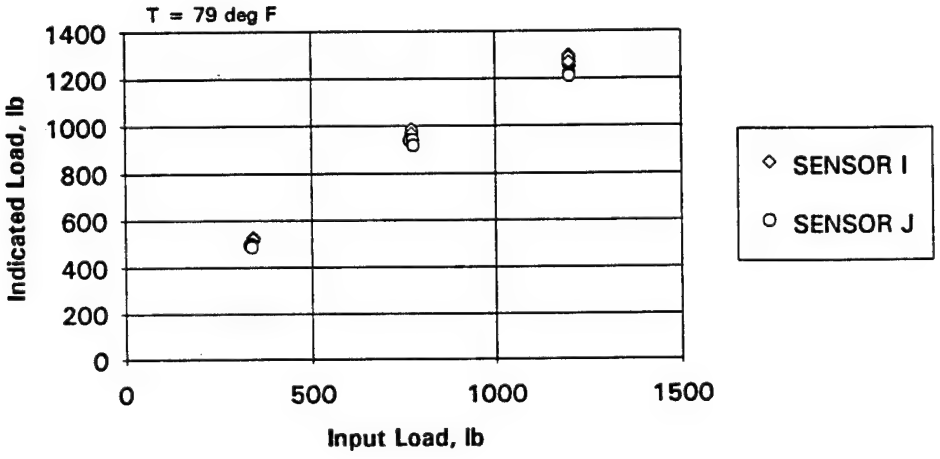

Figure 3-33. Non-uniform loading at 79 degrees and 90 degrees F - indicated load versus input load.

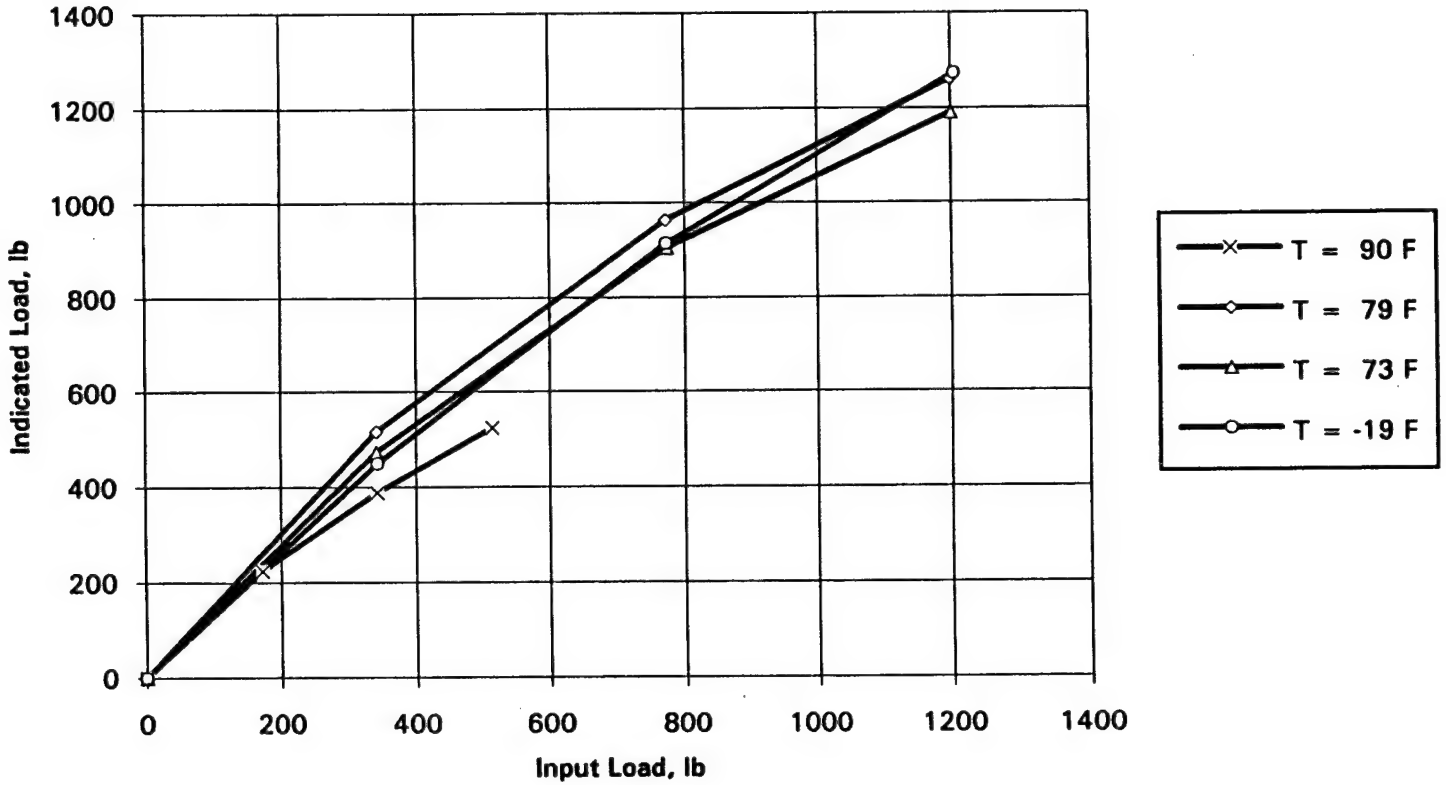

Figure 3-34. Summary of non-uniform loading. Reading versus input load.

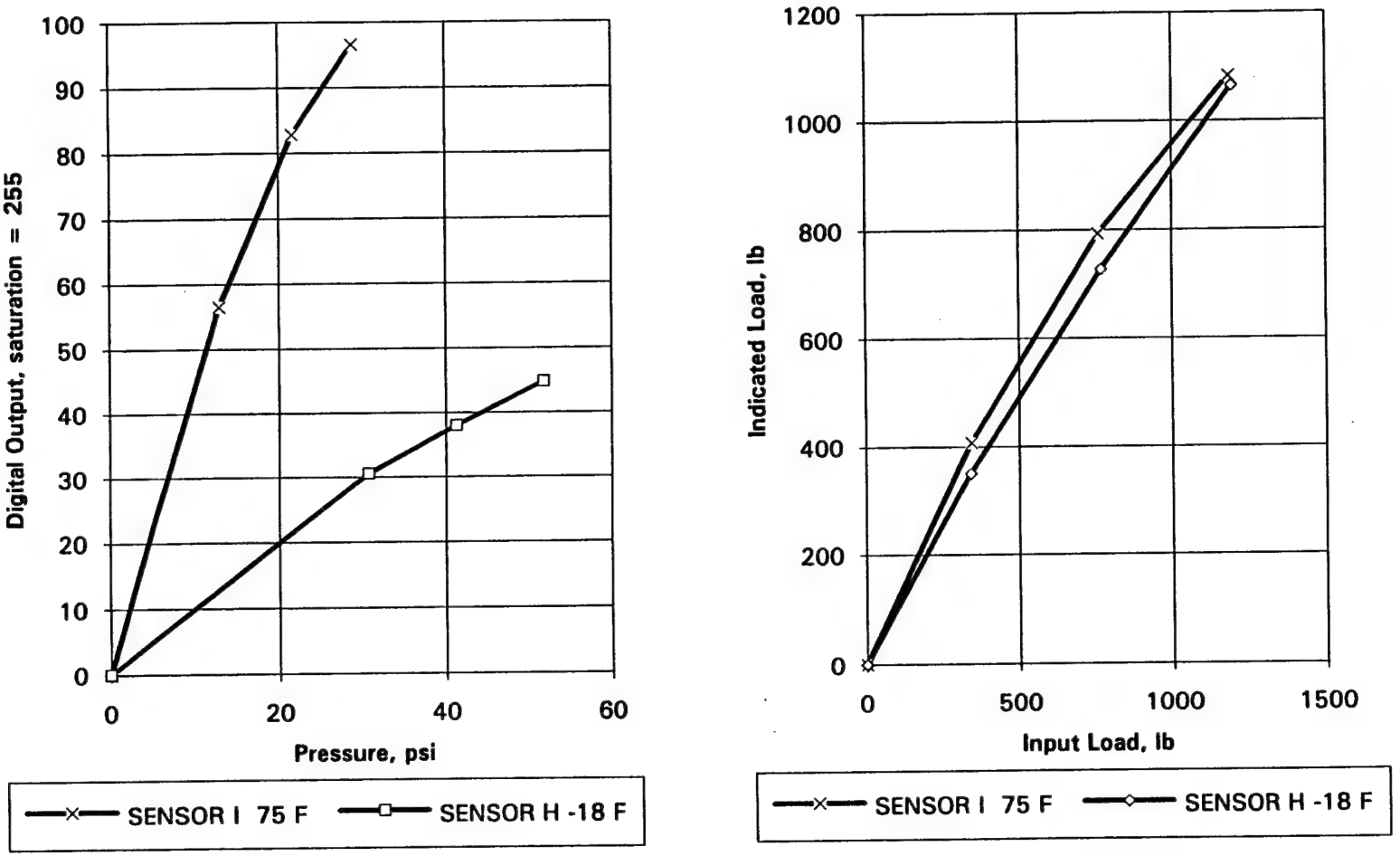

Figure 3-35. Pulse loadings at -18 degrees and 75 degrees F.

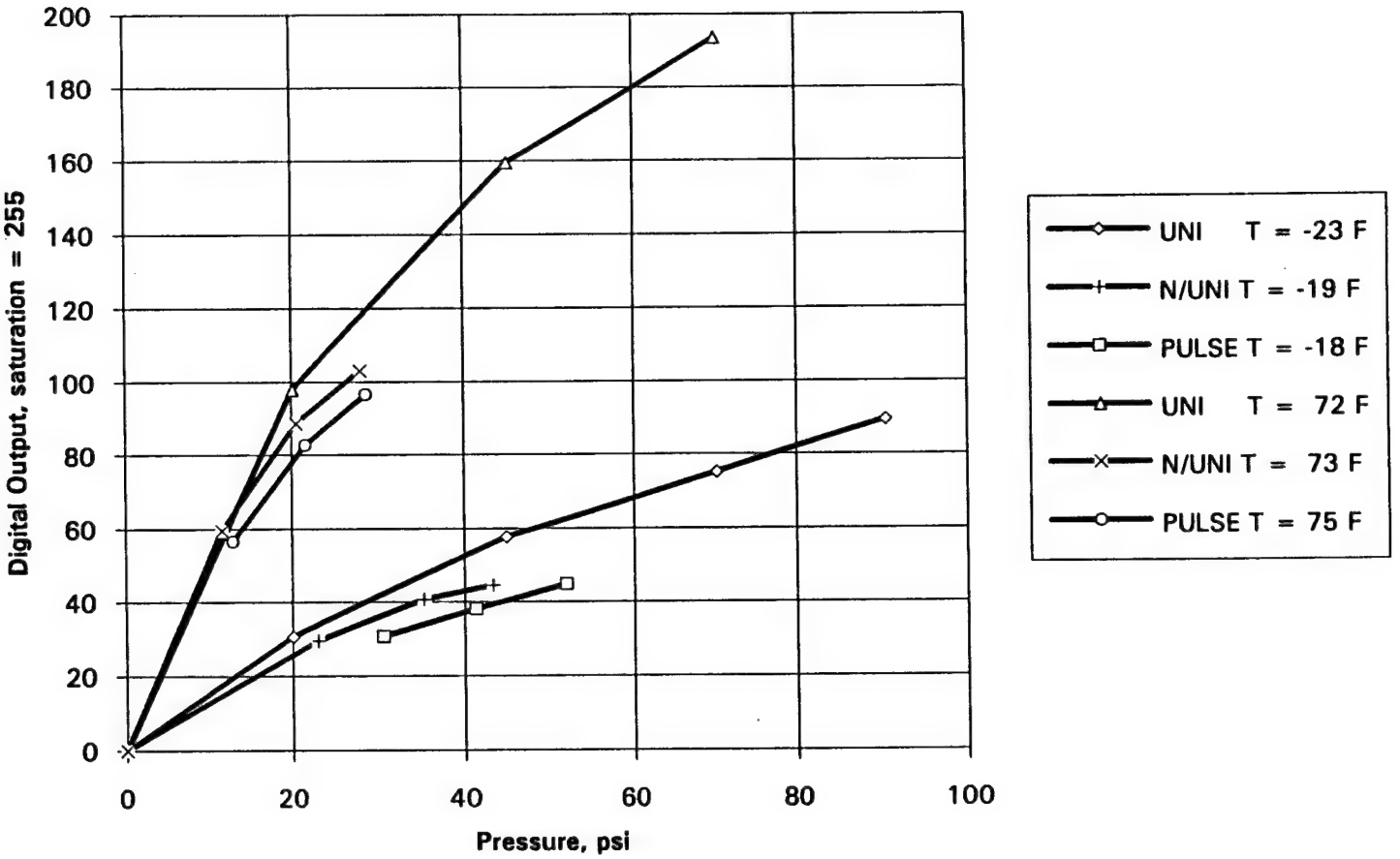

Figure 3-36. Comparison of uniform, non-uniform and pulse loadings.

creep, the pulse loading readings were low versus the static readings. The shorter duration pulse load data are also less nonlinear than the data obtained with static loadings. This can be seen by comparing data from pulse loads and static loads in Figure 3-37.

3.4.4 Nonlinearity Summary.

Nonlinearity was characterized for various temperature and loading conditions. A family of curves was obtained over a wide range of temperatures for both uniform and non-uniform static loading conditions. The sensor responds to pressure nonlinearly at all temperatures, but it is more nearly linear at low temperatures than at high temperatures. Nonlinearity also increases with load duration.

3.5. STATIC CREEP AND HYSTERETIC BEHAVIOR.

3.5.1 Static Creep.

Static creep was represented by Tekscan as bringing in a constant or nearly constant percent increase in indicated load for each factor of increase in the time that a constant load is applied; specifically, about 3 to 5 percent per decade. That is, there would be a 3 to 5 percent increase in indicated load (or pressure) during the time intervals 1 to 10 seconds, 10 to 100 seconds, 100 to 1000 seconds, and so forth. Accordingly, it was suggested that the most precise and repeatable measurements would be obtained with relatively long loading times, of the order of ten seconds or more, so that the indicated load would not be very sensitive to small variations in the time of application. Our data included static load durations over 20 seconds. These provided information on static creep as well as repeatability.

Tests with uniform loading by means of the air-bladder equilibration fixture provided good data on repeatability of indicated load or pressure after 20 second application, and on the effect of temperature on sensitivity, but the static creep aspect of these data was rendered questionable by occasional early-time trapping of an air pocket or bubble in the sensor itself. This can occur when all or a large part of the sensor is loaded uniformly. The sensors have air vents at their outer edges, but in a few cases, the loading air bladder can make first contact around the sensor periphery, preventing air trapped in the center region inside the sensor pocket from escaping immediately. The pressure of the trapped air then decreases the indicated pressure in the central region. Indeed, several recordings obtained with uniform loading by air bladder showed symptoms of an early-time trapped air pocket. The phenomenon is recognized by a secondary rise in the output time history, coinciding with an initial shallow bowl-like depression in the central region of the indicated pressure distribution rising up to the final, flat spatial distribution.

Techniques to prevent pockets of trapped air suggested by Tekscan involve perforating the sensors with pinholes (in regions in between the row-column junctions, or sensels) and inserting a layer of cloth between sensor and air bladder to help the air exiting via the pinholes escape to the edges. It is also a good idea to avoid pulling a partial vacuum inside the air bladder upon dumping the air, since that may tend to pull air into the sensor pocket. (Unfortunately, the air switch in the equilibration device provided by the manufacturer makes this difficult.)

Because of the occasional occurrence of an early-time air pocket and its effect on static creep data in particular, experimental analysis of static creep in this report is confined to tests with platen loading with the tire tread. Exceptions are some very long-duration data.

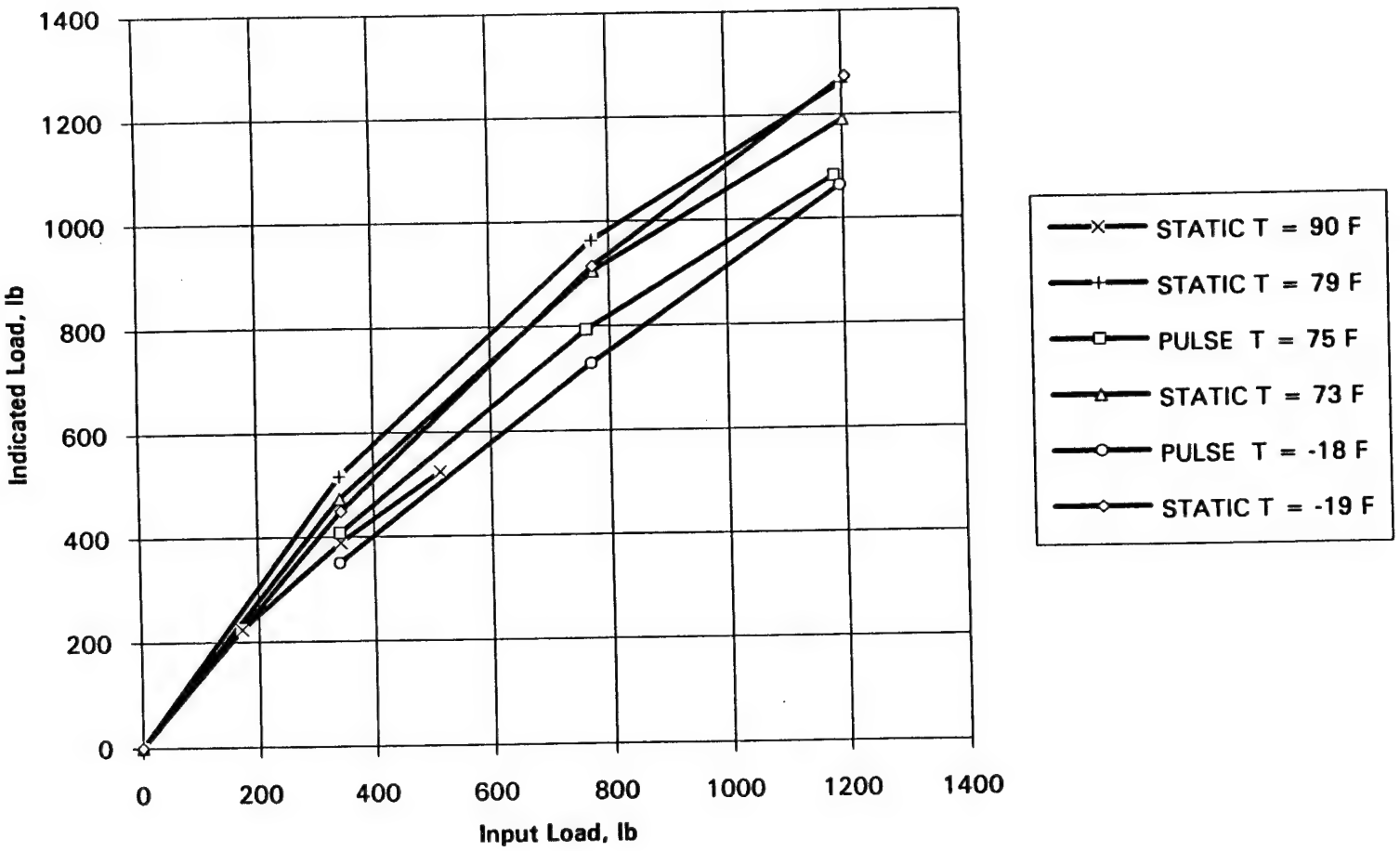

Figure 3-37. Non-uniform loadings - static versus pulse.

The time history of the platen loading consisted of a slight initial preload, of the order of one to five percent of the final applied load, then a programmed step rise to the final load. Sample Tekscan force versus time histories are shown in Figures 3-38 and 3-39. In order to save processing time, data-taking time, and data file space, a recording interval of 1 second was used in almost all static creep recordings. Thus, the 0.2-second rise does not show in the Tekscan time histories. Synchronization between applied load and the Tekscan recording time scale was manual, with the Tekscan operator counting "one, two, three, go" to the MTS loader operator. Initiation of the load increase was very close to the four-second mark on the Tekscan recording time scale, sometimes slightly above it, as in Figure 3-38, sometimes slightly below it, as with Figure 3-39.

In case of a Tekscan recording with a time history such as in Figure 3-38, the onset of nearly full applied load was assumed to be at the 4.5-second mark. The corresponding data are shown in Table 3-2. In Table 3-2, 0.5 second corresponds to the 5-second mark in Figure 3-38, 1.5 seconds to the 6-second mark (indicated by the vertical line in Figure 3-38), and so forth. Because there is some uncertainty as to whether the applied load had reached its full value after 0.5 seconds, the factor of increase data were normalized to the load at 1.5 seconds (Table 3-2).

In case of a Tekscan recording such as Figure 3-39, the onset of nearly full applied load was assumed to be at the 4-second mark. The corresponding data are in Table 3-3. In Table 3-3, time zero corresponds to the 4-second mark in Figure 3-39, 1 second to the 5-second mark (indicated by the vertical line in Figure 3-39), etc. The factor of increase data were normalized to the load at 1 second (Table 3-3).

Corresponding plots of factor of increase in indicated load versus time are shown in Figures 3-40 and 3-41. In the semilog plots as shown, with the log scale on the time axis (the abscissa), a constant percent increase in load per decade in time would show up as a straight line. Indeed, all recordings thus analyzed and plotted (most of the tables and plots are not shown in this report) fit a straight line rather well.

The first few points often tended to deviate. Examples are shown in Figures 3-42 and 3-43. In Figure 3-42, the first few points appear high, whereas in Figure 3-43, the first point appears low. This is a reflection of the uncertainty in accurately establishing time zero, the time that nearly the full applied load was reached. If time zero was actually earlier, the first few points would shift to the right (on the log scale) much more than the later-time points, and a plot such as in Figure 3-42 would fit a straight line more closely. On the other hand, if time zero was actually later, the first few points would shift to the left (on the log scale) more than the other points, and a plot such as in Figure 3-43 would fit a straight line more closely. Therefore, *the first two points were ignored in performing the fits.*

Figures 3-42 and 3-43 also show the effects of round-offs to three decimal places in the Tekscan software, with loads not far above 1000 pounds.

As in most other tests, generally the maximum load magnitudes were chosen so as to stay within the range of the sensor, suitably below saturation. In the room temperature range, a suitable maximum load on the tire patch was 1200 pounds. A stress distribution under 1200 lbs. at 77.8 degrees F is shown in Figure 3-44. The color scale in this and other (color) stress distributions in this section has been adjusted such that the deep red indicates saturation. A stress distribution under 514-pound load at 89.5 degrees F is shown in Figure 3-45. The closeness to saturation is comparable to that in Figure 3-44, though a bit lower in Figure 3-45 (more conservative) in view of other tests, such as fatigue and memory, involving pulse trains and longer effective durations. However, static creep data at low temperatures were limited to maximum loads around 1200 pounds. A stress distribution

Graph

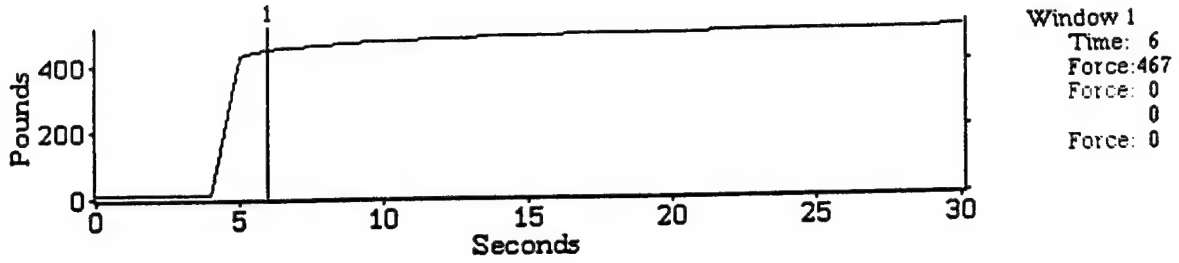

COMMENTS:
I4081607

Figure 3-38. Indicated force time history from static platen loading.

Graph

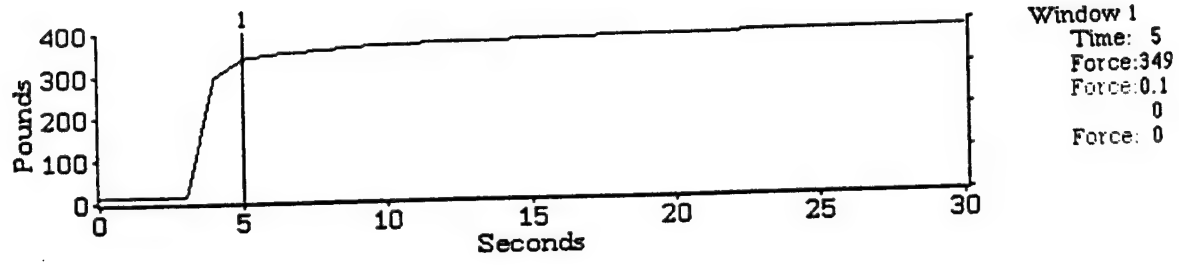

COMMENTS:
I4081616

Figure 3-39. Indicated force time history from static platen loading.

Table 3-2. Static creep, 89.5 degrees F, 514-pound load, sensor I.

Equilibration calibration pressure:	70.0 psi
Force calibration temperature:	89.3 degrees F
Calibration load:	514 lbs.
Calibration file:	I70089
Recording:	I4081607
Preload:	13.7 lbs

Time, sec	Indicated Load, lbs.	Factor of Increase in Indicated Load
0.5	447	
1.5	467	1.000
2.5	474	1.015
3.5	482	1.032
4.5	487	1.043
5.5	491	1.051
6.5	494	1.058
7.5	497	1.064
8.5	500	1.071
9.5	503	1.077
10.5	505	1.081
11.5	507	1.086
12.5	508	1.088
13.5	510	1.092
14.5	511	1.094
15.5	512	1.096
16.5	513	1.099
17.5	514	1.101
18.5	515	1.103
19.5	516	1.105
20.5	517	1.107
21.5	518	1.109
22.5	518	1.109
23.5	519	1.111
24.5	520	1.113
25.5	521	1.116

Table 3-3. Static creep, 89.7 degrees F, 343-pound load, sensor I.

Equilibration calibration pressure:	45.0 psi
Force calibration temperature:	89.5 degrees F
Calibration load:	534 lbs.
Calibration file:	I45089
Recording:	I4081616
Preload:	17.8 lbs

Time, sec	Indicated Load, lbs.	Factor of Increase in Indicated Load
0	305	
1	349	1.000
2	361	1.034
3	367	1.052
4	371	1.063
5	375	1.074
6	378	1.083
7	381	1.092
8	383	1.097
9	385	1.103
10	387	1.109
11	388	1.112
12	390	1.117
13	391	1.120
14	392	1.123
15	393	1.126
16	394	1.129
17	395	1.132
18	396	1.135
19	397	1.138
20	398	1.140
21	399	1.143
22	399	1.143
23	400	1.146
24	400	1.146
25	401	1.149
26	402	1.152

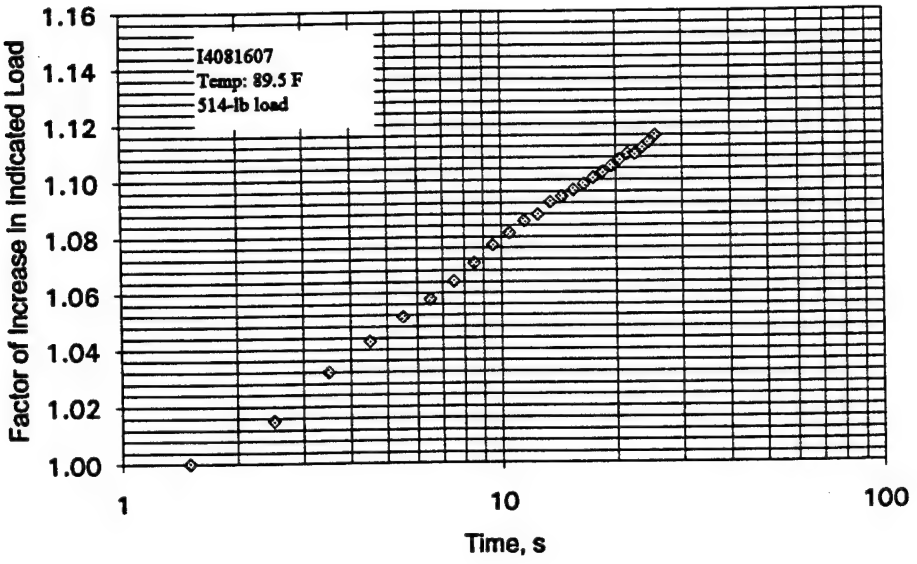

Figure 3-40. Static creep for 514-pound load at 89.5 degrees F.

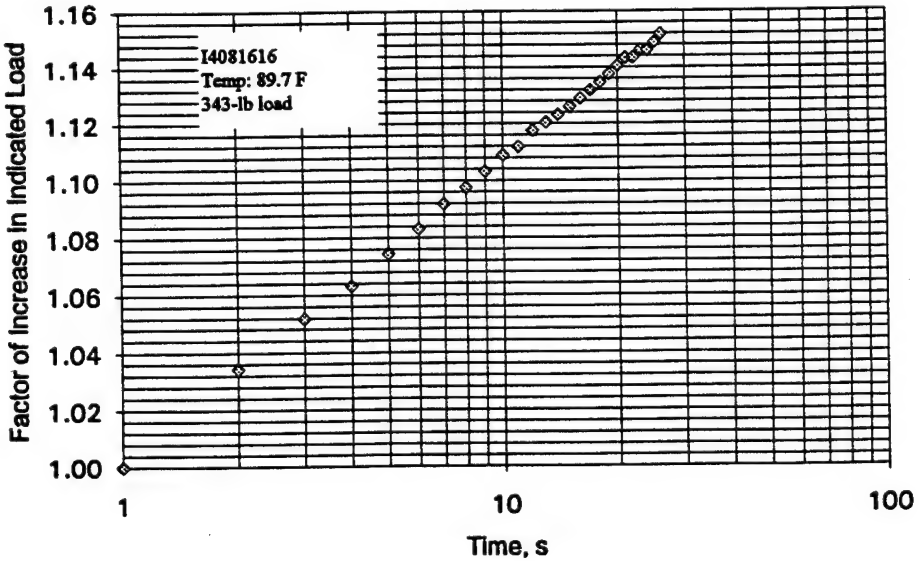

Figure 3-41. Static creep for 343-pound load at 89.7 degrees F.

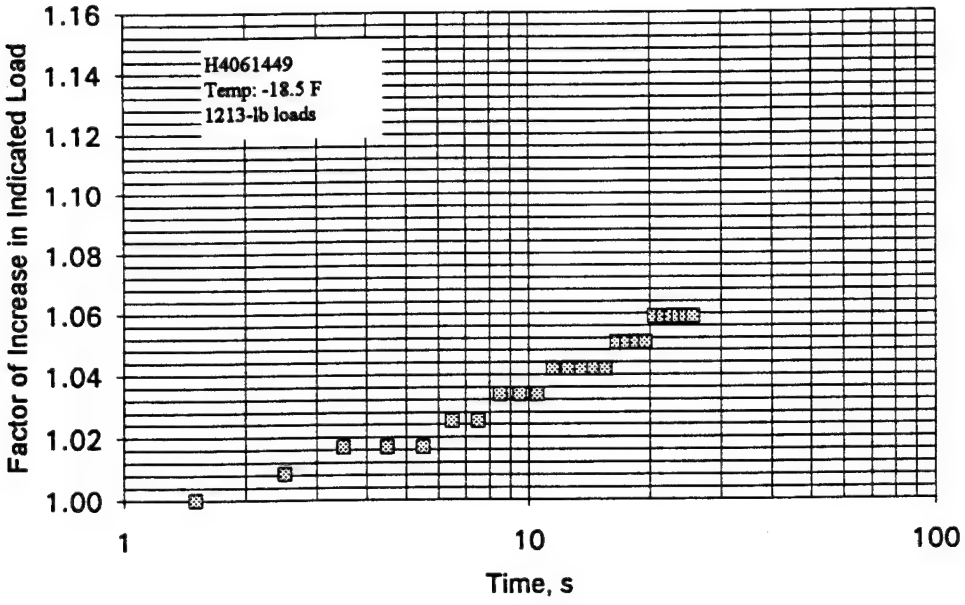

Figure 3-42. Static creep for 1213-pound load at -18.5 degrees F.

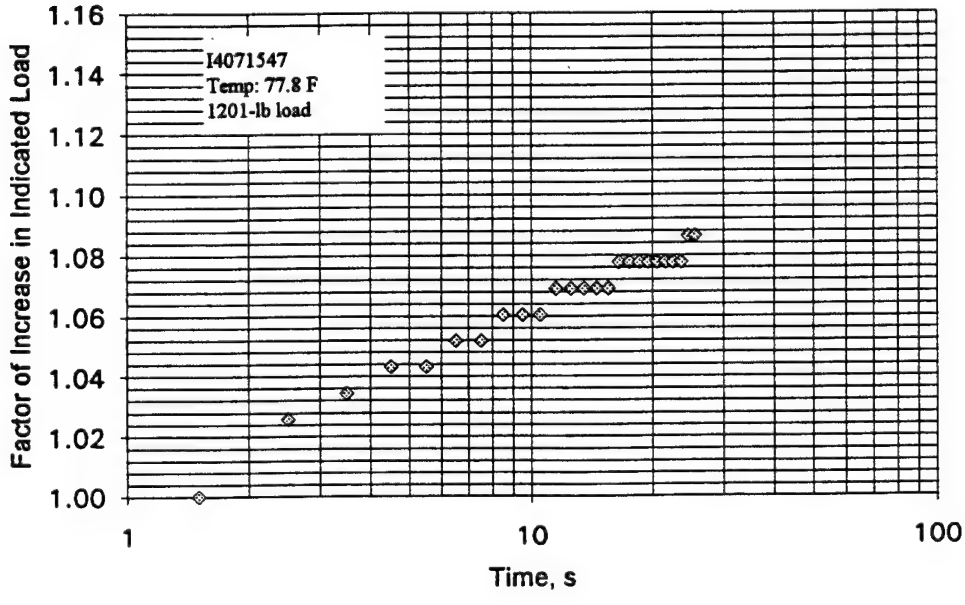

Figure 3-43. Static creep for 1201-pound load at 77.8 degrees F.

```
Playback Window 1
     Machine_Name:
    Machine_Ident:
             Date: 04/07/94,14:18
Area = 44.96 sq inches
 Frame   27 of   31
File D:\DATA\WEIGHMAT\I4071547.FSX
Saved 04/07/17  14:49
```

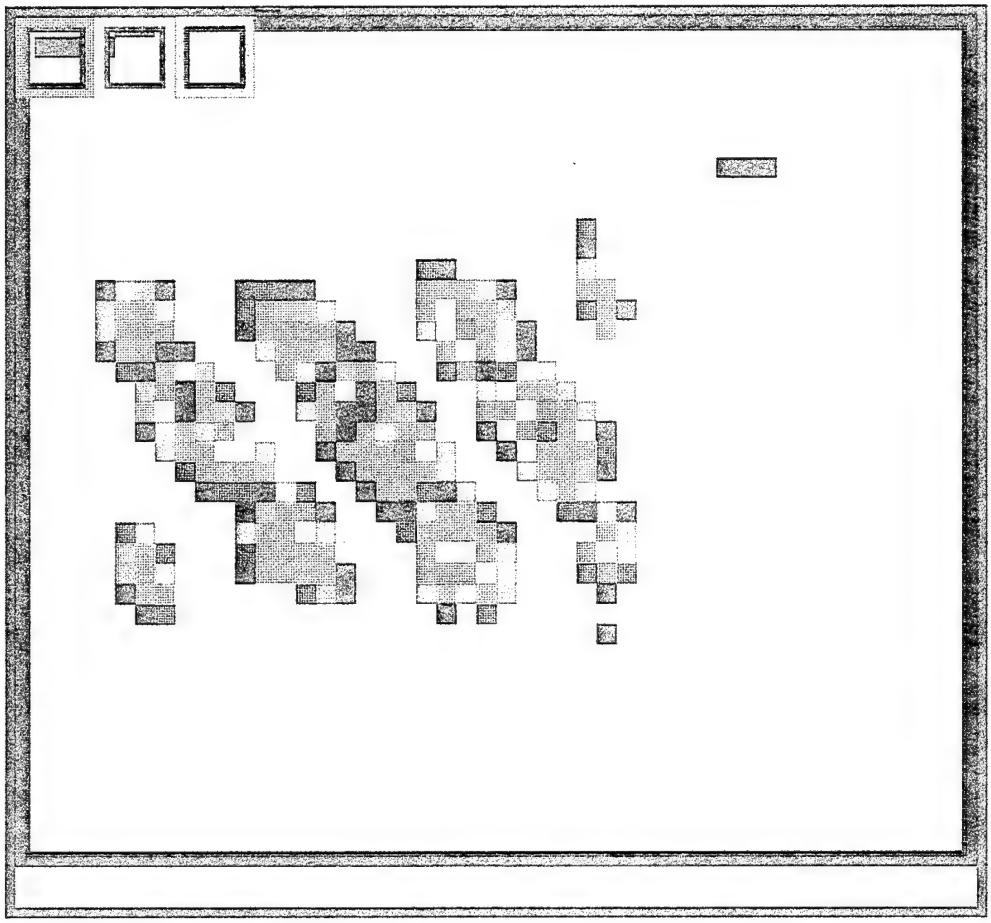

Key: 0.8 6.5 12.1 17.5 23.2 28.6 34.3 39.7 45.3 50.7 56.4 61.8 67.4 PSI

Figure 3-44. Stress distribution for 1200-pound load at 77.8 degrees F.

```
Playback Window 1
     Machine_Name:
    Machine_Ident:
             Date: 04/08/94,14:43
Area = 35.04 sq inches
 Frame    27 of    31
File D:\DATA\WEIGHMAT\I4081607.FSX
Saved 04/08/17  15:07
```

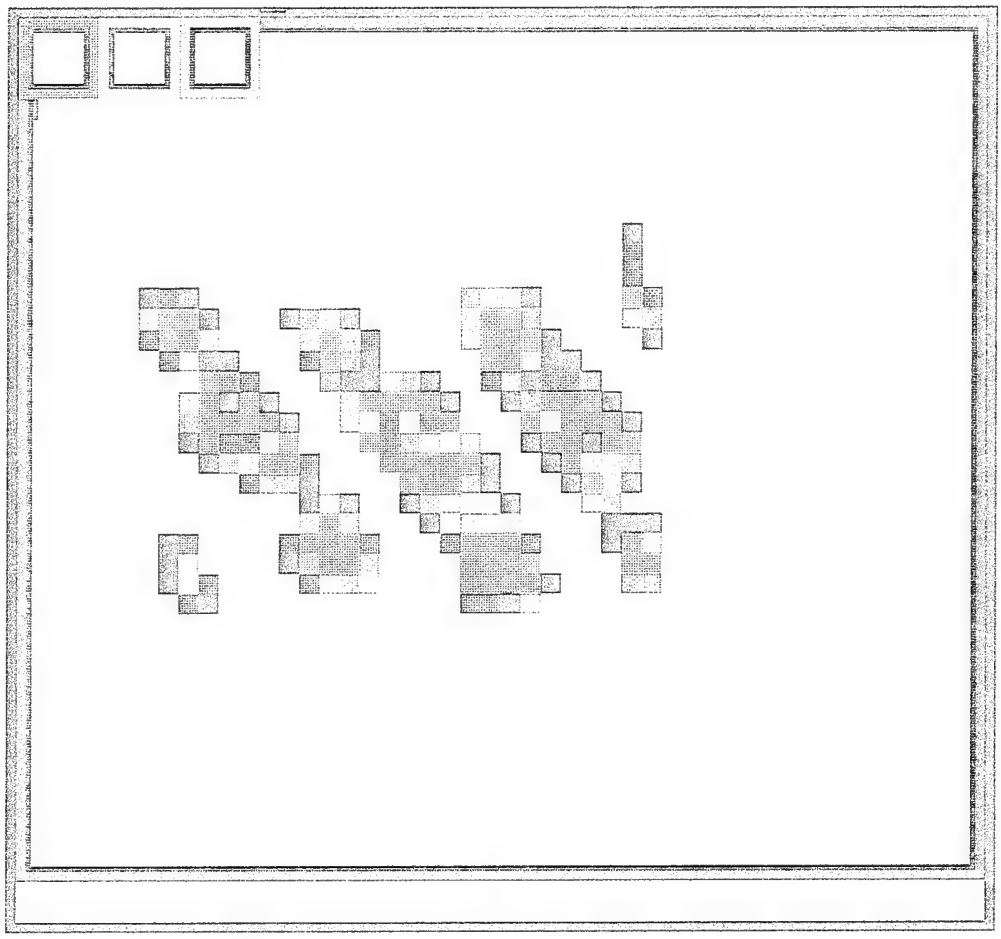

Key: 0.5 4.4 8.0 11.7 15.6 19.2 22.9 26.7 30.4 34.1 37.9 41.6 44.6 PSI

Figure 3-45. Stress distribution for 514-pound load at 89.5 degrees F.

```
Playback Window 1
     Machine_Name:
    Machine_Ident:
             Date: 04/06/94,13:45
Area = 28 sq inches
 Frame   27 of   31
File D:\DATA\WEIGHMAT\H4061449.FSX
Saved 04/06/17  13:52
```

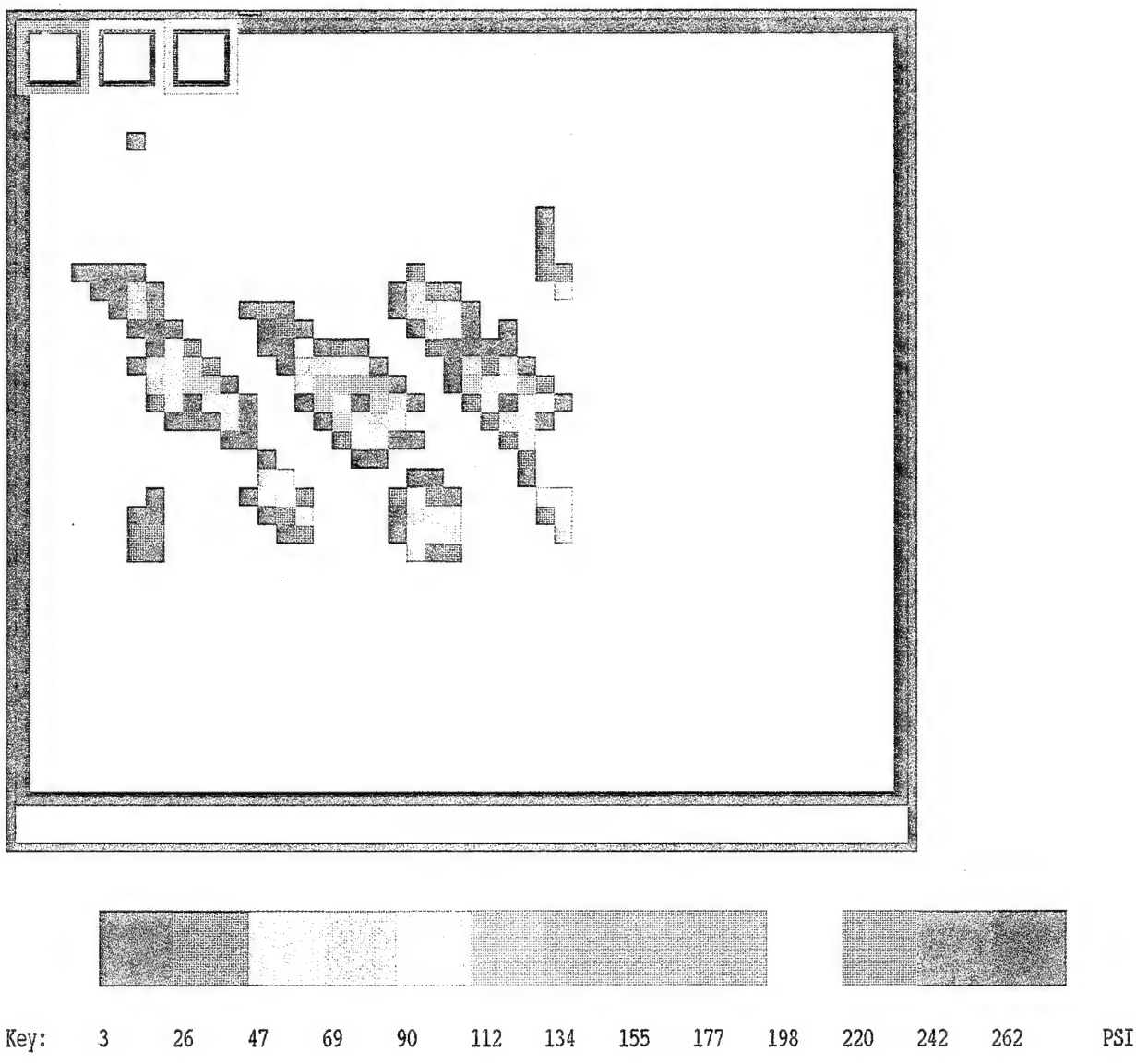

Key: 3 26 47 69 90 112 134 155 177 198 220 242 262 PSI

Figure 3-46. Stress distribution for 1213-pound load at -18.5 degrees F.

under 1213-lb. load at -18.5 degrees F is shown in Figure 3-46; the sensor is functioning significantly lower relative to saturation here.

The platen loading tests at room temperature involved three different positions on the sensor; we labeled them simply as Positions 1, 2, and 3. The three positions are shown in Figures 3-47, 3-48 and 3-49, respectively. Distances between the three loading positions were chosen so as to minimize the possibility of the tire lug locations staying in phase upon switching to either of the other positions. At lower and higher temperatures, the position on the sensor was constrained by the need to keep the door of the environmental chamber shut. That position was very close to Position 1.

All calibrations for the platen loading tests started with a previously generated equilibration file. All the equilibrations were performed at room temperature. The subsequent force calibrations were performed near the test temperature, with an applied load close to the maximum load used in the tests. (The only exception was a fatigue, memory and recovery test, with a train of pulses.) As with other calibrations for the laboratory data in this report, both equilibration and force calibration were established after 20 seconds at constant pressure or load.

The data on static creep from recordings which were analyzed in this way are summarized in Table 3-4. Where the data included recordings made with calibrations based on different equilibration pressures (there were three), the recording chosen involved an equilibration pressure roughly matching the applied load in that the recording with the highest load involved the highest equilibration pressure, the recording with the middle load involved the middle equilibration pressure, and the recording with the lowest load involved the lowest equilibration pressure. The standard error tabulated (last column in Table 3-4) reflects the effects of point scatter in the particular fit only and does not include effects of any systematic biases.

One of the features of the data is that *static creep is greater at lower loads*. This is brought out in Figure 3-50, in which the fitted static creep in percent per decade is plotted against the load, for different sensors at different temperatures. All show the same trend of greater static creep at lower loads.

The data taken around 90 degrees F show greater static creep even for the same load range (Figure 3-50). The difference is magnified further when comparing creep rates at loads corresponding to roughly the same degree of sensor saturation, such as the highest of the three loads at 90 degrees F to the corresponding highest loads at room temperature. The data taken around -19 degrees F show creep rates roughly in the same range as the room-temperature data, for the same loads. However, the same absolute loads are much lower when considered as relative to saturation, at -19 degrees F.

The data in Table 3-4 also provide some information on the repeatability of static creep rates when switching loading position on the sensor, and on variability from sensor to sensor. The recording file identifiers (fifth column in Table 3-4) all begin with the letter identifying the sensor. The greatest difference in creep rates upon changing loading position on the same sensor at roughly the same load was observed with Sensor O: 4.98 versus 3.21 percent per decade, a difference of 1.77 percent per decade. Averages of creep rates at maximum load at the three loading positions for the different sensors are as follows I:5.14, J:3.66, O:3.83, P:3.88, Q:4.49, and R:3.75 percent per decade. The biggest difference, approximately 1.5 percent per decade, is between Sensors I and J. However, part of this difference may have been due to more of the Sensor I data having been taken at a slightly higher temperature, in the range 78-80 F (Table 3-4). The data suggest that *differences in static creep rates on the order of one to two percent per decade at the same load level and*

```
Playback Window 2
     Machine_Name:
    Machine_Ident:
             Date: 04/11/94,10:52
Area = 42.72 sq inches
 Frame   26 of   31
File D:\DATA\WEIGHMAT\P4111058.FSX
Saved 04/11/17  10:56
```

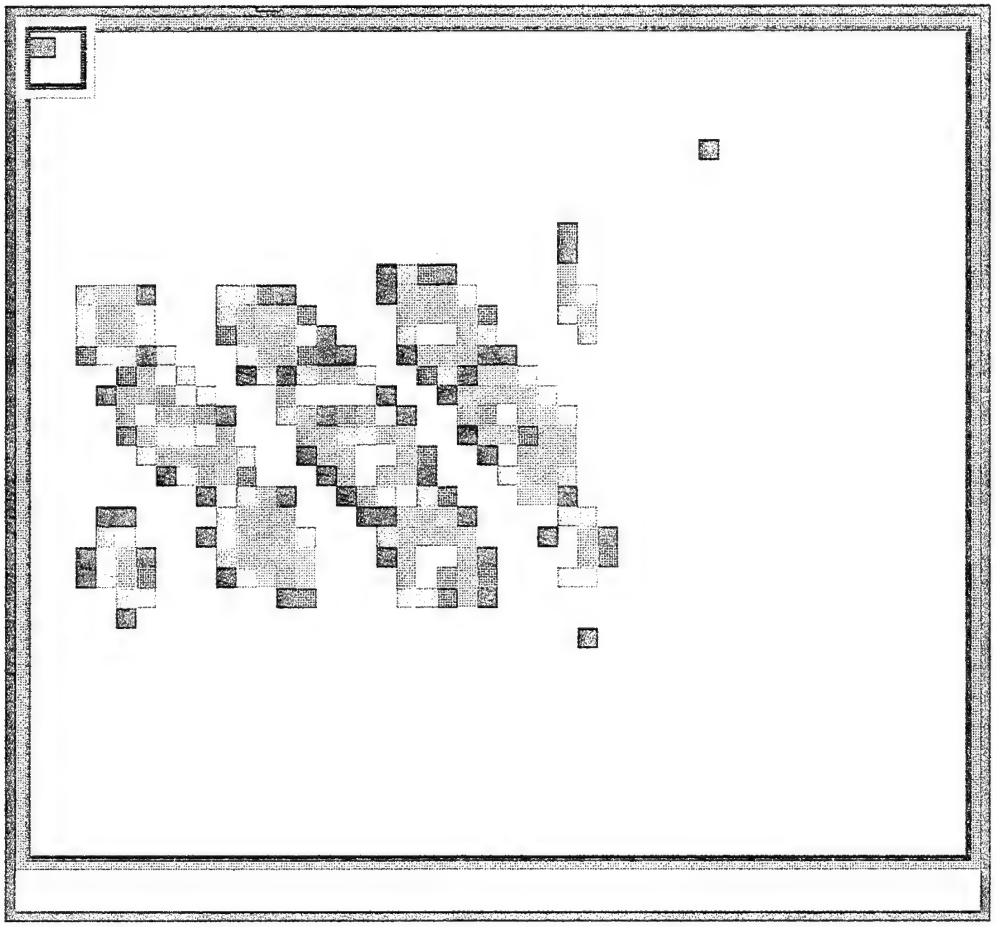

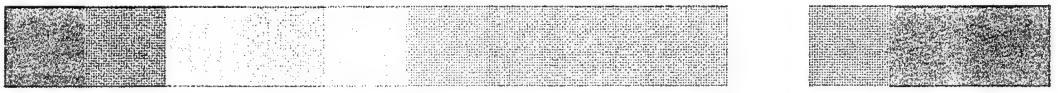

Key: 0.8 6.4 12.0 17.6 23.2 28.7 34.3 39.7 45.2 50.8 56.4 62.0 67.6 PSI

Figure 3-47. Position 1 on sensor.

```
Playback Window 1
     Machine_Name:
    Machine_Ident:
             Date: 04/11/94,09:45
Area = 44.48 sq inches
 Frame   26 of   31
File D:\DATA\WEIGHMAT\P4110958.FSX
Saved 04/11/17  09:56
```

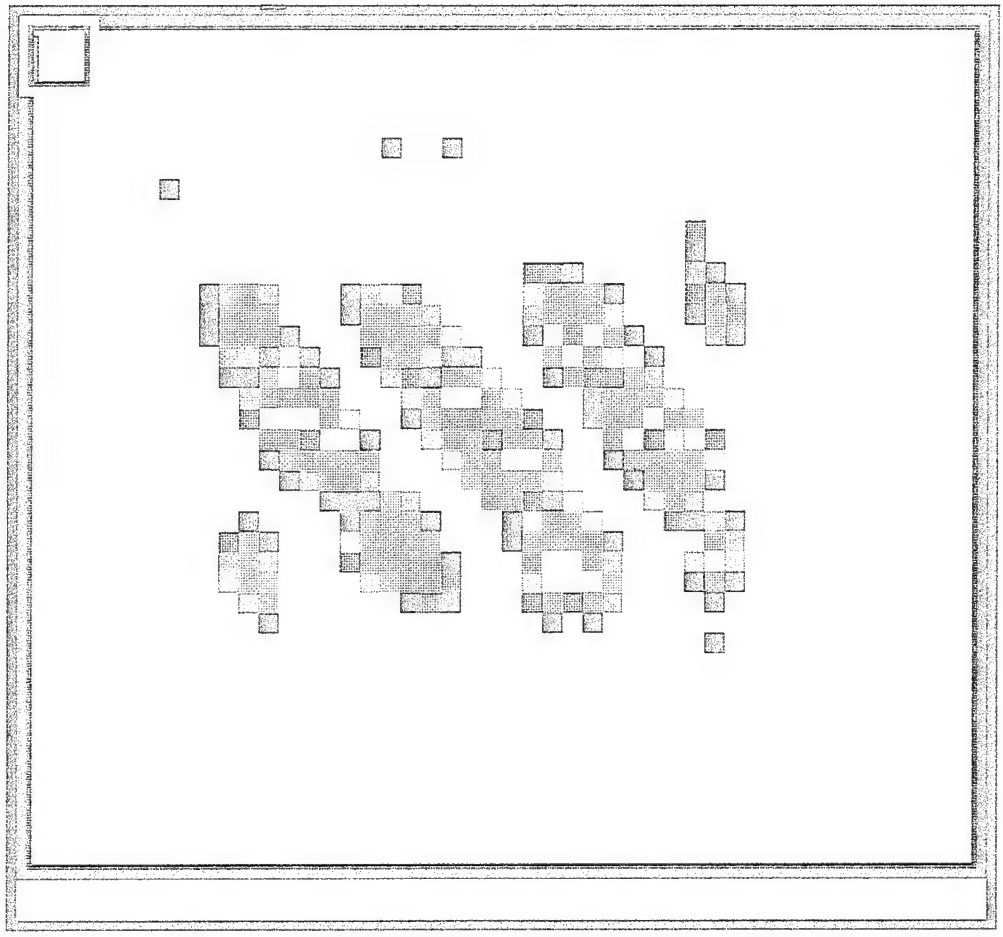

Key: 0.8 6.4 12.0 17.6 23.2 28.7 34.3 39.7 45.2 50.8 56.4 62.0 67.6 PSI

Figure 3-48. Position 2 on sensor.

```
Playback Window 1
     Machine_Name:
    Machine_Ident:
             Date: 04/11/94,12:09
Area = 44 sq inches
 Frame    26 of    31
File D:\DATA\WEIGHMAT\P4111214.FSX
Saved 04/11/17  12:12
```

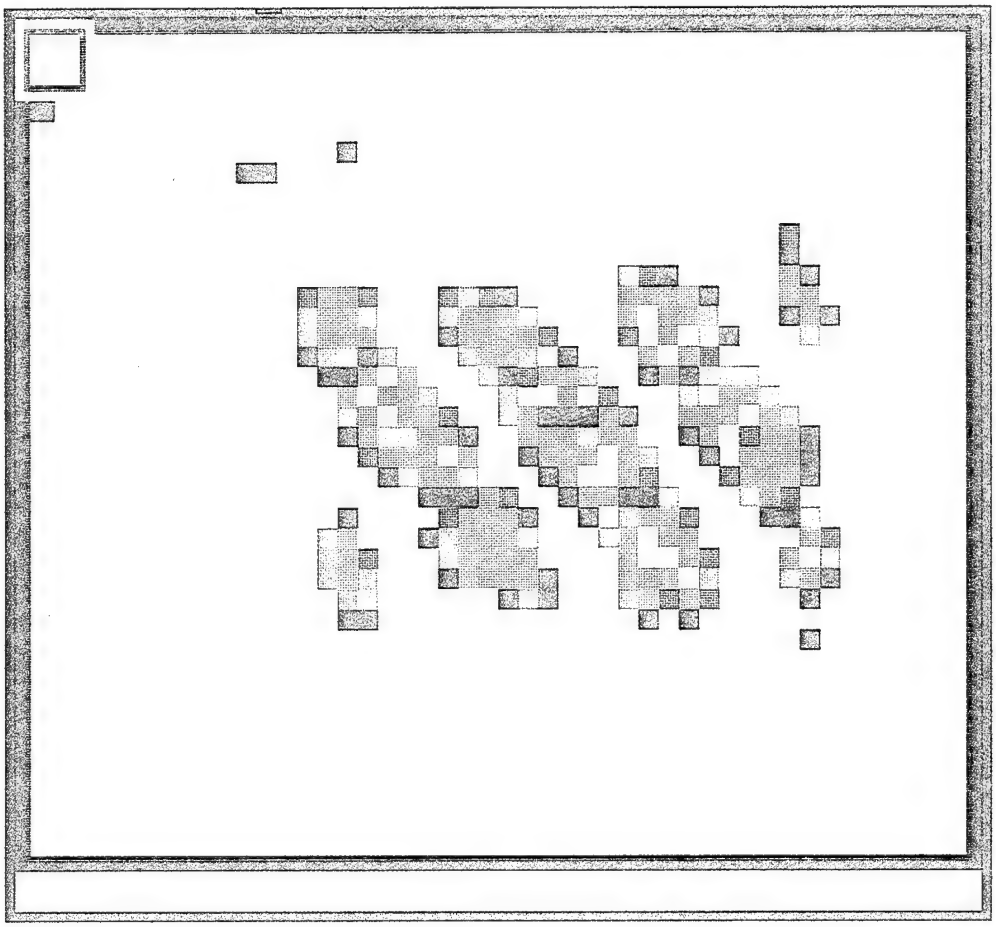

Key: 0.8 6.4 12.0 17.6 23.2 28.7 34.3 39.7 45.2 50.8 56.4 62.0 67.6 PSI

Figure 3-49. Position 3 on sensor.

Table 3-4. Static creep data summary.

Temperature, degrees F	Load, lbs.	Equilibration Calibration Pressure, psi	Platen Position on Sensor	Recording	Static Creep, percent per decade	Standard Error, percent per decade
-18.5	1213	70.0	1	H4061449	5.75	0.26
-18.6	772	45.0	1	H4061503	6.77	0.13
-18.7	342	19.5	1	H4061519	7.25	0.24
77.8	1201	70.0	1	I4071547	5.65	0.23
77.9	772	45.0	1	I4071601	6.25	0.08
78.0	344	19.0	1	I4071614	8.73	0.09
80.4	1200	70.0	2	I4071725	5.05	0.21
80.5	771	45.0	2	I4071734	6.66	0.14
80.4	343	19.0	2	I4071743	8.74	0.06
80.1	1200	70.0	3	I4071647	4.72	0.23
80.3	771	45.0	3	I4071658	5.59	0.13
80.4	343	19.0	3	I4071710	8.51	0.09
77.2	1201	70.5	2	J4081024	4.48	0.21
76.9	775	45.0	2	J4081037	6.01	0.08
76.6	340	19.5	2	J4081054	8.78	0.08
89.5	514	70.0	1	I4081607	9.64	0.12
89.7	343	45.0	1	I4081616	10.71	0.07
89.5	172	19.0	1	I4081629	11.52	0.42
73.3	1201	70.0	1	J4111041	3.46	0.24
73.4	1204	70.0	3	J4111145	3.05	0.22
72.4	1198	70.5	2	O4110943	3.29	0.20
73.2	1207	70.5	1	O4111051	4.98	0.23
73.4	1195	70.5	3	O4111200	3.21	0.20
72.9	1200	70.0	2	P4110958	3.96	0.22
73.2	1198	70.0	1	P4111058	3.95	0.20
73.5	1205	70.0	3	P4111214	3.72	0.19
72.9	1201	70.0	2	Q4111014	4.38	0.24
73.3	1194	70.0	1	Q4111105	4.96	0.25
73.6	1205	70.0	3	Q4111228	4.12	0.23
72.8	1199	70.0	2	R4111026	3.62	0.20
73.0	1205	70.0	1	R4111113	4.40	0.24
73.8	1200	70.0	3	R4111243	3.23	0.42
70-67	45psi*	45.0		M3220910	2.98**	0.02**
69.4-70.9	45psi*	45.0		M3221108	3.81	0.08
71.6	45psi*	45.0		M3221141	2.86	0.15

* These long-duration static creep data were obtained by uniform (pressure) loading See text for portions of sensor loaded.

** Only the first four points were included in this particular fit.

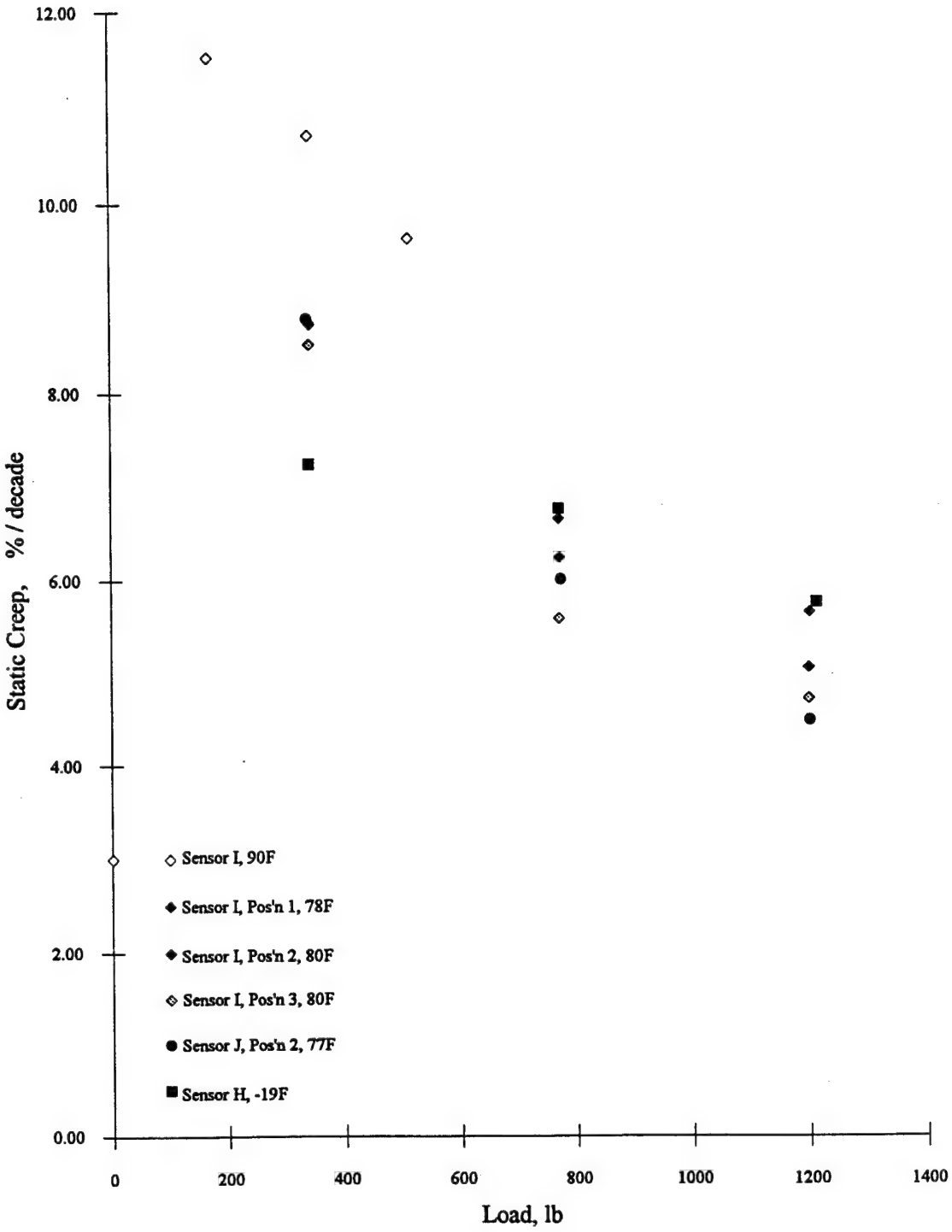

Figure 3-50. Static creep versus load.

under otherwise similar conditions should be expected.

Data on long-duration static creep were obtained from tests intended to check out possible static fatigue, using air bladder loading. Different portions of the sensor were loaded by varying the extent or reach of the sensor into the equilibration device. Loading of the sensor for the first recording taken in this way is shown in Figure 3-51. In the figure, the edge of the sensor inside the equilibration device is the lower edge of the green, while the upper edge is the edge of the air bladder in the equilibration device. The red box within the green area outlines the area over which the pressure was averaged, using the Tekscan software.

This 50,000-second (approximately 13.9-hour) recording ran overnight. The data are tabulated in Table 3-5 and plotted in Figure 3-52, in which the Tekscan graph is also shown, at the top. Unfortunately, the effects of static creep are ambiguous with the effects of temperature here. The temperature was not monitored overnight, but it was known to decrease as the air conditioner caught up in the evening, especially after the people left and the lights were turned off, shortly after starting this recording. Starting temperature was 69.6 degrees F. Next morning (9 AM) it was 68.5 F, but it had probably been lower during the night. Around 70 degrees F, the effect of temperature on sensitivity is approximately 1.1 percent per degree F. The first four points in Figure 3-52, which cover roughly the first seventeen minutes of this recording, give a slope of approximately 3.0 percent per decade. This is not out of range of the creep rates observed in tests with 25- to 26-second durations (Table 3-4).

For the next recording, the sensor was inserted further into the equilibration device; the portion loaded is shown in Figure 3-53. The sensor area loaded previously had only a couple of minutes at zero pressure to recover from the effects of the previous test. The outline of the blue box is the same as of the red box in Figure 3-51. Thus, the blue box outlines the same part of the sensor as was used to generate the data from the previous recording. The red box outlines the area of the sensor over which the pressure is averaged for the part of the sensor not loaded previously. Sensor edges and the air bladder edge (at the top in Figure 3-53) are avoided. The two sensor rows in between the boxes are excluded from pressure averaging in order to avoid the effects of a possible overload or a slight crease in the sensor active area imparted by the edge of the air bladder in the previous test.

The data from this 5000-second (approximately 1.4-hour) recording are tabulated in Table 3-6. The factor of increase in indicated pressure was normalized to the initial indicated output in the area *not* loaded previously, for both areas. The data are plotted in Figure 3-54; the Tekscan graph is included at the top in the figure. In the semilog plot, the filled triangles are for the area not loaded previously. A fit gives a static creep rate of 3.8 percent per decade (Table 3-4). The unfilled triangles are for the area loaded previously. These show the effects of memory of prior loading. (Recall that this area experienced only a couple of minutes at zero pressure after being loaded for nearly 14 hours.) The sensitivity starts out a bit higher but there is a trend toward convergence as the load duration increases.

During this test, the temperature increased by 1.5 degree F. Correction for this effect brings the static creep (in the area not loaded previously) from 3.8 percent per decade to approximately 3 percent per decade.

For the third long-duration recording, the sensor was again inserted further into the equilibration device. The portion loaded is shown in Figure 3-55. This time, the sensor areas loaded previously had approximately 12 minutes at zero pressure. The outline of the blue box is again the same as of the red box in Figure 3-51. The red box again outlines the area of the sensor over which the pressure is averaged for the part of the sensor not loaded previously. This time, the indicated pressure in the two areas were, for all practical

```
Playback Window 1
     Machine_Name:
    Machine_Ident:
             Date: 03/21/94,18:11
Area = 115.2 sq inches
 Frame    1 of 1001
File D:\DATA\WEIGHMAT\M3220910.FSX
Saved 03/22/17  09:13
```

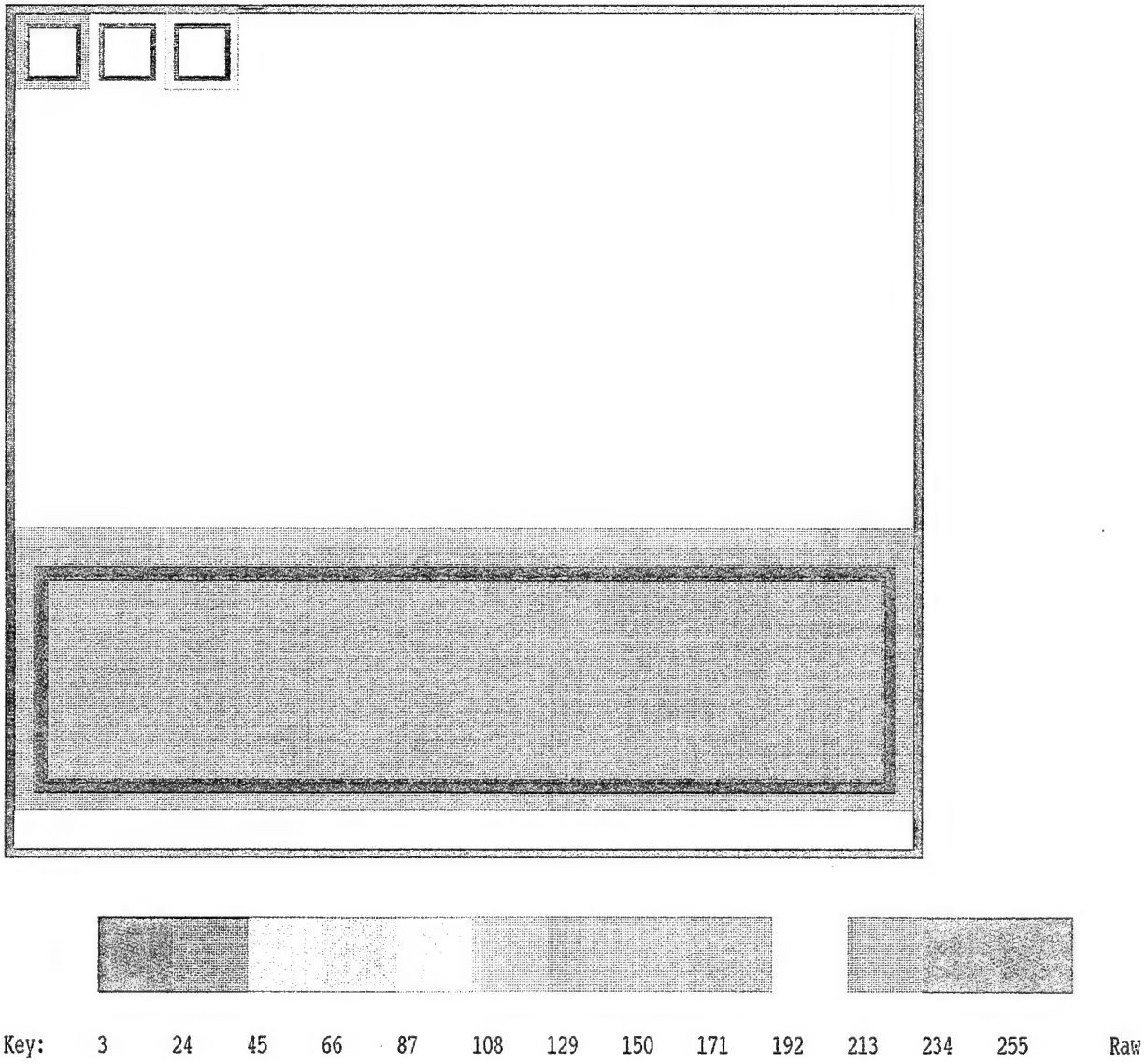

Key: 3 24 45 66 87 108 129 150 171 192 213 234 255 Raw

Figure 3-51. First recording of long duration static creep test.

Table 3-5. Long-duration static creep, 70-67 degrees F, 40.5-44.7 psi, sensor M.

Equilibration calibration pressure: 45.0 psi
Equilibration calibration temperature: 69.6 degrees F
Calibration file: M45P696
Recording: M3220910

Time From Start of Recording, sec	Approx. Time From Start of Pressure, lbs.	Indicated Pressure, digital output	Factor of Increase in Indicated Pressure
0	330	167	1.000
200	530	168	1.006
500	830	169	1.012
1000	1330	170	1.018
2000	2330	171	1.024
3000	3330	171	1.024
4000	4330	171	1.024
5000	5330	172	1.030
6000	6330	172	1.030
8000	8330	172	1.030
10000	10330	173	1.036
12000	12330	173	1.036
15000	15330	173	1.036
17000	17330	173	1.036
20000	20330	173	1.036
22000	22330	173	1.036
25000	25330	173	1.036
30000	30330	172	1.030
35000	35330	171	1.024
40000	40330	169	1.012
45000	45330	169	1.012
50000	50330	171	1.024

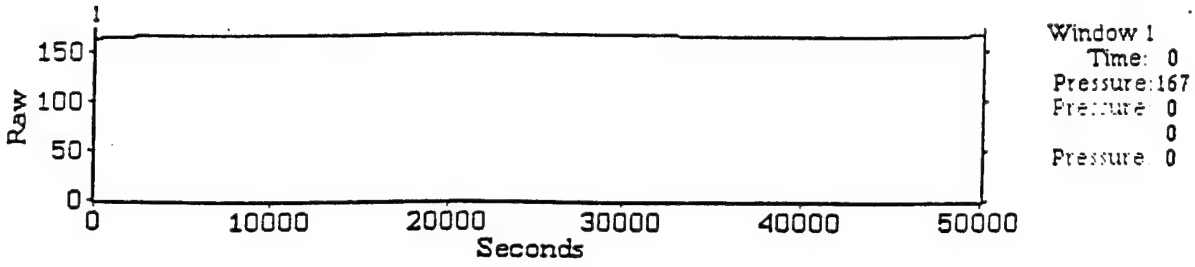

COMMENTS:
M3220910

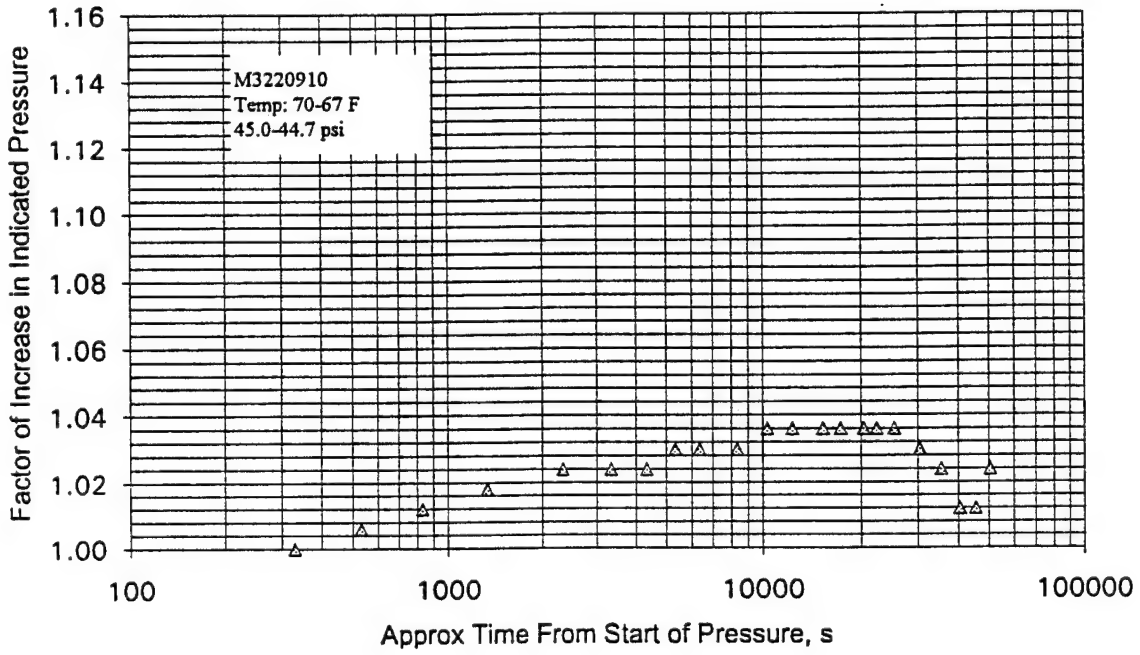

Figure 3-52. Long-duration static creep. The creep data in this plot are ambiguous with the effects of temperature.

```
Playback Window 1
     Machine_Name:
    Machine_Ident:
             Date: 03/22/94,09:36
Area = 184.32 sq inches
 Frame    1 of 1001
File D:\DATA\WEIGHMAT\M3221108.FSX
Saved 03/22/17  11:13
```

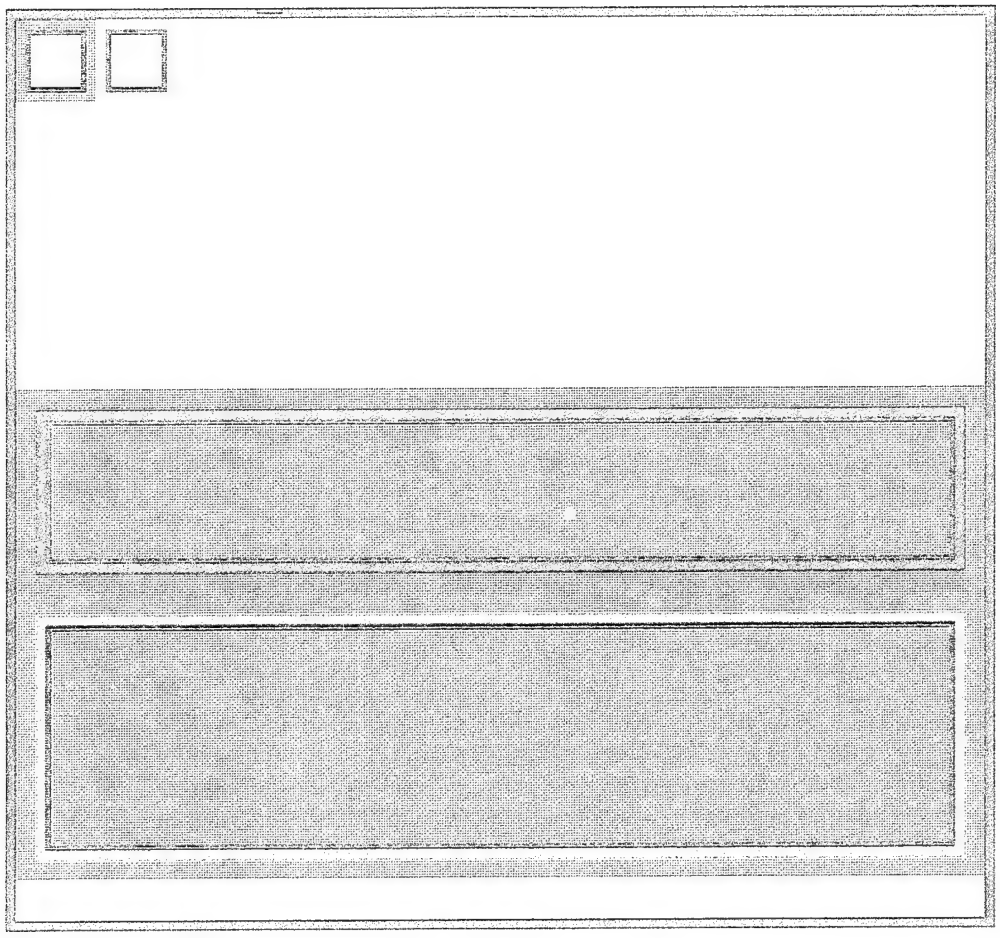

Key: 3 24 45 66 87 108 129 150 171 192 213 234 255 PSI

Figure 3-53. Second recording of long duration static creep test.

Table 3-6. Long-duration static creep, 69.4-70.9 degrees F, 45 psi, sensor M.

Equilibration calibration pressure: 45.0 psi
Equilibration calibration temperature: 69.6 degrees F
Calibration file: M45P696
Recording: M3221108

Time From Start of Recording, sec	Approx. Time From Start of Pressure, lbs.	Indicated Pressure, Digital Output: Area Not Loaded Previously	Indicated Pressure, Digital Output: Area Loaded Previously	Factor of Increase in Indicated Pressure: Area Not Loaded Previously	Factor of Increase in Indicated Pressure: Press. in Area Loaded Previously/154
0	140	154	159	1.000	1.032
50	190	155	159	1.006	1.032
100	240	155	160	1.006	1.039
200	340	156	160	1.013	1.039
300	440	157	160	1.019	1.039
400	540	157	161	1.019	1.045
500	640	158	161	1.026	1.045
600	740	158	161	1.026	1.045
800	940	159	162	1.032	1.052
1000	1140	159	162	1.032	1.052
1200	1340	160	162	1.039	1.052
1500	1640	160	162	1.039	1.052
1700	1840	160	163	1.039	1.058
2000	2140	161	163	1.045	1.058
2200	2340	161	163	1.045	1.058
2500	2640	161	163	1.045	1.058
3000	3140	162	164	1.052	1.065
3500	3640	162	164	1.052	1.065
4000	4140	163	164	1.058	1.065
4500	4640	163	165	1.058	1.071
5000	5140	163	165	1.058	1.071

Graph

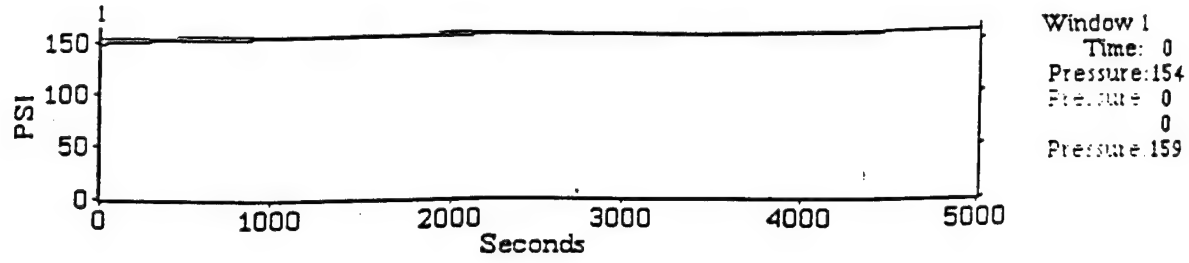

COMMENTS:
M3221108

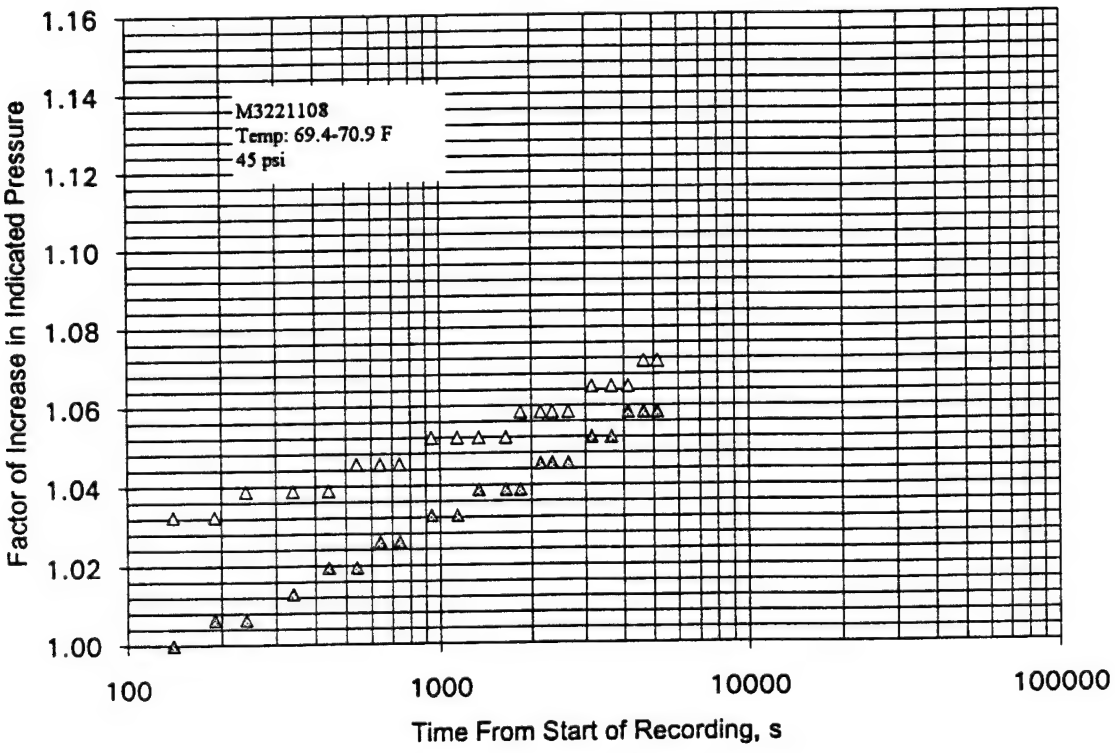

Figure 3-54. Long-duration static creep.

```
Playback Window 1
     Machine_Name:
    Machine_Ident:
             Date: 03/22/94,11:14
Area = 261.12 sq inches
 Frame    1 of 1001
File D:\DATA\WEIGHMAT\M3221141.FSX
Saved 03/22/17  11:47
```

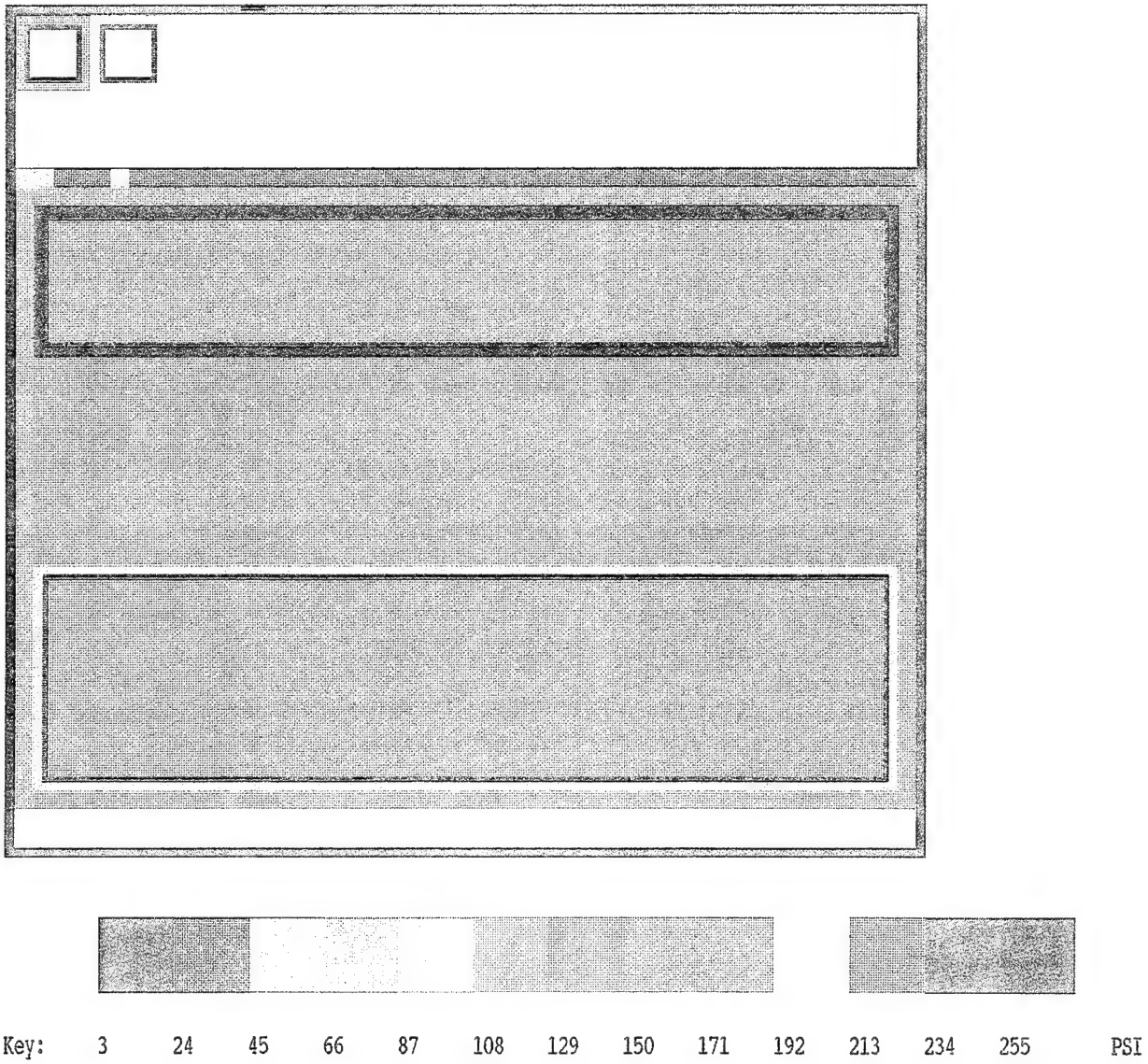

Key: 3 24 45 66 87 108 129 150 171 192 213 234 255 PSI

Figure 3-55. Third recording of long duration static creep test.

purposes, coincident throughout the 500-second (8.3-minute) recording, differing at most by one in the last significant digit. Thus, only the indicated pressure from the area not loaded previously (red box in Figure 3-55) is tabulated in Table 3-7 and plotted in Figure 3-56. A fit gives a slope of approximately 2.9 percent per decade (Table 3-4), consistent with the other creep tests involving this sensor.

Because of the ambiguities with effects of temperature in the 14-hour recording, effective investigation of long-duration static creep was limited to approximately 1.4 hours (83 minutes). Except for possible overload or a slight crease in the sensor active area imparted by the *edge* of the air bladder, *permanent* fatigue effects of long-duration static loading were not observed. Investigation of shorter duration static creep did not extend to times less than 1 second, and data fitting was limited to times greater than 3 seconds from load application.

3.5.2 Hysteresis.

3.5.2.1 Hysteresis With Uniform Loading; 20-Second Plateaus. Loading was by means of the air bladder equilibration device. The entire area of the sensor was loaded. However, the averaging area for the indicated pressure was chosen to exclude the last sensor rows and columns around the edges, to avoid possible effects of imperfect centering of the sensor in the equilibration device. The pressure was adjusted manually by means of a regulator.

The loading cycle was as follows. The pressure was increased from zero gage pressure to 20 psi and held for 20 seconds, then increased to 45 psi and held for 20 seconds, then increased to 70 psi and held for 20 seconds, then decreased to 45 psi and held for 20 seconds, then decreased to 20 psi and held for 20 seconds, and finally back to zero. Timing was coordinated between the regulator operator who also monitored the pressure, and the Tekscan operator so that the stabilization of each pressure as well as the end of each plateau could be correlated with the time scale on the Tekscan recording. Sample Tekscan pressure-time history shapes are shown in Figures 3-57 and 3-58. The pressure regulator operator was consistently successful in preventing overshoot upon increasing the pressure, but control of overshoot while reducing pressure was much more difficult. Signs of overshoot in reducing pressure can be seen in Figure 3-58.

Hysteresis data with uniform loads were taken at low temperatures, around 40 degrees F, 20 degrees F, and -24 degrees F as well as room temperature (69 degrees F in this case), but not at higher temperatures. The calibration file used in all cases was generated at room temperature. This started with equilibration at 70 psi, followed by a force calibration under uniform load at 70 psi.

The results for the hysteresis tests with uniform loading are summarized in Table 3-8 and plotted in Figures 3-59 through 3-62. In these plots, the vertical scales (applied pressure) are all the same, but the horizontal scales (indicated pressure) were adjusted so that a line drawn from the origin to the start of the highest pressure plateau makes a 45-degree angle. This makes it easier to visualize and compare hysteretic effects as percentages of indicated pressure or load. There appears to be no clear trend of change in hysteresis with temperature, over this temperature range.

It is evident both from Table 3-8 and from the figures that the percent increases in indicated pressure during the main plateau and the *loading* plateaus are greater at lower pressures. This is consistent with the observation in the static creep tests with platen loading that static creep is greater at lower loads (Figure 3-50). Also, there appears to be no clear trend in the effect of temperature on the percent increases in indicated load during the loading plateaus and the main plateau (Table 3-8) over this temperature range. This, too, is consistent with the observation in the static creep tests with platen loading that the creep rates near -19 F

Table 3-7. Long-duration static creep, 71.6 degrees F, 45 psi, sensor M.

Equilibration calibration pressure: 45.0 psi
Equilibration calibration temperature: 69.6 degrees F
Calibration file: M45P696
Recording: M3221141

Time From Start of Recording, sec	Approx. Time From Start of Pressure, lbs.	Indicated Pressure, digital output	Factor of Increase in Indicated Pressure
0	70	154	1.000
5	75	154	1.000
10	80	154	1.000
20	90	155	1.006
30	100	155	1.006
40	110	155	1.006
50	120	155	1.006
60	130	155	1.006
80	150	156	1.013
100	170	156	1.013
120	190	156	1.013
150	220	156	1.013
170	240	157	1.019
200	270	157	1.019
220	290	157	1.019
250	320	157	1.019
300	370	157	1.019
350	420	157	1.019
400	470	158	1.026
450	520	158	1.026
500	570	158	1.026

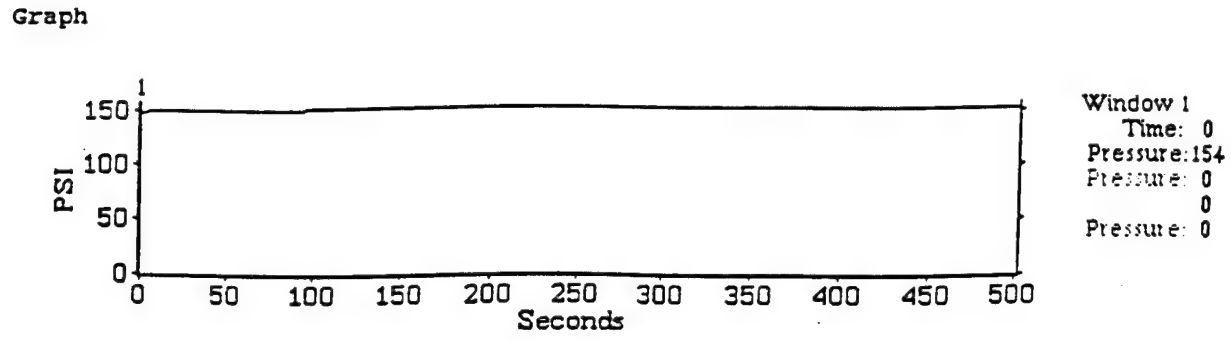

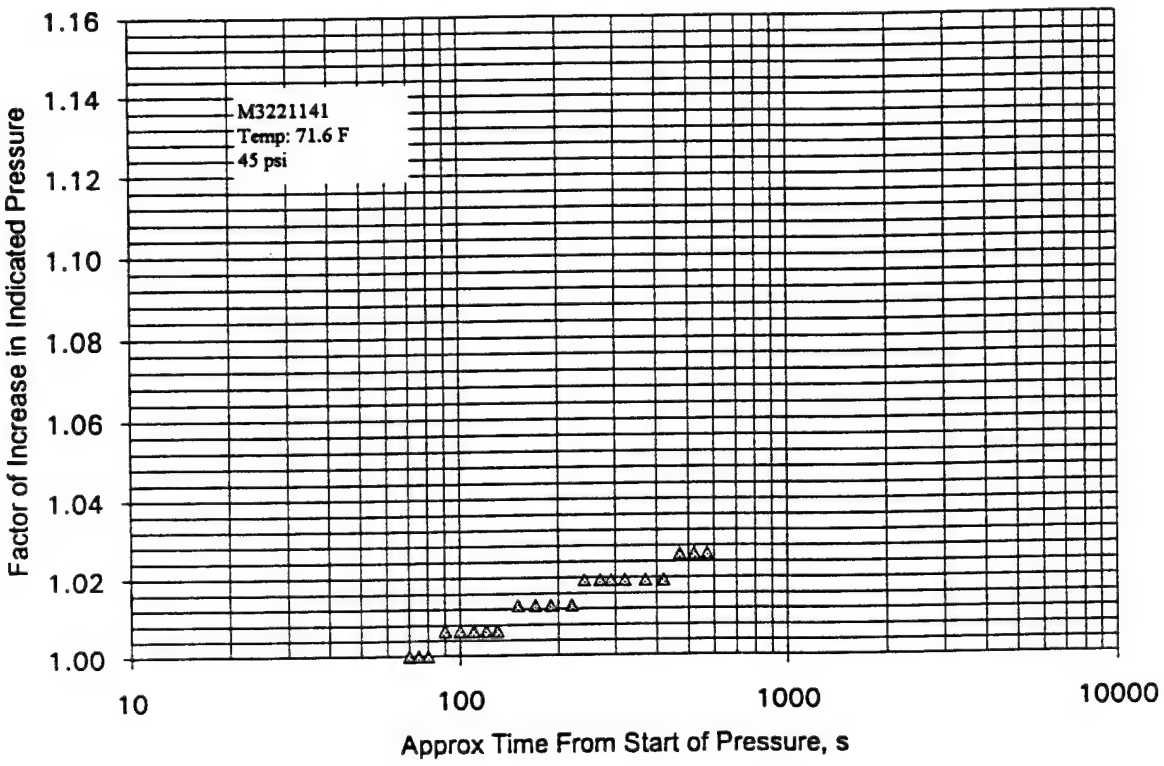

Figure 3-56. Long-duration static creep.

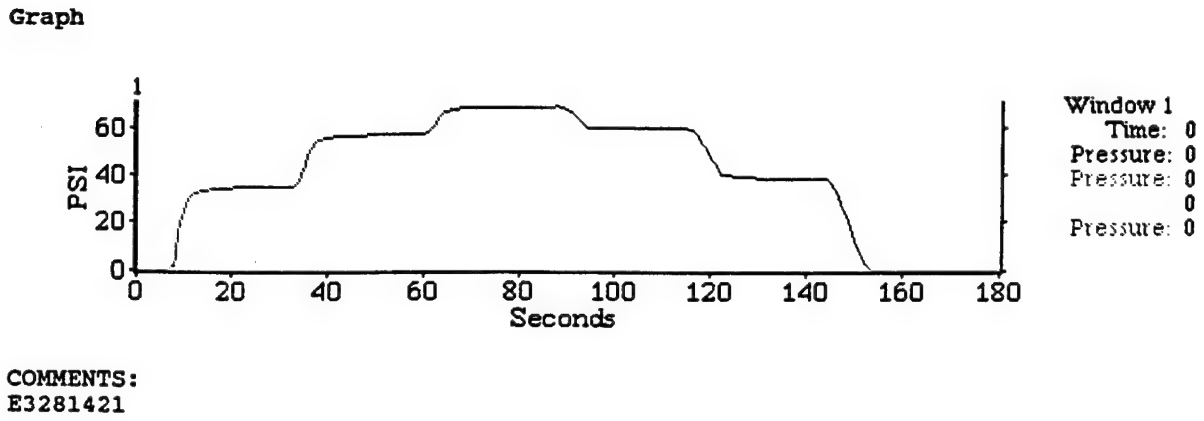

Figure 3-57. Hysteresis time histories from bladder loading.

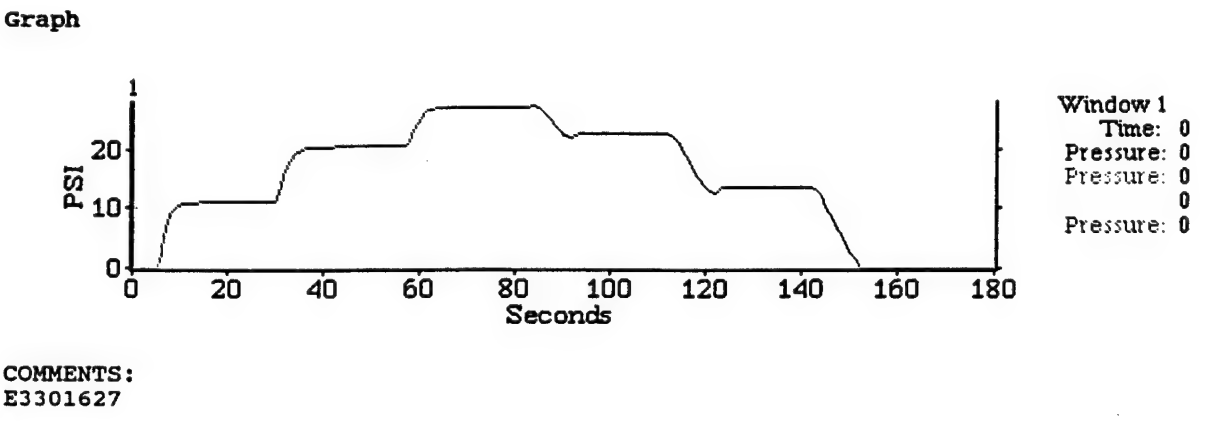

Figure 3-58. Hysteresis time histories from bladder loading.

Table 3-8. Hysteretic behavior, uniform loading.

Applied Pressure (psi)	E3281421 Temperature: 69.1 F Time (sec)	Indic'd Press. (psi)	Final / Init'l Indic'd Press.	E3291356 Temperature: 40.3 F Time (sec)	Indic'd Press. (psi)	Final / Init'l Indic'd Press.	E3291648 Temperature: 19.7 F Time (sec)	Indic'd Press. (psi)	Final / Init'l Indic'd Press.	E3301627 Temperature: -24.1 F Time (sec)	Indic'd Press. (psi)	Final / Init'l Indic'd Press.
0	7	0		8	0		5	0		5	0	
20	13	34.4		15	27.2		10	19.8		10	11	
20	33	36.8	1.070	35	28.9	1.062	30	21.2	1.070	30	11.8	1.073
45	41	58.4		42	45.0		35	33.5		37	21.1	
45	60	59.8	1.024	62	46.3	1.029	55	34.5	1.030	57	21.6	1.024
70	68	71.1		70	56.1		61	41.9		64	28.1	
70	88	71.8	1.010	90	56.7	1.011	81	42.7	1.019	84	28.4	1.011
45	96	62.8		97	48.7*		88	36.4		92	23.1*	
45	115	62.5	0.995	117	49.1	1.008	108	36.2	0.995	112	23.7	1.026
20	124	42.0		127	33.3†		117	22.1		122	13.3†	
20	144	40.1	0.955	146	33.0	0.991	137	20.7	0.937	142	14.3	1.075
0	157	0		158	0		148	0		153	0	

*max 49.1 @ 99-117
†max 33.5 @ 128-131
Above initial lows were caused by dips (overshoot) in reducing pressure

*max 23.7 @ 96-112
†max 14.3 @ 125-142
Above initial lows were caused by dips (overshoot) in reducing pressure

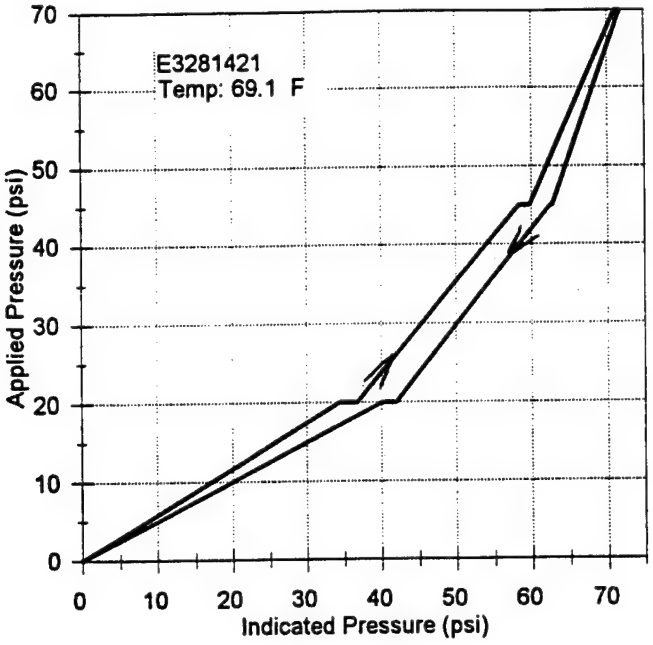

Figure 3-59. Hysteresis from uniform loading.

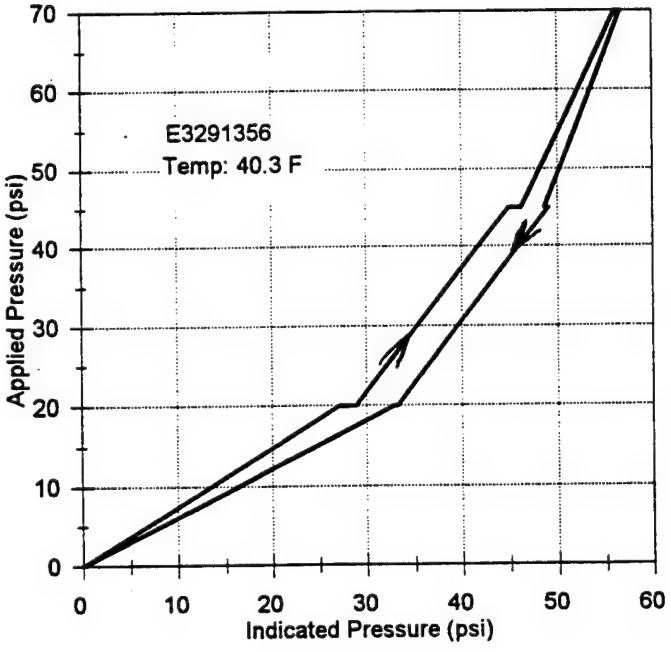

Figure 3-60. Hysteresis from uniform loading.

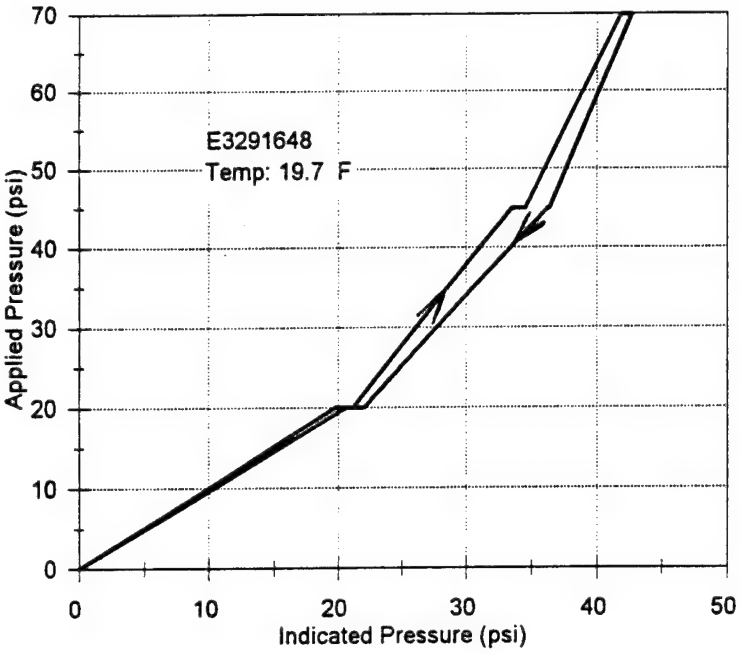

Figure 3-61. Hysteresis from uniform loading.

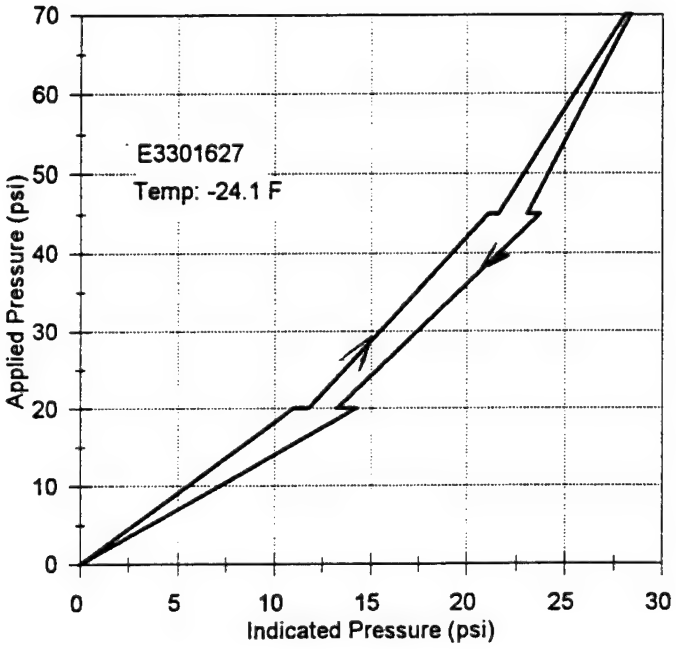

Figure 3-62. Hysteresis from uniform loading.

were not very different from creep rates at room temperature for the same loads. (However, higher creep rates were observed at 90 F.) The backwards plateaus in the *unloading* portions in Figures 3-60 and 3-62 arise from the effects of overshoot in reducing pressure, as in Figure 3-58.

3.5.2.2 Hysteresis Tests With Platen Loading; Half-Second and One-Second Plateaus. The loading pulses for hysteresis tests with platen loading with the tire tread were programmed as a series of abrupt steps, each with duration x, three of these rising to a maximum, followed by two downward steps back to zero load. Most of the sensors in these tests were tested with both 1/2-second plateaus (x=0.5) and 1-second plateaus (x=1). Due to loading machine limitations, each actual rise and fall in applied load was not totally abrupt. It took on the order of 0.1 second to approach close to the full load, and a constant value was reached in approximately a total of 0.4 second. Sample recordings of *indicated* load are shown in Figures 3-63 and Figure 3-64.

At each step or plateau, values of applied load were read off the loader's oscilloscope screen, one to each plateau, and correlated with approximate time as displayed by the horizontal position on the scope screen. Because of greater variation of load with time (greater slopes at the early parts of the plateaus), the data from the tests with the 1/2-second plateaus are not as accurate as the data from tests with the 1-second plateaus.

Calibrations for these tests were performed in the same way as in the platen loading tests of static creep. These started with equilibration files generated at room temperature. For all these tests, the equilibration pressure was 70 psi. This was followed by a force calibration at or near test temperature, with an applied load close to the maximum load used in the test. As with other calibrations for the laboratory data in this report, both the equilibration and force calibration were established after 20 seconds at constant pressure or load.

The results are summarized in Table 3-9 and plotted in Figures 3-65 through 3-78. Where there was significant uncertainty in correlating the applied load with the indicated load (indicated by the series of numbers preceded by question marks in Table 3-9), their median or sometimes average value was plotted.

Comparing the plots of data from recordings with 1/2-second plateaus with data plots from recordings with 1-second plateaus with the same sensor under otherwise the same test conditions shows no clear difference. Evidently, the factor of two difference in durations is not enough to resolve a difference in hysteresis. Uncertainties in matching loads and times, especially in the tests with 1/2-second plateaus, may be part of the reason. Similarly, no clear differences appear when comparing the results at -18.5 degrees F (Figure 3-65) and 89.6 F (Figures 3-67 and 3-68) to the results obtained in tests at room temperature.

Comparing the results of the hysteresis tests with platen loading to the much longer-duration tests with uniform loading (Figures 3-59 through 3-62) brings out the significantly greater upward concavity (nonlinearity) in the longer-duration tests. The tests with uniform (pressure) loading involved not only much longer (20-second) plateaus but also longer rise times, as it typically took about 10 seconds before the first or any next subsequent plateau pressure was reached. Thus, the tests with pressure loading were much more subject to the influence of static creep, which has been observed to be significantly greater at lower pressures and lower loads. Greater percent increases in the lower indicated pressures or loads tend to increase upward concavity in plots of applied versus indicated pressure or load. Thus, the degree of nonlinearity also depends on the rate of load application, in tests of this kind.

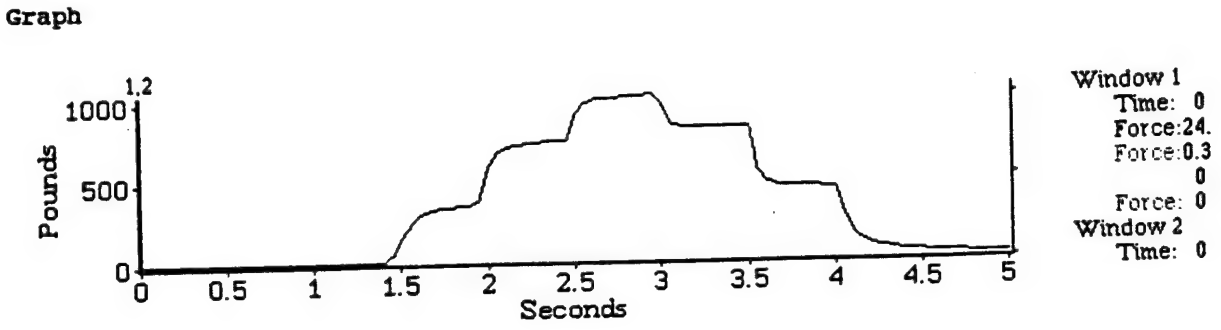

Figure 3-63. Hysteresis time history from platen loading - 1/2-second plateaus.

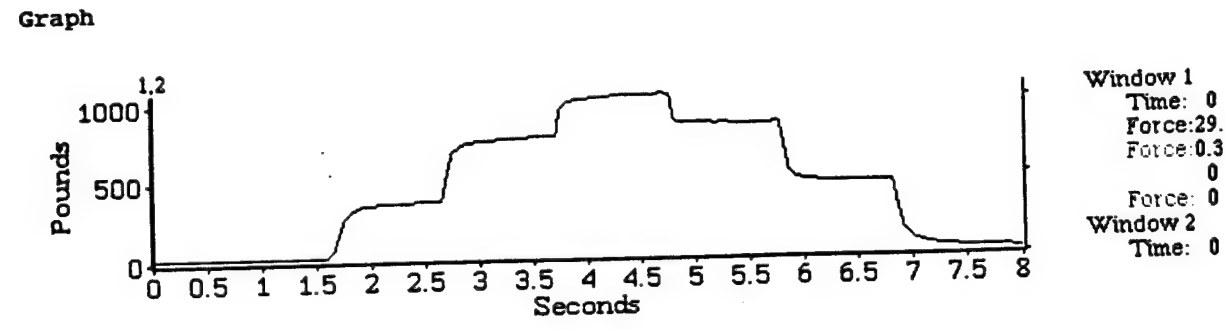

Figure 3-64. Hysteresis time history from platen loading - 1-second plateaus.

Table 3-9. Hysteretic behavior, platen loading.

Sensor	H
Calfile	H700-19
Temp	-18.5
Preload	0
Recording	H4061321
1 sec plateaus	
Applied Load	Indicated Load
0	0
340	346
760	726
1170	1060
760	817
340	412
0	0

Sensor	I
Calfile	I70075
Temp	75
Preload	22.6
Recording	I4070932
1-sec plateaus	
Applied Load	Indicated Load
0	0
350	406
810	817
1212	1120
820	910
350	520
0	0

Sensor	I
Calfile	I70089
Temp	89.6
Preload	15
Recording	I4081722
1/2 sec plateaus	
Applied Load	Indicated Load
0	0
139	139
329	319
508	457
349	364
149	205
0	0

Sensor	I
Calfile	I70089
Temp	89.6
Preload	9.7
Recording	I4081730
1-sec plateaus	
Applied Load	Indicated Load
0	0
144	152
340	331
512	468
351	373
160	206
0	0

Sensor	J
Calfile	J70578
Temp	73.5
Preload	29.3
Recording	J4111138
1/2-sec plateaus	
Applied Load	Indicated Load
0	0
326	367
784	777
1196	1060
804	861
362	473
0	0

Sensor	J
Calfile	J70578
Temp	73.1
Preload	29.2
Recording	J4111131
1-sec plateaus	
Applied Load	Indicated Load
0	0
343	394
808	810
1212	1090
808	885
364	486
0	0

Sensor	O
Calfile	O70073
Temp	73.5
Preload	6.4
Recording	O4111153
1/2 sec plateaus	
Applied Load	Indicated Load
0	0
331	360
763	763 ?71877467763
1184	1090
803	902 ?897?908
361	511 ?502?520
0	0

Sensor	O
Calfile	O70073
Temp	73.8
Preload	12.3
Recording	O4111157
1 sec plateaus	
Applied Load	Indicated Load
0	0
327	380
793	835
1204	1130
803	925
341	502
0	0

Sensor	P
Calfile	P70073
Temp	73.7
Preload	27.4
Recording	P4111212
1/2 sec plateaus	
Applied Load	Indicated Load
0	0
333	387
788	810 ?807?814
1192	1110
808	920 ?922?919
364	520 ?529?520?516
0	0

Sensor	P
Calfile	P70073
Temp	73.4
Preload	25.6
Recording	P4111208
1 sec plateaus	
Applied Load	Indicated Load
0	0
341	396 ?39073967401
787	844
1204	1150
803	948
361	530
0	0

Sensor	Q
Calfile	Q70073
Temp	73.5
Preload	36.8
Recording	Q4111222
1/2 sec plateaus	
Applied Load	Indicated Load
0	0
341	395
783	823
1204	1110
823	918
361	516
0	0

Sensor	Q
Calfile	Q70073
Temp	73.6
Preload	38.8
Recording	Q4111225
1 sec plateaus	
Applied Load	Indicated Load
0	0
343	405
798	837
1212	1120
808	930
364	517
0	0

Sensor	R
Calfile	R70073
Temp	73.5
Preload	15.2
Recording	R4111239
1/2 sec plateaus	
Applied Load	Indicated Load
0	0
324	356
791	788
1196	1100
800	890
345	490
0	0

Sensor	R
Calfile	R70073
Temp	73.6
Preload	14.3
Recording	R4111236
1 sec plateaus	
Applied Load	Indicated Load
0	0
333	372 ?364737073747378
788	806 ?80278067811
1212	1130
808	922
354	504
0	0

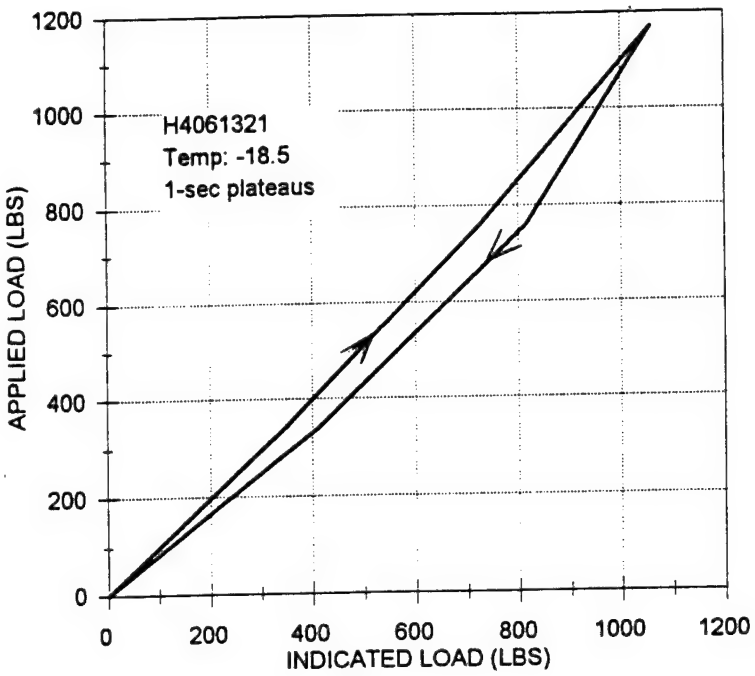

Figure 3-65. Hysteresis from platen loading.

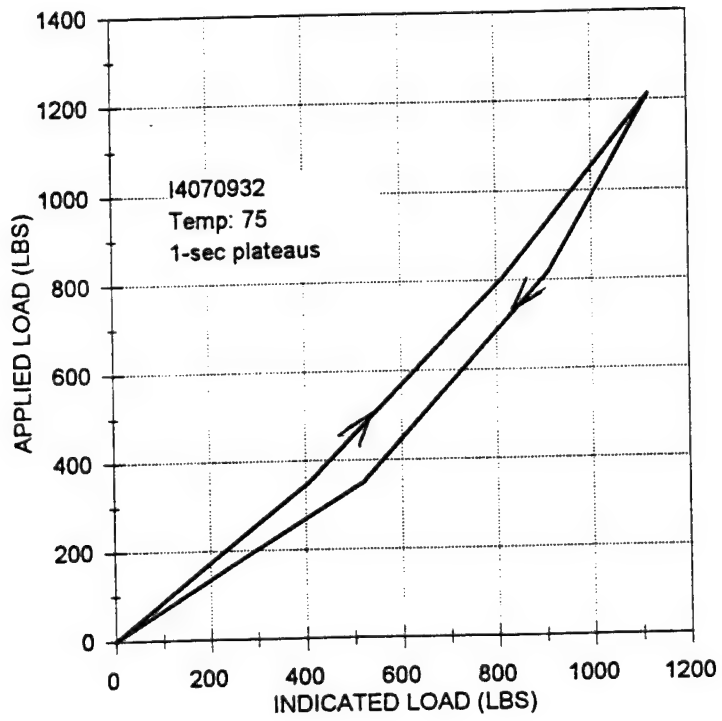

Figure 3-66. Hysteresis from platen loading.

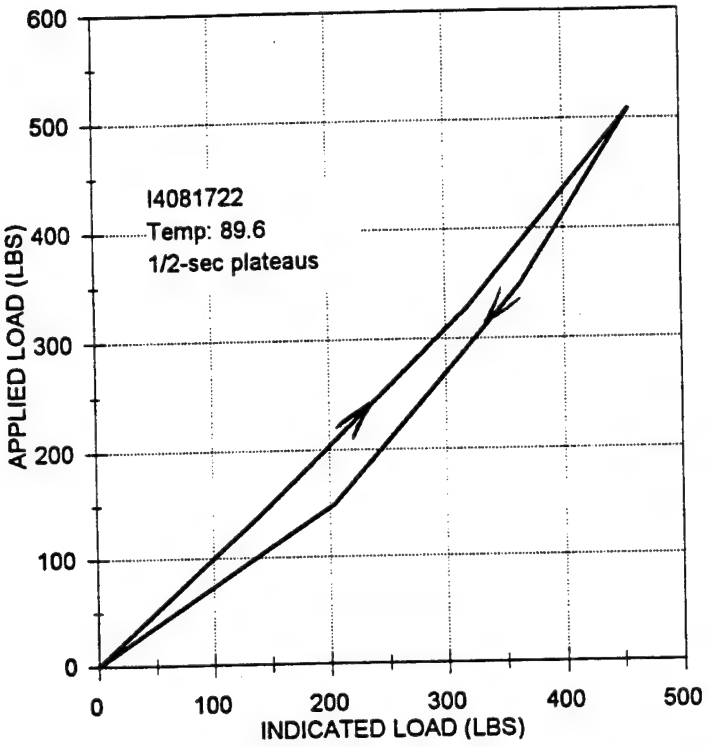

Figure 3-67. Hysteresis from platen loading.

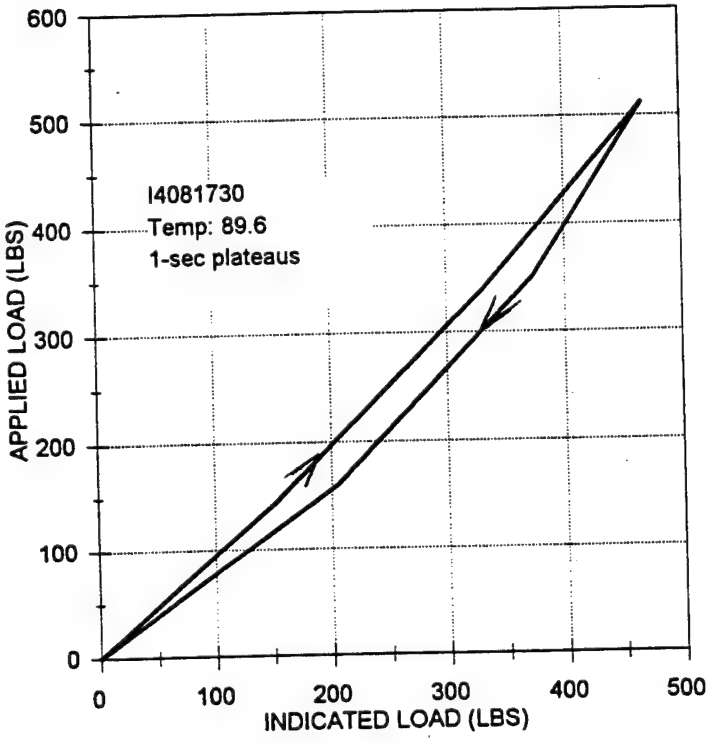

Figure 3-68. Hysteresis from platen loading.

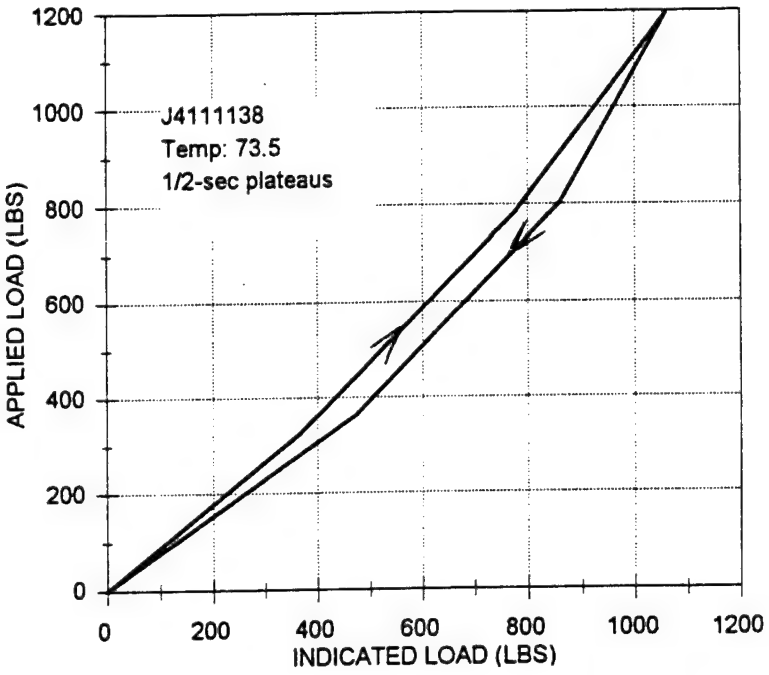

Figure 3-69. Hysteresis from platen loading.

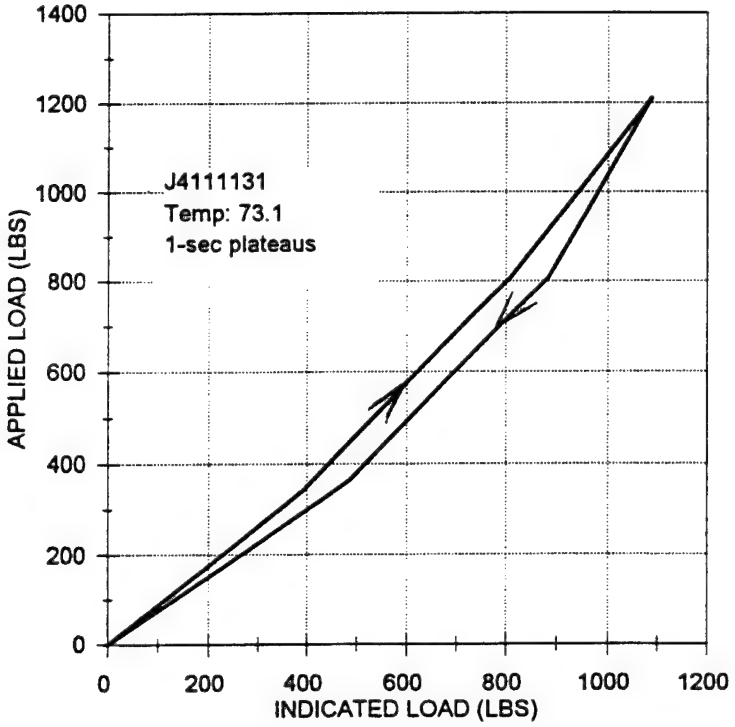

Figure 3-70. Hysteresis from platen loading.

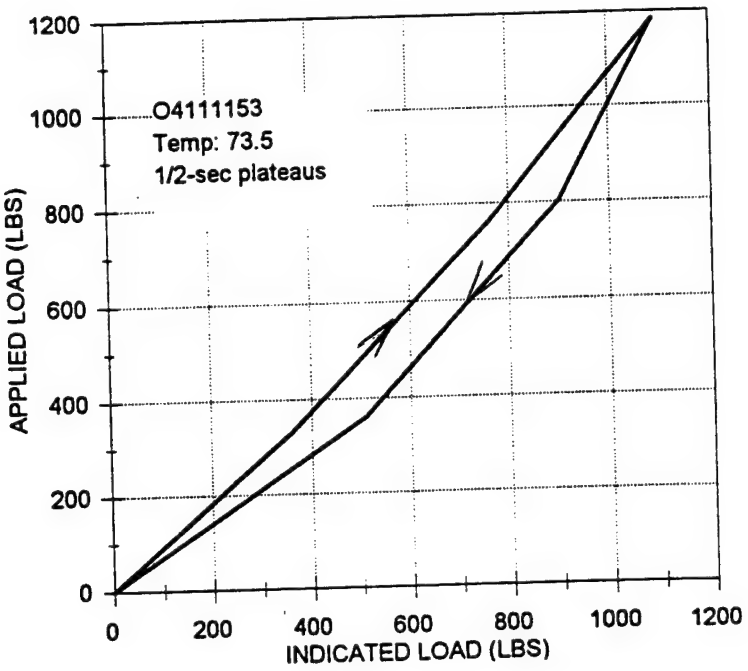

Figure 3-71. Hysteresis from platen loading.

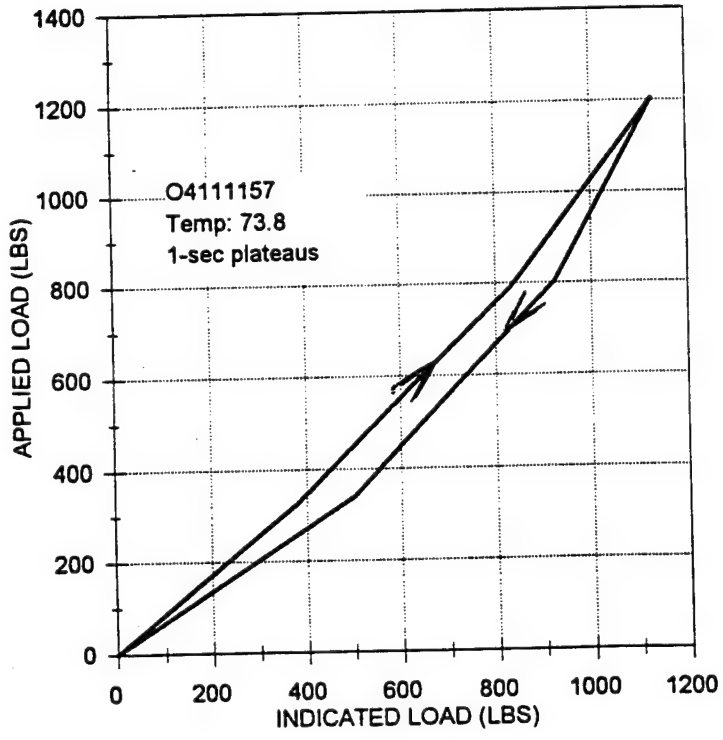

Figure 3-72. Hysteresis from platen loading.

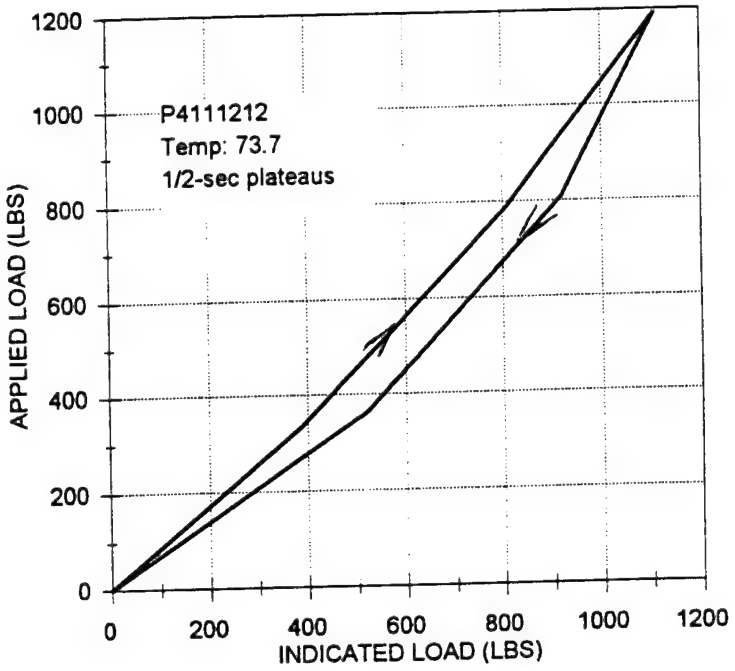

Figure 3-73. Hysteresis from platen loading.

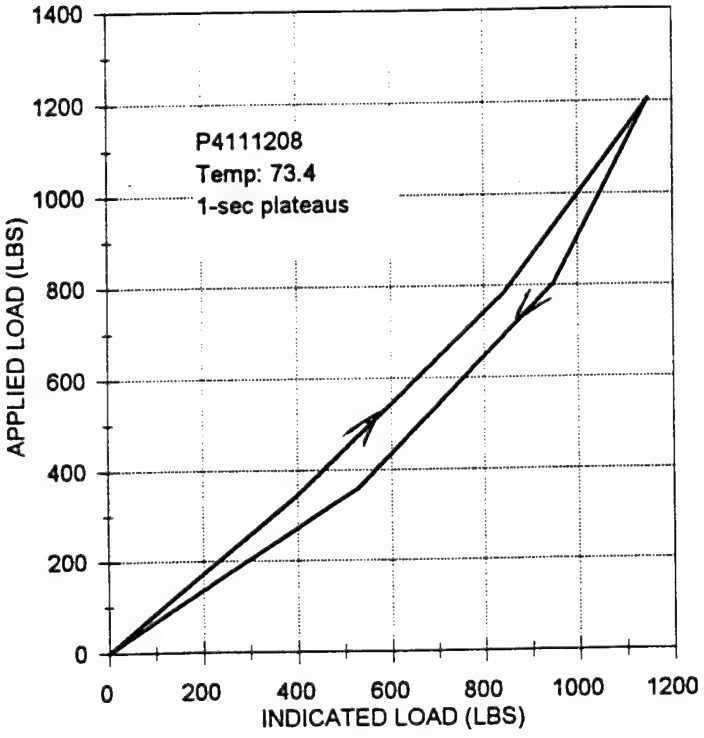

Figure 3-74. Hysteresis from platen loading.

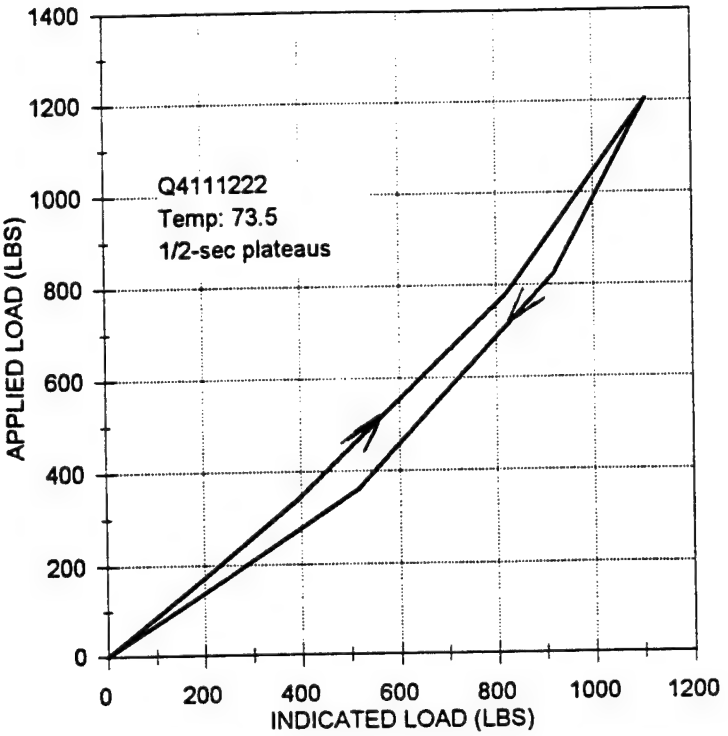

Figure 3-75. Hysteresis from platen loading.

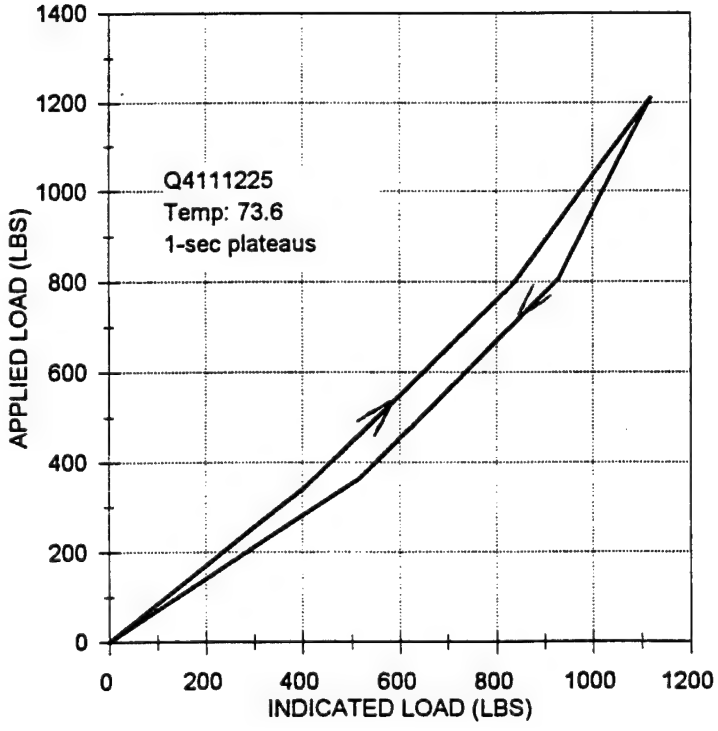

Figure 3-76. Hysteresis from platen loading.

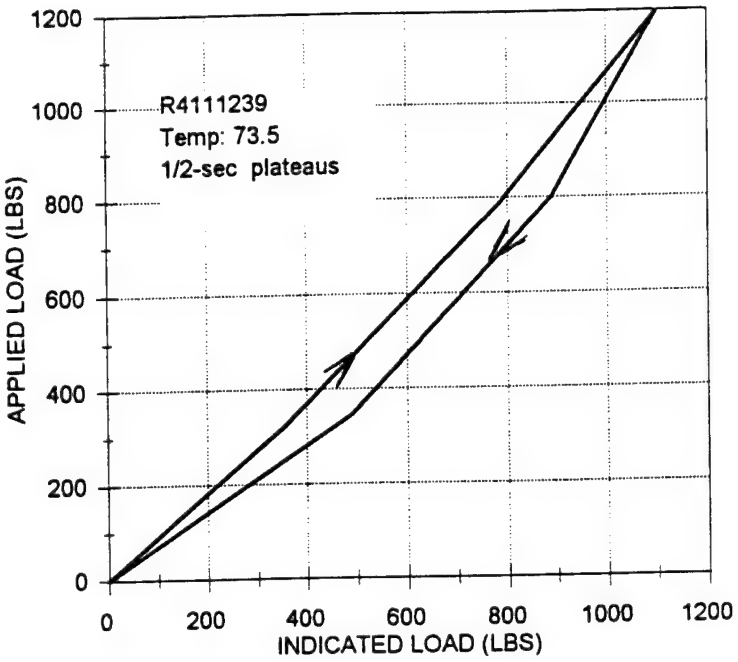

Figure 3-77. Hysteresis from platen loading.

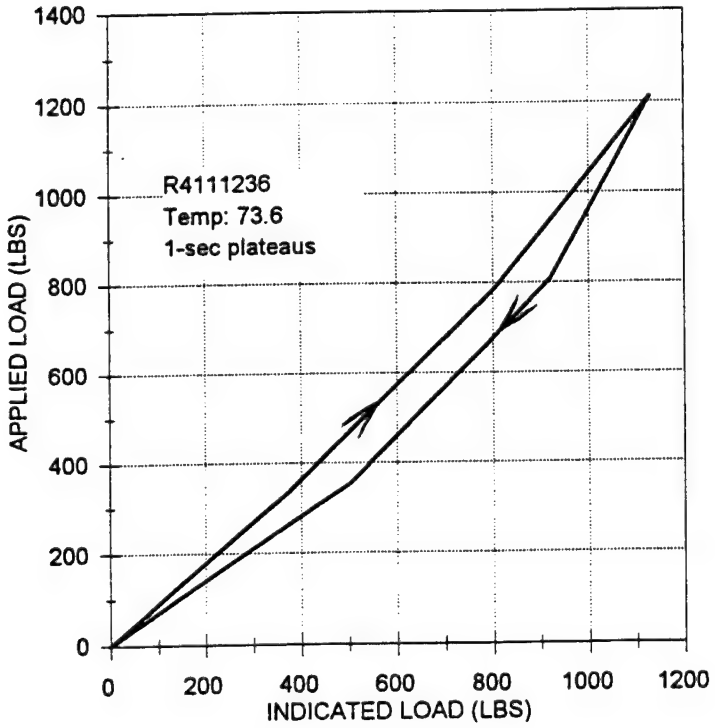

Figure 3-78. Hysteresis from platen loading.

3.5.3 Fatigue, Memory and Recovery. Tests With Pulse Trains.

While it would be possible to weigh vehicles in the field by stopping each axle on the Weighmats, it is expected that a relatively slow driveover at constant speed (of the order of one mile per hour) would be much more convenient. Rolling of a tire in this way over a sensor mat imparts a relatively short pulse to each loaded sensel, or row-column junction. Separation of successive pulses is also determined by the distance(s) between axles, and in case several vehicles are weighed in succession, also by the distance between vehicles. Tests with pulse trains under controlled conditions help answer questions regarding presence or absence of permanent fatigue effects, memory, and recovery.

3.5.3.1 Conduct of Pulse Train Tests. The waveform of the pulse train as programmed into the MTS loader is shown in Figure 3-79. This simulates the loading history of a loaded sensel in the sensor mat, when the tire contact patch length in the direction of travel is 18 inches and the axles are six feet center-to-center, or any other combination with a four to one ratio of axle separation to contact patch length. The ramps at the beginning and end of each pulse simulate reduced ground contact pressure at the beginning and end edges of the contact patch. These regions of reduced pressure arise from a nonzero transition radius in the tire carcass at the beginning and end of the contact patch, and were observed directly in the previous Proof of Concept tests.

Most of the tests were done with the total duration, D, of each pulse (Figure 3-79) equal to 1 second. This corresponds to a vehicle with axles 6 feet center-to-center and tire contact patch length 18 inches, moving at 1 mile per hour.

An example of the beginning of a pulse train in indicated load is shown in Figure 3-80. Figure 3-81 shows a pulse train for which the loading system was turned on at an instant when it was programmed to be in mid-pulse.

The peak applied load for each pulse monitored was recorded manually from a peak-reading meter. The only exception was a test in which the time scale was compressed by a factor of four, in which case the peak loads were scaled off the oscilloscope. The indicated peak loads in the tables and plots are the averages of the three highest loads in each given pulse in the Tekscan recording. Recording interval was 0.05 second except in the test in which the time scale was compressed by a factor of four, in which it was 0.01 second.

Calibrations for the tests with pulse trains started with an equilibration file previously generated at room temperature, using 70 psi pressure. Subsequent force calibrations were performed near the test temperature. Calibration loads were close to 1200 pounds in the tests close to -20 degrees F and at room temperature, and 514 pounds at 89 degrees F. As with other calibrations for the laboratory data in this report, both equilibration and force calibration were established after 20 seconds at constant pressure or load.

3.5.3.2 Investigation for Permanent Fatigue from Repeated Loadings. The question of presence or absence of permanent fatigue effects under pulsed loading can also be phrased in the following way: How many vehicle-weighings is a single sensor good for? Considering four-axle vehicles, a train of 400 pulses would simulate weighing 100 vehicles in close succession, bumper-to-bumper. An axle-to-axle distance of 6 feet is near the short end of the practical range; this makes the test probably conservative in that less time is allowed for recovery between pulses.

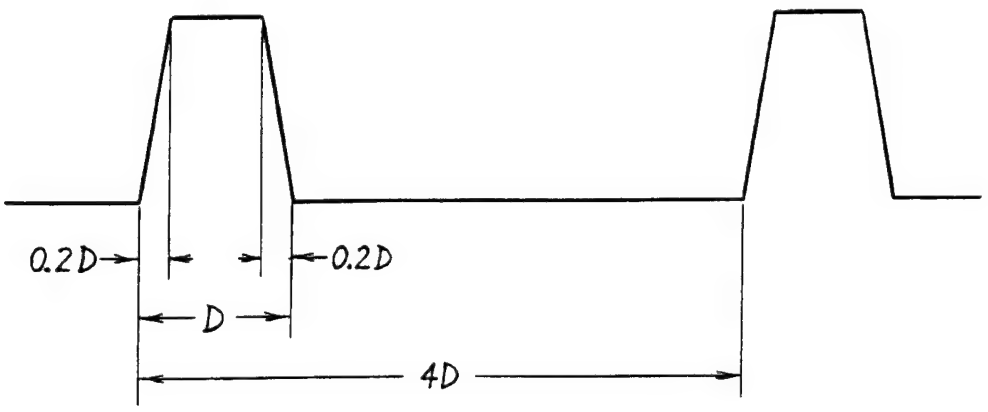

Figure 3-79. Programmed pulse-train waveform.

Graph

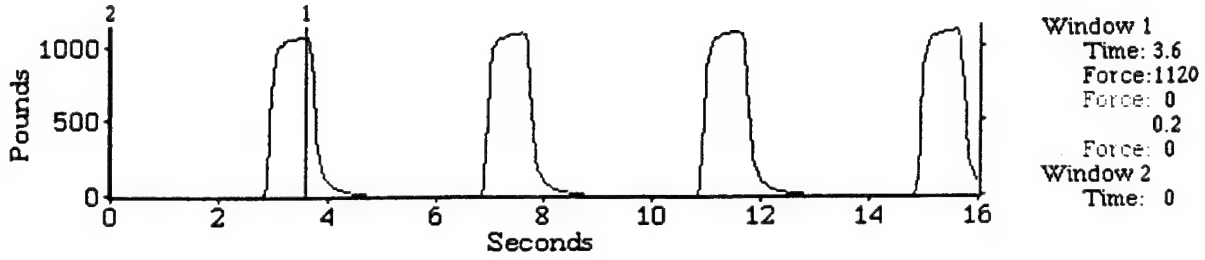

COMMENTS:
I4080847

Figure 3-80. Beginning of a pulse-train in indicated load.

Graph

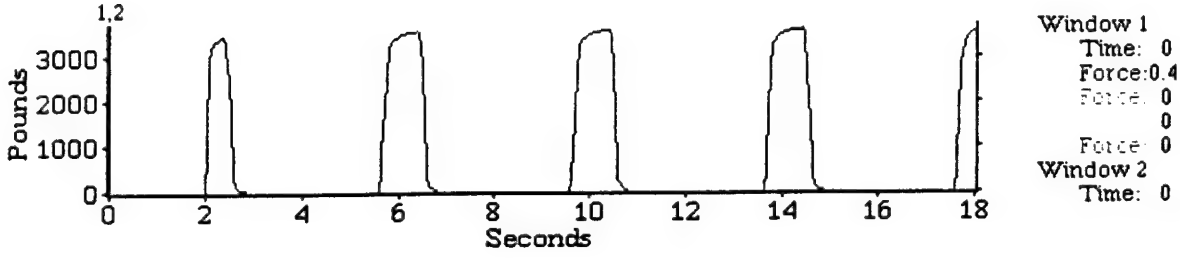

COMMENTS:
H4061716

Figure 3-81. Beginning of a pulse-train in indicated load. Loading system turned on when programmed to be in mid-pulse.

Results of tests near -20 degrees F with pulse trains slightly exceeding 400 pulses are tabulated in Tables 3-10 and 3-11. The peak load level employed in the first test, 1200 pounds, was a suitable maximum for tests at room temperature (Figure 3-44) but only used the lower part of its sensing range, without getting close to saturation, at temperatures close to -20 F (Figure 3-46). In these figures, the color scale was adjusted such that the deep red indicates saturation. The same is true for the stress distributions shown in Figures 3-82 and 3-83; these were produced by close to 5000-pound loads at approximately -19.5 F. The stress distribution in Figure 3-82 is associated with the highest indicated load in a single frame in the first pulse. The stress distribution in Figure 3-83 is associated with the highest indicated load in a single frame in the last pulse of the last recording made during the run: pulse number 377. Closeness to saturation is now comparable to the effect of a 1200-pound load at 77.8 F (Figure 3-44).

The results for these two tests are plotted in Figures 3-84 and 3-85. The points from the checks on recovery are unfilled (white) while the points from the long runs themselves are filled with dot-matrix. At the higher pulse numbers, the number of overlapping points in a less than distinct cluster is indicated by a digit next to the cluster.

Comparison of the check on recovery with the first points from the original run in Figure 3-84 shows essentially complete recovery from over 400 pulses with 1200-pound loads after an approximately 8.5-minute rest. Recovery after about 10.5 minutes subsequent to over 400 pulses with 5000-pound loads (Figure 3-85) is perhaps less complete, as three of the four points (hollow squares) from the check on recovery lie above the points from the original, long run. A slightly compressed, not fully recovered metal powder and resin matrix would show greater sensitivity. Still, the degree of nonrecovery in Figure 3-85 is within 2 percent.

3.5.3.3 Comparison of Pulse Train Data with Static Creep. The pulse train data were plotted in the semilog format in order to see whether they are like the static creep data in showing a nearly constant percent increase in indicated load per decade, which would produce a straight line on these plots. Indeed, the data seem to fit straight lines fairly well. A departure is the slight J-shape, brought about by the first few points (Figures 3-84 and 3-85). Several other observations suggest that such an initial J-shape may be the result of loading shortly before the test (trial runs to adjust load level, etc.). For example, in one case, data from a 16-pulse train were taken immediately after an abortive run; these particular data showed a very shallow slope, only a little over 1 percent per decade. (The data from this run are not shown in this report.)

In fitting the data in Figures 3-84 and 3-85, the first three points were excluded from the fit. These fits give slopes of 3.31 plus or minus 0.06 percent per decade, and 5.84 plus or minus 0.06 percent per decade, respectively. The significantly greater percent increase per decade with the higher loads differs from the behavior in the static creep tests, which consistently show greater creep rates at *lower* loads. The explanation for this difference probably lies in lower rates of *recovery* between pulses with higher loads. Considering the nature of the resin-metal matrix, such behavior is not unexpected. The matrix compacts easily at first (greater static creep at lower loads); increased compaction becomes more difficult as the degree of compaction increases. But the greater the compaction, the slower the recovery.

A similar test at room temperature (Table 3-12 and Figure 3-86) pointed to longer recovery times. Recovery was clearly insufficient after a 10-minute rest, marginal after 13 minutes additional rest, but could be considered complete after a rest exceeding two hours. It should be mentioned here that the last check on recovery, after two hours additional rest, also involved a drop in temperature of 1.2 degrees F relative to the beginning of the original long run. Correction with the 1.1 percent per degree F effect of temperature on sensitivity in the

Table 3-10. Fatigue, memory, and recovery, -19.1 to -19.5 degrees F, 1200-pound loads.

Force calibration temperature: -18.7 degrees F
Calibration load: 1200 lbs.
Calibration file: H700-19

Pulse Number	Recording	Temp, deg. F	Applied Peak Load, lbs.	Indicated Peak Load, lbs.	Factor of Increase Over Starting Indicated Peak Load
1	H4061533	-19.1	1200	1143	1.000
2				1150	1.006
3				1150	1.006
4				1153	1.009
92	H4061540	-19.2	1200	1210	1.059
93				1210	1.059
94				1210	1.059
95				1210	1.059
237	H4061549	-19.2	1200	1223	1.070
238				1227	1.073
239				1227	1.073
240				1223	1.070
375	H4061558	-19.3	1200	1233	1.079
376				1237	1.082
377				1237	1.082
378				1237	1.082
406	Pulse loading stopped, after 27 minutes 33 seconds total.				
Restart to check recovery, after 8 minute 36 second rest.					
1	H4061610	-19.5	1200	1133	0.991
2				1140	0.997
3				1147	1.003
4				1153	1.009

Table 3-11. Fatigue, memory, and recovery, -19.5 to -20.4 degrees F, 5000-pound loads.

Force calibration temperature: -18.7 degrees F
Calibration load: 1200 lbs.
Calibration file: H700-19

Pulse Number	Recording	Temp, deg. F	Applied Peak Load, lbs.	Indicated Peak Load, lbs.	Factor of Factor of Increase Over Starting Indicated Peak Load
1	H4061634	-19.6	4998	3620	1.000
2			4998	3647	1.007
3			5000	3673	1.015
4			4998	3690	1.019
37	H4061636	-19.6	4998	3877	1.071
38			4998	3880	1.072
39			4998	3880	1.072
40			4998	3880	1.072
92	H4061640	-19.7	4998	3960	1.094
93			4998	3963	1.095
94			4998	3963	1.095
95			4998	3963	1.095
226	H4061649	-19.5	4998	4050	1.119
227			4998	4050	1.119
228			4998	4047	1.118
229			5000	4059	1.119
374	H4061659	-19.5	4998	4093	1.131
375			5000	4093	1.131
376			4998	4097	1.132
377			4998	4097	1.132
453	Pulse loading stopped, after 27 minutes 33 seconds total.				

Restart to check recovery, after 10 minute 23 second rest.

0.5*	H4061716	-20.4	4998	3610**	0.997
1.5			4998	3710	1.025
2.5			4998	3737	1.032
3.5			4998	3757	1.038

* Looks like loading system was turned on at an instant when it was programmed to be in mid-pulse. That is why the first pulse is considered to be a half-pulse, the second the 1.5 pulse, etc. here.

** Because of the possibly greater variation in applied load (greater rate of increase) in this half-pulse, the peak load tabulated is the highest in just one recording frame, not the average of the three highest loads as in other cases.

```
Playback Window 1
     Machine_Name:
    Machine_Ident:
             Date: 04/06/94,15:35
Area = 40.48 sq inches
 Frame   55 of  361
File D:\DATA\WEIGHMAT\H4061634.FSX
Saved 04/06/17  15:37
```

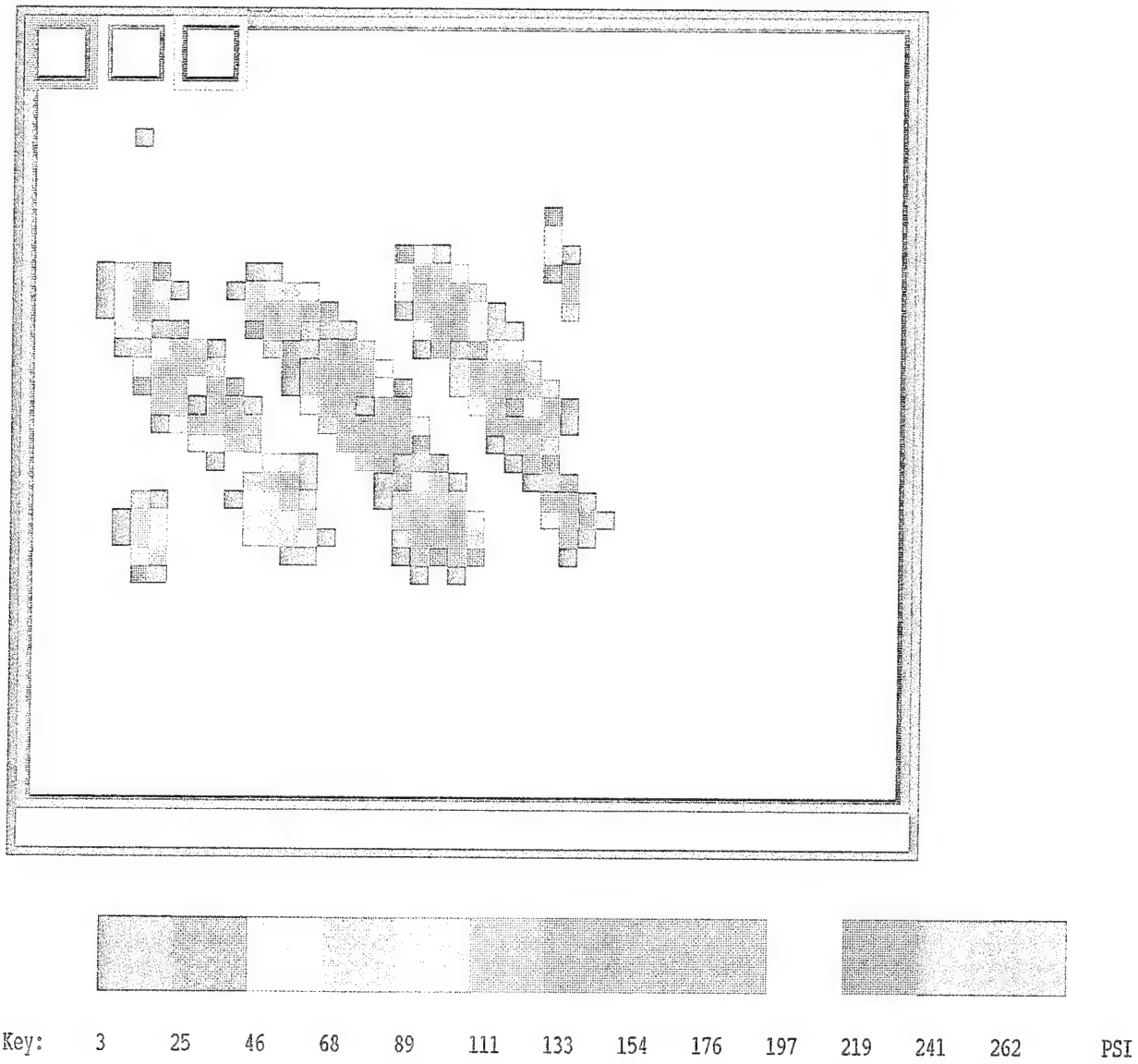

Key: 3 25 46 68 89 111 133 154 176 197 219 241 262 PSI

Figure 3-82. 4998 pounds at -19.5 degrees F, first pulse.

```
Playback Window 1
     Machine_Name:
    Machine_Ident:
             Date: 04/06/94,15:54
Area = 43.52 sq inches
 Frame   39 of  361
File D:\DATA\WEIGHMAT\H4061659.FSX
Saved 04/06/17  16:03
```

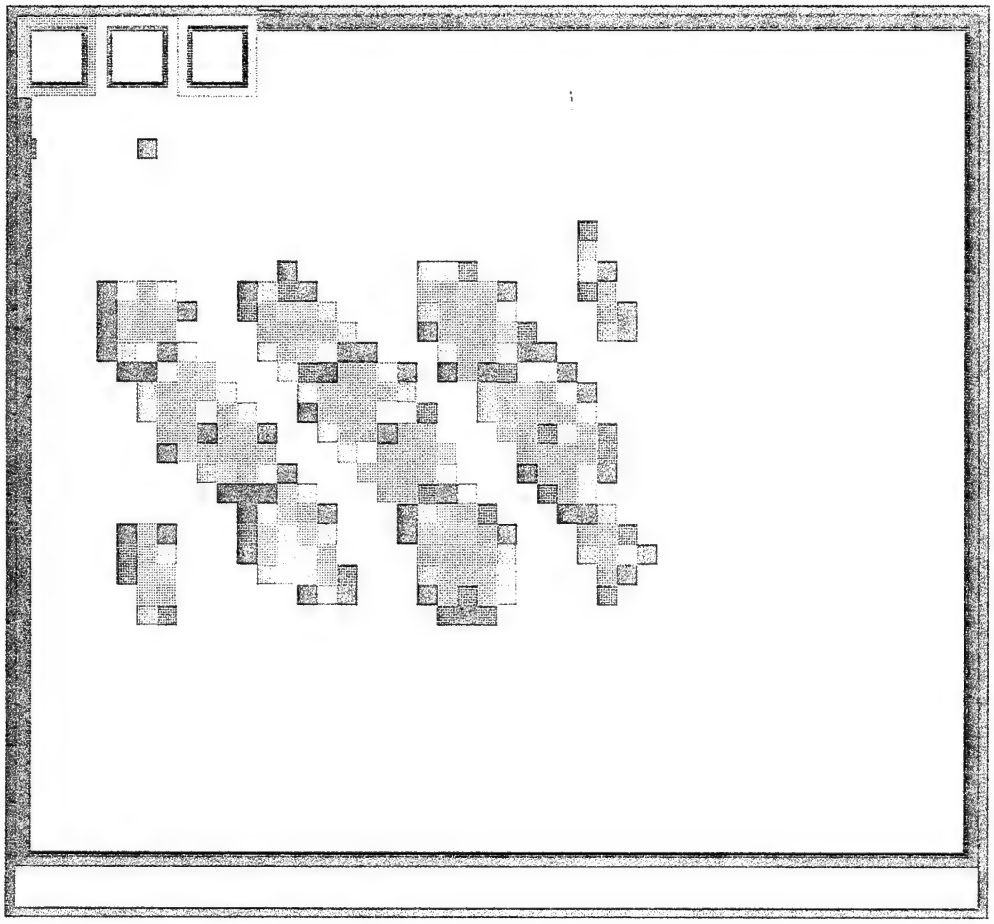

Key: 3 25 46 68 89 111 133 154 176 197 219 241 262 PSI

Figure 3-83. 4998 pounds at -19 degrees F, pulse 377.

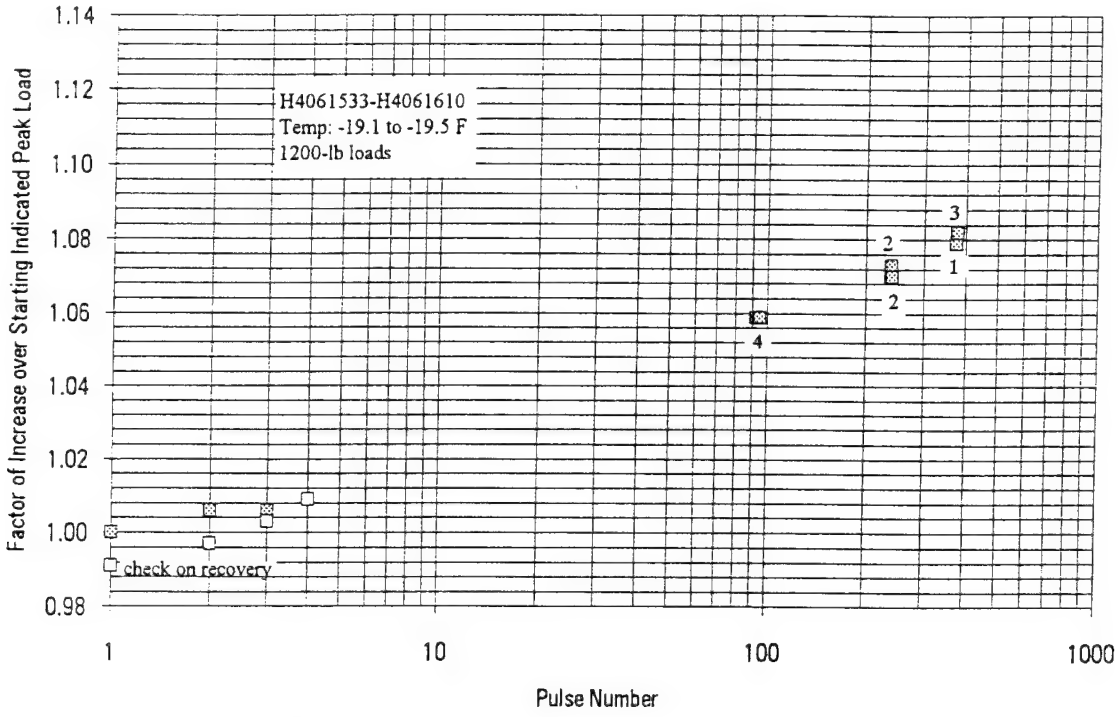

Figure 3-84. Creep of pulse train readings.

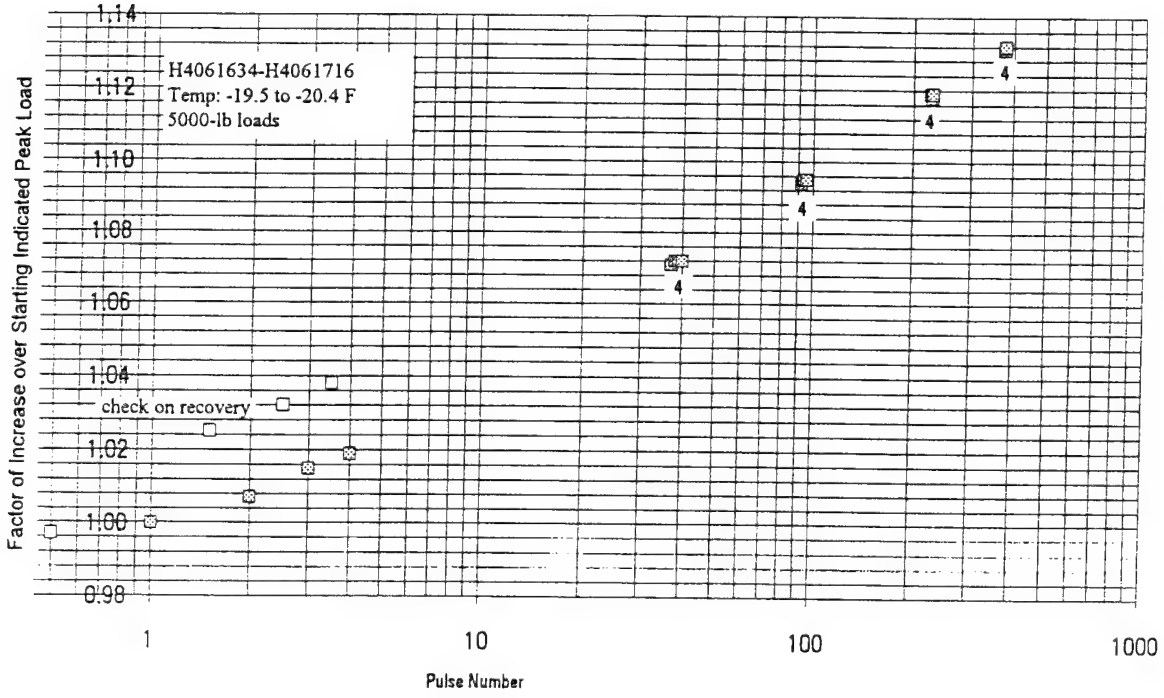

Figure 3-85. Creep of pulse train readings.

70 F range moves the points from the last check on recovery upward by 1.3 percent, to where they are pretty well in line with the first four points from the original, long run.

Continuous recordings of the first 16, and of the first 32 pulses were also taken; a Tekscan graph of the first 32 pulses in a train is shown in Figure 3-87. Data from the first 16 pulses, 1200-pound loads at room temperature, are displayed in Table 3-13 and Figure 3-88, and data from the first 32 pulses are shown in Tables 3-14 and 3-15, and Figures 3-89 and 3-90, all at room temperature. Data from the first 32 pulses with 500-pound loads at 89.6 degrees F are tabulated in Table 3-16 and plotted in Figure 3-91.

In Figure 3-91, the jog at pulse numbers 6 through 9 was a puzzle at first. Then it was noticed that it coincided with a drop in the preload between pulses, which is tabulated in the middle column in Table 3-16. In the pulse interval 6 through 9, the indicated preload dropped from an average of 26.5 psi to an average of 21 psi. Effects of variations in the slight preload were *not* observed in the static creep tests and in the hysteresis tests. It may be that the preload has an effect on *recovery* between pulses.

The results of fits to all of the above tests with pulse-trains are summarized in Table 3-17. The effect of the jog in the data at 89.6 F (Figure 3-91) was avoided by excluding the first eight points from the fit.

3.5.3.4 Sensor Response to a Succession of Vehicles. We now proceed to address the question of separation between vehicles in successive driveover weighings. Specifically, to what extent would the indicated weight of the second vehicle be influenced by the previous passage of the first over the Weighmats, at various separations. For simplicity, we restricted ourselves to only attempt to simulate the effects of two *identical* four-axle vehicles, with equal axle weights and equal distances between all four axles. These tests (as well as the other pulse-train tests) were also restricted to the case where the center-to-center distance between axles is four times the length of the tire contact patch (Figure 3-79).

An example of a Tekscan graph of indicated load is shown in Figure 3-92. This particular recording involved a nominal interval of 8 seconds between the two four-pulse trains. The train intervals were varied between 8 seconds and 64 seconds. With four-axle vehicles with 6-foot separation between axles and tire contact patches 18 inches long, these correspond to separations of 12 and 96 feet, respectively, between the last axle of the previous vehicle and the first axle of the subsequent vehicle. In all the tests except one, the simulated speed of the vehicles described above was one mile per hour. The Tekscan graph of indicated load from the one exception is shown in Figure 3-93. In this test, the time-scale was shrunk by a factor of four relative to the other tests, attempting to simulate the passage of two vehicles as described above, moving at 4 miles per hour. The separation of these two vehicles would be 48 feet.

Data from the test run for which the Tekscan graph is displayed in Figure 3-92 are displayed in Table 3-18 and Figure 3-94. In Figure 3-94 and in all subsequent plots on pulse-train results, the first train of four pulses is displayed by the symbols filled with dot-matrix, and the second train of four pulses is displayed by the unfilled (white) symbols. The data in Figure 3-94 show clear effects of memory of the passage of the previous train of four pulses. The indicated loads in the second train start out high but converge toward the loads in the first train. Similar behavior still appears when the nominal interval between pulse trains is increased to 16 seconds (Table 3-19 and Figure 3-95).

When the nominal interval between the four-pulse trains is increased to 32 seconds (corresponding to a 48-foot separation between two four-axle vehicles as described above), as in the tests with results in Table 3-20, Figure 3-96, Table 3-21, Figure 3-97, Table 3-22, and

Table 3-12. Fatigue, memory, and recovery, 75.6 to 77.5 degrees F, 1200-pound loads.

Force calibration temperature: 74.8 degrees F
Calibration load: 1200 lbs.
Calibration file: I70075

Pulse Number	Recording	Temp, deg. F	Applied Peak Load, lbs.	Indicated Peak Load, lbs.	Factor of Increase Over Starting Indicated Peak Load
1	I4080847	76.8	1180	1113	1.000
2			1184	1133	1.018
3			1180	1140	1.024
4			1184	1147	1.030
56	I4080850	76.9	1180	1180	1.060
57			1188	1180	1.060
58			1184	1180	1.060
59			1180	1183	1.063
107	I4080854	76.8	1180	1193	1.072
108			1176	1193	1.072
109			1180	1193	1.072
110			1180	1193	1.072
226	I4080902	76.9	1188	1220	1.096
227			1192	1220	1.096
228			1188	1220	1.096
229			1192	1220	1.096
386	I4080912	77	1188	1220	1.096
387			1188	1227	1.102
388			1184	1223	1.099
389			1188	1220	1.096
419	Pulse loading stopped, after 27 minutes 55 seconds total.				
Restart to check recovery, after 10 minute rest.					
1	I4080925	77.1	1176	1153	1.036
2			1176	1173	1.054
3			1180	1183	1.063
4			1176	1190	1.069
Restart to check recovery after 13 minute rest.					
1	I4080947	77.5	1192	1133	1.018
2				1147	1.03
3			1184	1160	1.042
4			1184	1167	1.048
Restart to check recovery after additional rest of approximately 2 hours.					
1	I4081153	75.6	1212	1100	0.988
2			1208	1110	0.997
3			1204	1120	1.006
4			1208	1130	1.015

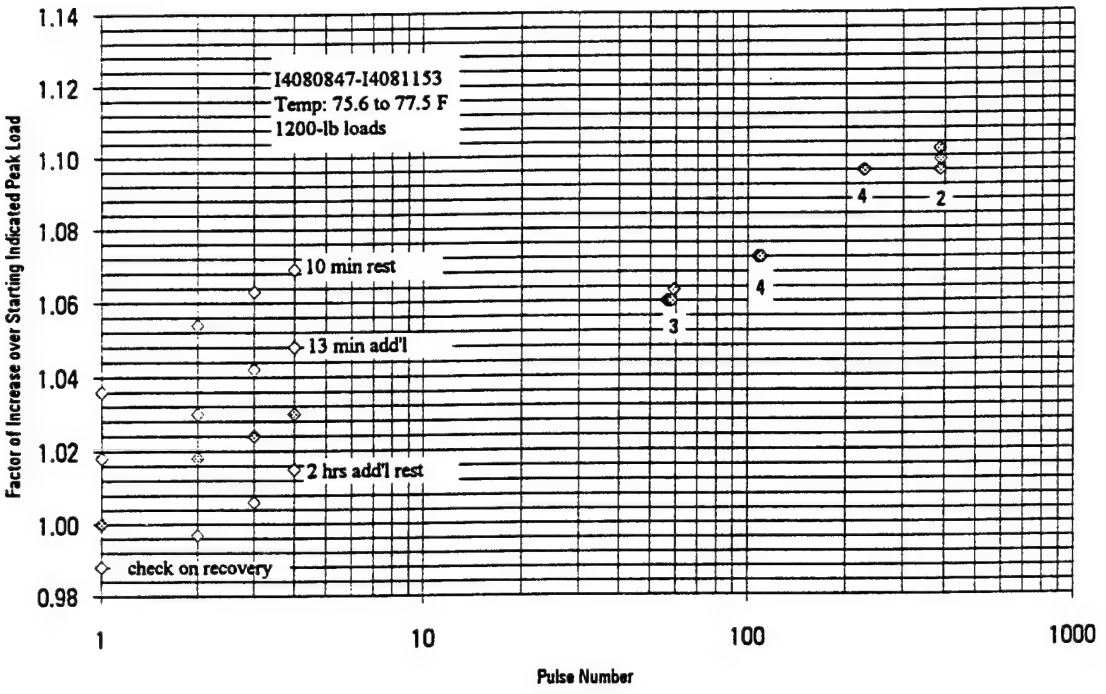

Figure 3-86. Creep of pulse train readings.

Graph

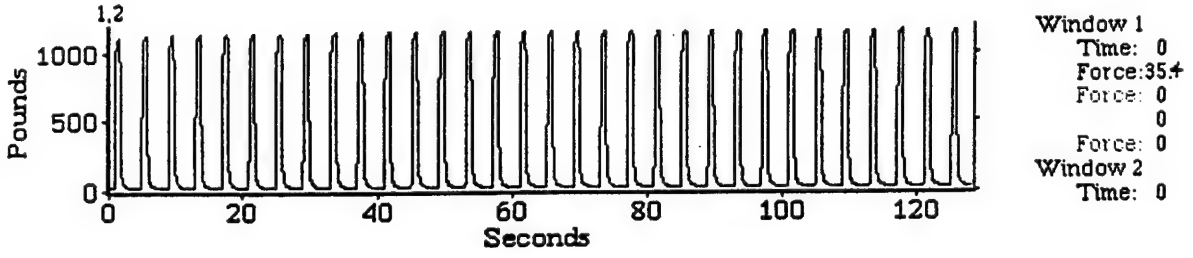

COMMENTS:
R4111302

Figure 3-87. Thirty-two pulse train.

Table 3-13. Memory, 16-pulse train, 75 degrees F, 1200-pound loads.

Force calibration temperature:	74.8 degrees F
Calibration load:	1200 lbs.
Calibration file:	I70075
Recording:	I4071010

Pulse Number	Applied Peak Load, lbs.	Indicated Peak Load, lbs.	Factor of Increase Over Starting Indicated Peak Load
1	1200	1100	1.000
2	1204	1110	1.009
3	1204	1120	1.018
4	1208	1127	1.024
5	1204	1127	1.024
6	1208	1130	1.027
7	1204	1130	1.027
8	1208	1133	1.030
9	1204	1137	1.033
10	1208	1137	1.033
11	1204	1137	1.033
12	1208	1140	1.036
13	1204	1140	1.036
14	1208	1140	1.036
15	1204	1140	1.036
16	1208	1140	1.036

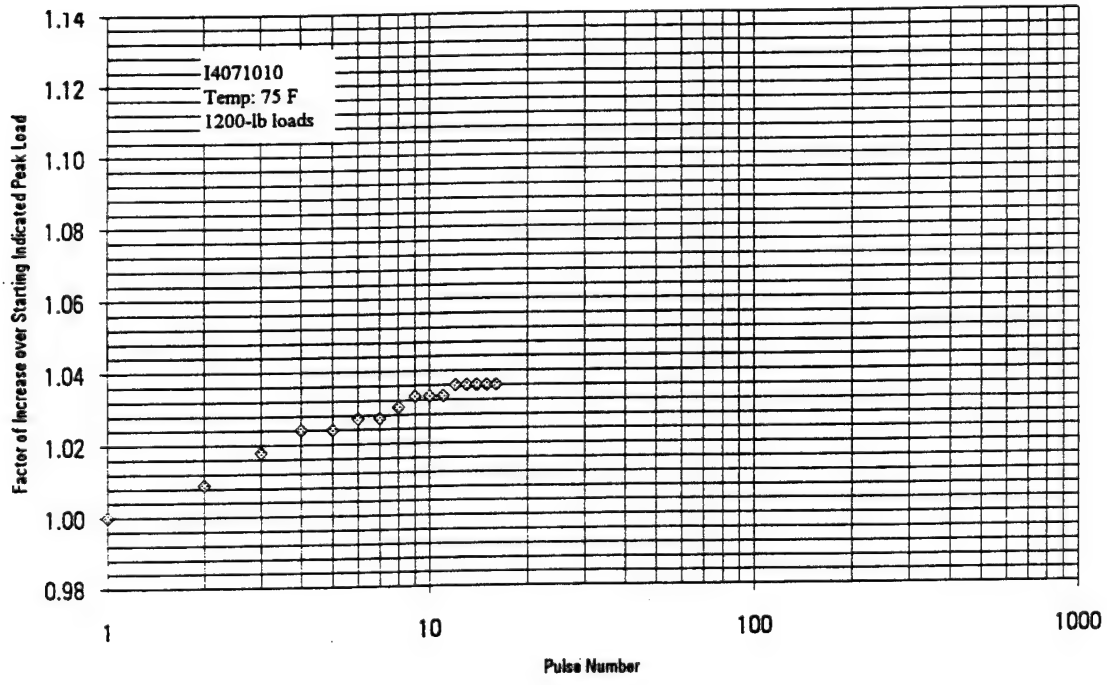

Figure 3-88. First 16 pulses for 1200-pound load.

Table 3-14. Memory, 32-pulse train, 75.2 degrees F, 1200-pound loads, sensor I.

Force calibration temperature:	74.8 degrees F
Calibration load:	1200 lbs.
Calibration file:	I70075
Recording:	I4071039

Pulse Number	Applied Peak Load, lbs.	Indicated Peak Load, lbs.	Factor of Increase Over Starting Indicated Peak Load
1	1192	1090	1.000
2	1188	1103	1.012
3	1196	1110	1.018
4		1117	1.025
5	1196	1120	1.028
6	1192	1123	1.030
7	1196	1130	1.037
8	1192	1130	1.037
9	1196	1130	1.037
10	1192	1130	1.037
11	1196	1130	1.037
12	1188	1130	1.037
13	1196	1133	1.040
14	1188	1133	1.040
15	1196	1130	1.037
16	1188	1130	1.037
17	1196	1130	1.037
18	1192	1130	1.037
19	1196	1137	1.043
20	1192	1130	1.037
21	1196	1130	1.037
22	1192	1133	1.040
23	1196	1133	1.040
24	1192	1130	1.037
25	1196	1130	1.037
26	1196	1133	1.040
27	1188	1133	1.040
28	1192	1133	1.040
29	1196	1133	1.040
30	1196	1133	1.040
31	1196	1133	1.040
32	1196	1130	1.037

Table 3-15. Memory, 32-pulse train, 73.6 degrees F, 1200-pound loads, sensor R.

Force calibration temperature:	73.1 degrees F
Calibration load:	1200 lbs.
Calibration file:	R70073
Recording:	R4111302

Pulse Number	Applied Peak Load, lbs.	Indicated Peak Load, lbs.	Factor of Increase Over Starting Indicated Peak Load
1	1204	1160	1.000
2	1204	1170	1.009
3	1208	1180	1.017
4	1208	1183	1.020
5	1208	1187	1.023
6	1208	1190	1.026
7	1208	1190	1.026
8	1208	1190	1.026
9	1208	1190	1.026
10	1204	1190	1.026
11	1208	1193	1.029
12	1208	1193	1.029
13	1208	1197	1.032
14	1204	1197	1.032
15	1208	1197	1.032
16	1204	1200	1.034
17	1208	1200	1.034
18	1204	1200	1.034
19	1208	1200	1.034
20	1204	1200	1.034
21	1208	1200	1.034
22	1204	1200	1.034
23	1208	1200	1.034
24	1208	1200	1.034
25	1208	1200	1.034
26	1204	1203	1.037
27	1208	1203	1.037
28	1208	1203	1.037
29	1208	1203	1.037
30	1204	1203	1.037
31	1208	1207	1.040
32	1208	1203	1.037

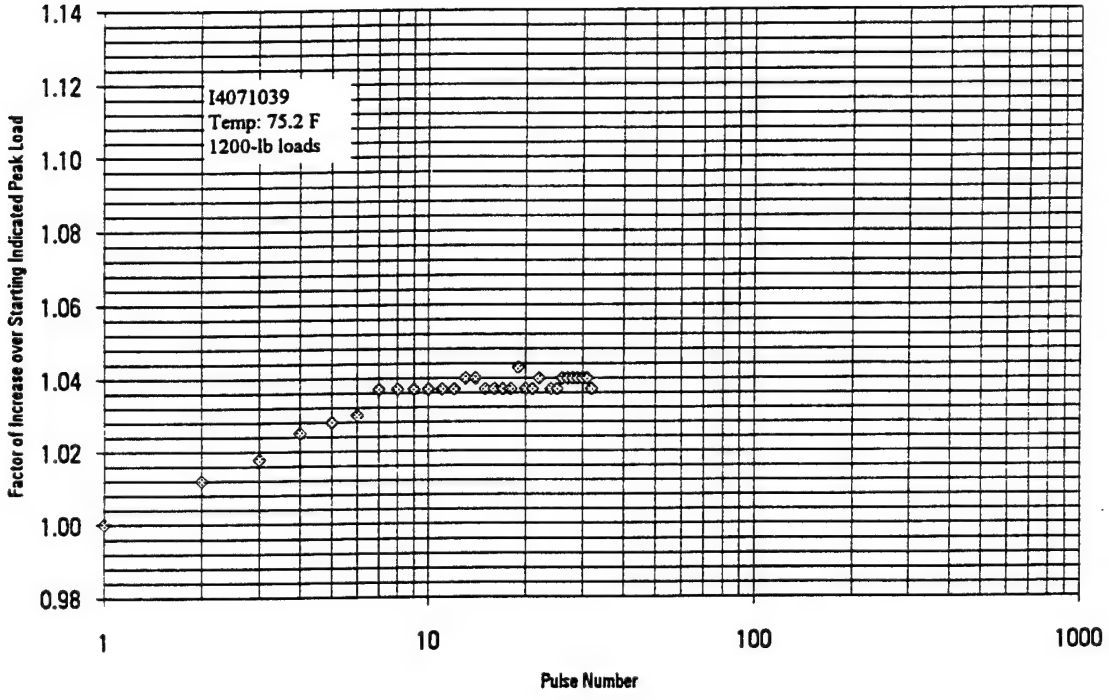

Figure 3-89. First 32 pulses for 1200-pound load.

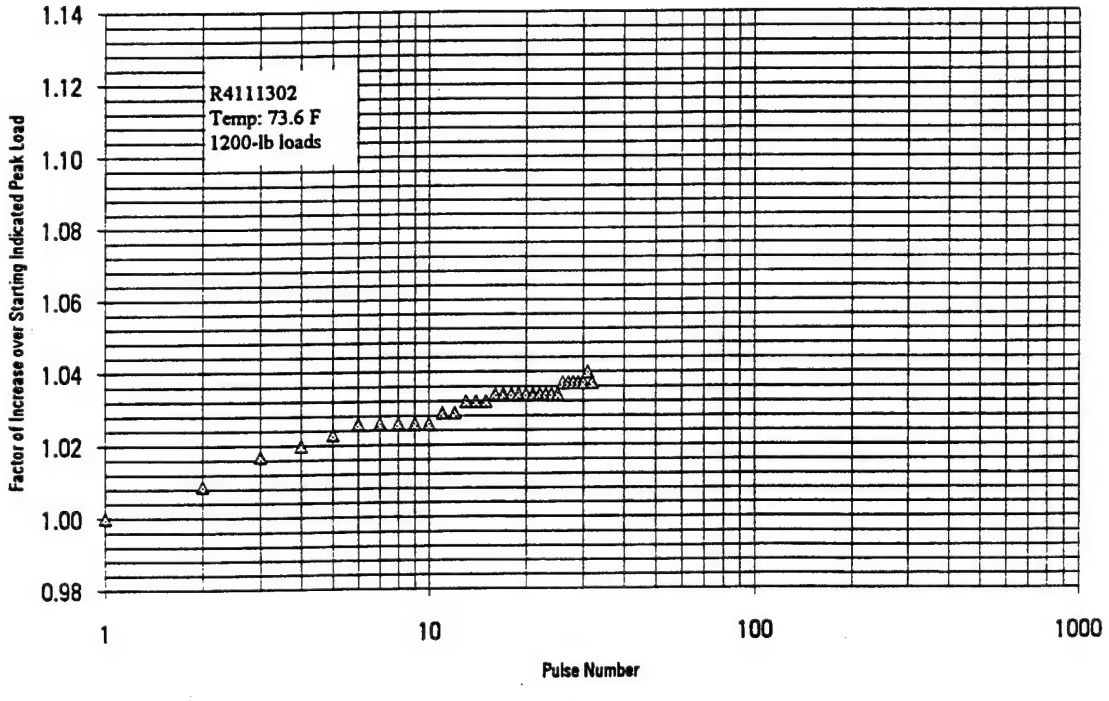

Figure 3-90. First 32 pulses for 1200-pound load.

Table 3-16. Memory, 32-pulse train, 89.6 degrees F, 500-pound loads.

Force calibration temperature: 89.3 degrees F
Calibration load: 514 lbs.
Calibration file: I70089
Recording: I4081711

Pulse Number	Applied Peak Load, lbs.	Indicated Preload, lbs.	Indicated Peak Load, lbs.	Factor of Increase Over Starting Indicated Peak Load
1	508	24.9	439	1.000
2	504	27.9	446	1.016
3	512	28.1	450	1.025
4	508	26.8	452	1.030
5	508	25.5	453	1.032
6	508	25.8	455	1.036
7	512	22.9	453	1.032
8	504	21.4	453	1.032
9	508	21.1	454	1.034
10	504	21.0	455	1.036
11	508	21.1	455	1.036
12	504	20.9	456	1.039
13	508	21.1	456	1.039
14	508	20.9	457	1.041
15	508	21.0	457	1.041
16	504	20.8	458	1.043
17	508	21.2	458	1.043
18	504	20.8	459	1.046
19	508	21.1	459	1.046
20	512	21.0	459	1.046
21	508	21.1	460	1.048
22	504	20.9	460	1.048
23	508	21.0	461	1.050
24	504	20.9	461	1.050
25	508	20.9	461	1.050
26	508	21.1	461	1.050
27	508	20.9	462	1.052
28	508	20.9	462	1.052
29	508	20.9	463	1.055
30	508	20.9	463	1.055
31	508	20.9	464	1.057
32	504	20.9	463	1.055

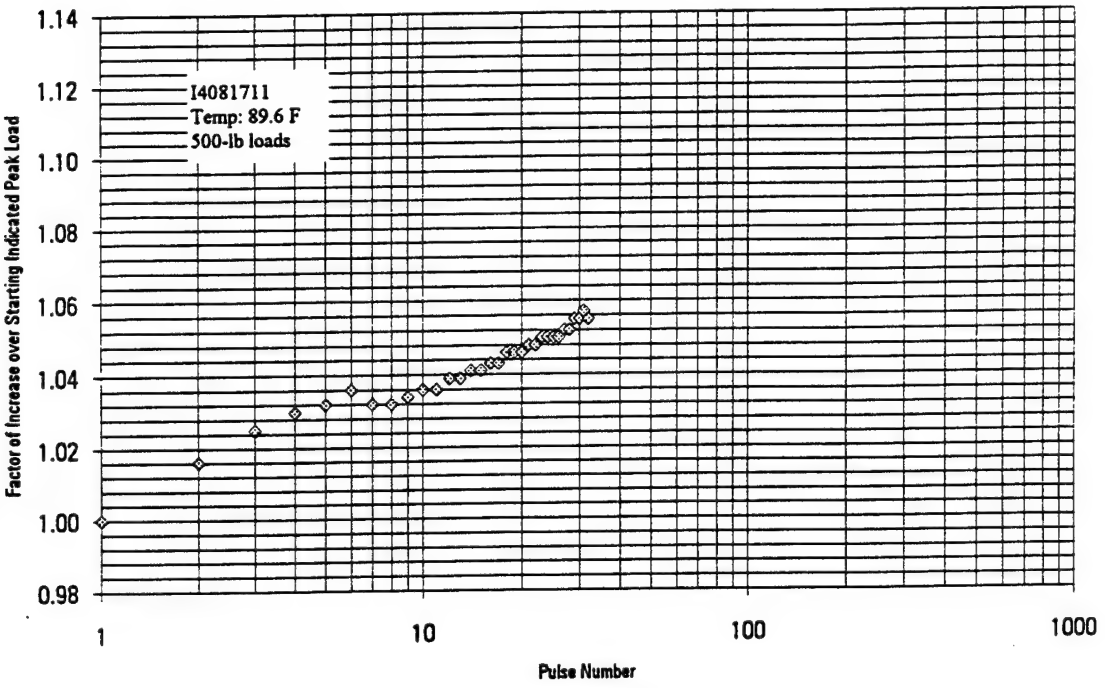

Figure 3-91. First 32 pulses for 500-pound load.

Table 3-17. Fatigue and memory slopes.

Temperature, degrees F	Load, lbs.	Recording	Slope, percent per decade	Error in Slope, percent per decade
-19.1 to -19.5	1200	H4061533-H4061558	3.31*	0.06*
-19.1 to -20.4	5000	H4061634-H4061659	5.84*	0.06*
75.6 to 77.5	1200	I4080847 I4080912	3.67	0.16
75.0	1200	I4071010	3.04	0.13
75.2	1200	I4071039	2.19	0.20
73.6	1200	R4111302	2.27	0.09
89.6	500	I4081711	4.00**	0.12**

* The first three points were excluded from this fit.

**The first eight points were excluded from this fit.

Graph

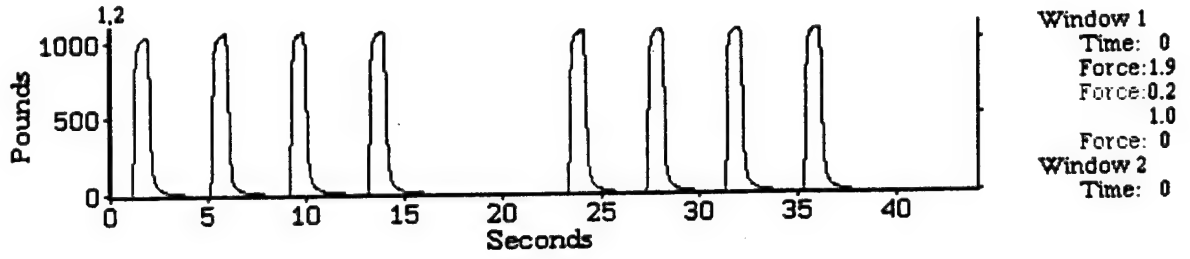

COMMENTS:
I4071141

Figure 3-92. Trains of four pulses with 8-second nominal interval in between.

Graph

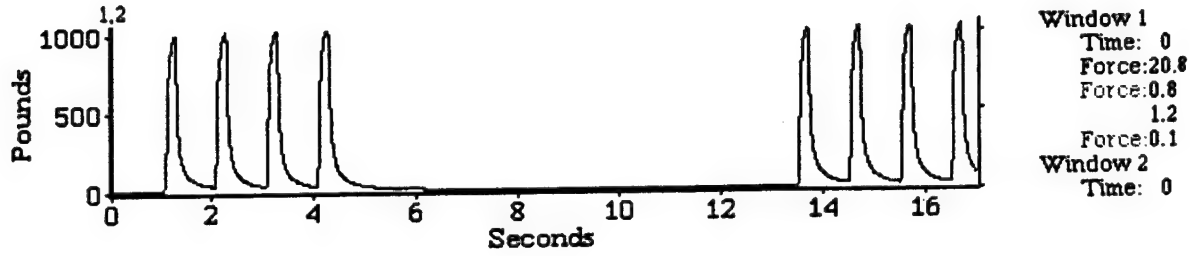

COMMENTS:
I4071503

Figure 3-93. Trains of four pulses with an interval in between. Time-scale shrunk by a factor of four relative to the other tests.

Table 3-18. Memory, two four-pulse trains, 8-second nominal interval, 75.7 degrees F, 1200-pound loads.

Load calibration temperature:	74.8 degrees F
Calibration load:	1200 lbs.
Calibration file:	I70075
Recording:	I4071141

Pulse Number	Applied Peak Load, lbs.	Indicated Peak Load, lbs.	Factor of Increase Over Starting Indicated Peak Load
1	1184	1083	1.000
2	1184	1100	1.016
3	1184	1100	1.016
4	1184	1100	1.025

Nominal interval: 8 seconds. Time from beginning of last pulse in first train to beginning of first pulse in second train: 10.15 seconds

1	1184	1100	1.016
2	1184	1100	1.025
3	1184	1100	1.025
4	1184	1100	1.025

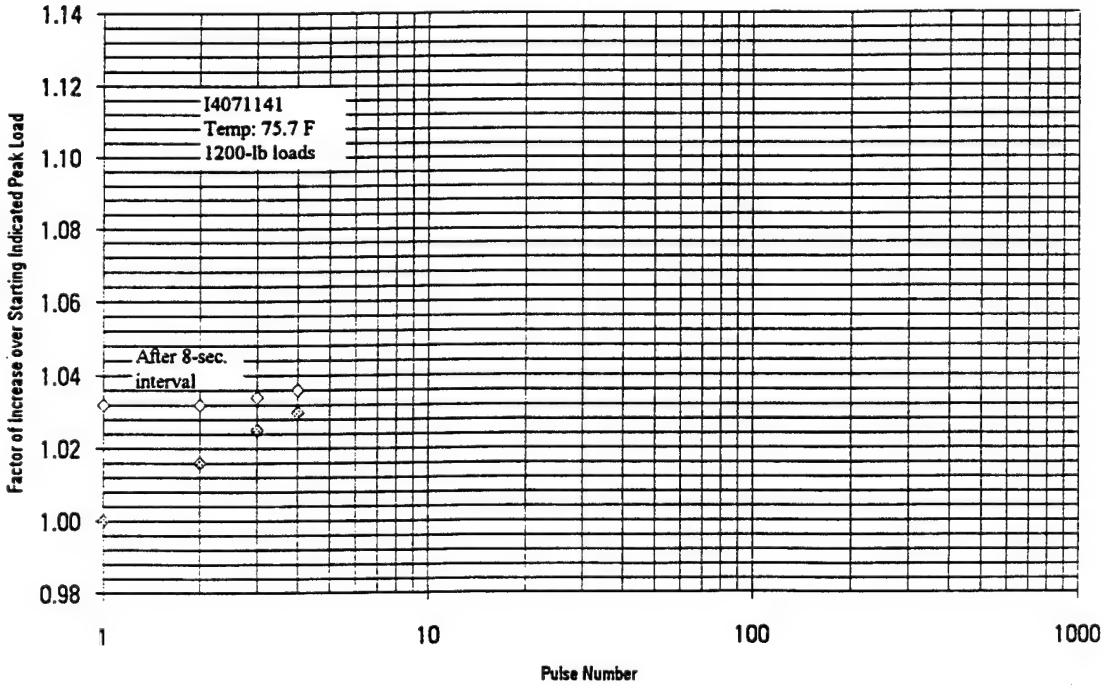

Figure 3-94. Memory, two four-pulse trains, 8-second nominal interval, 75.7 degrees F, 1200-pound loads.

Table 3-19. Memory, two four-pulse trains, 16-second nominal interval, 75.8 degrees F, 1200-pound loads.

Load calibration temperature:	74.8 degrees F
Calibration load:	1200 lbs.
Calibration file:	I70075
Recording:	I4071153

Pulse Number	Applied Peak Load, lbs.	Indicated Peak Load, lbs.	Factor of Increase Over Starting Indicated Peak Load
1	1196	1090	1.000
2		1100	1.009
3	1192	1110	1.018
4	1192	1110	1.018

Nominal interval: 16 seconds. Time from beginning of last pulse in first rain to beginning of first pulse tin second train: 17.25 seconds

1	1192	1107	1.015
2	1196	1110	1.018
3	1196	1113	1.021
4	1196	1117	1.024

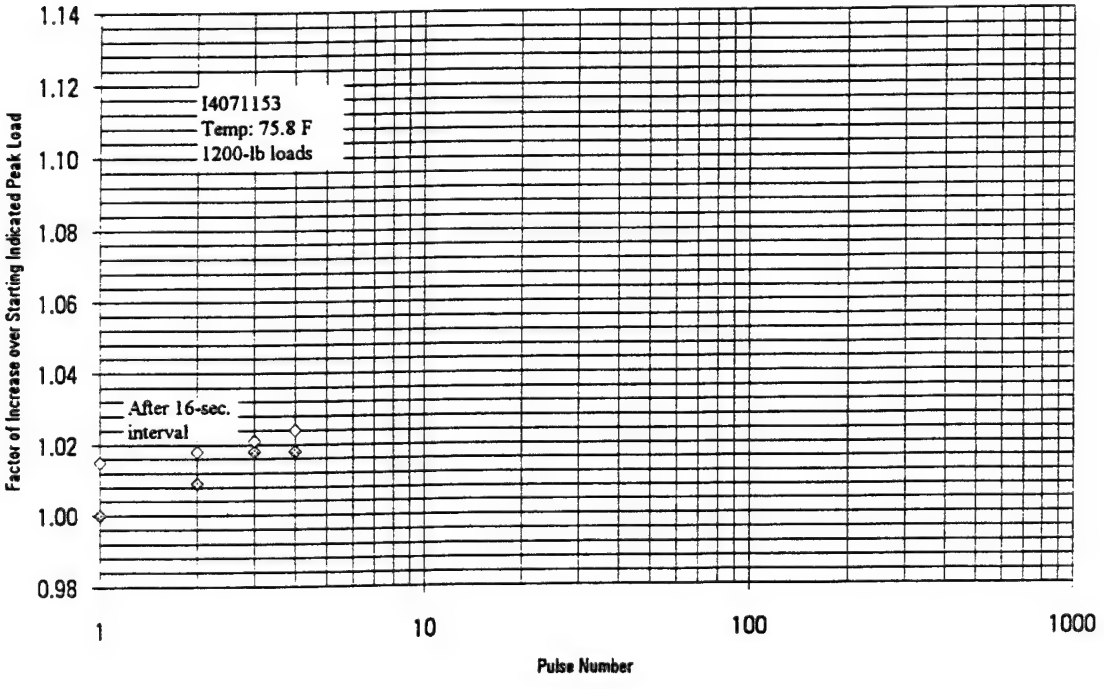

Figure 3-95. Memory, two four-pulse trains, 16-second nominal interval, 75.8 degrees F, 1200-pound loads.

Table 3-20. Memory, two four-pulse trains, 32-second nominal interval, 75.8 degrees F, 1200-pound loads, sensor I.

Force calibration temperature:	74.8 degrees F
Calibration load:	1200 lbs.
Calibration file:	I70075
Recording:	I4071212

Pulse Number	Applied Peak Load, lbs.	Indicated Peak Load, lbs.	Factor of Increase Over Starting Indicated Peak Load
1	1188	1100	1.000
2	1192	1103	1.003
3	1188	1110	1.009
4	1192	1110	1.009

Nominal interval: 32 seconds. Time from beginning of last pulse in first train to beginning of first pulse in second train: 34.15 seconds.

1	1192	1103	1.003
2	1192	1113	1.012
3	1188	1117	1.015
4	1192	1120	1.018

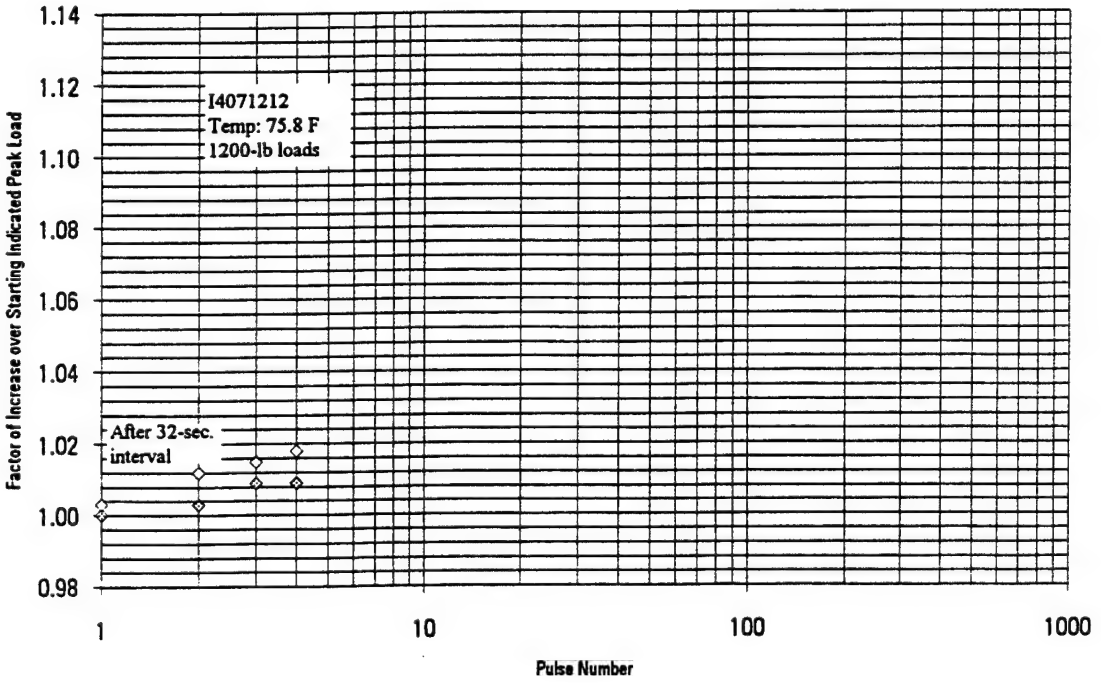

Figure 3-96. Memory, two four-pulse trains, 32-second nominal interval, 75.8 degrees F, 1200-pound loads, sensor I.

Table 3-21. Memory, two four-pulse trains, 32-second nominal interval, 77.1 degrees F, 1200-pound loads, sensor I.

Force calibration temperature:	74.8 degrees F
Calibration load:	1200 lbs.
Calibration file:	I70075
Recording:	I4071427

Pulse Number	Applied Peak Load, lbs.	Indicated Peak Load, lbs.	Factor of Increase Over Starting Indicated Peak Load
1	1200	1110	1.000
2	1204	1120	1.009
3	1200	1120	1.009
4	1204	1127	1.015

Nominal interval: 32 seconds. Time from beginning of last pulse in first train to beginning of first pulse in second train: 34.1 seconds

1	1200	1110	1.000
2	1200	1120	1.009
3	1200	1127	1.015
4	1200	1130	1.018

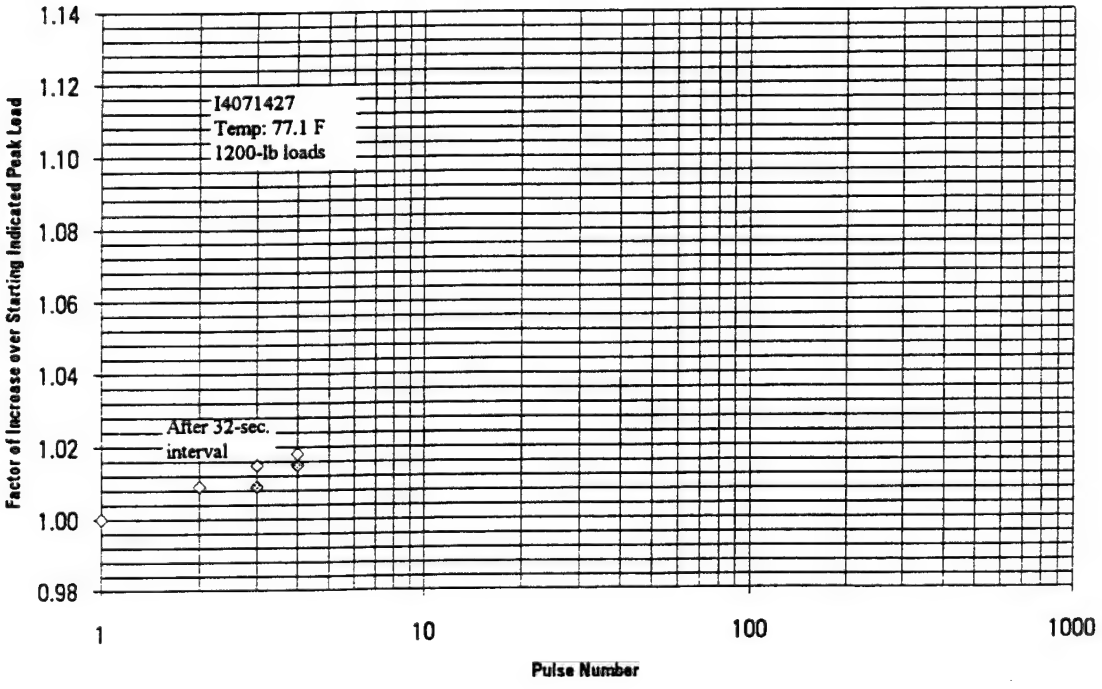

Figure 3-97. Memory, two four-pulse trains, 32-second nominal interval, 77.1 degrees F, 1200-pound loads, sensor I.

Table 3-22. Memory, two four-pulse trains, 32-second nominal interval, 75.8 degrees F, 1200-pound loads, sensor J.

Force calibration temperature:	77.8 degrees F
Calibration load:	1205 lbs.
Calibration file:	J70578
Recording:	J4081117

Pulse Number	Applied Peak Load, lbs.	Indicated Peak Load, lbs.	Factor of Increase Over Starting Indicated Peak Load
1	1196	1107	1.000
2	1188	1117	1.009
3	1196	1127	1.018
4	1192	1133	1.023

Nominal interval: 32 seconds. Time from beginning of last pulse in first train to beginning of first pulse in second train: 34.05 seconds

1	1196	1107	1.000
2	1188	1120	1.012
3	1196	1130	1.021
4	1196	1137	1.027

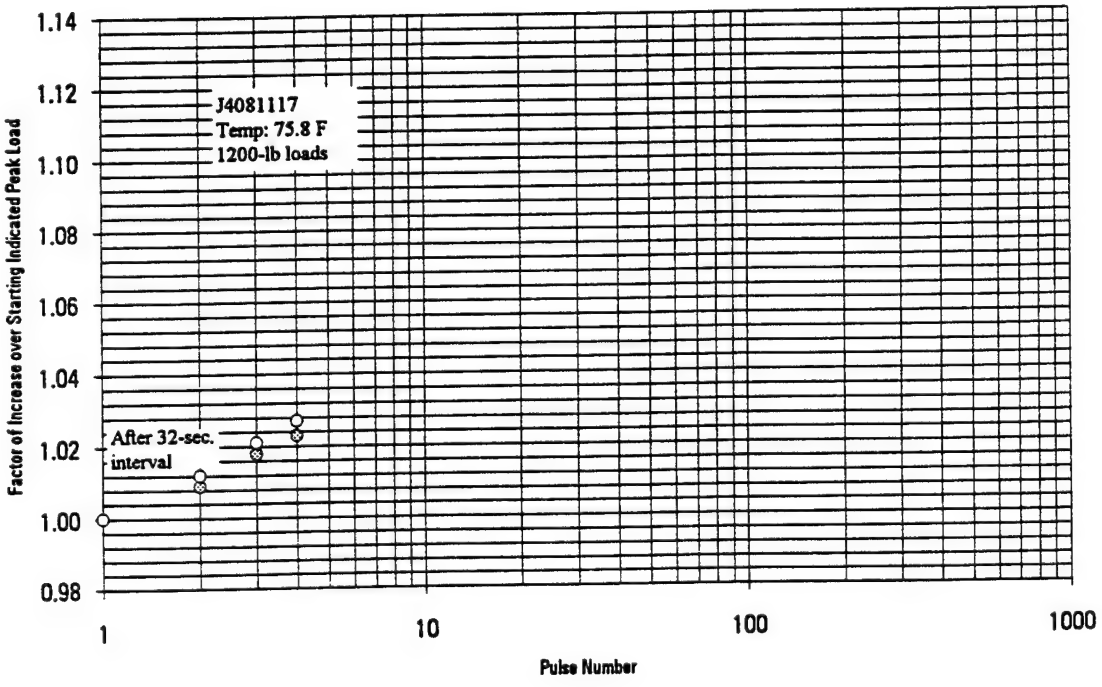

Figure 3-98. Memory, two four-pulse trains, 32 second nominal interval, 75.8 degrees F, 1200-pound loads, sensor J.

Figure 3-98, differences decrease to approximately 1 percent, sometimes less. The same can be said for the results of a test with a 64-second nominal interval (Table 3-23 and Figure 3-99). It appears that a separation of about 50 feet between two successive identical vehicles as described above would be a good guideline for keeping memory effects within 1 percent.

The memory results from the test with the time-scale compressed by a factor of four (Table 3-24 and Figure 3-100) are very similar to the corresponding previous results, with 32-second nominal intervals.

Results from a test at higher temperature, 89.5 degrees F, are displayed in Table 3-25 and Figure 3-101. Memory of the previous pulse train may be slightly greater at the higher temperature, but the difference is on the borderline of the limit of resolution.

3.6 VEHICLE WEIGHINGS.

Vehicle weighings of the previous Weighmat study indicated a worst case accuracy of plus or minus 9 percent between Weighmat readings and truck scale readings. Equilibration of the sensor and application of empirically derived correction factors for non-linearity and temperature effects were proposed in order to improve accuracy. In order to assess the influence of equilibration and statistical corrections on accuracy of the sensor, a series of vehicle drive over tests were performed in this project.

Testing was performed in a WES warehouse building which is part of the Geotechnical Laboratory. All vehicle weighings were conducted at a temperature of 81 degrees F. Two sensors (sensor H and sensor O) were placed side by side so that each side of a vehicle could be weighed for a single drive over as can be seen in Figure 3-102. Two vehicles were weighed: a Bobcat forklift which weighed 7000 pounds and a large 19,000-pound forklift. The Bobcat vehicle was small enough so that it could turn around outside the building, thus weighing in both directions (north and south) was accomplished with the smaller vehicle. With the large vehicle, it was necessary to drive around the building for each test. The large forklift was weighed travelling in one direction (north) only.

Each sensor was "sandwiched" between printing blankets for protection. This sandwich configuration was the same configuration used in the platen loadings tests. The package consisted of two top blankets (r15) and one bottom blanket (r9). Teflon sheets were inserted between the blankets and the sensor to alleviate shearing (see Figure 3-103). Each sensor sandwich was placed on a sheet of 1/8 inch aluminum plate.

Prior to testing, the vehicles were weighed on static scales at WES. The weights obtained for each wheel of both forklifts are shown in Table 3-26. Spread of the static scale readings was at worst plus or minus 11 percent of an average reading; however, in most cases the spread of the readings versus the average was within a few percent.

3.6.1 Bobcat Weighings (Force Calibration Based on Static Scale).

The Bobcat loader was weighed first. Equilibration calibrations which were obtained by 70 psi bladder loadings at 70 degrees F were loaded for each sensor. A force calibration was performed for each sensor based on the average of the static scale readings of the back left wheel of the Bobcat (1805 pounds). In order to compensate for static creep, force calibrations were obtained while the forklift was traversing the sensor at approximately the same speed at which the sensors were tested. Six drive overs (three in each direction) were performed so that each sensor recorded each wheel weight three times.

Table 3-23. Memory, two four-pulse trains, 64-second nominal interval, 75.9 degrees F, 1200-pound loads.

Force calibration temperature:	74.8 degrees F
Calibration load:	1200 lbs.
Calibration file:	I70075
Recording:	I4071234

Pulse Number	Applied Peak Load, lbs.	Indicated Peak Load, lbs.	Factor of Increase Over Starting Indicated Peak Load
1	1192	1090	1.000
2	1188	1103	1.012
3	1192	1110	1.018
4	1192	1113	1.021

Nominal interval: 64 seconds. Time from beginning of last pulse in first train to beginning of first pulse in second train: 66.15 seconds

1	1192	1103	1.012
2	1188	1113	1.021
3	1192	1120	1.028
4	1192	1120	1.028

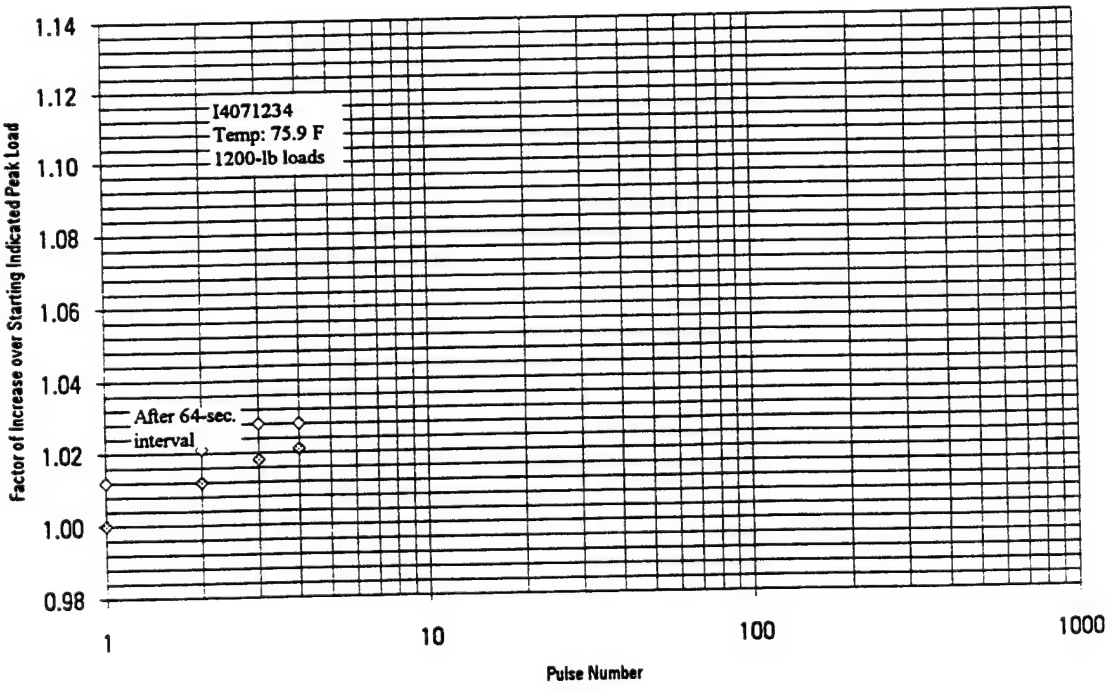

Figure 3-99. Memory, two four-pulse trains, 64-second nominal interval, 75.9 degrees F, 1200-pound loads.

Table 3-24. Two four-pulse trains with time-scale compressed by a factor of four, 8-second nominal interval, 77.3 degrees F, 1200-pound loads.

Force Calibration temperature:	74.8 degrees F
Calibration load:	1200 lbs.
Calibration file:	I70075
Recording:	I4071503

Pulse Number	Applied Peak Load, lbs.	Indicated Peak Load, lbs.	Factor of Increase Over Starting Indicated Peak Load
1	1172	1047*	1.000
2	1184	1057	1.010
3	1184	1067	1.019
4	1184	1067	1.019

Nominal interval: 8 seconds. Equivalent to 32-second interval when time-scale is not compressed.
Time from beginning of last pulse in first train to beginning of first pulse in last train: 9.44 seconds.

1	1184	1057	1.010
2	1184	1067	1.019
3	1184	1070	1.022
4	1184	1077	1.029

* This load was normalized to an applied load of 1184 lbs, by multiplying by 1184/1172.

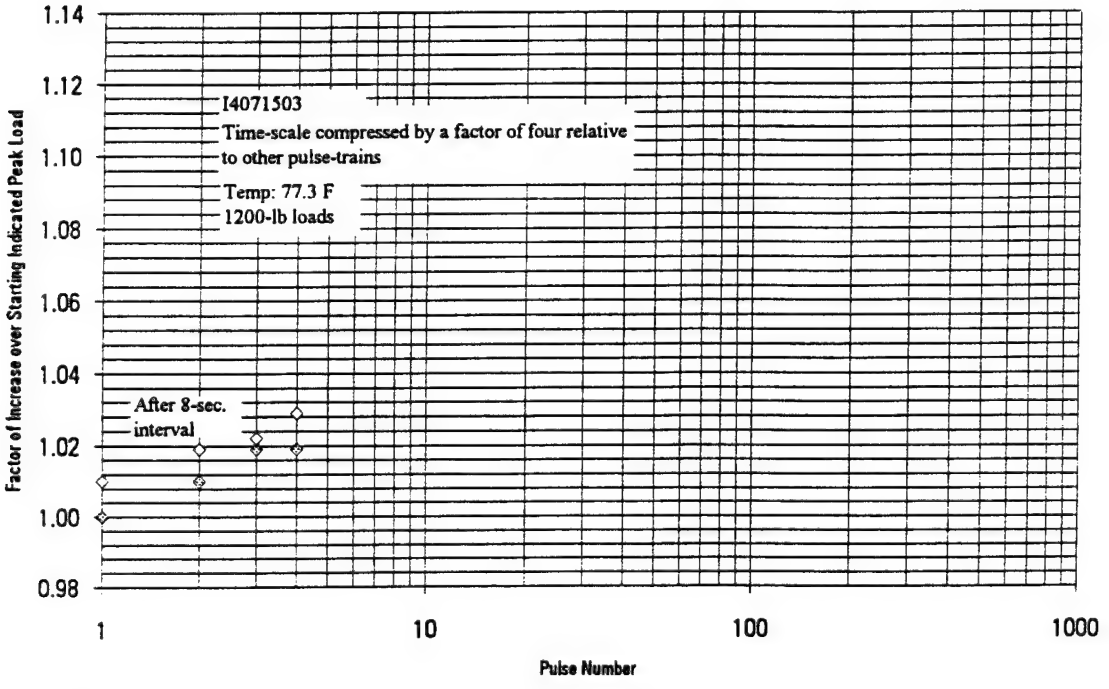

Figure 3-100. Two four-pulse trains with time-scale compressed by a factor of four, 8-second nominal interval, 77.3 degrees F, 1200-pound loads.

Table 3-25. Memory, two four-pulse trains, 32-second nominal interval, 89.5 degrees F, 500-pound loads.

Force calibration temperature:	89.3 degrees F
Calibration load:	514 lbs.
Calibration file:	I70089
Recording:	I4081650

Pulse Number	Applied Peak Load, lbs.	Indicated Peak Load, lbs.	Factor of Increase Over Starting Indicated Peak Load
1	512	442	1.000
2	508	449	1.016
3	512	452	1.023
4	508	454	1.027
Nominal interval: 32 seconds. Time from beginning of last pulse in first train to beginning of first pulse in second train: 33.95 seconds			
1	512	448	1.014
2	512	454	1.027
3	512	455	1.029
4	508	456	1.032

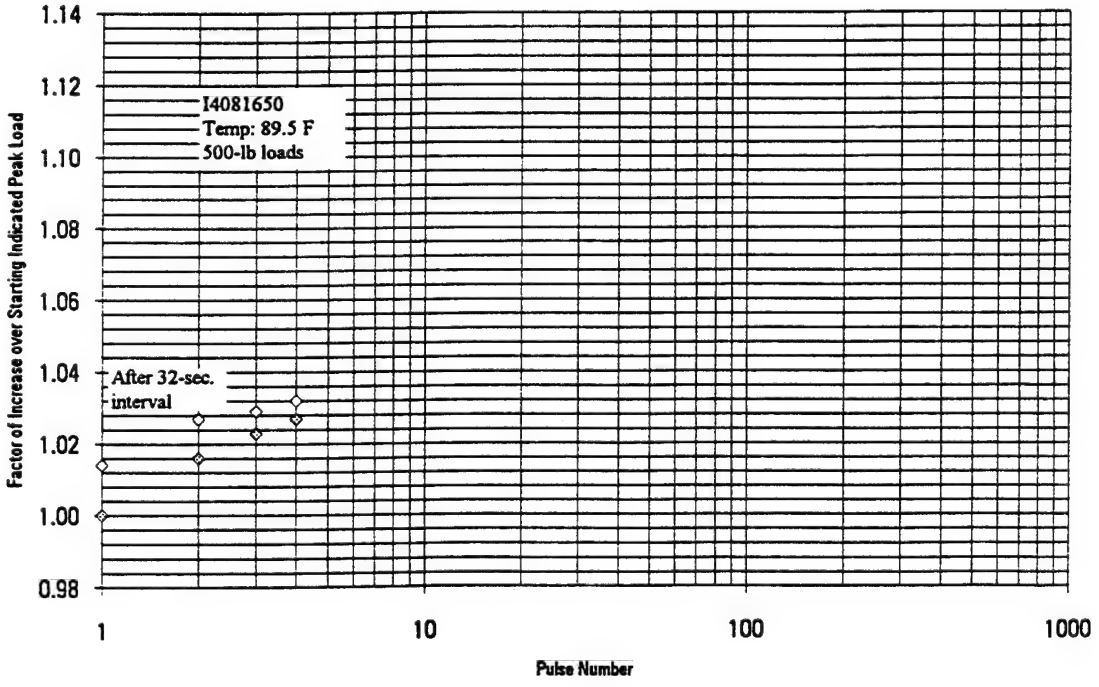

Figure 3-101. Memory, two four-pulse trains, 32-second nominal interval, 89.5 degrees F, 500-pound loads.

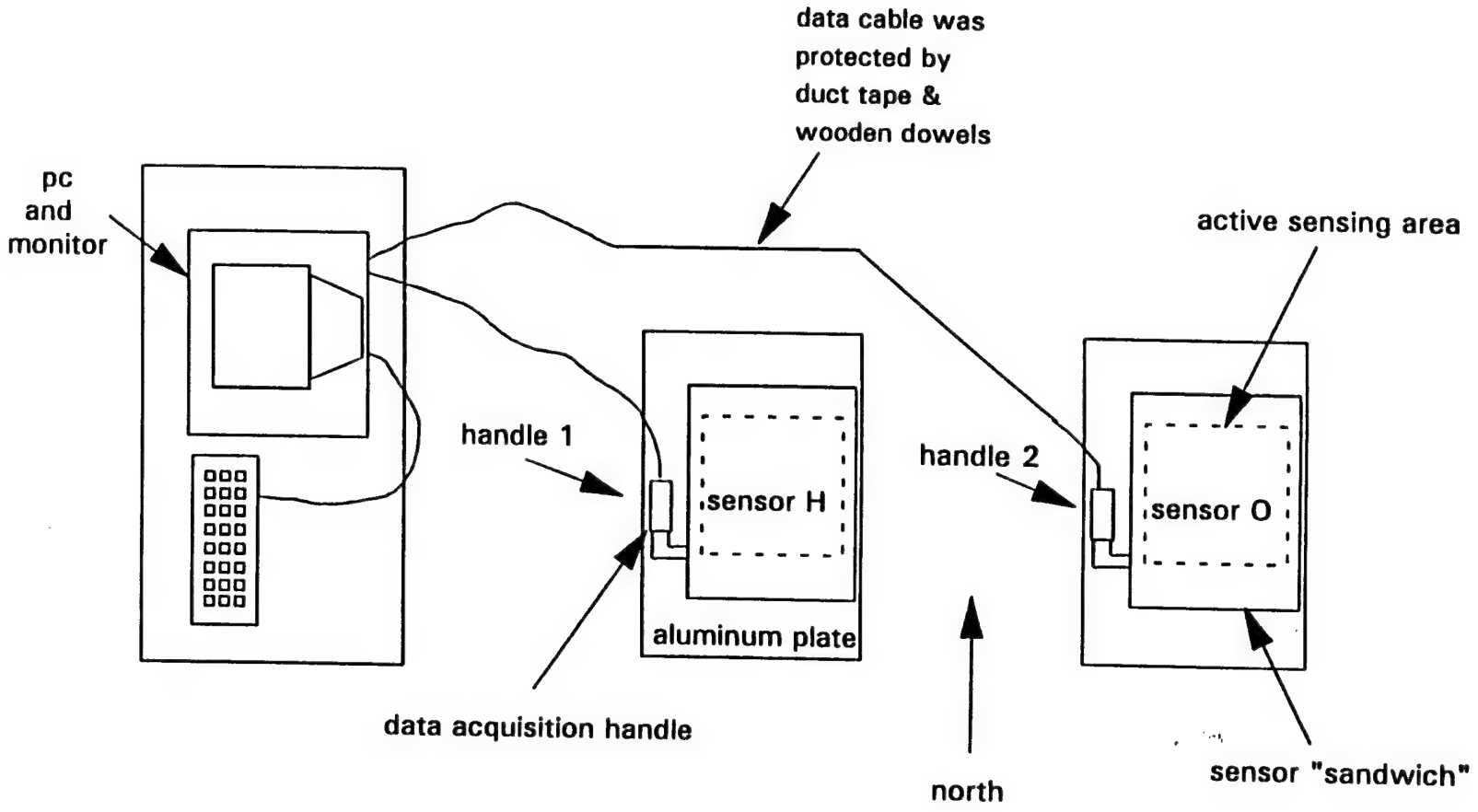

Figure 3-102. Vehicle weighings test layout.

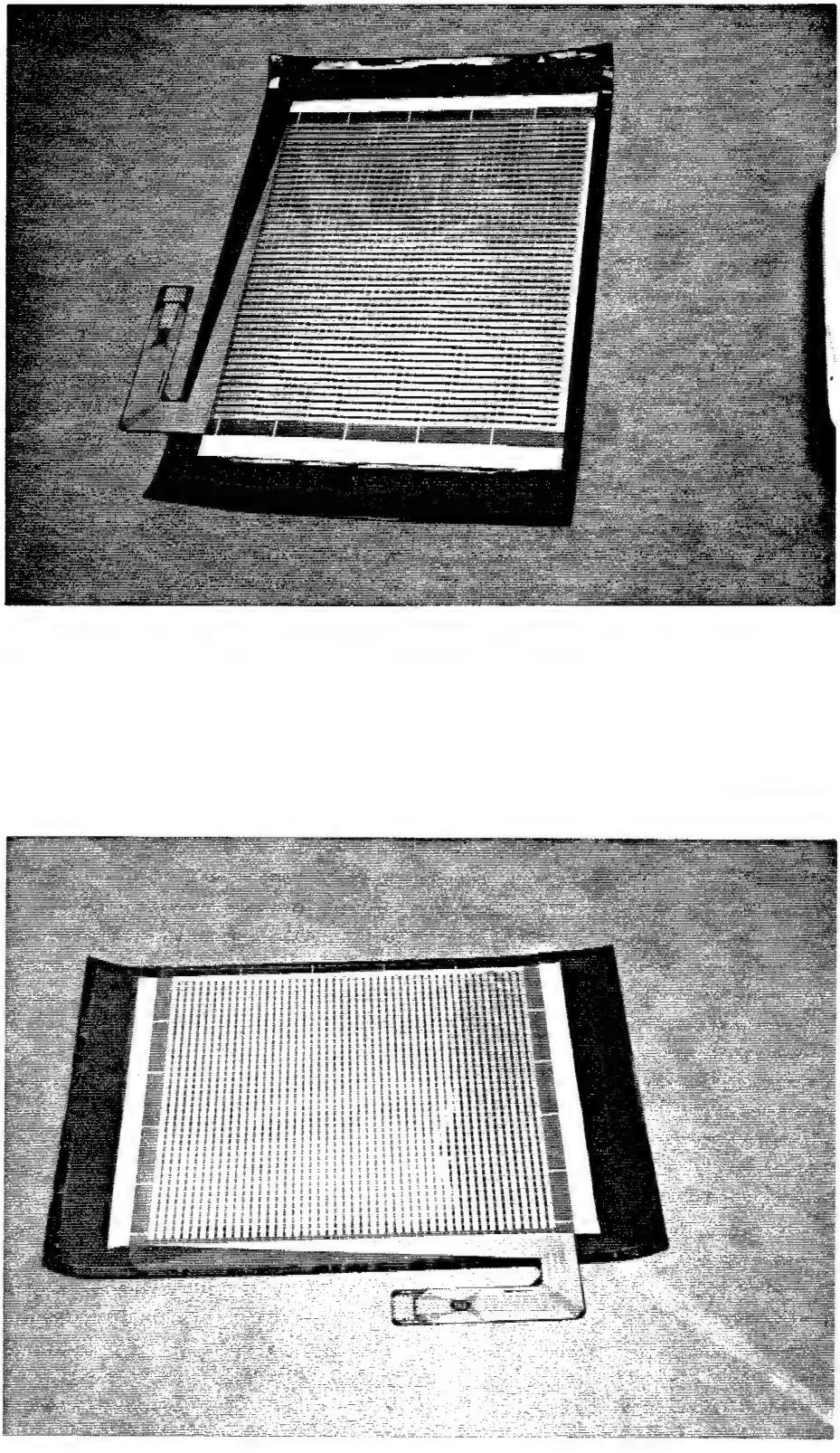

Figure 3-103. Sensor, teflon, and printing blanket.

Table 3-26. Static scales data.

Weights From WES Static Scales

* all weights in lb

Bobcat Loader

direction	left front (lb)	right front (lb)	left back (lb)	right back (lb)	**total weight**
s	1640	560	1840	2740	**6780**
s	1760	580	1820	2760	**6920**
n	1700	700	1780	2680	**6860**
n	1740	680	1780	2640	**6840**
avg	**1710**	**630**	**1805**	**2705**	**6850**

19,000 lb Forklift

direction	left front (lb)	right front (lb)	left back (lb)	right back (lb)	**total weight**
s	3480	4160	5960	5680	**19280**
s	3580	4080	5900	5680	**19240**
n	3680	3600	5960	6000	**19240**
n	3620	3560	5960	5900	**19040**
avg	**3590**	**3850**	**5945**	**5815**	**19200**

Drive over speeds for the first six weighings varied from .95 mph to 1.64 mph with an average of 1.31 mph. Weight readings were taken at 20 Hertz for all drive overs. For the Bobcat drive overs, this sampling rate allowed for six readings for each wheel. Examples of the footprints of Bobcat tires are shown in Figures 3-104 and 3-105.

Results from the first six bobcat weighings can be seen in Tables 3-27 - 3-29. Data denoted "% static" represent the average weight read by the Weighmat as a percent of the static scale reading; "% error" is the difference in the Weighmat reading and the static scale reading over the static scale reading times 100. Because there was not enough static scale data to warrant typical spread indications such as a standard deviation, the spread of the data, i.e., the maximum reading minus the minimum reading from a given set of data was reported here. Also, one should note that there is no correlation between a north static scale reading and a north Weighmat reading; nor is there a correlation between a south static scale reading and a south Weighmat reading. Directionality is indicated here only to distinguish directionality effects of each weighing system.

In general, the Weighmat readings were off by several percent. The average error for a total Bobcat weighing for all six drive overs was 14.2 percent. This large amount of error in the readings is quite high compared to that of previous readings made with unequilibrated sensors (previous Weighmat readings showed a worse case of plus or minus 9 percent). Dynamic motion, specifically bouncing of the Bobcat loader, is believed to be primarily to blame for the variation in the readings. The Bobcat has a short wheelbase with its weights in front of the front wheels (bucket) and behind the rear wheels (counterweight). These vehicle characteristics combine to induce the vehicle to pitch continually. To compound the problem, it was noted that the Bobcat driver was varying the location of the loader bucket between weighings which varied the load distribution causing further variation in the readings. In all cases the Weighmat readings were low. Inaccurate force calibrations caused by dynamic motion during the calibration process are believed to be the cause of the tendency of all readings to be low.

A force calibration is based on a single frame of sensor response. Force calibrations for static loads are therefore more accurate than for dynamic loads. Care must be taken, then, to ensure that force calibrations are made carefully for moving vehicles. Certain short-wheelbase or poorly-suspended vehicles that are prone to excessive pitch may not be suitable for force calibration purposes. Once the system is calibrated, however, it can be used to weigh those troublesome vehicles because weighings capture a time history of wheel loads which may be averaged. A longer Weighmat would allow more data to be obtained for averaging.

Bouncing and/or rocking motion of the Bobcat can be seen in the force time histories of the weighings shown in Figures 3-106 and 3-107. In all cases, the red time history is sensor H and the green time history is sensor O. An even loading of a wheel would result in a flat-topped time history for each loading. Nearly all histories recorded show unevenness in the force while the vehicle load was being applied. The average pressure of the foot print for a varying force was nearly constant (see Tables 3-30 and 3-31) for a given reading. This behavior is indicative of rocking and bouncing dynamic motion of the vehicle. Considering the short wheelbase of the vehicle, some bouncing is reasonable. Also, both vehicles weighed were "unsprung" vehicles with no suspension; all cushion in the ride is given by tire deformation.

Force calibration inaccuracies caused by dynamic motions during the force calibration process are believed to be the reason for the tendency of the readings to be low. The scale factors from all the force calibrations performed during the drive overs are shown in the following table:

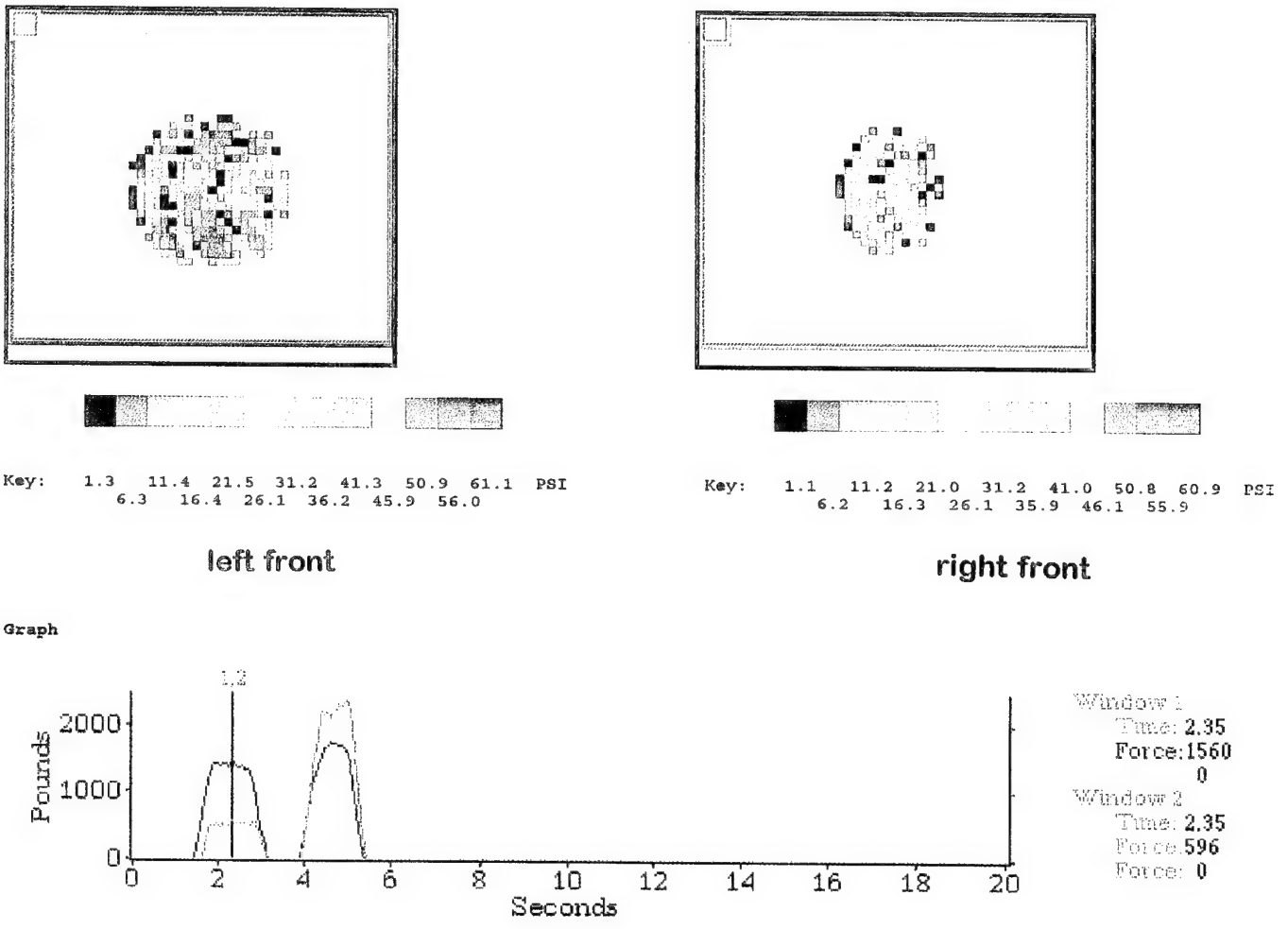

Figure 3-104. Bobcat weighing #1 - front wheels. Vehicle motion is from left to right on page.

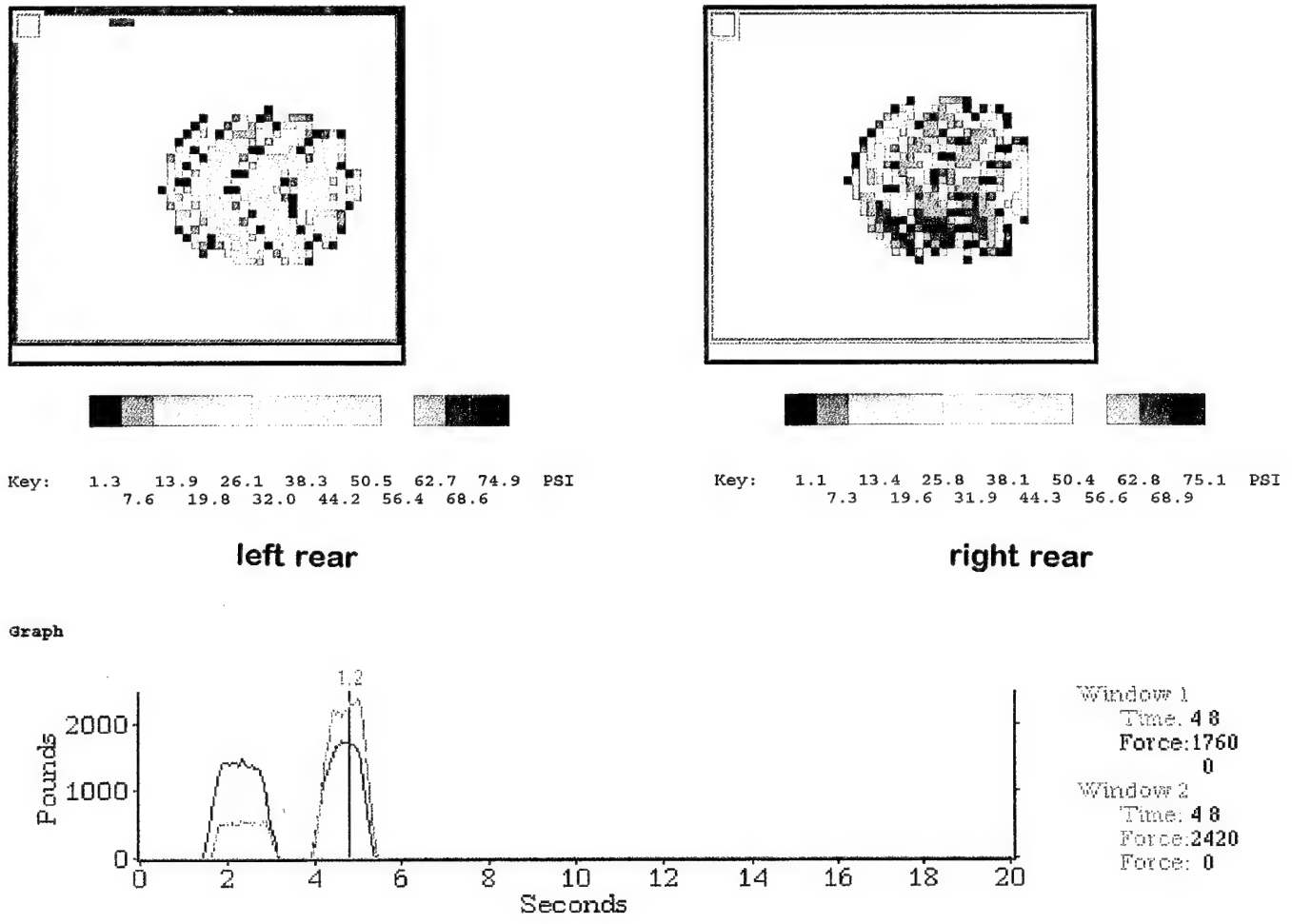

Figure 3-105. Bobcat weighing #1 - rear wheels. Vehicle motion is from left to right on page.

Table 3-27. Bobcat data based on force calibration from left rear wheel of Bobcat.

Bobcat Drive Over Data

* all weights in lb

force cal from bobcat loading - left back wheel (1805 lb - static scales)

driveover 1		v=0.9535 mph			driveover 2		v=1.240 mph		
sensor	H	O	H	O	sensor	O	H	O	H
	left front	right front	left back	right back		left front	right front	left back	right back
	1430	547	1830	2220		1460	535	1630	2240
	1490	607	1820	2290		1380	538	1590	2320
	1560	596	1810	2300		1390	584	1490	2270
	1500	576	1810	2340		1350	575	1550	2290
	1450	572	1766	2420		1350	560	1560	2290
	1450	577	1770	2390		1380	582	1610	2250
avg	1480	579.16667	1801	2326.66667	avg	1385	562.333333	1571.6667	2276.6667
% static	86.549708	91.931217	99.778393	86.0135551	% static	80.99415	89.2592593	87.072946	84.165126
% error	13.450292	8.0687831	0.2216066	13.9864449	% error	19.00585	10.7407407	12.927054	15.834874

driveover 3		v=1.033 mph			driveover 4		v=1.637 mph		
sensor	H	O	H	O	sensor	O	H	O	H
	left front	right front	left back	right back		left front	right front	left back	right back
	1420	588	1740	2290		1310	413	1770	2240
	1400	579	1710	2340		1430	495	1650	2250
	1380	562	1710	2300		1410	538	1550	2200
	1410	597	1750	2280		1410	469	1540	2290
	1400	608	1680	2370		1290	447	1470	2220
	1400	620	1670	2350		1290	421	1460	2270
avg	1401.6667	592.33333	1710	2321.66667	avg	1356.667	463.833333	1573.3333	2245
% static	81.968811	94.021164	94.736842	85.8287123	% static	79.33723	73.6243386	87.165282	82.994455
% error	18.031189	5.978836	5.2631579	14.1712877	% error	20.66277	26.3756614	12.834718	17.005545

driveover 5		v=1.471 mph			driveover 6		v=1.522 mph		
sensor	H	O	H	O	sensor	O	H	O	H
	left front	right front	left back	right back		left front	right front	left back	right back
	1420	493	1640	2100		1390	404	1810	2310
	1490	549	1630	2180		1440	519	1700	2240
	1420	594	1640	2170		1430	493	1640	2170
	1440	584	1640	2270		1340	506	1610	2250
	1410	618	1660	2220		1310	486	1610	2220
	1470	619	1650	2320		1270	562	1620	2240
avg	1441.6667	576.16667	1643.3333	2210	avg	1363.333	495	1665	2238.3333
% static	84.307992	91.455026	91.043398	81.7005545	% static	79.7271	78.5714286	92.243767	82.747998
% error	15.692008	8.5449735	8.956602	18.2994455	% error	20.2729	21.4285714	7.7562327	17.252002
avg of 3	1441.1111	582.55556	1718.1111	2286.11111	avg of 3	1368.333	507.055556	1603.3333	2253.3333
% static	84.275504	92.469136	95.186211	84.514274	% static	80.01949	80.4850088	88.827331	83.302526
% error	15.724496	7.5308642	4.8137889	15.485726	% error	19.98051	19.5149912	11.172669	16.697474

Table 3-28. Weighmat data versus static scales.

Bobcat Drive Over Data

* all weights in lb

force cal from bobcat loading - left back wheel (1805 lb - static scales)

Weighmat vs. Static Scales

	left front	right front	left back	right back	total
weighmat north readings					
driveover 1	1480	579.1667	1801	2326.667	6186.83
driveover 3	1401.667	592.3333	1710	2321.667	6025.67
driveover 5	1441.667	576.1667	1643.333	2210	5871.17
avg	**1441.111**	**582.5556**	**1718.111**	**2286.111**	**6027.89**
spread	**78**	**16**	**158**	**117**	**316**
weighmat south readings					
driveover 2	1385	562.3333	1571.667	2276.667	5795.67
driveover 4	1356.667	463.8333	1573.333	2245	5638.83
driveover 6	1363.333	495	1665	2238.333	5761.67
avg	**1368.333**	**507.0556**	**1603.333**	**2253.333**	**5732.06**
spread	**28**	**98**	**93**	**39**	**157**
static scale north readings					
reading 1	1700	700	1780	2680	6860
reading 2	1740	680	1780	2640	6840
avg	**1720**	**690**	**1780**	**2660**	**6850**
spread	**40**	**20**	**0**	**40**	**20**
static scale south readings					
reading 1	1640	560	1840	2740	6780
reading 2	1760	580	1820	2760	6920
avg	**1700**	**570**	**1830**	**2750**	**6850**
spread	**120**	**20**	**20**	**20**	**140**

Table 3-29. Summary of Bobcat data based on force calibration from left rear wheel of Bobcat.

Bobcat Weighings

Summary - force cal from bobcat left-back wheel load

* all weights in lb

avg v = 1.309 mph

	left front	right front	left back	right back	total
Average Weight - All Weighings					
weighmat	1405	545	1661	2270	5880
static	1710	630	1805	2705	6850
% static	82.16374	86.507937	92.02216	83.91867	85.83942
% error	17.83626	13.492063	7.977839	16.08133	14.16058
Maximum Spread - Weighings In One Direction					
weighmat	78	16	158	117	316
weighmat	28	98	93	39	157
static	40	20	0	40	20
static	120	20	20	20	140
Maximum Spread - All Weighings					
weighmat	290	207	370	320	548
static	120	60	140	120	140

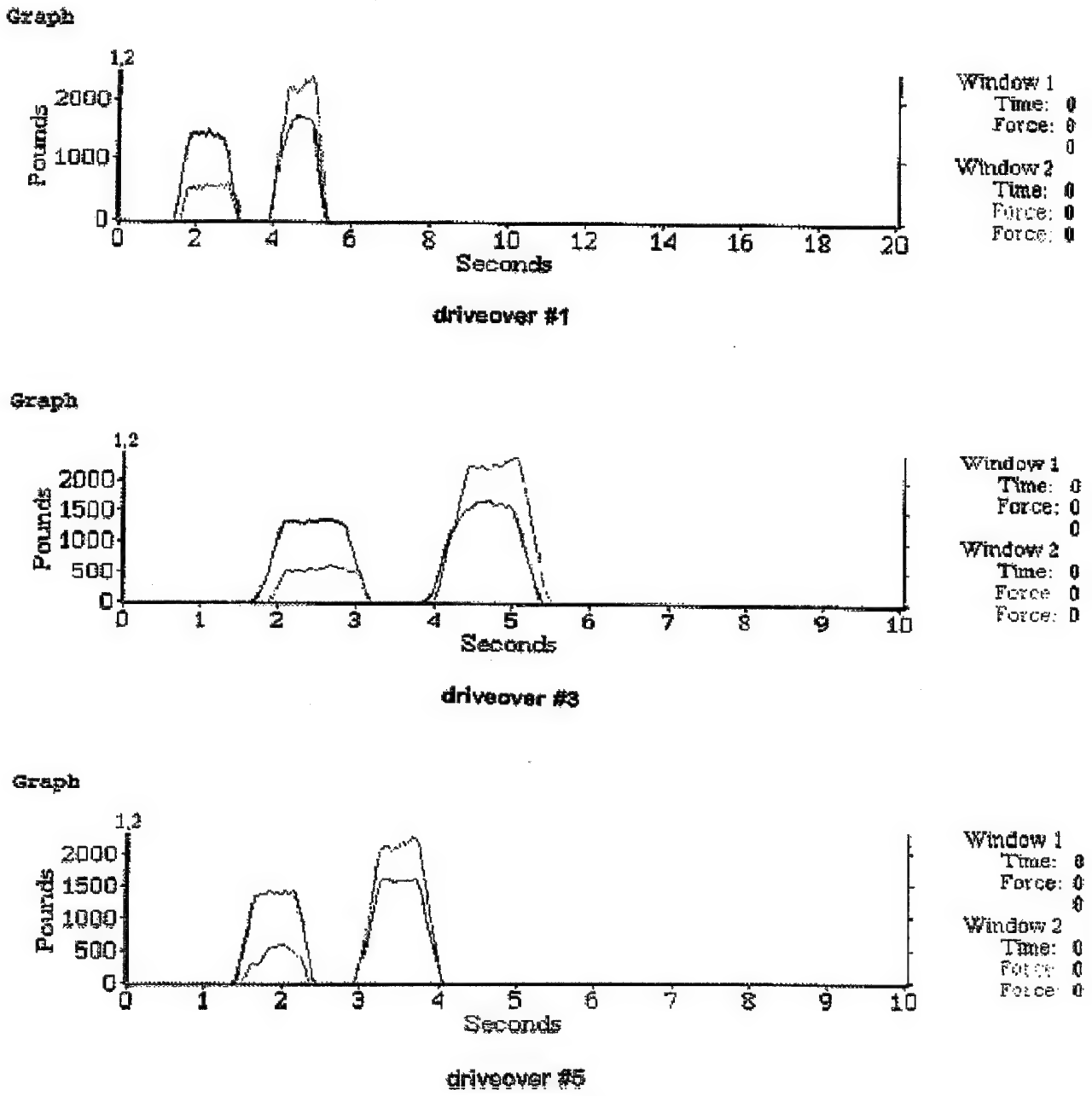

Figure 3-106. Northward weighings of Bobcat.

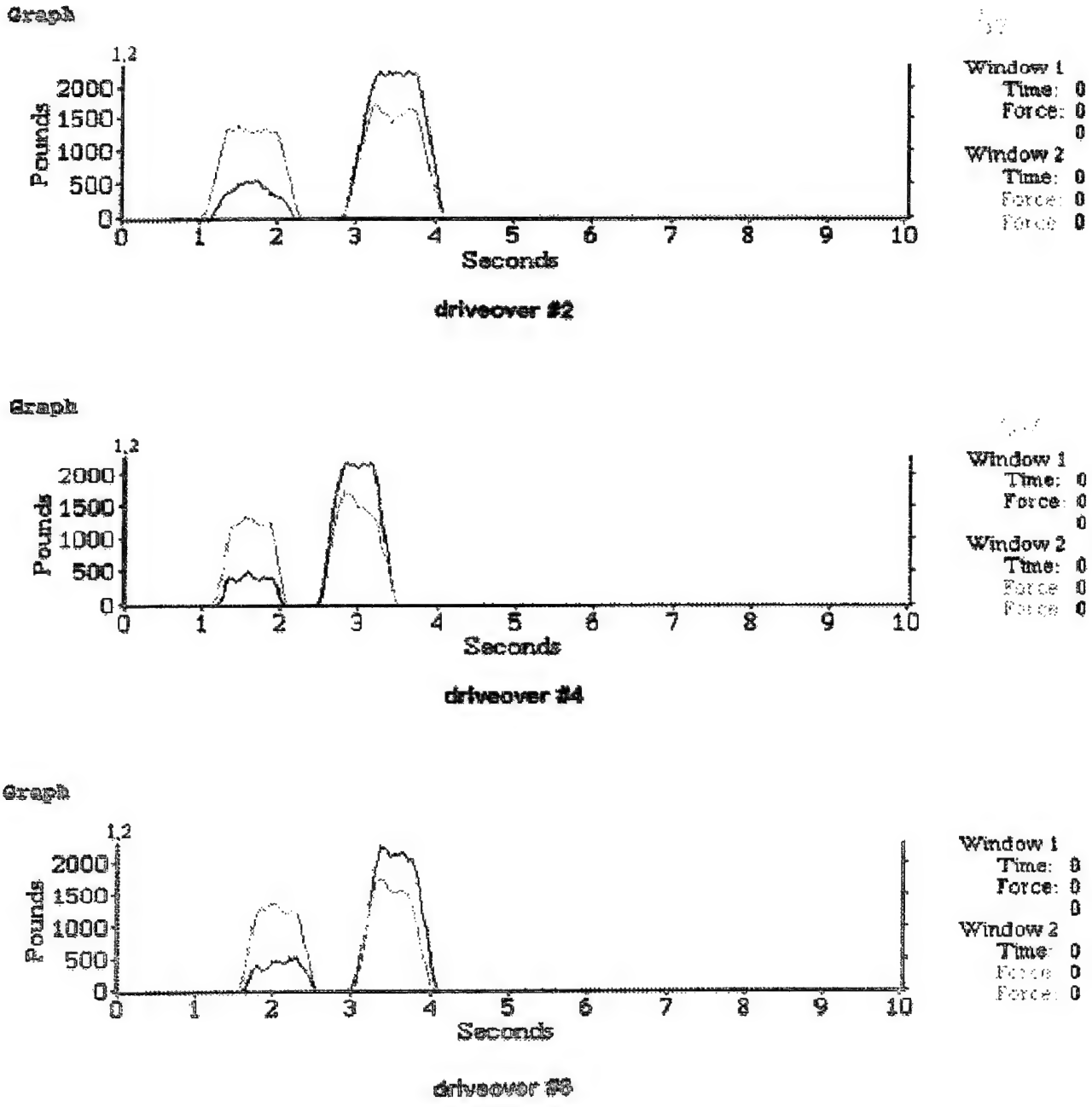

Figure 3-107. Southward weighings of Bobcat.

Table 3-30. Bobcat data including average pressures.

Bobcat Drive Over Data

* all weights in lb, areas in in^2, and pressures in psi
force cal from bobcat loading - left back wheel (1805 lb - static scales)

driveover 1 v=0.9536 mph

sensor	H			O			H			O		
	left front	area	pressure	right front	area	pressure	left back	area	pressure	right back	area	pressure
	1430	38.72	36.93182	547	13.28	41.18976	1830	56.96	32.12781	2220	37.12	59.806
	1490	40.64	36.66339	607	15.2	39.93421	1820	56.96	31.95225	2290	39.36	58.1809
	1560	42.56	36.65414	596	15.2	39.21053	1810	51.36	35.24143	2300	39.2	58.6735
	1500	42.56	35.24436	576	14.08	40.90909	1810	53.12	34.0738	2340	39.04	59.9385
	1450	40.32	35.9623	572	13.6	42.05882	1766	52	33.96154	2420	41.44	58.3977
	1450	41.76	34.72222	577	14.4	40.06944	1770	49.28	35.91721	2390	40.8	58.5784
avg	1480		36.0297	579.16667		40.56198	1801		33.87901	2326.6667		58.9292
% static	86.54971			91.931217			99.77839			86.013556		
% error	13.45029			8.0687831			0.221607			13.986445		

driveover 2 v=1.240 mph

sensor	O			H			O			H		
	left front	area	pressure	right front	area	pressure	left back	area	pressure	right back	area	pressure
	1460	30.4	48.02632	535	19.04	28.09874	1630	35.68	45.68386	2240	47.84	46.8227
	1380	28.96	47.65193	538	20.32	26.47638	1590	35.36	44.96606	2320	49.44	46.9256
	1390	29.6	46.95946	584	20.16	28.96825	1490	33.12	44.98792	2270	48.64	46.6694
	1350	28.96	46.61602	575	21.6	26.62037	1550	34.24	45.26869	2290	47.2	48.5169
	1350	28.8	46.875	560	19.68	28.45528	1560	34.72	44.93088	2290	50.24	45.5812
	1380	29.6	46.62162	582	21.44	27.14552	1610	35.84	44.92187	2250	46.88	47.9949
avg	1385		47.12506	562.33333		27.62742	1571.667		45.12655	2276.6667		47.0851
% static	80.99416			89.259259			87.07295			84.165126		
% error	19.00585			10.740741			12.92705			15.834874		

driveover 3 v=1.033 mph

sensor	H			O			H			O		
	left front	area	pressure	right front	area	pressure	left back	area	pressure	right back	area	pressure
	1420	39.2	36.22449	588	14.56	40.38462	1740	51.36	33.8785	2290	39.52	57.9453
	1400	40.96	34.17969	579	14.08	41.12216	1710	51.36	33.29439	2340	40.96	57.1289
	1380	36	38.33333	562	14.08	39.91477	1710	49.76	34.36495	2300	40.48	56.8182
	1410	37.92	37.18354	597	15.2	39.27632	1750	51.36	34.07321	2280	39.52	57.6923
	1400	40.48	34.58498	608	15.68	38.77551	1680	50.88	33.01887	2370	40.96	57.8613
	1400	36.96	37.87879	620	16	38.75	1670	47.68	35.02517	2350	41.6	56.4904
avg	1401.667		36.39747	592.33333		39.7039	1710		33.94252	2321.6667		57.3227
% static	81.96881			94.021164			94.73684			85.828712		
% error	18.03119			5.978836			5.263158			14.171288		

Table 3-31. Bobcat data including average pressures.

Bobcat Drive Over Data

* all weights in lb, areas in in^2, and pressures in psi
force cal from bobcat loading - left back wheel (1805 lb - static scales)

driveover 4		v=1.637 mph										
sensor	O			H			O			H		
	left front	area	pressure	right front	area	pressure	left back	area	pressure	right back	area	pressure
	1310	27.52	47.60174	413	14.88	27.75538	1770	37.92	46.67722	2240	53.12	42.1687
	1430	31.2	45.83333	495	18.56	26.67026	1650	36.16	45.63053	2250	51.36	43.8084
	1410	30.24	46.62698	538	18.4	29.23913	1550	35.04	44.23516	2200	50.4	43.6508
	1410	30.08	46.875	469	19.04	24.63235	1540	35.04	43.94977	2290	51.84	44.1744
	1290	26.24	49.16159	447	17.44	25.63073	1470	32.96	44.59951	2220	48	46.25
	1290	27.52	46.875	421	16.16	26.05198	1460	32.16	45.39801	2270	50.72	44.7555
avg	1356.667		47.16227	463.83333		26.66331	1573.333		45.0817	2245		44.1346
% static	79.33723			73.624339			87.16528			82.994455		
% error	20.66277			26.375661			12.83472			17.005545		

driveover 5		v=1.471 mph										
sensor	H			O			H			O		
	left front	area	pressure	right front	area	pressure	left back	area	pressure	right back	area	pressure
	1420	38.24	37.13389	493	12.32	40.01623	1640	50.4	32.53968	2100	36.8	57.0652
	1490	42.4	35.14151	549	14.08	38.99148	1630	47.84	34.07191	2180	39.36	55.3862
	1420	38.72	36.67355	594	15.84	37.5	1640	49.6	33.06452	2170	39.36	55.1321
	1440	40.96	35.15625	584	15.36	38.02083	1640	49.12	33.38762	2270	40.8	55.6373
	1410	37.28	37.82189	618	15.84	39.01515	1660	51.2	32.42188	2220	39.68	55.9476
	1470	42.88	34.28172	619	14.88	41.59946	1650	49.76	33.15916	2320	41.28	56.2016
avg	1441.667		36.0348	576.16667		39.19053	1643.333		33.10746	2210		55.896
% static	84.30799			91.455026			91.0434			81.700565		
% error	15.69201			8.5449735			8.956602			18.299445		

driveover 6		v=1.522 mph										
sensor	O			H			O			H		
	left front	area	pressure	right front	area	pressure	left back	area	pressure	right back	area	pressure
	1390	29.28	47.47268	404	14.56	27.74725	1810	39.84	45.43173	2310	51.28	45.0468
	1440	31.36	45.91837	519	17.76	29.22297	1700	36.96	45.99567	2240	53.12	42.1687
	1430	31.36	45.59949	493	18.56	26.5625	1640	36.64	44.75983	2170	55.52	39.085
	1340	29.12	46.01648	506	18.56	27.26293	1610	35.36	45.53167	2250	54.4	41.3603
	1310	28.16	46.51989	486	16.8	28.92857	1610	35.36	45.53167	2220	55.04	40.3343
	1270	26.88	47.24702	562	18.72	30.02137	1620	36.48	44.40789	2240	52.32	42.8135
avg	1363.333		46.46232	495		28.29093	1665		45.27641	2238.3333		41.8014
% static	79.7271			78.571429			92.24377			82.747998		
% error	20.2729			21.428571			7.756233			17.252002		

vehicle	wheel	sensor	scale factor
Bobcat	left rear, 1805 lb	H	0.362741
Bobcat	left rear, 1805 lb	O	0.421052
19,000-lb forklift	front left, 3590 lb	H	0.447613
19,000-lb forklift	front right, 3850 lb	O	0.436160

The scale factor is simply the conversion from raw digital output read by the sensor to a force. These scale factors should be the same number at a given temperature and input pressure. The temperature remained constant (81 degrees F) throughout the experiment. Contact pressures for all wheels weighed ranged from 35 to 60 psi which is a significant range. However, it is interesting to note that the two force calibrations which were performed with the 19,000-pound forklift were performed at around 35 psi for the left wheel and around 55 psi for the right. With this big a difference in the input pressure the scale factors varied only slightly. The 19,000-pound forklift weighings, which will be discussed later in detail, showed very good accuracy indicating accuracy of the scale factors. Scale factors from the Bobcat calibrations should have been basically the same as the scale factors obtained by the forklift based on the fact that the Bobcat scale factors were obtained at pressures in the same range as those of the forklift (Bobcat pressures for the left rear calibration wheel varied from 33 psi to 45 psi). The Bobcat scale factors were slightly lower, however, and thus subsequent readings with these scale factors all tended to be low. The indication is that the Bobcat vehicle was experiencing dynamic motion when the calibration was made.

3.6.2 Bobcat Weighings (Force Calibration From 1200-pound Platen Load @ -19F).

Five additional Bobcat drive overs were performed using sensor H only. Sensor H had been previously tested in the environmental chamber at -19 degrees F. Prior to testing sensor H at this low temperature, the equilibration calibration for a 70 psi bladder loading at 70 degrees F was loaded and a force calibration was made for a platen loading of 1200 pounds. This force calibration was used for the five additional drive overs. The purpose of using this calibration file was to see how well empirically derived corrections could improve the weight readings.

Results of the additional Bobcat weighings can be seen in Table 3-32. The readings for all wheel weights were approximately twice that of the static scale weights. The high reading of the sensor is consistent with expected behavior. That is, it is expected that this sensor would tend to be more sensitive if it was calibrated at a low temperature and tested at a higher temperature. Spread of the weight data was somewhat small regardless of the fact that some dynamic motion was noted in the time histories. Dynamic motion was extreme for drive over #10, however, the average reading for weighing #10 varied little from that of the other data.

These weighings were performed in order to see if corrections based on lab data could be implemented to improve accuracy of the readings under field conditions. Two methods were implemented to correct the data. The first correction (denoted "cor-1" on data sheets) was

simply to use the ratio of scale factors from two force calibrations at the two temperatures. The corrected weight was calculated as:

$$W^* = W\,(SF_{81}/SF_{-19})$$

where:
- W^* = corrected weight
- W = weight reading
- SF_{81} = scale factor for cal @ 81 degrees F
- SF_{-19} = scale factor for cal @ -19 degrees F.

Based on accuracy of the 19-kip forklift weighings, it was believed that the force calibration performed with the forklift was more accurate than that obtained with the Bobcat. It is for this reason that the scale factor from the calibration made with the forklift was used as SF_{81}.

The second method utilized the nonlinear data fit which is included in the appendix of this report. The data fit performed gives raw digital output as a function of pressure and temperature:

$$R = f(P,T)$$

where:
- R = raw digital output
- P = input pressure in psi
- T = temperature in degrees Rankine.

The second correction process (denoted cor-2 on the data sheets) was performed in the following manner. The force read by the Weighmat was divided by the loaded area of the foot print in order to obtain an average pressure. This pressure and each temperature (81 degrees F and -19 degrees F) were used to get two raw digital output values from the data fit equation. The ratio of the values was used to correct the reading:

$$W^* = W(DO_{P,-19}/DO_{P,81})$$

where:
- W^* = corrected weight
- W = weight reading
- $DO_{P,-19}$ = digital output calculated from data fit based on avg pressure and T = -19 deg F
- $DO_{P,81}$ = digital output calculated from data fit based on avg pressure and T = 81 deg F.

Corrected data are shown in Tables 3-33 and 3-34. Corrections based on the first method did a fair job of improving accuracy. The average error was on the order of 10 to 12 percent which is comparable to accuracy obtained for the first six Bobcat drive overs. Corrections based on the second method improved accuracy significantly; worst-case errors were on the order of 7 percent. One interesting observation was that with the second

Table 3-32. Bobcat data based on force calibration from platen load at -19 degrees F.

Bobcat Drive Over Data

Force cal from 1200 lb platen load @ -19 F
Sensor H Only
* all weights in lb

driveover 7	v=1.496 mph	
north	left front	left back
	3400	4120
	3490	4170
	3670	4040
	3440	4100
	3390	3950
	3220	3980
avg	3435	4060
% static	200.8772	224.9307
% error	100.8772	124.9307

driveover 8	v=1.205 mph	
south	right front	right back
	1210	5720
	1340	5530
	1240	5590
	1240	5370
	1230	5470
	1260	5500
avg	1253.333	5530
% static	198.9418	204.4362292
% error	98.9418	104.4362292

driveover 9	v=1.735 mph	
north	left front	left back
	3210	4140
	3490	4280
	3560	4120
	3440	4120
	3460	4030
	3360	4050
avg	3420	4123.333
% static	200	228.4395
% error	100	128.4395

this south drive over was not recorded due to operator error

driveover 10	v=1.972 mph	
north	left front	left back
	2810	3540
	2870	3390
	2950	4180
	3390	4350
	3710	4380
	3750	4330
avg	3246.667	4028.333
% static	189.8635	223.1764
% error	89.86355	123.1764

driveover 11	v=1.496 mph	
south	right front	right back
	1120	5570
	1310	5300
	1190	5490
	1260	5370
	1240	5570
	1350	5340
avg	1245	5440
% static	197.619	201.1090573
% error	97.61905	101.1090573

Table 3-33. Bobcat data corrections.

Bobcat Drive Over Data

Corrections To Readings Taken With Force Cal From -19 Deg F

driveover 7			
north	left front	left back	left total
avg	3435	4060	7495
% static	200.8772	224.9307	213.22902
% error	100.8772	124.9307	113.22902
cor-1	1495.932	1768.118	3264.05
% static	87.4814	97.95668	92.860597
% error	12.5186	2.043324	7.1394026
cor-2	1633.2	2016.32	3649.52
% static	95.50877	111.7075	103.82703
% error	4.491228	11.70748	3.827027

driveover 8			
south	right front	right back	right total
avg	1253.333	5530	6783.333
% static	198.94175	204.43623	203.39829
% error	98.941746	104.43623	103.39829
cor-1	545.6229	2408.2984	2954.1213
% static	86.638556	89.031365	88.57935
% error	13.361444	10.968635	11.42065
cor-2	636.444	2515.77	3152.214
% static	101.02286	93.004436	94.51916
% error	1.0228571	6.9955638	5.4808396

driveover 9			
north	left front	left back	left total
avg	3420	3481.333	6901.33
% static	200	192.8716	196.339
% error	100	92.87163	96.3395
cor-1	1489.4	1516.11	3005.51
% static	87.09942	83.99501	85.5053
% error	12.90058	16.00499	14.4947
cor-2	1643.48	2002.94	3646.42
% static	96.10994	110.9662	103.739
% error	3.890058	10.9662	3.73883

driveover 10			
north	left front	left back	left total
avg	3246.667	4028.333	7275
% static	189.8635	223.1764	206.97013
% error	89.86355	123.1764	106.97013
cor-1	1413.914	1754.327	3168.241
% static	82.68503	97.19263	90.134879
% error	17.31497	2.807368	9.8651209
cor-2	1579.32	2016.47	3595.79
% static	92.35789	111.7158	102.29844
% error	7.642105	11.71579	2.2984353

driveover 11			
south	right front	right back	right total
avg	1245	5440	6685
% static	197.61905	201.10906	200.44978
% error	97.619048	101.10906	100.44978
cor-1	542.1938	2369.1037	2911.2975
% static	86.062508	87.582391	87.295277
% error	13.937492	12.417609	12.704723
cor-2	632.999	2473.3	3106.299
% static	100.47603	91.434381	93.142399
% error	0.4760317	8.5656192	6.8576012

Table 3-34. Summary of Bobcat data based on force calibration from -19 degrees F.

Bobcat Drive Over Data

Summary - Force cal from 1200 lb platen load @ -19 F
Sensor H Only
* all weights in lb

avg v = 1.581 mph

	left front	right front	left back	right back	left total	right total
	3 readings	2 readings	3 readings	2 readings		
avg	3367.222	1249.1667	4070.556	5485	7437.778	6734.167
% static	196.9136	198.28042	225.5155	202.7726	211.6011	201.924
% error	96.91358	98.280423	125.5155	102.7726	111.6011	101.924
cor-1	1466.415	544.00835	1679.518	2388.701	3145.934	2932.709
% static	85.75528	86.350532	93.04811	88.30688	89.50025	87.93731
% error	14.24472	13.649468	6.951893	11.69312	10.49975	12.06269
cor-2	1618.665	634.72188	2011.909	2494.535	3630.574	3129.257
% static	94.65876	100.7495	111.4631	92.21942	103.288	93.8308
% error	5.341237	0.7495041	11.46309	7.78058	3.288011	6.1692

correction the data consistently bounded the static scale reading. The front wheels read a lower weight than the static scale reading and the back wheels read higher. The total of the front and back readings yielded good agreement with the total weight for one side of the vehicle. Vehicle pitching and the shifting of the bucket by the driver of the Bobcat which was noted during the weighings explains the cause of the load distribution change from front to back.

3.6.3 Forklift Weighings.

The 19,000-pound forklift was weighed five times. Because the forklift was tested in only one direction, each sensor weighed only one side of the vehicle; sensor H weighed the left side of the forklift and sensor O weighed the right. Force calibrations were based on the static weights of each of the front wheels. Drive overs with the 19,000-pound forklift were performed at slightly higher speeds than those of the Bobcat forklift. The Bobcat forklift was weighed at speeds of around 1.4 mph while the larger forklift traveled at speeds of 2 mph over the sensors. Examples of the footprints for each of the tires on the forklift are shown in Figures 3-108 and 3-109.

Results from the forklift weighings are shown in Table 3-35. Because of the large tire footprint and the faster speed of the vehicle, fewer data readings were available. Three data points were averaged to obtain a front wheel reading while only one data point was available for rear wheel readings. Nevertheless, weights obtained were in quite good agreement with static scale data. In fact, the average of all readings was within 2 percent of the average static scale reading. Good accuracy is the result of equilibration, accurate force calibrations, and repeatability of the input load. Had the forklift been subject to severe pitching or heaving, neither an accurate force calibration could have been obtained nor would repeatability of the loads have been realized. Thus, it is believed that the forklift, which had a much longer wheelbase and compliant rough terrain tires, was less susceptible to the dynamic forces which plagued the Bobcat. The Bobcat, however, provides a glimpse of the loading conditions which may be encountered with certain tandem axle combinations found on tractor-trailer vehicles.

3.6.4 Weighmat Damage from Vehicle Loads.

It was noted that while the vehicles were travelling across the mat/plate configurations, the mats and printing blankets curled up at the edges (see Figure 3-110). This curling was particularly notable for the 19-kip loader; therefore, it was not surprising that wrinkling of the Weighmat sensor was noted upon disassembly of the Weighmat/printing blanket sandwiches. A sketch of the damage is shown in Figure 3-111 and photographs are shown in Figures 3-112 - 3-114. Both sensors showed wrinkling on the side opposite the handle. This edge damage reached into the sensing area on sensor O. Sensor O, which showed the most damage of the two mats, also showed wrinkling in a strip of the mat 5 inches from the side opposite the handle. Sensor H showed only minor creases in the sensing area.

All sensor damage was in the form of Z-shaped creases approximately 0.05 inches in width. Damage at the edge of the sensor showed as creases at 20-30 degree angles to the edge. This damage is due to a shearing which took place when the vehicle was allowed to traverse the mat too closely to the edge where the sensor was secured to the printing blankets. This type damage could be eliminated by making the sensor mat wider and keeping the sensor area the same size. The other creases in the sensing area were caused by localized shearing effects of the aggressive treads of the vehicles. This type of damage can be eliminated by a protective covering which would resist the shear loading without deflecting the vertical load. Teflon would still be needed to deter shearing between the protective cover and the mat.

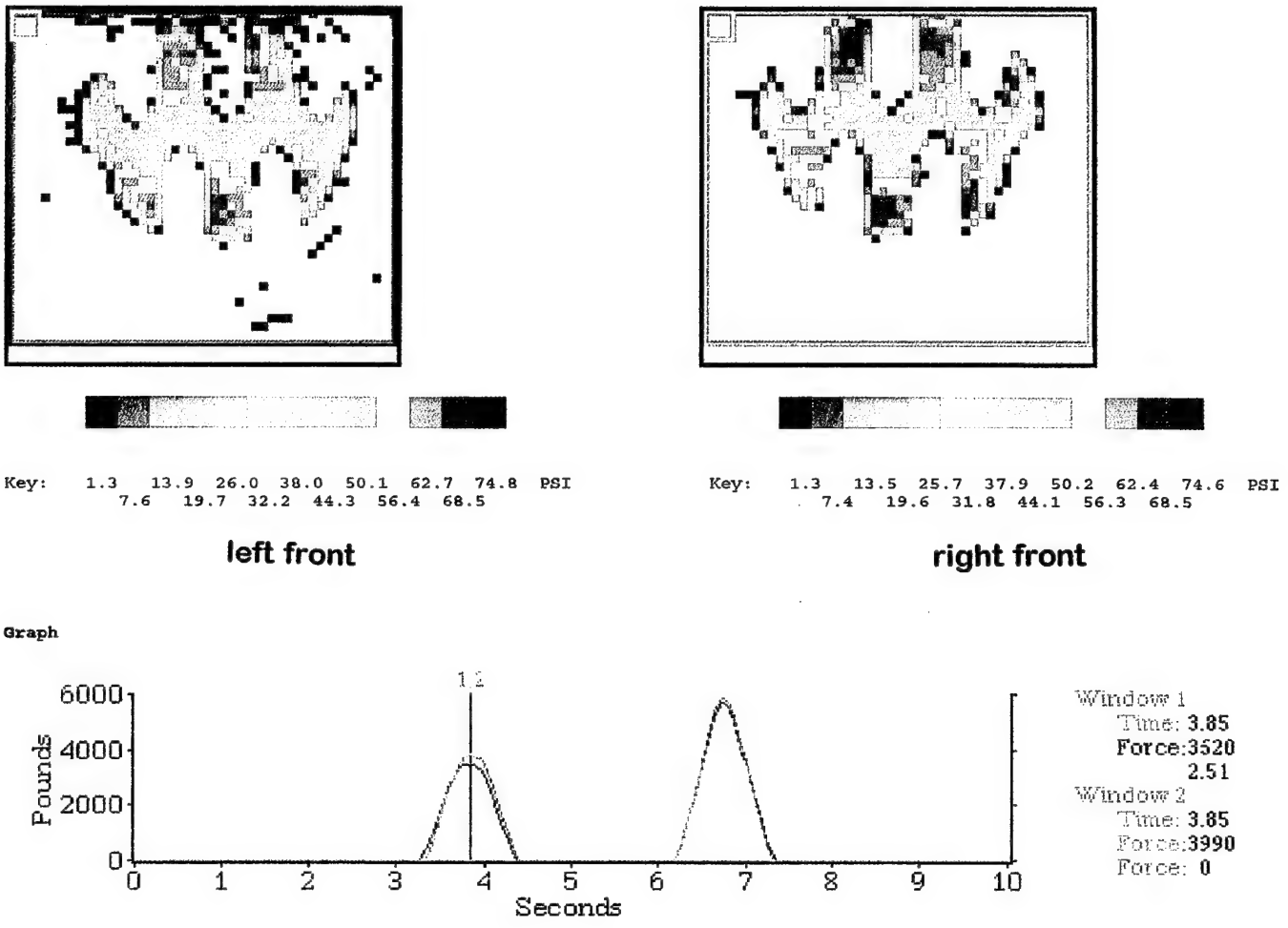

Figure 3-108. 19 kip loader weighing #1 - front wheels. Vehicle motion is from left to right on page.

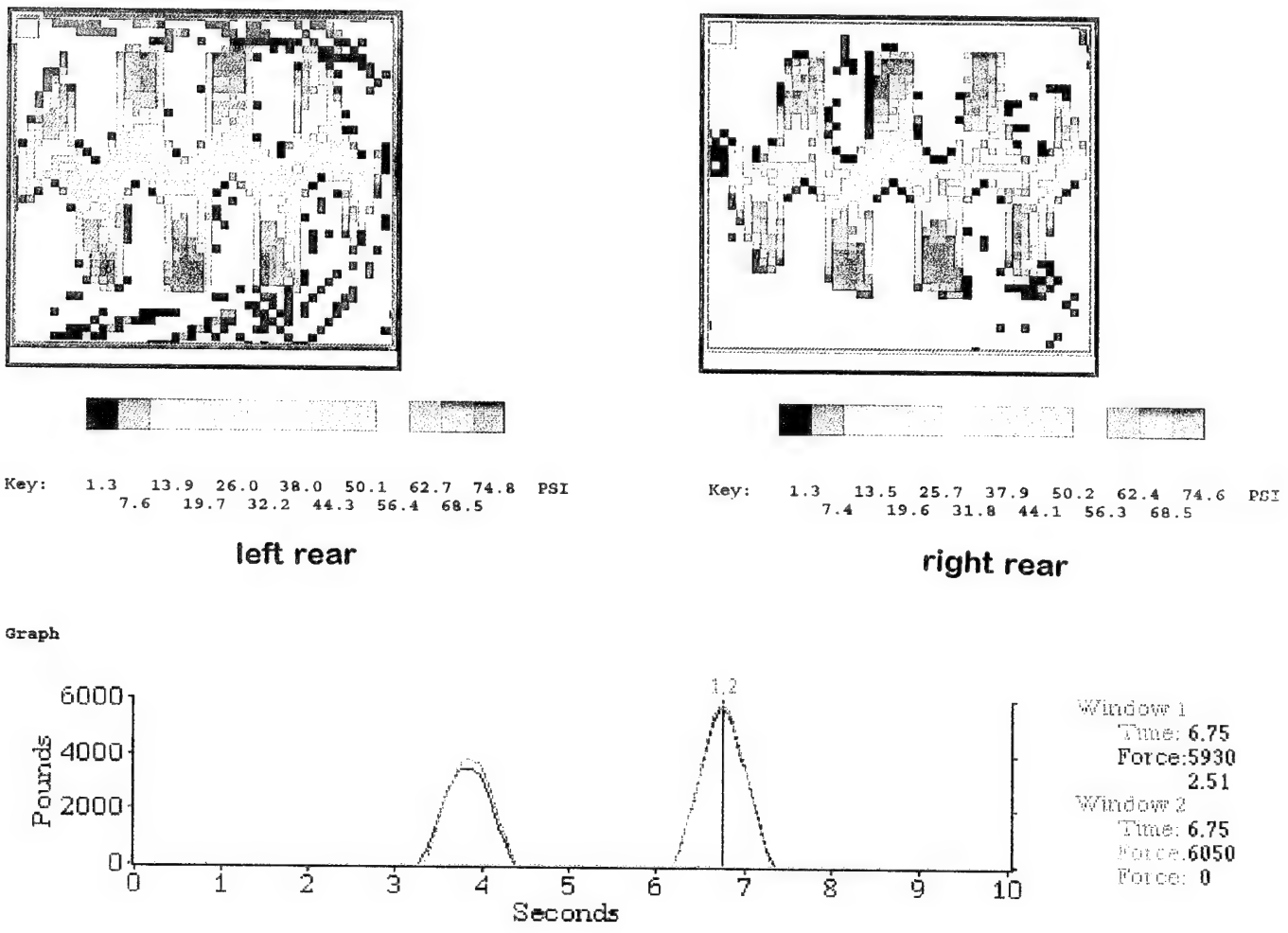

Figure 3-109. 19 kip loader weighing #1 - rear wheels. Vehicle motion is from left to right on page.

Table 3-35. 19,000-pound forklift drive over data.

19,000 lb Forklift Drive Over Data

* all weights in lb

	left front	right front	left back	right back	total
static scale	3590	3850	5945	5815	19200

driveover 1 v=1.808 mph

sensor	H	O	H	O
	left front	right front	left back	right back
	3590		5930	6050
	3620	3920		
	3620	3990		
	3590	3950		
avg	3605	3953.333	5930	6050
% static	100.418	102.684	99.7477	104.0413
% error	0.41783	2.683983	0.25231	4.041273

driveover 2 v=1.808 mph

sensor	H	O	H	O
	left front	right front	left back	right back
	3430		5850	5860
	3490	3690		
	3560	3760		
	3590	3770		
avg	3517.5	3740	5850	5860
% static	97.9805	97.14286	98.402	100.774
% error	2.019499	2.857143	1.59798	0.77386

driveover 3 v=2.169 mph

sensor	H	O	H	O
	left front	right front	left back	right back
	3410		5660	5980
	3380	3800		
	3320	3870		
		3870		
avg	3370	3846.667	5660	5980
% static	93.8719	99.91342	95.2061	102.8375
% error	6.12813	0.08658	4.79394	2.837489

driveover 4 v=1.808 mph

sensor	H	O	H	O
	left front	right front	left back	right back
	3320		5850	5720
	3360	3730		
	3430	3790		
		3810		
avg	3370	3776.667	5850	5720
% static	93.87187	98.09524	98.402	98.3663
% error	6.128134	1.904762	1.59798	1.63371

driveover 5 v=2.116 mph

sensor	H	O	H	O
	left front	right front	left back	right back
	3300		5620	5660
	3280	3670		
	3250	3710		
		3690		
avg	3276.67	3690	5620	5660
% static	91.2721	95.84416	94.5332	97.33448
% error	8.72795	4.155844	5.46678	2.66552

SUMMARY avg v = 1.942 mph

sensor	H	O	H	O
	left front	right front	left back	right back
avg	3427.83	3801.333	5782	5854
avg % err	4.68431	2.337662	2.7418	2.39037
% static	95.4828	98.73593	97.2582	100.6707
% err	4.51718	1.264069	2.7418	0.670679

Vehicle Total Weighing
average of all driveovers

18865.16667
2.448784722
98.25607639
1.743923611

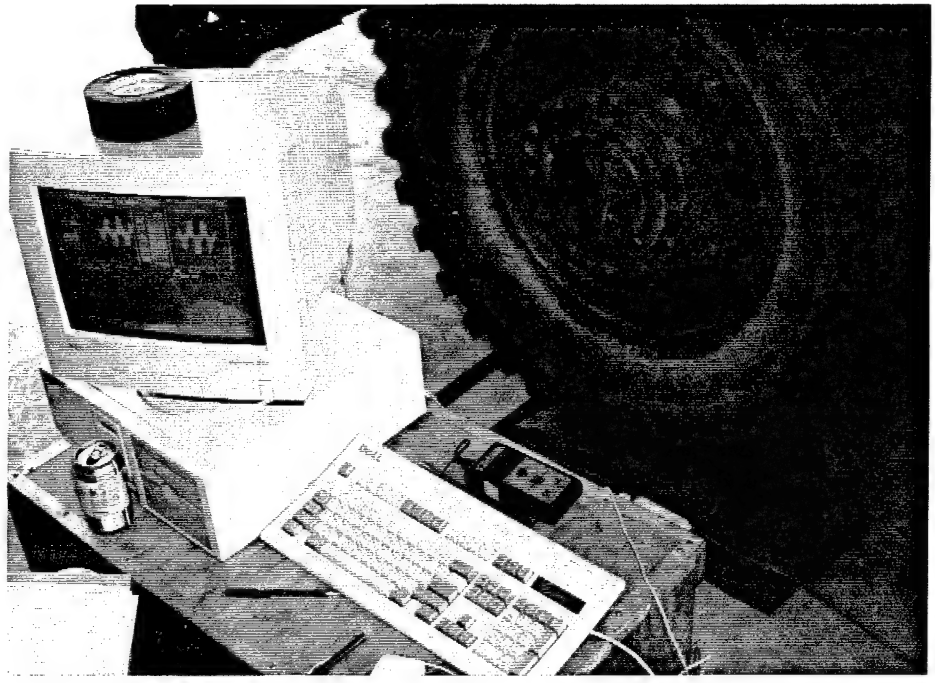

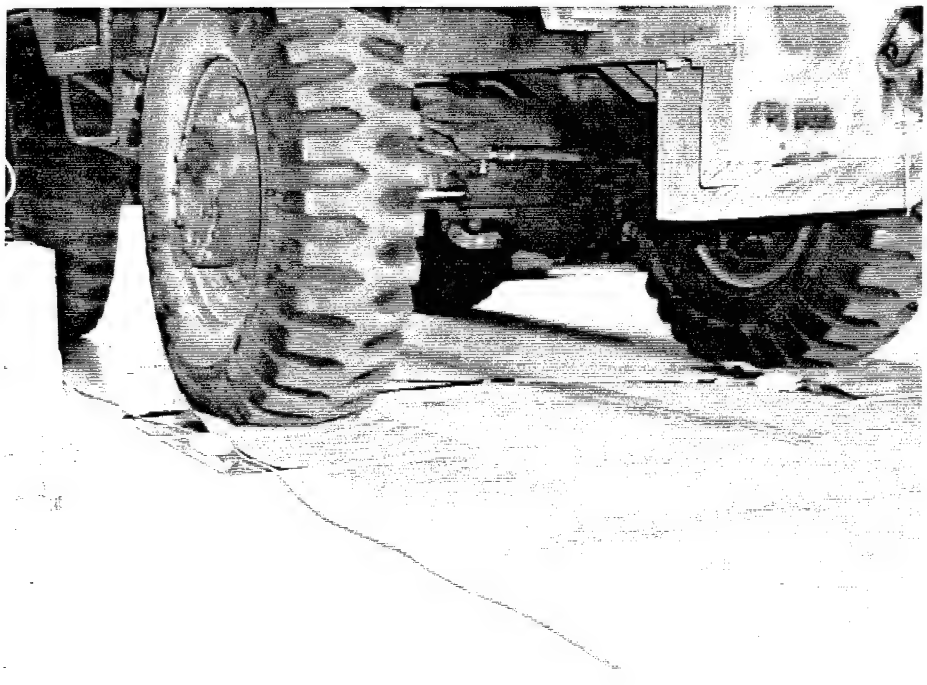

Figure 3-110. Curling of sensor sandwich occurred with the 19-kip loader.

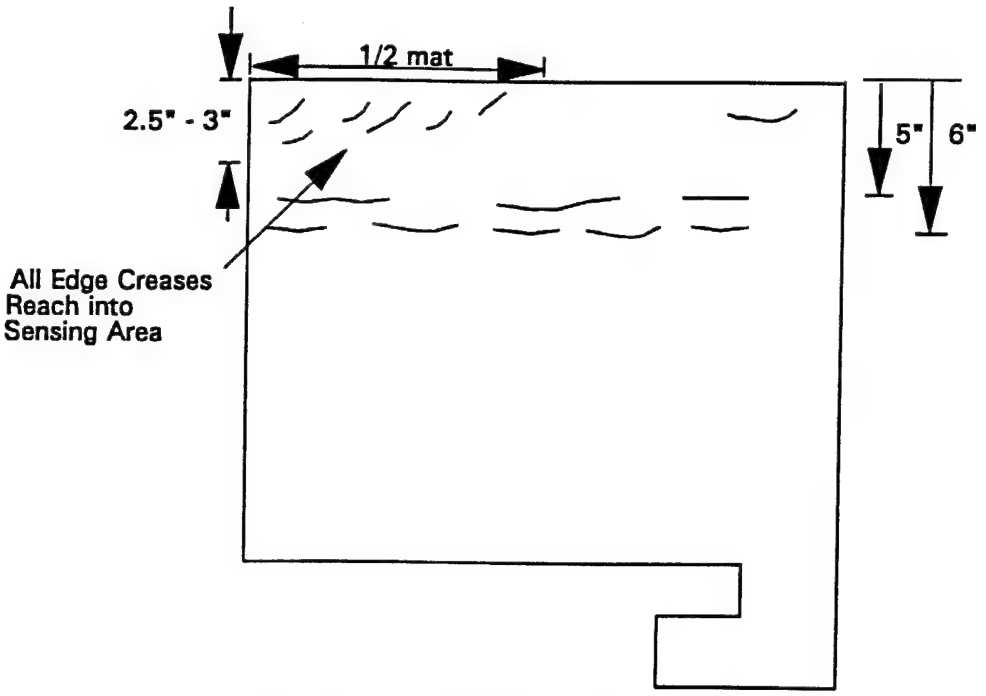

Sensor O - Sustained Most Damage

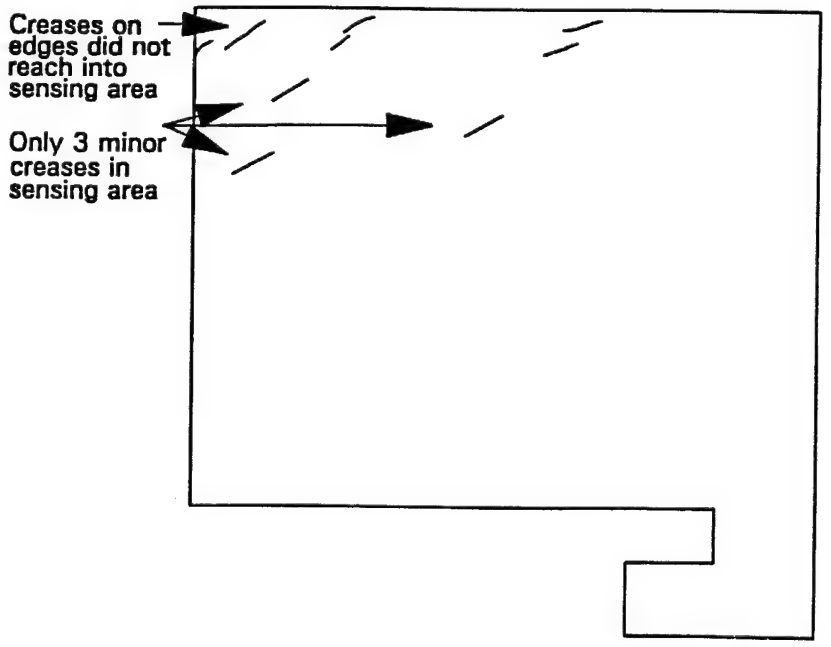

Sensor H - Minor Damage to Sensing Area

Figure 3-111. Summary of damage.

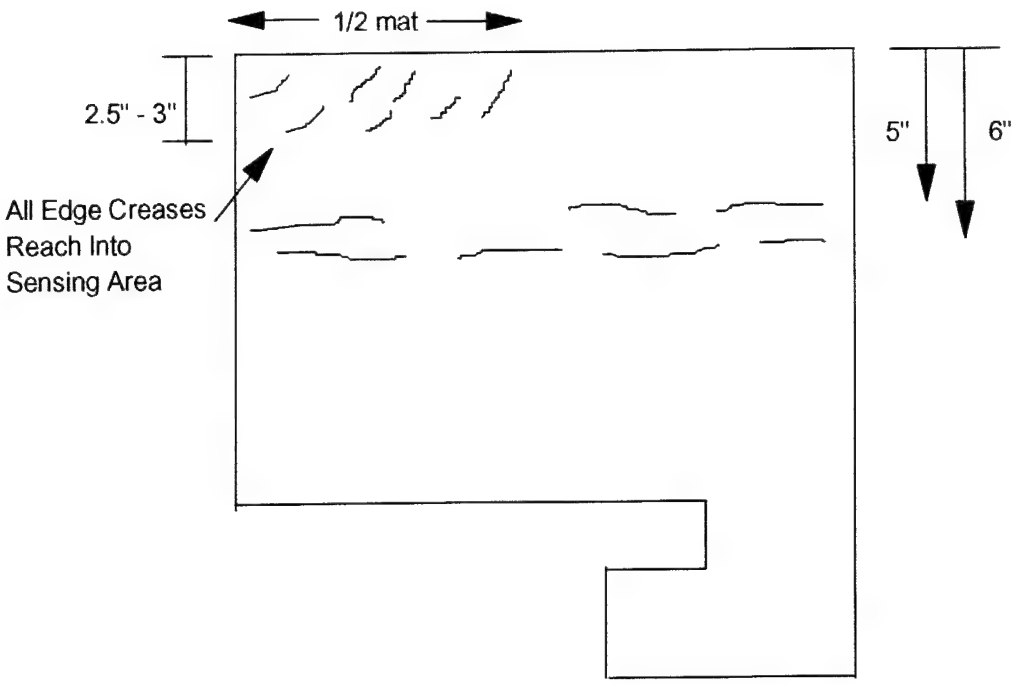

Sensor O - Sustained Most Damage

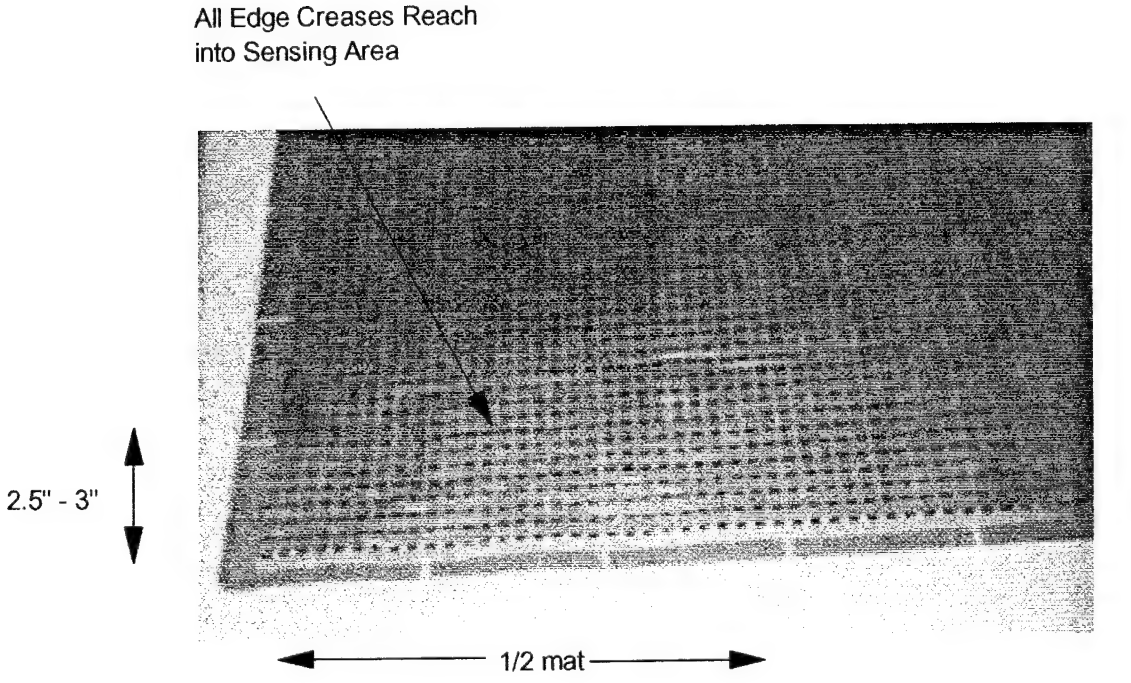

Figure 3-112. Damage of sensor O.

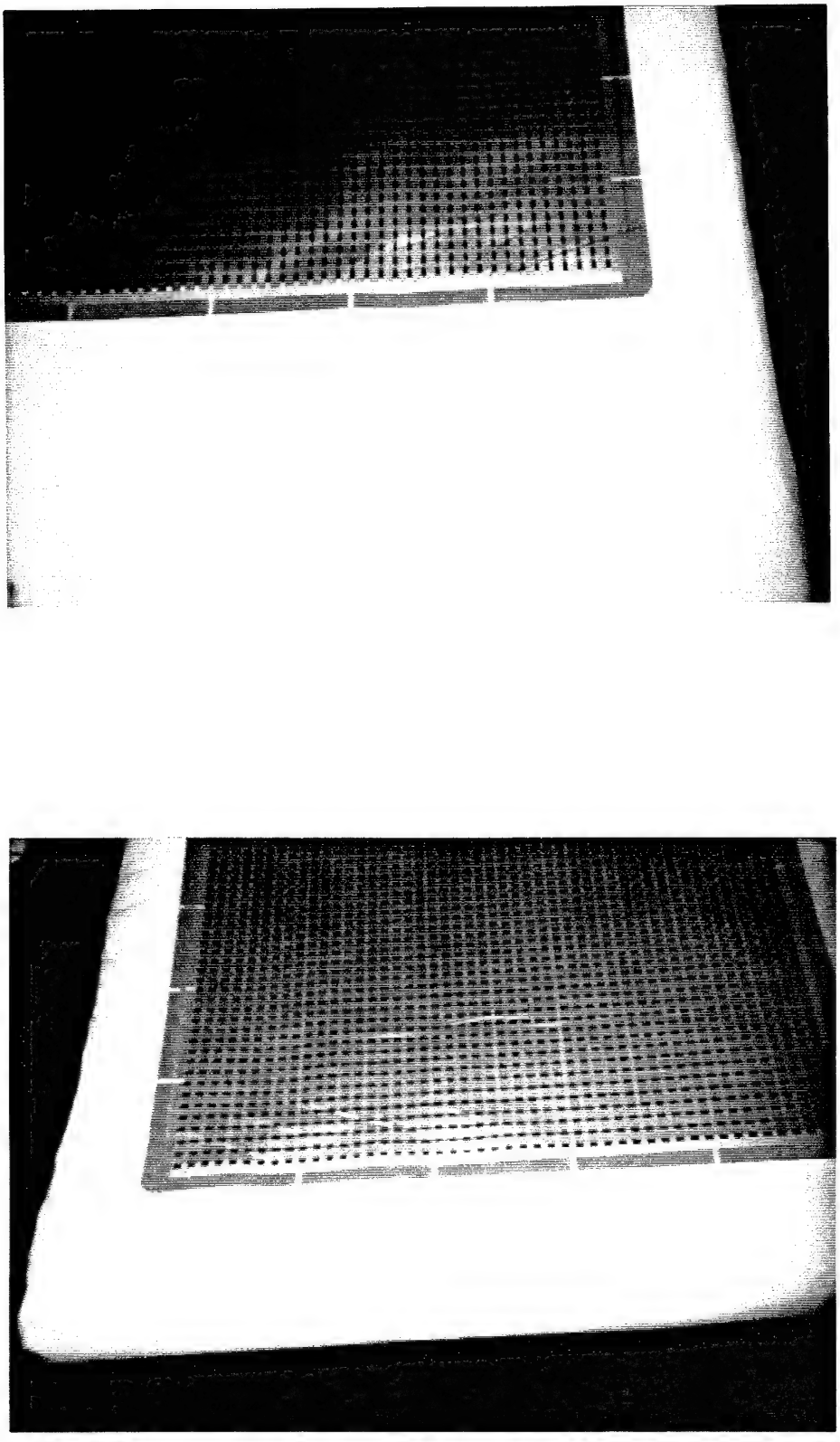

Figure 3-113. Damage of sensor O.

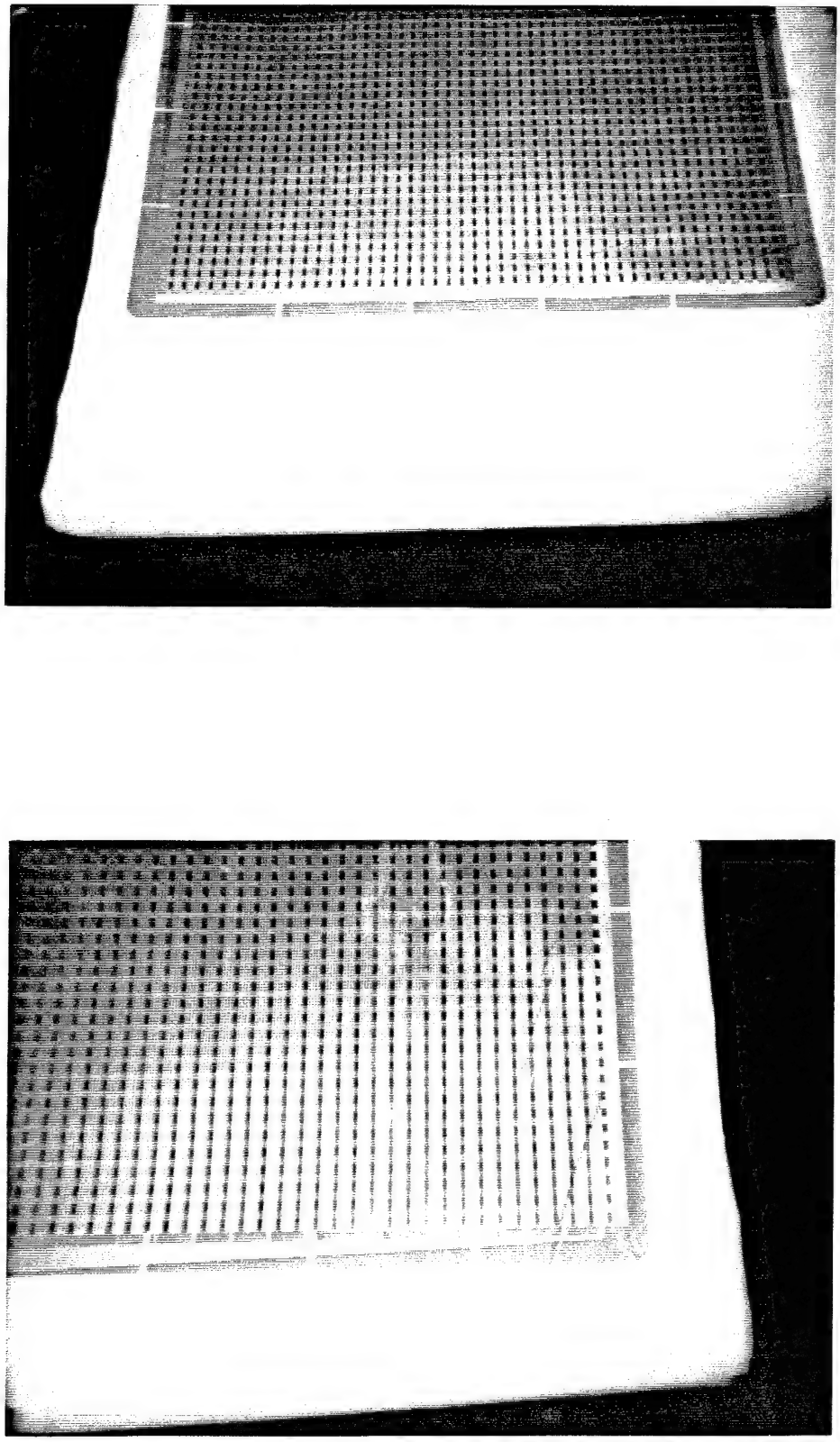

Figure 3-114. Damage of sensor O.

Each damaged sensor was placed in the equilibration device and a recording was made using the original equilibration at 70 degrees F. Damage to sensor O was visible as losses in signal at the creases (Figure 3-115). Sensor H showed no signs of damage in the equilibration device.

3.6.5 Vehicle Weighings - Summary.

It was found that heaving and pitching of a short-wheelbase vehicle or a vehicle subassembly could adversely affect repeatability. Because the repeatability varies, an accurate force calibration made from a wheel weighing of such a vehicle is not likely. Force calibrations made for such a vehicle should be performed under controlled conditions to eliminate error due to dynamic vehicle motion. Force calibrations taken as the average of several samples for a given drive over would probably improve the accuracy, although this is not an option that is currently available in the software. A longer Weighmat would allow more data for averaging and would also allow for more information on dynamic responses of the wheels so that corrections for such responses could be obtained. Tandem axle vehicles are probably subject to similar problems with dynamic wheel motion based on the fact that the closeness of the tandems is similar to a short wheelbase.

Empirically derived corrections were used to correct data readings obtained at one temperature (80 degrees F) with a force calibration obtained at another temperature (-19 degrees F). Corrected readings were within 7 percent of the static scale readings. Considering that the nonlinear fit to the data was a marginally good fit, this degree of accuracy can be considered quite good.

Sensor damage due to localized and edge shearing effects can alter readings. Creases caused by such damage induced losses in signal. Protective measures should be further studied in order to see if mat damage can be eliminated.

Equilibration of the sensor, accurate scale factors, and repeatability of the wheel loads of the forklift yielded good accuracy for the forklift weighings. An average of the five weighings resulted in an accuracy of less than 2 percent.

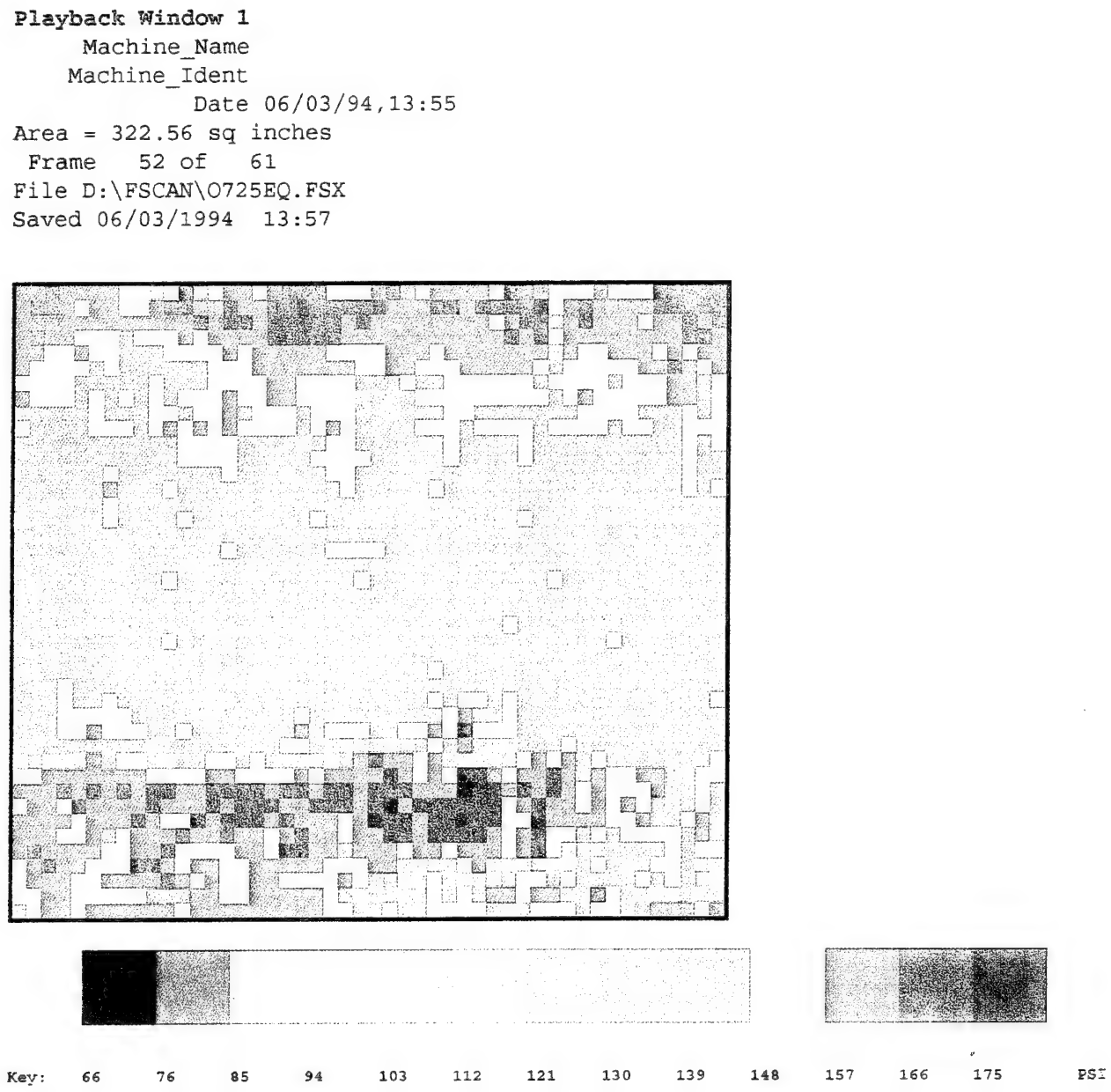

Figure 3-115. Damage shows as loss of signal in the equilibration device.

SECTION 4

CONCLUSIONS

4.1 SENSOR SYSTEM.

We found the sensor elements, hardware and software to be generally satisfactory. Care should be taken by a user to thoroughly check system components and response prior to use as a measurement tool. The data handles provided by Tekscan have different responses to the same sensor element. Care, therefore, should be taken when calibrating and using multi-handle systems. The system software provided by Tekscan is generally excellent in functionality, ease of use and stability. Quality control of sensor elements shipped to us was poor; four of ten sensors in one shipment required exchange due to row ghosting.

4.2 SENSEL-TO-SENSEL VARIATIONS AND EQUILIBRATION.

The equilibration feature greatly reduces sensel-to-sensel variations, but is most effective when performed at a temperature, pressure, and duration close to measurement conditions. However, equilibration cannot overcome error encountered by performing a force calibration on a fluctuating load. Conditions to beware of include unsprung vehicles, vehicles with non-compliant or high pressure tires, short wheelbase vehicles, and tandem axle assemblies, among others. For a fielded system, equilibrations and force calibrations could be performed on a sensor at the factory prior to shipment, with calibration files included on a disk. Correction factors can be applied to substantially compensate for differences in conditions.

Calibration at conditions near those to be encountered when testing will greatly improve accuracy, but generation of equilibration files at room temperature could be considered adequate for many purposes.

4.3 REPEATABILITY.

Repeatability is generally good (when care is taken). Uniform loads produce better repeatability than non-uniform loads. Aggressively treaded tires (particularly with small lugs) will be harder to measure. Sensors very repeatable:

Uniform static	0.836%	Coefficient of variation
Non-uniform static	2.62%	Coefficient of variation
Non-uniform pulses	2.86%	Coefficient of variation

4.4 TEMPERATURE SENSITIVITY.

These sensors are sensitive to temperature changes. Digital output changes about 1 percent per 1 degree change in Fahrenheit temperature between about 10 degrees and 80 degrees F. The sensitivity rate increases sharply above about 90 degrees F, and becomes hypersensitive above about 100 degrees F.

4.5 LINEARITY.

These sensors are nonlinear as the manufacturer says. The nonlinearity increases with temperature, with the sensor responding most linearly at -20 degrees F and very nonlinearly above 100 degrees F. Nonlinearity also increases with load duration.

4.6 STATIC CREEP AND HYSTERETIC BEHAVIOR.

4.6.1 Static Creep.

Static creep is predictable for these sensors. It is greater at lower loads than at higher loads and greater at higher temperatures than at lower temperatures. Different sensors may have differences in static creep rates on the order of 1 to 2 percent per decade.

4.6.2 Hysteresis.

Hysteretic response for a given load is relatively unaffected by temperature changes between -20 degrees F and room temperature. A significant difference could not be resolved in hysteretic response between one half second and one second load plateaus. Hysteresis is a very minor factor in weighing vehicles. For a rolling vehicle measurement, hysteresis would affect no more than 20% of the tire contact area (the trailing portion which is unloading), so that a 10% effect would result in no more than a 2 percent change to overall accuracy.

4.6.3 Fatigue, Memory and Recovery. Tests With Pulse Trains.

The sensor element did not exhibit permanent change in response after a simulated passage of 100 successive vehicles. Fatigue does not appear to be a problem for the application of the sensor in a portable device. However, permanent installation of the sensor for weighing vehicles would require an investigation of the effects of thousands, rather than hundreds of vehicles. Permanent fatigue from long duration static loads was not observed (on the order of 1.4 hours to 14 hours). Permanent fatigue effects were not observed from one single test. Short-term memory of the sensors can affect measurements of vehicles following one another in succession. For an application of weighing a line of vehicles, separation of vehicles by approximately 50 feet would keep this effect within 1 percent.

4.7 VEHICLE TESTS.

Equilibration improves sensor response and repeatability, particularly for narrow tires which could travel across different sides of the mat. Empirically derived corrections and equilibration improve accuracy.

Heaving and pitching of poorly suspended vehicles and potentially some subassemblies necessitate averaging of readings for rolling measurements. For greatest accuracy, vehicles prone to heaving/pitching should be statically weighed; high accuracy measurements may be impossible when these type vehicles are in motion regardless of sensor type.

Current protection of sensor is insufficient for vehicle weighing purposes. Packaging to resist shear forces from tires would be needed for a fielded system.

4.8 SUMMARY.

This sensor technology continues to offer great promise as a portable weighing device. However, this element is presently too immature for use in a high precision vehicle weighing device. It is most severely limited by its inability to behave properly at temperatures above 100 degrees F. Tekscan, the element manufacturer, has indicated that development of a high temperature-tolerant resistive ink is under development, but is unable to predict an availability date. Near term applications should be able to attain accuracy within 10 percent of true weight, making the current technology suitable for screening and gating measurements at mild temperatures.

SECTION 5

RECOMMENDATIONS

This project has confirmed many of the preliminary conclusions from the Proof of Concept project and thus our recommendations from that effort remain largely unchanged. However, our conclusion here of the loss of linearity and repeatability at temperatures above 100 degrees Fahrenheit makes further development of the technology into a system usable under all field conditions premature until a heat resistant element can be manufactured or another type element can be found which can be used in the grid type pressure sensor.

1. A sensor ink capable of yielding repeatable measurements under temperature conditions exceeding 100 degrees Fahrenheit and approaching 160 degrees Fahrenheit must be developed before this technology will be suitable for weighing vehicles under all field conditions.

2. Application of these sensors for weighing should routinely include equilibration, careful force calibration, temperature monitoring, and correction for changes in temperature, pressure, load duration, and load frequency. For development of a robust system, automated monitoring and correction should be incorporated.

3. The manufacturer's software should be modified to allow for multi-frame calibration. For example, a calibration recording could be made over a user-specified duration and sampling rate which could be averaged to produce the calibration scale factor. (This feature would be an addition to the current procedure and should not be confused with the current equilibration technique which we found to be quite valuable.) A real-time output of a rolling average of total load would also be a desirable software feature.

4. In the near term until a new high temperature ink is formulated, these sensors could be used as screening/gating measurement devices provided they are employed on pavements which are shaded or otherwise protected from attaining temperatures greater than 100 degrees F. Development of the technology toward this application has wide potential within the civilian sector as well as in certain military uses (such as for weighing vehicles prior to airlift).

5. For any future vehicle application, packaging must be designed to protect the elements from scuffs and punctures as well as shear stresses from tires. The package would require anchorage to the pavement for measurements conducted above a crawling speed. Furthermore, sensor element design would require modification to move the data handle well away from the path of the vehicle's tires. A number of other obvious hardening measures would also be required.

APPENDIX

DATA FIT

Three data fit equations which give raw digital output as a function of temperature and pressure were obtained. The data fitted was the uniform loadings data obtained with the equilibration device. The first fit was performed with a linear regression analysis using the power equation. The second and third fits were nonlinear regression fits using the Powell method. The first two fits were performed with all uniform loading data while the third fit omitted data for temperatures greater than 80 degrees F.

The first fit was obtained by use of a linear regression using the power equation:

$$R = a0 * T^{a1} * P^{a2}$$

where:

R = raw digital output
T = temperature in deg R
P = pressure in psi
a0, a1, a2 = fitting constants.

The following fit equation was obtained:

$$R = 5.427E\text{-}10 * T^{3.961} * P^{0.3436}$$

The surface defined by the data was not fit very well by this equation. A nonlinear fit which introduced two more fitting constants was pursued in order to find a better fit. The nonlinear data fit equation is shown below. The equation is the same as the linear fit with the addition of the fitting constants a1 and a3.

$$R = a0 * (a1 * T)^{a2} * (a3 * P)^{a4}$$

The nonlinear fit was calculated with the Powell method which is a Gauss-Newton based iterative type method with corrections for divergence due to instabilities which can occur with Gauss-Newton regressions. The Powell method minimizes the sum of the squares of the residuals between the data and the proposed function. A Taylor series expansion is used to approximate the nonlinear equation in a linear form and least squares theory is then used to minimize the residuals. Both Gauss-Newton and steepest descent corrections are calculated for the current parameter estimates. The actual correction is a linear combination of these two. Because the nonlinear fit is an iterative type regression analysis, initial guesses are required for the fitting constants. An initial value of one was assumed for a1 and a3. Initial guesses for a0, a2, and a4 were those obtained with the linear fit. A summary of the initial guesses is as follows:

$a0_i$ = 5.427E-10
$a1_i$ = 1.
$a2_i$ = 3.961
$a3_i$ = 1.
$a4_i$ = 0.3436

A solution was converged upon after 167 iterations for the first nonlinear fit. The resulting equation is shown below:

$$R = 4.713E\text{-}10*(0.2082 * T)^{5.384} *(0.9581 * P)^{0.3458}$$

Both the linear and the first nonlinear fit equations are compared to the data in Figures A-1 and A-2. The green surface is the linear fit, the blue surface is the nonlinear fit, and the red symbols represent the lab data. It can be seen that the nonlinear fit is much better than the linear fit. The nonlinear equation is a good fit to the data except at the higher temperatures. Data fit statistics for the first nonlinear fit are given in Tables A-1 and A-2. The coefficient of determination (COD) is a measure of the fraction of the total variance which is accounted for by the model. The COD for the nonlinear fit was 86 percent which is good, especially when considering the simple form of the assumed data fit equation.

Because the sensor begins erratic behavior at the high temperatures, high temperature data was omitted for the second nonlinear fit. The point at which the sensor begins poor behavior is 90 degrees F. No data was taken between 80 degrees F and 100 degrees F; thus, the data fit was performed for data obtained at temperatures less than 80 degrees F. The Powell method was used for the second nonlinear fit with the same initial guesses used in the first nonlinear fit. The solution found is shown below:

$$R = 4.793E\text{-}10*(0.4155 * T)^{4.531} *(0.9574 * P)^{0.5487}$$

Data fit statistics are included in Tables A-3 and A-4 and the fit is plotted versus the data in Figures A-3 and A-4. The COD was 93 percent which is a 7 percent improvement over the first nonlinear data fit. Based on this measure of accuracy, the fit can be considered quite satisfactory.

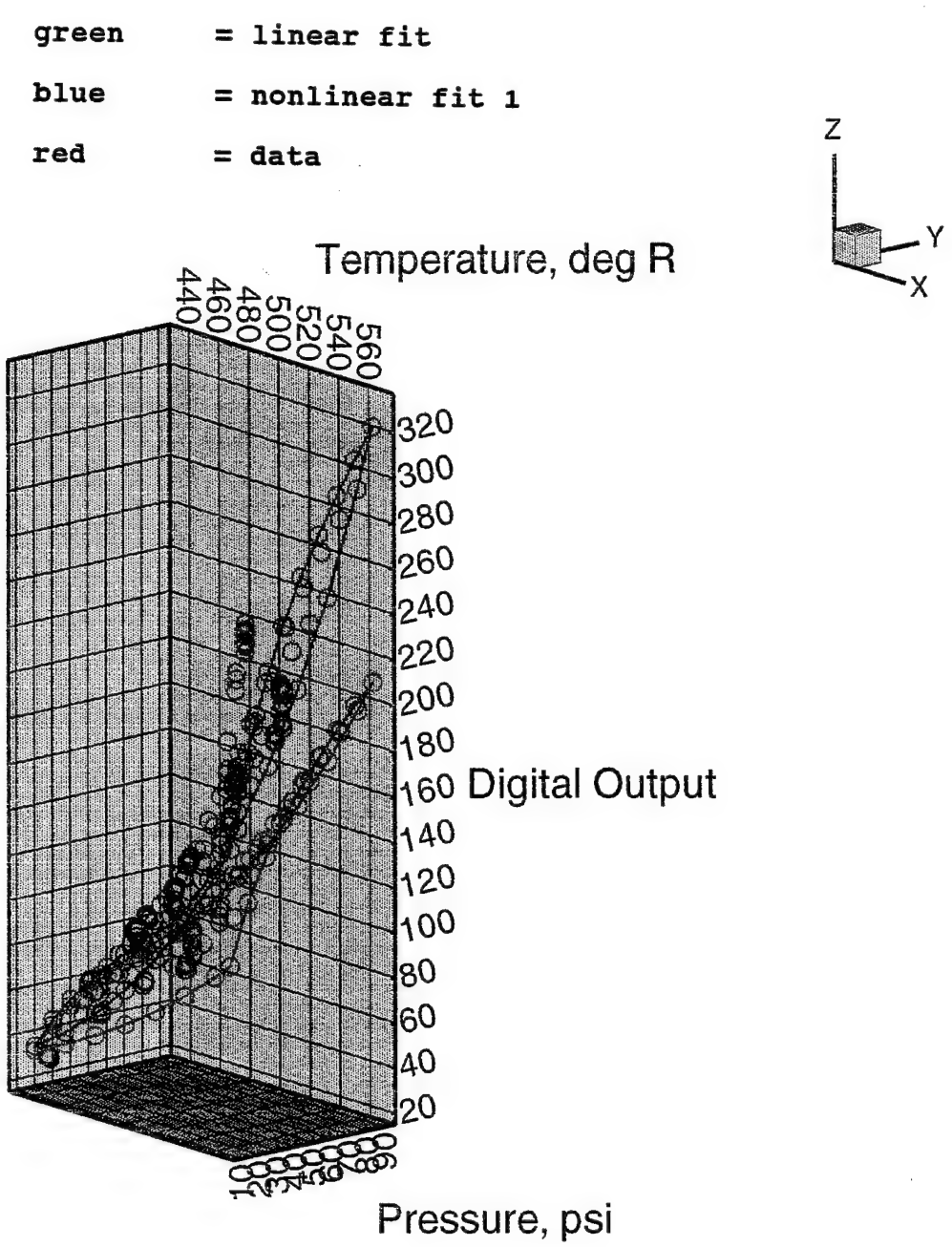

Figure A-1. Linear fit and nonlinear fit 1 compared to data.

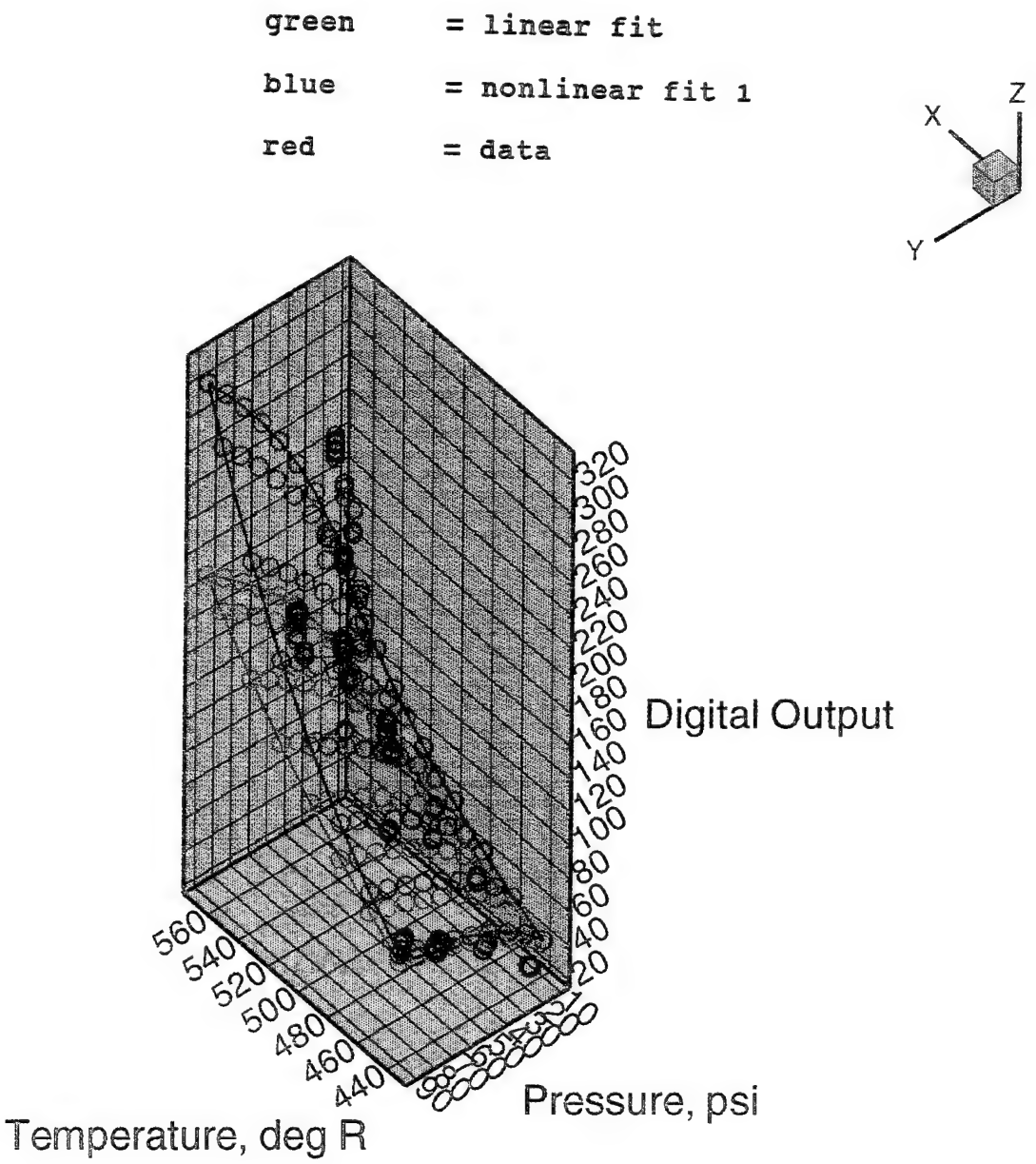

Figure A-2. Linear fit and nonlinear fit 1 compared to data.

Table A-1. Nonlinear fit 1 statistics.

```
Goodness of Fit Statistics ...
  C O D:       0.859660984
  Corrl:       0.927432351
  M S C:        1.91844537

Parameter Statistics
   95.00% Confidence Intervals
Parameter P[1]:    4.71297076E-10
StdDev:      0.00149765937
   Uninvariant ...
   LOW:     -0.00295189734
  HIGH:      0.00295189828
   Supporting Plane:
   LOW:     -0.00502984001
  HIGH:      0.00502984096
   95.00% Confidence Intervals
Parameter P[2]:       0.208177383
StdDev:      0.0337739741
   Uninvariant ...
   LOW:        0.141608627
  HIGH:        0.274746138
   Supporting Plane:
   LOW:       0.0947485849
  HIGH:        0.321606180
   95.00% Confidence Intervals
Parameter P[3]:        5.38348765
StdDev:      0.0449610285
   Uninvariant ...
   LOW:         5.29486912
  HIGH:         5.47210617
   Supporting Plane:
   LOW:         5.23248749
  HIGH:         5.53448780
   95.00% Confidence Intervals
Parameter P[4]:       0.958053171
StdDev:    0.000471813238
   Uninvariant ...
   LOW:        0.957123223
  HIGH:        0.958983118
   Supporting Plane:
   LOW:        0.956468601
  HIGH:        0.959637740
   95.00% Confidence Intervals
Parameter P[5]:       0.345815996
StdDev:      0.0637842247
   Uninvariant ...
   LOW:        0.220096813
  HIGH:        0.471535180
   Supporting Plane:
   LOW:        0.131598744
  HIGH:        0.560033249
```

Table A-2. Nonlinear fit 1 statistics.

```
Fitting Result ...
Parameter: Before
Param[1]:=   5.40000000E-10
Param[2]:=      1.000000000
Param[3]:=       3.96000000
Param[4]:=      1.000000000
Param[5]:=      0.340000000
Using Powell's method
Save Data
Parameter: After
Number of Function Calls: 167
Param[1]:=   4.71297076E-10
Param[2]:=      0.208177383
Param[3]:=       5.38348765
Param[4]:=      0.958053171
Param[5]:=      0.345815996
SumSqr       106705.0666
Covariance Matrix:
  cvm[1,1] :=    4.54040724E-9
  cvm[2,1] :=    1.02391504E-7
  cvm[2,2] :=    2.30904843E-6
  cvm[3,1] :=   -1.35878487E-7
  cvm[3,2] :=   -3.06421913E-6
  cvm[3,3] :=    4.09205239E-6
  cvm[4,1] :=    1.43038149E-9
  cvm[4,2] :=    3.22567789E-8
  cvm[4,3] :=   -4.28063084E-8
  cvm[4,4] :=   4.50618433E-10
  cvm[5,1] :=   -1.03131278E-7
  cvm[5,2] :=   -2.32573119E-6
  cvm[5,3] :=    2.70340097E-6
  cvm[5,4] :=   -3.24898325E-8
  cvm[5,5] :=    8.23560052E-6
```

Table A-3. Nonlinear fit 2 statistics.

```
Goodness of Fit Statistics ...
  C O D:        0.934090975
  Corrl:        0.966799041
  M S C:         2.66628840

Parameter Statistics
   95.00% Confidence Intervals
 Parameter P[1]:     4.79271486E-10
 StdDev:      0.00579006874
   Uninvariant ...
     LOW:      -0.0114238741
    HIGH:       0.0114238751
   Supporting Plane:
     LOW:      -0.0194785573
    HIGH:       0.0194785583
   95.00% Confidence Intervals
 Parameter P[2]:        0.415509871
 StdDev:       0.0560181671
   Uninvariant ...
     LOW:        0.304985360
    HIGH:        0.526034382
   Supporting Plane:
     LOW:        0.227057341
    HIGH:        0.603962401
   95.00% Confidence Intervals
 Parameter P[3]:         4.53050413
 StdDev:       0.0286980672
   Uninvariant ...
     LOW:         4.47388250
    HIGH:         4.58712576
   Supporting Plane:
     LOW:         4.43396003
    HIGH:         4.62704823
   95.00% Confidence Intervals
 Parameter P[4]:        0.957465848
 StdDev:      0.00294511798
   Uninvariant ...
     LOW:        0.951655095
    HIGH:        0.963276601
   Supporting Plane:
     LOW:        0.947558081
    HIGH:        0.967373615
   95.00% Confidence Intervals
 Parameter P[5]:        0.548724059
 StdDev:       0.0578382627
   Uninvariant ...
     LOW:        0.434608478
    HIGH:        0.662839641
   Supporting Plane:
     LOW:        0.354148486
    HIGH:        0.743299632
```

Table A-4. Nonlinear fit 2 statistics.

```
Fitting Result ...
Parameter: Before
Param[1]:=    5.40000000E-10
Param[2]:=       1.000000000
Param[3]:=        3.96000000
Param[4]:=       1.000000000
Param[5]:=       0.340000000
Using Powell's method
Save Data
Parameter: After
Number of Function Calls: 101
Param[1]:=    4.79271486E-10
Param[2]:=       0.415509871
Param[3]:=        4.53050413
Param[4]:=       0.957465848
Param[5]:=       0.548724059
SumSqr         30947.2021
Covariance Matrix:
  cvm[1,1] :=     1.98242670E-7
  cvm[2,1] :=     1.91797222E-6
  cvm[2,2] :=     1.85561335E-5
  cvm[3,1] :=    -9.74921730E-7
  cvm[3,2] :=    -9.43224180E-6
  cvm[3,3] :=     4.87006767E-6
  cvm[4,1] :=     1.00836118E-7
  cvm[4,2] :=     9.75576412E-7
  cvm[4,3] :=    -4.95893857E-7
  cvm[4,4] :=     5.12902828E-8
  cvm[5,1] :=    -4.07801222E-7
  cvm[5,2] :=    -3.94542414E-6
  cvm[5,3] :=     8.16368342E-7
  cvm[5,4] :=    -2.07428057E-7
  cvm[5,5] :=     1.97815436E-5
```

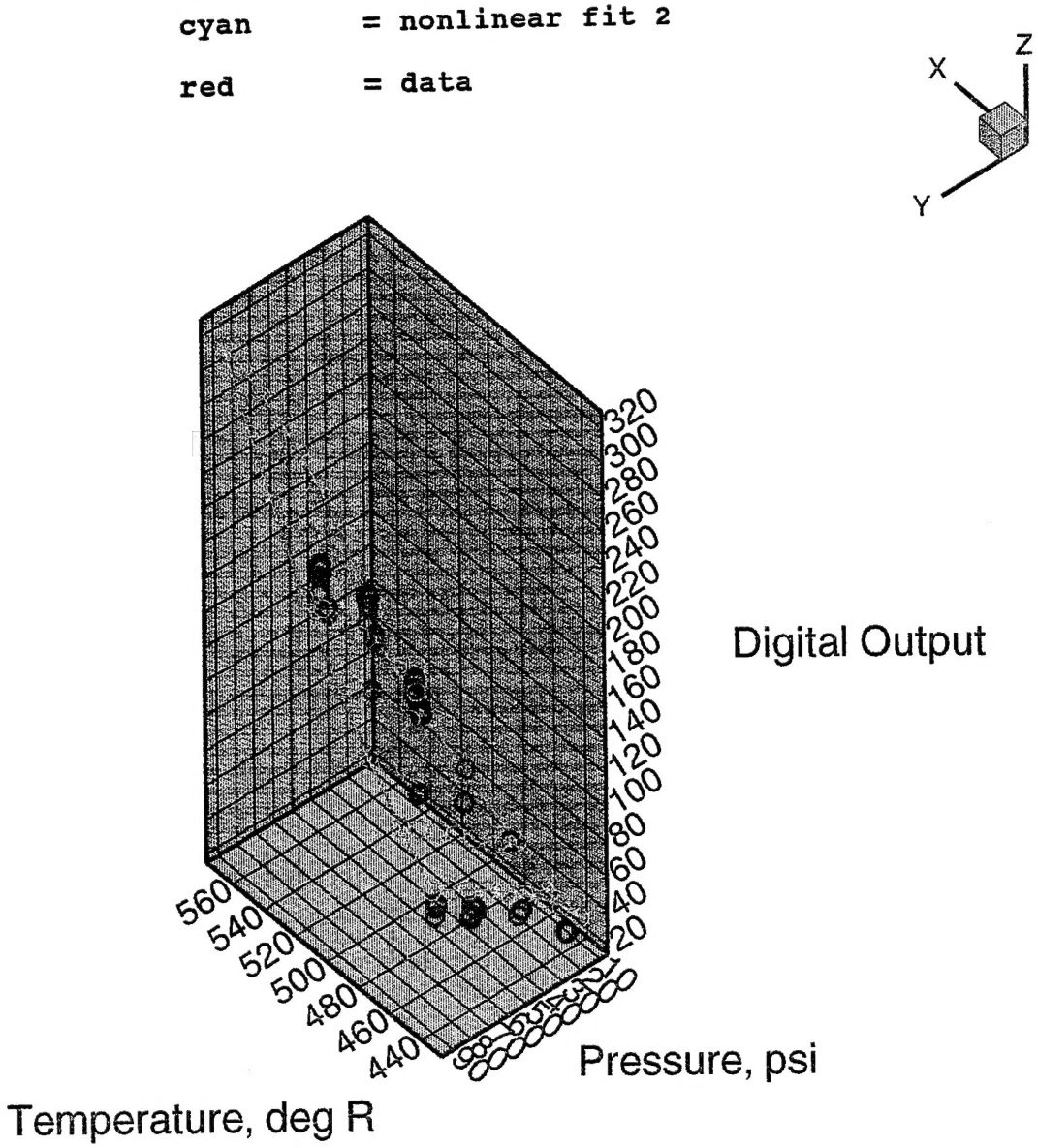

Figure A-3. Nonlinear fit 2 compared to data.

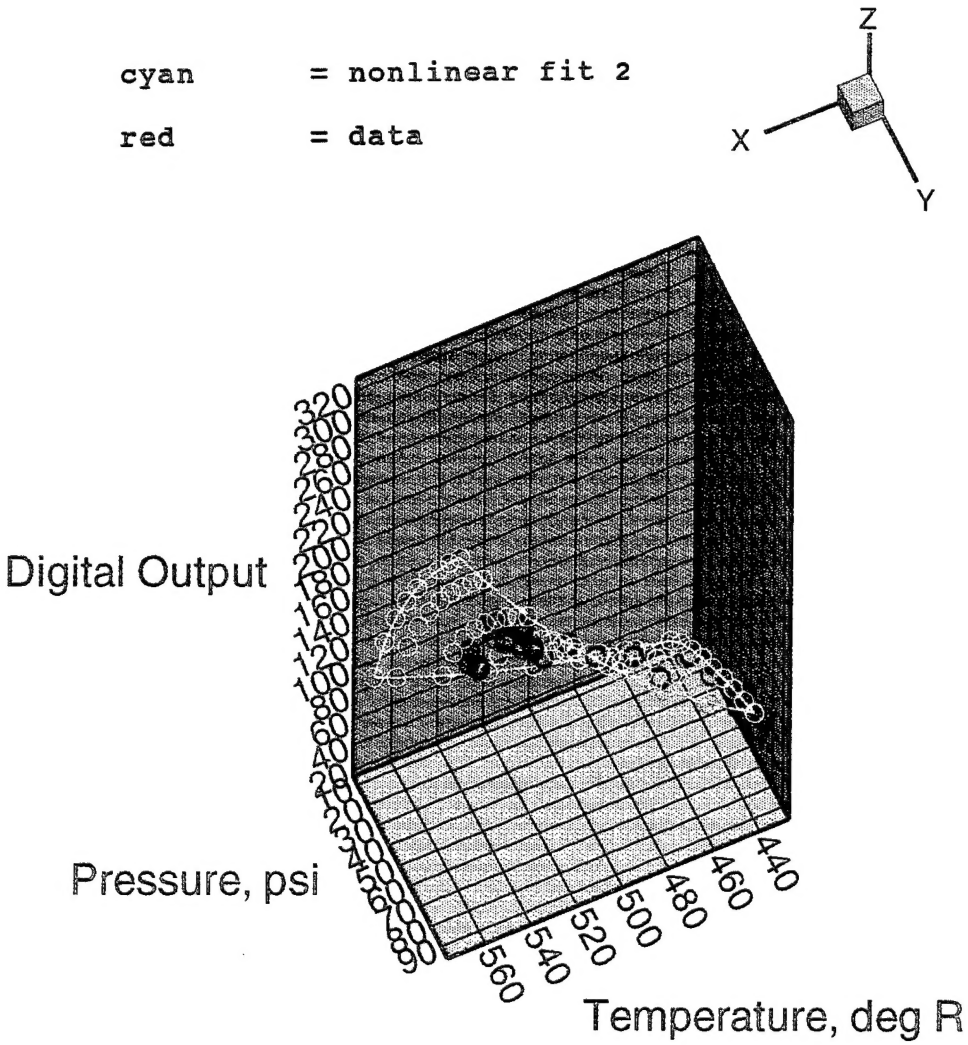

Figure A-4. Nonlinear fit 2 compared to data.

DISTRIBUTION LIST

DNA-TR-94-124

DEPARTMENT OF DEFENSE

ASSISTANT SECRETARY OF DEFENSE
INTERNATIONAL SECURITY POLICY
ATTN: VERIFICATIONS POLICY

DEFENSE INTELLIGENCE AGENCY
ATTN: DI-5
ATTN: DT
ATTN: PAM-1D
ATTN: PGI-4

DEFENSE NUCLEAR AGENCY
5 CY ATTN: OPAC LT COL B SIMELTON
2 CY ATTN: SSTL

DEFENSE TECHNICAL INFORMATION CENTER
2 CY ATTN: DTIC/OC

FIELD COMMAND DEFENSE NUCLEAR AGENCY
ATTN: FCPR

FIELD COMMAND DEFENSE NUCLEAR AGENCY
ATTN: FCTO

ON-SITE INSPECTION AGENCY
2 CY ATTN: DR MENZEL

DEPARTMENT OF THE AIR FORCE

AIR UNIVERSITY LIBRARY
ATTN: AUL-LSE

HQ 497 IG/INOT
ATTN: INT

DEPARTMENT OF DEFENSE CONTRACTORS

APPLIED RESEARCH ASSOCIATES, INC
2 CY ATTN: R B UNDERWOOD III
2 CY ATTN: S C LOFTON

INNOVATIVE MECHANICS, INC
2 CY ATTN: A PEEKNA

JAYCOR
2 CY ATTN: CYRUS P KNOWLES

KAMAN SCIENCES CORP
ATTN: DASIAC

KAMAN SCIENCES CORPORATION
ATTN: DASIAC